VNIVERSITAT D VALÈNCIA Facultat de Física
Departament de Física de la Terra i Termodinàmica

Departament de Física de la Terra i Termodinàmica

Tesis Doctoral

OPTICAL AND RADAR REMOTE SENSING APPLIED TO AGRICULTURAL AREAS IN EUROPE

TELEDETECCIÓN EN EL ÓPTICO Y EN EL RADAR APLICADA A REGIONES AGRÍCOLAS EN EUROPA

Memoria presentada por
María del Carmen González Sanpedro
para optar al grado de Doctor en Física
Valencia, Octubre, 2008

A mis padres,
y a Pere

ACKNOWLEDGEMENTS

I would like to thank my advisors, Dr. Tuy Le Toan and Dr. José Moreno for giving me the opportunity of working with them at CESBIO and at the University of Valencia respectively, as well as for helping me to accomplish this thesis. I am also very grateful with Dr. Martine Guèrif, Dr. Francesco Mattia, and Dr. José Sobrino who, as reviewers of my report, provided careful corrections.

I am extremely grateful with my friends and colleagues at CESBIO. In particular I would like to mention Dr. Laurent Kergoat for his priceless scientific discussions and encouragement.

Pendant cette étape dans le monde de la recherche, j'ai eu la chance de rencontrer des personnes qui sont devenues très importantes pour moi. Je tiens donc à remercier toutes ces personnes et à leur transmettre ici toute mon amitié. Sans aucun doute, vous avez été le meilleur de cette étape.

Au CESBIO je remercie spécialement Manuela Grippa (et à la *famiglia* Balochi au complet: Andrea, Mattia et Gaia). Également je remercie Nicolas Delbart, Claire Gruhier, Silvia Juglea, Iskander Benhadj, Arnaud Mialon, Philippe Richaume, Olivier Merlin, Alex Bouvet, Frederic Frappart et Ahmad Albitar. Merci aussi à Julie Gardelle, qui a eu le courage de partager un bureau avec moi a la fin de ma thèse (bonne chance pour la suite!). Je remercie aussi d'autres amis qui ont passé par ce laboratoire il y a quelque temps: Erick Lopez, Daniel Kristoff (et Andrea "*la otra*"), Joost Hodges, Sergio Vicente, Alberto García,

Julien l'Hermitte, Yannick Lepage, Mª José Escorihuela, Sylvie Duthoit, Laurent Coret, et Ferran Gascon. J'ai de très bons souvenirs du temps passé à Toulouse avec Lizbeth Guijarro qui sera toujours une bonne amie, même si elle est de l'autre côté de l'Atlantique. Un grand merci aussi aux permanents et "quasi-permanets" du CESBIO qui ont toujours été très aimables avec moi, spécialement je veux remercier à François Cabot (est-ce que tu sais où il est Laurent?), Olivier Hagolle, Valérie Le Dantec, Valérie Demarez, Philippe Maisongrande (vive le Tour!), Pierre Hiernaux, Eric Mougin, et encore à Laurent et à Thuy.

Je pense aussi tout particulièrement à Françoise Guichard, toujours très douce et très gentille avec moi.

También quiero agradecer de corazón a quienes han sido mis compañeros de laboratorio en la Universidad de Valencia y con quienes compartí muchas risas: Luis Alonso (por los momentos frikis), José Carlos García, Carlos Cuñat, José Manuel Martínez, Luis Guanter, Juan Carlos Fortea y Gloria Fernández. También quiero agradecer muy especialmente a Siham Lanjeri todo su cariño y amistad. Por supuesto que no puedo olvidar tampoco a otros compañeros del departamento como Fernando Camacho. Tengo también un recuerdo para los buenos ratos pasados allá bajo el sol de la Mancha junto con Michael Whiting, Bob Zomer, y la lista es demasiado larga.., (gracias!). Y a mis compañeros de la facultad: Ana Campos, Antonio Pérez, Oscar Soler, Javier Cervera, José Juan Esteve, Julio Trujillo, María José Yusá, muy particularmente a Víctor Estellés, quien siempre supo ser un gran amigo incluso a distancia.

Tengo un recuerdo muy bueno de mis amigas en Valencia: Laura, Pilar, Maribel y Meriam. Finalmente, quiero agradeceros a vosotras: Desirée, Carmen María, Rosaura, Ana, María Jesús, Rosa y Maite por vuestra paciencia y todas las veces que os dije "tengo que trabajar".

A mis padres.

I moltes, moltíssimes gràcies a tu Pere, per ser al meu costat. *Dankon belulo*!

ABSTRACT

The global population growth, as well as the social and economic importance that the agricultural sector has in many regions of the world, makes it very important to develop methods to monitor the status of crops, to improve their management, as well as to be able to make early estimates of the agricultural production. One of the main causes of uncertainty in the production of crops is due to the weather, for example, in arid and semiarid regions of the world, periods of drought can generate big losses in agricultural production, which may result in famine. Thus, FAO, during their summit in June 2008, stressed the need to increase agricultural production as a measure to strengthen food security and reduce malnutrition in the world.

Concern for increasing crop production, has generated, during the last decades, significant changes in agricultural techniques. For example, there has been a widespread use of pesticides, genetically modified crops, as well as an increase in intensive farming. In turn, the market influences crop rotations, and as a consequence, changes in the spatial distribution of crops are very common. Therefore, in order to make estimates of agricultural production, it is also necessary to map regularly the crop fields, as well as their state of development.

The aim of this thesis is to develop methods based on remote sensing data, in the radar and optical spectral regions, in order to monitor crops, as well as a to map them. The results of this thesis can be combined with other techniques, especially with models of crop growth, to improve the prediction of crops.

The optical remote sensing methods for classifying and for the cartography of crops are well established and can be considered almost operational. The disadvantage of the methods based on optical data is that they are not applicable to regions of the world where cloud coverage is frequent. In such cases, the use of radar data is more advisable. However, the classification methods using radar data are not as well established as the optical ones, therefore, there is a need for more scientific studies in this field. As a consequence, this thesis focuses on the classification of crops using radar data, particularly using AIRSAR airborne data and ASAR satellite data.

The monitoring of crops by remote sensing is based on the estimation of biophysical parameters and their evolution over time. These parameters are, among others, LAI (leaf area index), chlorophyll and biomass. In this thesis, satellite data from LANSAT-TM are used for the inversion of LAI, and ENVISAT-MERIS data for estimating LAI and chlorophyll. Finally, ENVISAT-ASAR radar data are used to investigate its potential in the estimation of the biomass of cereals.

Chapter 1 of the thesis introduces the context of this study and its scientific objectives.

Chapter 2 presents the theoretical basis of optical remote sensing.

Chapter 3 is dedicated to the inversion of LAI in the region of Barrax (Castilla-La Mancha, Spain) using 12 LANDSAT-TM images acquired during the same agricultural season. The LAI is calculated using LUTs (Look Up Tables) to invert the radiative transfer model SAIL, which is coupled to the model of leaf reflectance PROSPECT. The results are validated with experimental measurements acquired during the field campaign ESA SPARC-2003, showing a good correlation.

Chapter 4 proposes a method to invert, at the same time, LAI and chlorophyll data from ENVISAT-MERIS. This method involves an inversion of the same model, PROSPECT + SAIL, which was used in Chapter 3, but with the special addition of a temporal constraint. Thus, instead of inverting a single value of LAI and chlorophyll for each date, a curve for the entire crop cycle is inverted. This method seeks to take as much information as possible from the temporal dimension of the data. The results show that the multitemporal method works better than the inversions on a single date. However, the inversion of chlorophyll still requires further study.

Chapter 5 introduces the concepts related to the radar remote sensing, which will be used along the second part of this thesis.

In Chapter 6 a method of hierarchical classification of crops is developed. It uses polarimetric data in C band, from the airborne instrument AIRSAR. The method is applied to images in Flevoland (Netherland) and is validated with field observations.

Chapter 7 investigates the use of ENVISAT-ASAR data for agricultural applications in the region of Toulouse. The first part discusses the possibilities for classification of crops. The second part investigates the potential of the polarization ratio HH / VV to estimate the biomass of wheat. It is confirmed that there is a clear link between this ratio and the biomass of wheat, however, this relationship depends on many other factors and seems to be dependent on the experimental site. Therefore, more studies needs to be conducted.

The findings of this study, as well as their prospects are outlined in greater detail in Chapter 8.

To sum up, this thesis investigates the use of optical and radar remote sensing to the monitoring of agricultural areas. Four different instruments, three on board satellites (LANDSAT-TM, ENVISAT-MERIS, and ENVISAT-ASAR) and 1 airborne instrument (AIRSAR) are used, in three areas of study in Europe (Barrax, Toulouse and Flevoland), as well as an important number of field measurements. This study highlights the importance of the multi-temporal aspect in agricultural studies using remote sensing.

RESUMÉ

À cause de l'importance sociale et économique que le secteur agricole a dans des nombreuses régions du monde, il est très important de développer des méthodes pour surveiller l'état des cultures, pour améliorer leur gestion et pour pouvoir faire une estimation précoce de la production agricole. L'une des principales causes d'incertitude dans la production des cultures est due aux conditions météorologiques, par exemple dans les zones arides et semi-arides du monde, des longues périodes de sécheresse peuvent générer des grandes pertes dans la production agricole, ce qui, parfois, provoque des famines. Ainsi, la FAO, au cours du sommet de juin 2008, a souligné la nécessité d'accroître la production agricole comme une mesure visant à renforcer la sécurité alimentaire et réduire la malnutrition dans le monde.

Le souci d'améliorer la production agricole a suscité, au cours des dernières décennies, des changements importants dans les techniques agricoles. Par exemple, il y a eu une utilisation généralisée des produits phytosanitaires, une augmentation des cultures génétiquement modifiées, ainsi qu'une augmentation de l'agriculture intensive. Quant à, la rotation des cultures, elle est de plus en plus influencée par le marché. En conséquence, des changements dans la répartition spatiale des cultures sont très fréquents. Ainsi, afin de faire des estimations de la production agricole, il est nécessaire de pouvoir produire, régulièrement des cartes des cultures ainsi que leur état de développement.

L'objectif de cette thèse est de développer des méthodes basées sur des données de télédétection, radar et optiques, afin d'assurer le suivi des cultures, ainsi que leur cartographie. Les résultats de cette thèse pourront être

combinés avec d'autres techniques, notamment avec des modèles de croissance des cultures, pour améliorer la prévision des récoltes.

Les méthodes de télédétection optique pour classifier et cartographier les cultures sont bien établies et peuvent être considérées comme quasi opérationnelles, mais leur inconvénient est qu'elles ne sont pas applicables à des régions du monde où la couverture nuageuse est fréquente. Dans ce cas, l'utilisation des données radar est plus souhaitable. Toutefois, les méthodes de classification basées sur des données radar n'étant pas aussi bien établies que celles qui sont basées sur l'optique, il y a donc un besoin de plus d'études scientifiques dans ce domaine. En conséquence, cette thèse porte sur la classification des cultures utilisant des données radar, en particulier des données aéroportées AIRSAR et de données ASAR du satellite ENVISAT.

La surveillance des cultures par télédétection est basée sur l'estimation des paramètres biophysiques et de leur évolution au fil du temps. Ces paramètres sont, entre autres, le LAI (indice de surface foliaire), la chlorophylle et la biomasse. Dans cette thèse, les données satellitaires LANSAT-TM sont utilisées pour l'inversion du LAI et les données ENVISAT-MERIS sont utilisées pour l'estimation combinée du LAI et de la chlorophylle. Enfin, le potentiel des données radar ENVISAT ASAR pour étudier leur potentiel dans l'estimation de la biomasse des céréales est évalué.

Le premier chapitre de la thèse présente le contexte de cette étude et ses objectifs scientifiques.

Le deuxième chapitre présente les fondements théoriques de la télédétection optique.

Le troisième chapitre est consacré à l'inversion du LAI dans la région de Barrax (Castilla-La Mancha, Espagne) à l'aide de 12 images LANDSAT-TM acquises au cours du même cycle de culture. Le LAI est calculé en utilisant des

LUTs (Look Up Tables) pour inverser le modèle de transfert radiatif SAIL, qui est couplé au modèle de réflexion des feuilles PROSPECT. Les résultats sont validés avec des mesures expérimentales acquises au cours de la campagne sur le terrain ESA SPARC-2003, montrant une bonne corrélation.

Le Chapitre 4 propose une méthode inverser à la fois le LAI et la chlorophylle avec les données ENVISAT-MERIS. Cette méthode implique une inversion du même modèle, PROSPECT + SAIL, utilisé dans le Chapitre 3, mais avec une contrainte temporelle. Ainsi, au lieu d'inverser une valeur unique du LAI et de la chlorophylle pour chaque date, une courbe pour l'ensemble du cycle de culture est inversée. Cette méthode cherche à tirer parti, autant que possible, de la dimension temporelle des données. Les résultats montrent que la méthode multitemporelle fonctionne mieux que les inversions sur une date unique. Toutefois, l'inversion de la chlorophylle nécessite encore une étude plus approfondie.

Le Chapitre 5 présente les concepts liés à la télédétection radar, qui seront utilisés le long de la deuxième partie de cette thèse.

Dans le Chapitre 6, une méthode de classification hiérarchique des cultures est développée. Elle utilise des données polarimétriques en bande C de l'instrument aéroporté AIRSAR. La méthode est appliquée à des images dans le Flevoland (Pays-Bas) et est validée avec des observations sur le terrain.

Le Chapitre 7 examine l'utilisation des données ENVISAT ASAR pour les applications agricoles dans la région de Toulouse. La première partie examine les possibilités offertes pour obtenir une classification des cultures. La deuxième partie étudie le potentiel du rapport de polarisation HH / VV pour estimer la biomasse du blé. Il est confirmé qu'il existe un lien entre ce rapport et la biomasse du blé, cependant, cette relation dépend de nombreux facteurs

et semble être dépendante du site d'expérimentation. Par conséquent, une étude plus approfondie est nécessaire.

Les conclusions de cette étude, ainsi que ses perspectives, sont décrites plus en détail dans le Chapitre 8.

En résumé, la thèse porte sur la télédétection optique et radar pour le suivi des zones agricoles. Quatre instruments différents, 3 satellitaires (LANDSAT-TM, ENVISAT-MERIS, ENVISAT-ASAR) et 1 aéroporté (AIRSAR) sont utilisés dans trois régions d'étude en Europe (Barrax, Toulouse et Flevoland), ainsi qu'un nombre important de mesures sur le terrain. Cette étude souligne l'importance de l'aspect multitemporel dans les études agricoles au moyen de la télédétection.

RESUMEN

El aumento de la población mundial, así como la importancia social y económica que el sector agrícola tiene en muchas regiones del mundo, hace que sea muy importante desarrollar métodos que permitan hacer un seguimiento del estado de los cultivos, mejorar la gestión de los mismos, así como poder realizar una estimación temprana de la producción. La principal causa de incertidumbre en la producción de las cosechas es debida a las condiciones meteorológicas, por ejemplo, en las regiones áridas y semiáridas del mundo los períodos de sequía generan grandes pérdidas en la producción agrícola, la cuales se traducen en hambrunas. Así, la FAO, durante su cumbre de Junio 2008, insistió en la necesidad de aumentar a producción agrícola como una medida para reforzar la seguridad alimentaria y reducir la desnutrición en el mundo.

La preocupación por aumentar la producción de cultivos, ha generado, durante las últimas décadas, importantes cambios en las técnicas agrícolas. Por ejemplo, se ha producido un uso generalizado de productos fitosanirios, de cultivos modificados genéticamente, así como un aumento de la agricultura intensiva. A su vez, la rotación de cultivos está cada vez más influenciada por el mercado, siendo los cambios en la distribución espacial de los cultivos muy frecuentes. Por lo tanto, para poder hacer estimaciones de la producción agrícola, es necesario producir periódicamente mapas de cultivos, así como cartografiar su estado de desarrollo.

La presente tesis doctoral tiene como objetivo desarrollar métodos basados en datos de teledetección, en la región del óptico y en la región del radar, que permitan realizar un seguimiento de los cultivos, así como una

cartografía de los mismos. Los resultados de esta tesis pueden combinarse con otras técnicas, especialmente con los modelos de crecimiento de cultivo, para mejorar la predicción de las cosechas.

Los métodos de teledetección para la clasificación y la cartografía de cultivos utilizando datos en la región del óptico están bien establecidos y pueden considerarse casi operacionales. La desventaja de estos estudios basados en datos ópticos es que no pueden aplicarse a regiones donde la cobertura nubosa es frecuente. En esos casos, la utilización de datos radar es más recomendable. Sin embargo, los métodos de clasificación utilizando datos radar no están tan bien establecidos y es necesario realizar más estudios científicos en este campo. Es por ello, que esta tesis se centra en la clasificación de cultivos mediante datos radar, concretamente datos aerotransportados AIRSAR y datos ASAR del satélite ENVISAT.

El seguimiento de los cultivos mediante teledetección se basa en la estimación de parámetros biofísicos y su evolución en el tiempo. Estos parámetros son, entre otros, LAI (índice de área foliar), clorofila y biomasa. En esta tesis se han utilizado datos del satélite LANSAT-TM para la inversión de LAI, y datos ENVISAT-MERIS para la estimación de LAI y clorofila. Finalmente, se ha investigado el uso de datos radar ENVISAT-ASAR para investigar su potencial en la estimación de la biomasa de los cereales.

El Capítulo 1 de la tesis presenta el contexto y los objetivos científicos de este estudio.

El Capítulo 2 presenta las bases teóricas sobre la teledetección en el óptico.

El Capítulo 3 está dedicado a la inversión de LAI en la región de Barrax, en Castilla-La Mancha, utilizando 12 imágenes LANDSAT-TM adquiridas durante la misma temporada agrícola. El LAI se ha calculado

utilizando LUTs (Look Up Tables) para invertir el modelo de transferencia radiativa SAIL acoplado al modelo de reflectividad de hoja PROSPECT. Los resultados se han validado con medidas experimentales adquiridas durante la campaña de campo de ESA, SPARC-2003, mostrando una muy buena correlación.

El Capítulo 4 propone un método para invertir a la vez LAI y clorofila a partir de datos ENVISAT-MERIS. Este método consiste en una inversión de mismo modelo PROSPECT+SAIL que se utilizó en el Capítulo 3, pero con la particularidad de que se añade una ligadura temporal. De esta forma, en vez de invertir un único valor de LAI y clorofila para cada fecha, se invierte una curva válida para todo el ciclo del cultivo. Este método intenta aprovechar al máximo la dimensión temporal de los datos. Los resultados obtenidos muestran que el método multitemporal da mejores resultados que las inversiones fecha a fecha. Sin embargo, la inversión de clorofila todavía requiere más estudio.

El Capítulo 5 introduce los conceptos relacionados con la teledetección radar que se manejan a lo largo de la segunda parte de esta tesis.

En el Capítulo 6 se ha desarrollado un método de clasificación de cultivos jerarquizado, que utiliza datos polarimétricos en banda C, del instrumento aerotransportado AIRSAR. El método se ha aplicado a imágenes en Flevoland (Paises Bajos) y se ha validado con observaciones de campo.

El Capítulo 7 se investiga el uso de los datos ENVISAT-ASAR para aplicaciones agrícolas en la región de Toulouse. En la primera parte se analizan las posibilidades para la clasificación de cultivos. Finalmente se investiga el potencial del cociente de polarizaciones HH/VV para estimar la biomasa del trigo. Se ha confirmado que hay una relación clara entre este cociente y la

biomasa del trigo, sin embargo, dicha relación depende de muchos otros factores y parece ser dependiente del lugar de estudio. Por lo tanto, los algoritmos de inversión necesitan mucho más análisis.

Las conclusiones de este estudio, así como sus perspectivas, están expuestas con mayor detalle en el Capítulo 8.

En resumen, esta tesis doctoral ilustra las aplicaciones de la teledetección en el óptico y en el radar para el estudio de zonas agrícolas. Se han utilizado cuatro instrumentos distintos, tres a bordo de satélites (LANDSAT-TM, ENVISAT-MERIS, ENVISAT-ASAR y uno aerotransportado (AIRSAR) en tres zonas de estudio europeas (Barrax, Toulouse y Flevoland), así como una serie importante de medidas de campo. Este estudio pone de manifiesto la importancia del aspecto multitemporal en los estudios agrícolas mediante teledetección.

TABLE OF CONTENTS

CHAPTER 6: C Band Polarisation data for the classification

-Adiós -dijo Ana,
reteniendo la mano de Levin y mirándole a los ojos con
una mirada que le conturbó-. Me siento muy dichosa
de que la glace soit rompue.

Leon Tolstoi, Ana Karenina

CHAPTER 1:
INTRODUCTION

1.1. Scientific context.

1.1.1. Need for an agricultural monitoring.

The economic and social importance of the agricultural sector in many regions of the world, together with the concern about world population increase, economic development and the uncertainty in the changes of production caused by climate change, made necessary the development of procedures and techniques to monitor the conditions of crops, to improve the crop field management and also to be able to make early prediction of crop production. This need for an efficient crop monitoring and management, as well as, the prediction of crop production is thus enhanced by climate change issues and by the changes in agriculture related to human activities.

Regarding human activities, the Food and Agricultural Organization of the United Nations (FAO) states that the world population will increase at a rate of 43 millions per year in the period 2045-2050 (Bruinsma, 2003). This rise of human beings in the world will be a consequence of the population growth

in developing countries (45 millions), and prognosis is that half of this accruement will occur in the sub-Saharan Africa (23 millions). In those developing countries, especially in Africa, the increase of population will aggravate even more the current world undernourished state. It is expected that industrial countries will have some reactions for increasing food production in concordance to this population growth. Thus, there is a matter of fact that it exists a general concern about increasing agricultural production.

Furthermore in the frame of what is also known as food security strategies, there is an interest in predicting problems like pest infections and drought periods than can damage the crop production. In the large arid and semiarid regions of the world droughts are frequent and they commonly cause a decrease or a total failure of crop production, important economic losses in developed countries, and famine in undeveloped countries. An increase of some of these problems is expected with climate change, mainly in the Mediterranean region, which might be one of the most vulnerable regions to global change in Europe. Climate change projections for the Mediterranean region show a reduction of agricultural areas and losses of agricultural potential during the twentieth century (Schröter et al., 2005) due to the pronounced decrease in precipitation that is predicted (Giorgi and Lionello, 2008).

The current change of alimentary habits in some important emerging countries, like India and China is increasing the demand for agricultural products. In these countries, a growing sector of the population is becoming wealthy enough to change from a mostly vegetarian diet, based on rice and other cereals, to a diet that includes more meat. Livestock needs to be fed with cereals, which increases the demand and, therefore, market prices. Furthermore, some developed countries are increasing their production of biofuels, which diminishes the quantity of crops used for human consumption. This is also helping to increase the prices of cereals. Last, but not least, the

upward trend of prices is attracting speculators to the markets. This increase of prices is causing political tensions, as happened during the spring of 2008 in countries like Haiti, where the prime minister had to resign, Cameroon, Senegal, but also Egypt or Thailand. A means for limiting price increases would be to increase production, which would need an increase of agricultural productivity. In fact, during the FAO summit of June 2008, it was stated that more investments should be done to increase agricultural productivity.

The need for an increase of production has induced important changes in the agricultural practises during the last decades. For example the use of fertilizers has been extended worldwide and genetically modified crops are used as a solution for a "sustainable" production increase (Qaim and Wilberman, 2003). There is also a concern about the impacts associated with these new agricultural practises. The expansion of agriculture needs to be done in a sustainable way as the generalized use of fertilizers or over exploitation of water resources represents environmental risks and can even have consequences for human health. The increase intensive processes like irrigation and/or the abuse of fertilizers also might produce some negative consequences on water quality and the degradation of irrigated lands for instance as a consequence of salinisation.

Finally, another noticeable change in modern agriculture is that more and more frequently crop rotations are decided by market fluctuations and policy regulations (especially in the E.U.). This introduces an additional dynamics in crop distribution, which make necessary to update crop maps with a high temporal frequency.

The other important issue that requires a system for crop monitoring is the impacts of climate change in agriculture. Studies conducted over the last decades have provided evidence about the modifications of several climatic parameters (Solomon et al., 2007). For instance, noticeable trends in surface

temperatures have been recorded during the twentieth century at the global scale (Jones and Moberg, 2003). Satellite observations using AVHRR and ATSR data confirmed an increase in global sea temperature (+0.13ºC in a decade). An increase of extreme events such as hot waves, droughts and extreme precipitation events has also been recorded in different regions (Karl and Easterling, 1999). The existing models of climate agree on the increase of global surface temperatures for the second half of the 21st century. For instance, after a doubling of the concentration of CO_2, the increase in temperature is likely to be in a range that goes from 2 to 4.5°C, with a best estimate of about 3°C. Nevertheless, although this is the general pattern predicted at the global scale, models indicate an important spatial diversity in the manifestation of the effects of climate (Räisänen, 2007).

The feedback effect of climate change on agriculture is complex. The increase in temperature and the increase in the concentration of atmospheric CO_2 could affect the plant biological processes (photosynthesis, respiration, growth, etc) (Barnes et al., 1995; Booker et al., 2005). The fertilizing effect of the atmospheric carbon could produce a general increase of the vegetation activity and production (Long et al., 2005). Nevertheless, the positive response of vegetation activity and production to climate change is only expected in areas with an adequate availability of water, on the contrary, the areas affected by an increase of temperatures and evapotranspiration together with a decrease of precipitation will suffer from a higher water stress in vegetation, which, in turn, would cause a decrease of the production (Vicente-Serrano et al., 2006). Finally, extreme events (hot waves, droughts, extreme rainfalls) have a negative effect in crop production (Vicente-Serrano, 2007). The undesirable impacts that climatic change can have in crop production show the strong requirement for the monitoring of crops at present and to be maintained in the future.

1.1.2. Crop monitoring.

In the previous section it was highlighted that the relationship between agriculture and climate and the important changes in agriculture practises during the last part of the 20th century shows that agricultural monitoring systems are necessary. To be efficient, such systems should satisfy at least the three requirements listed hereafter: they should be able to provide a map of crops timely, to survey the growth of crops and if possible to predict the yields. Below, each of these requirements is discussed in more detail.

Crop mapping.

The substantial increase of intensive agriculture together with the influence of the policy regulations and market demands leads to frequent changes in the surface meant to agriculture and in the distribution of crops within the land devoted to agriculture. Therefore, the timely identification, inventory and cartography of crops becomes necessary for estimations of crop yield. In addition to the crop production assessment, crop mapping is also useful for the management of water resources or the estimations of sequestration of carbon by the soil, among others.

Crop growth survey.

Crop growth survey consists in the monitoring during the growth period of several crop and soil parameters, which are indicators of the plant condition, together with the actual plant phenological stage. Those parameters are for example plant height, LAI (Leaf Area Index), biomass or nitrogen content. Typically, the survey of crop growth is focused in the following issues, which are in-turn interconnected:

- Phenology development: which is the succession of biological events during the plant life. The survey of phenology implies, for example, the observation of the exact moment in which certain crop organs appear (ex. wheat ears). Phenology is often simulated in terms of the sum of degree-days and crop specific characteristics, for instance vernalisation factors.

- Canopy development: it can be quantified by the measurement of the LAI, the plant biomass of the plant height. In terms of biological processes, canopy development is the result of photosynthesis, respiration and biomass allocation. The amount of energy received and the capacity of the plant to use this energy will determine the biomass production. The amount of intercepted radiation is a function of the LAI. Only a part of the intercepted radiation, denoted as fPAR, is efficiently used by the crop and will be used for biomass accumulation. The way in which biomass partitioning is performed is specific to each cultivar type. In the modelling of canopy development the high vegetative structural diversity is controlled by genetic variables that intervene in this partitioning.

- Roots growth and uptake ability: the function of plant roots is to uptake water and nutrients from the soil. This is closely related to the soil chemical and physical properties as well as the soil moisture conditions. Any lack of nutrients, especially nitrogen, or any water deficiencies would negatively impact the plant development. The shortages in mineral content or basic nutrients in the soil can be detected with periodical analysis of soil samplings and compensate with fertilization. The monitoring of moisture conditions is also necessary. Regarding biological aspects, there is a big difference between the root system of annual crops (ex. wheat, corn, potatoes…) and perennial crops (ex. vineyards).

- Water balance among the plant, the soil and the atmosphere. The water requirements of a crop in a particular moment depend on the

environmental variables (ex. air temperature), the soil conditions and the crop phenology. The processes involved in the water balance include evaporation and transpiration, both in the soil and in the plant. The list of variables that take part in the water balance, mainly describing the soil status and soil water behaviour, can be very extensive (soil albedo, drainage coefficients, etc….) but the most important is soil moisture.

- Nitrogen balance in the soil and in the plant. The content of nitrogen in the soil can change as a result of organic decompositions, fertilisation, etc. Crops absorb nitrogen through the roots system and fix it in their elements. The nitrogen content in the leaves is related to the chlorophyll content, which is easier to measure than nitrogen content.

The information obtained from the survey of the previous points through the quantification of several parameters is of great valuable for the management of fields and are the basis of the human interventions like the use of fertilizers or a particular irrigation schedule. However, the monitoring of the parameters of crops along a growing season is expensive and time consuming, and therefore, there is a need for developing remote sensing techniques that will be useful in this context.

Prediction of crop yield.

Several techniques have been used to obtain an early prediction of crop production, most of them based on previous climate conditions summarised by means of drought indices, vegetation indices obtained from remote sensing data (e.g., Mkhabela et al., 2005; Kalularme et al., 2003; Royo et al., 2003) and both of them (Vicente-Serrano et al., 2006). These methods are based on regression models between the final crop yields, the climate data and vegetation indices. Although these methods are widely used, they have the problem that predictions are site specific from local measurements and

sometimes the spatial extrapolation is difficult, as a consequence of the geographic and topographic diversity and the different crop types. To solve these problems, more complex models, based on biophysical processes, can also be used. These are likely to be more general than the statistical methods based on local regressions. A model of crop growth describes how a plant grows, that is, how the carbon is allocated in the plant. These models require daily meteorological data: incoming solar radiation, temperature and precipitation. Many models have been developed or adapted to a unique cultivar, a reduced number of them or to particular crop conditions like water stress, nitrogen stress, salinity conditions, etc. and make use of many parameters. Thus, the benefits of using a monitoring system that provides crop parameters describing canopy development, for instance LAI would be very important for model calibration, forcing, etc.

A huge diversity of crop growth models exists in the scientific literature. Some well-known models and their related 'families' are SUCROS (Simple and Universal Crop Growth Simulator) (Spitters et al., 1989), CERES (Crop Environment Resource Synthesis) (Jones and Kiriny, 1986; Ritchie et al., 1985) that was developed for cereals, CROPGRO (Hoogenboom, 1992) is a family of grain legumes models and STICS (Simulateur mulTIdisciplinaire pour les Cultures Standard) (Brisson et al., 1998) developed at the INRA, France. There are also software "packages" like DDSAT (Decision Support System for Agrotechnology Transfer) (Jones et al., 2003) and APSIM (Agricultural Production Systems sIMulator) (McCown, 1986) that integrate several of the previously cited models.

Nevertheless, despite the great usefulness of these models, there are noticeable limitations concerning its calibration. Crop parameters describing canopy development and dynamic are commonly needed for the calibration of the models. This involves time and cost consuming field samplings and very

often there is a lack of spatial representation, mainly in areas in which spatial diversity of crops, soil characteristics and climate are important.

Therefore, due to these limitations, there is a need to develop methods based on remote sensing data, which allow the monitoring of crop parameters over large areas, to improve the yield prediction.

1.2. The role of remote sensing in crop monitoring.

The monitoring of crops can be done by means of ground survey at the local scale. However, at a regional scale, remote sensing appears appropriate booth in terms of spatial and temporal coverage.

Crop mapping.

As it was said before, crop mapping is necessary in land change studies, climate change, hydrological studies and other applications like yield prediction and the efficient management of water resources, the later usually based in the estimates of evapotranspiration (Simonneaux et al., 2008). Crop maps are usually used in combination with crop growth models for yield prediction or to model for example soil carbon sequestration (Doraiswamy et al., 2007).

Because of the amount of applications, the classification of crops using remote sensing images is an important topic in remote sensing research. The advantages of using remote sensing techniques, instead of field survey, are the lower cost and the possibility of covering large areas. Another important reason is that it is easier to update the classifications, due to the possibility of repeated time frequency of the data.

The use of optical remote sensing data is well established for crop mapping and the methodologies have been proved to be quasi operational. Crop classification using optical data is often performed with data with a spatial resolution compatible with the field size: in general Landsat-TM or SPOT-HRV data at regional scale are used. Medium-resolution data (200 Km - 1Km) and coarse resolution data (> 1Km) are often considered as insufficient with regard to the size of the fields. Those data (AVHRR, MODIS, MERIS, SPOT-VGT) are mostly used for multi-year temporal surveys, and to obtain land use/land cover maps at continental or global scales (Loveland et al., 2000; Strahler et al., 1999; Bartholomé and Belward, 2005). A well-known limitation of optical data is the presence of the cloud cover that prevents the acquisition of images at the desiderate time. Radar data, in contrast, has the advantage of being independent from cloud cover and thus show a high potential for crop classification. It may also happen that vegetation needs to be monitored at a specific phenology stage. This is the case, for example, when two crops have similar behaviour during the growing season except for a specific development stage. However, satellite radar data have not often been used for this purpose, (Saich and Borgeaud, 2000; Schotten et al., 1995; Tso and Mather, 1999) mainly because, until very recently, satellites were only able to measure single linear polarisations at a single frequency: ERS-1 and ERS-2 operate at C Band at VV polarisation, RADARSAT operated at C band and HH polarisation, JERS operated at L Band, HH polarisation. Future missions will measure the complete scattering matrix at a single frequency and there is a need for developing adequate classification methods.

Several algorithms use radar data for the classification of crops. In a general way, they can be classified into knowledge-based approaches, classification by scattering mechanism and statistical data-driven methods (Oliver and Quegan, 1998). Knowledge-based approaches are based on the

analysis of the physics that determines the measured backscattering for each crop type. Those classifiers have the advantage of being more robust and easier to adapt to the specific conditions of the area to classify.

Crop condition and growth survey using remote sensing data.

Remote sensing data can be used to estimate biophysical parameters, which are indicators of the crop condition along the growing season. Multi-temporal estimations of these parameters contribute to the growth survey. Biophysical variables like LAI, fraction of photosynthetically active radiation (fPAR), biomass or nitrogen content are important because they contribute to the understanding of the crops dynamics and environmental dynamic at any spatial scale. In spite of the availability of radar data under any weather conditions, the retrieval of biophysical parameters is more frequently done using optical data, mainly because the interaction between the radar signal and the vegetation is more complex than with the optical signal and it is more difficult to establish the biophysical relationships. Generally they can only be established for one type of crop, because it has a particular structure. In addition it is complex to handle radar data compared with optical data. A large amount of papers were published on the derivation of biophysical parameters at leaf and canopy level from optical data. Many examples can also be found for LAI (Turner et al., 1999; Weiss et al. 2000; Combal et al, 2002a), Duchemin et al., 2006), fPAR, canopy water content and leaf chlorophyll content. For agricultural crops, for which temporal changes are more rapid than for instance forest surfaces, multi-temporal observations are very important. Few papers have addressed the effective inversion of multi-temporal and high-resolution satellite images for various crop types. Thus, more work needs to be done on the retrieval of biophysical parameters using multi-temporal data.

In the radar domain, multi-angular, polarimetric and interferometric data have been shown to be of interest for the retrieval of biogeophysical parameters like crop height, plant water content, LAI and biomass (Le Toan et al., 1984). Those studies were mainly conducted with the X and C Bands. It has been demonstrated that if the vegetation cover has components with specific orientations, the penetration depth, the volume scattering, and the attenuation may be different at different polarisation states (Ferrazzoli et al., 1999; Picard et al., 2003, and Mattia et al. 2003). This phenomenon was the base used to develop an algorithm to map rice fields (Le Toan et al., 1989).

As with crop mapping the retrieval of biophysical parameters using radar satellite data have been limited by type of data. The ASAR sensor onboard ENVISAT allowed, for the first time, to measure two simultaneous polarisations HH/VV, HH/HV and VV/HV at different non-simultaneous incidence angles in Band-C. This motivated studies on the use of polarimetry for biomass retrieval of wheat (Mattia et al., 2003). This work studies the potential of polarized radar data in the derivation of biomass for small grain cereals using ENVISAT-ASAR data.

The role of Remote Sensing in combination with crop growth models for crop yield prediction.

It is difficult for the models to account for the spatial heterogeneity in vegetation and soil conditions as well as the inherent difficulties of phenology modelling. Crop growth depends on many factors (weather, species, soil status, soil characteristics and management strategies) and, as a result, models need many parameters. For instance STICS v3.0 depends on 132 parameters (Ruget et al., 2002). It is frequent that some of these parameters, like the sowing date, are unknown, or need to be adjusted for each crop type or geographical location. One solution consists in calibrating the models using measurements

of biophysical parameters (e.g. Brisson et al., 1998; Spitters et al., 1989; Bondeau et al., 1999; Launay and Guerif; 2005). LAI, which accounts for the leaf surface intercepting in-coming radiation, and biomass are key variables to calibrate crop growth models.

The calibration can be done with in-situ measurement of biophysical parameters. However, in-situ measurements are expensive and time consuming and generally can only be done at a limited number of fields. Thus, calibration has the risk of becoming site and cultivar-specific. In this context satellite remote sensing is useful when integrated in the models of crop growth as it provides spatial information on actual vegetation status. Remote sensing can be used to estimate key variables in the models: LAI, aboveground biomass and other crop characteristics like chlorophyll or nitrogen content. This information can be integrated in the calibration process using for example forcing methodologies (Clevers and van Leeuwen, 1996; Moulin et al., 1998).

1.3. Objectives of this study.

The general objective of this thesis is the assessment and development of methods based on remote sensing data, which are useful to the monitoring of crops, and can contribute, when combined with other methods, to improve yield prediction. The thesis focuses on two main topics: the classification of crop types and the retrieval of vegetation parameters. Furthermore, a relevant aspect addressed in this thesis is the benefits of using multi-temporal data. To achieve the goals of this study it has been necessary to deal with the complexity of using many different instruments, data types, test sites and ground measurements.

This study is based on two types of remote sensing data: optical and radar. The satellite optical instruments that are used are LANDSAT-TM and ENVISAT-MERIS. The radar data come from the satellite instrument, ENVISAT-ASAR, as well as from an airborne sensor, JPL-AIRSAR. More details about these sensors and satellites are commented in the following chapters.

For agricultural applications, the use of both optical and radar data is needed to overcome the limitations that each type of data have on their own. For example, although there are operational methods for the classification of crops using optical data, these methods cannot be applied in regions with a frequent presence of clouds. In this sense, this study is a demonstration of the complementarities of both types of data in crop studies. Optical data are used to perform a multi-temporal LAI monitoring, and to retrieve LAI & Chlorophyll. Forthcoming and recent satellite radar data are used for crop mapping. Finally, the retrieval of biomass using radar data is also investigated.

Concerning the retrieval of biophysical parameters, the objectives of this study are three:

- The derivation of seasonal LAI variations from LANDSAT images the different crops in an agricultural area.
- The development of multi-temporal method for the inversion of LAI & Chlorophyll using MERIS-FR data.
- To investigate the crop monitoring of small grain cereals with ASAR-APP data and the possibilities of biomass retrieval of small grain cereals.

Regarding crop mapping the objective in this thesis is the development of a hierarchical classification method and its validation. In view of applications to present and future satellite data fully polarimetric C-Band

AIRSAR data are used. The potential of ENVISAT-ASAR data is also investigated in the last part of this work.

This study has been developed in three agricultural areas in Europe:

- Barrax in Castilla-La Mancha, Spain. **Chapter 3** describes more in detail the region as well as the ground measurements acquired during the ESA/SPARC-2003 campaign.
- Flevoland, North of The Netherlands. More details are given in **Chapter 6**.
- Toulouse, South of France. The description of the experiment developed in a wheat field for the collection of wheat biomass and other measurements is done in **Chapter 7**.

1.4 Organisation of the thesis report.

The present thesis has been organised in two parts: optical and radar. The thesis will provide background information needed for the understanding of the remote sensing signal with respect to the agricultural crops. **Chapter 1** is a general introduction.

Part I presents the results obtained from the optical data in the area of Barrax.

- **Chapter 2** gives the physical basis of the optical remote sensing. A description of the models used for the inversion of optical data is presented, as well as a review of existing algorithms for LAI, Chlorophyll and biomass retrieval is presented. The atmospheric correction method that was applied to the optical data is also described.

- **Chapter 3** focus on the retrieval of LAI using LANDSAT-TM data. The study was conducted in the region of Barrax. LAI was inverted using images at twelve dates during year 2003 and validated with ground measurements from the ESA/SPARC-2003 campaign.

- **Chapter 4** gives results on the retrieval of LAI & Chlorophyll with MERIS-FR from multi-temporal inversion. The study was also in the region of Barrax.

Part II refers to the work done using radar data. The three study areas are involved. **Chapters 5** to **7** are organised as follows:

- **Chapter 5** gives the theoretical context or radar remote sensing necessary for **Chapters 6** and **7**.

- **Chapter 6** reports the performance of a hierarchical crop classification method, based on C-Band polarimetric measurements from synthetic aperture radar. AirSAR data collected on the Flevoland site in the frame of the ESA MAC-Europe campaign, and the European RAdar-Optical Research Assemblage (ERA-ORA) library (http://eraora.disp.uniroma2.it/) were used. The results obtained in classifying 5 types of crops and a soil class were validated with a ground truth map of the site. Some of the algorithm rules were also tested in the region of Barrax.

- **Chapter 7** deals with the applications of ASAR-APP data in crop classification, and the retrieval of biomass for small grain cereals using ENVISAT ASAR data, in the Toulouse region. The field campaing that was conducted in Toulouse to measure the biophysical parameters of a wheat field is presented. Results on the use of ASAR-APP data in Barrax for crop classification are also shown. Finally, the processing applied to ENVISAT-ASAR data is also described in that chapter.

- **Chapter 8** contains the general conclusions and perspectives of this work.

¿Dónde está mi ciencia? He sido un testarudo,
he perseguido un simulacro de orden, cuando debía saber
muy bien que no existe orden en el universo.
-Pero, sin embargo, imaginando órdenes falsos
habéis encontrado algo...

Umberto Eco, El Nombre de la Rosa

CHAPTER 2:
BIOPHYSICAL PARAMETERS AND OPTICAL DATA

Prior to the assessment of optical remote sensing methods, this chapter gives a brief introduction to the conceptual basis of optical remote sensing. Those are presented as the background relevant to the thesis, with the aim of understanding the relationships between the signal measured by the optical sensors and the vegetation properties. First, a general scheme of the remote sensing problem is outlined. The effect of the atmosphere on the sun radiation is explained and the atmospheric correction method that has been applied to the data is presented. The models that have been used in this work to describe the interaction of solar radiation with the vegetation canopy are also presented. The chapter ends with a review of bibliography concerning the derivation of biophysical parameters, LAI and Leaf Chorophyll Content using optical data.

2.1. Physical definitions.

In this section the definition of some physical magnitudes used in radiometry are given. They will be used along this work.

Flux, (W):	Φ	Energy coming from or arriving to a surface per unit of time. It is also called power.
Intensity, ($W \cdot sr^{-1}$):	I	Flux per unit of solid angle.
Irradiance, ($W \cdot m^{-2}$):	E	The incident flux on a surface.
Radiance, ($W \cdot sr^{-1} \cdot m^{-2}$):	L	Flux per unit solid angle per unit projected source area. $$L = \frac{d^2\phi}{dA d\Omega \cos\theta}$$ [Eq. 2.1]
Spectral radiance, ($W \cdot sr^{-1} \cdot m^{-2} \cdot \mu m^{-1}$):	L_λ	It is the radiance at a single wavelength. The radiance is the integral of all spectral radiances from a surface.
Reflectance,(unit-less):	ρ	The reflectance is the ratio between the incident flux (irradiance) and the reflected flux (reflected irradiance) from a surface. It is a unit-less quantity. $$\rho = \frac{E_{(reflected)}}{E_{(incident)}}$$ [Eq. 2.2]

BRDF, (sr^{-1}):	$f_r(\vec{\Omega}_r,\vec{\Omega}_i)$	The bidirectional reflectance distribution function (BRDF) is the ratio of reflected radiance coming from a surface in a particular direction $\vec{\Omega}_r$ to the irradiance incident on the surface from direction $\vec{\Omega}_i$. It is dimensionless.
Spectral BRDF , ($sr^{-1}nm^{-1}$):	$f_r(\lambda;\vec{\Omega}_i,\vec{\Omega}_r)$	The spectral BRDF describes the BRDF as a function of wavelength.

For a much more complete summary of radiation related magnitudes see, the classical reference Nicodemus (1977).

2.2. Optical remote sensing system.

The elements involved in the observation of vegetation using an optical remote sensing system are outlined in **Figure 2.1**. Basically, the system is composed of the following elements: the sun, the atmosphere, the observed surface and the satellite sensor. The solar radiation is transmitted through the atmosphere before interacting with the surface. Part of the solar radiation that

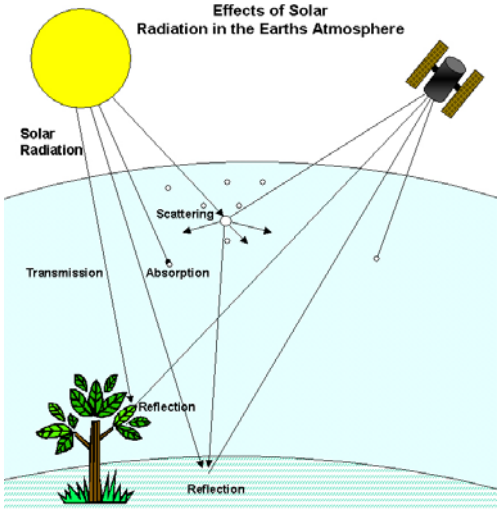

Figure 2.1. Basic scheme of the remote sensing system.
(Source : http://landsat.usgs.gov/)

reaches the surface is reflected and transmitted back through the atmosphere towards the sensor.

The sun is the source of energy of the system. The sun radiation on top of the atmosphere is close to the radiation emitted by a black body with a surface temperature of around 5900 K (see, **Figure 2.2**). The sun radiation on top of the atmosphere is well characterised. It is strongly directional and in the remote sensing problem it is considered as a punctual source of energy placed in the infinite. Thus, the geometry of the sun is defined with the sun zenith and azimuth angles.

Before reaching the surface, the sun radiation crosses the atmosphere, in which absorption and dispersion processes occur. The absorptions produced by the atmospheric gases are well known (see **Figure 2.3**). The main spectral regions for which atmospheric absorption is small are called the atmospheric windows. The part of the radiation that is absorbed will be re-emitted in another wavelength range. The constituents of the atmosphere also diffuse part of the solar radiation in all directions. The angular distribution of atmospheric radiance is difficult to be described; it depends on the particles size, quantity and shape, and can be very variable spatially.

The sunlight reaching the surface can be reflected or absorbed. There are two types of reflection: diffuse and specular. In remote sensing, specular reflection of sunlight is not frequently observed, it may occur for instance on a free water surface. Most of the natural surfaces show diffuse reflection. In diffuse reflection, the returning reflection of the directional incoming radiation flux is scattered in many directions. Diffuse reflectance is often characterised by means of the bidirectional reflectance distribution function (BRDF). A particular case of diffuse reflection is that of a Lambertian surface. The intensity of light scattered from a point on a reflecting lambertian surface follows a cosine relationship:

$$I(\theta_s) \propto I_0 \cos\theta_s \qquad \text{[Eq. 2.3]}$$

where I_0 is the incident light intensity and $\theta_s$is the angle of the scattered light. In lambertian surfaces, no dependence on azimuthal angle of the incident or scattered light is assumed. The lambertian case is the ideal case corresponding to a rough surface, in which many random reflections occur before the light leaves the surface.

Finally, the reflected light reaches the remote sensing sensor. In the solar domain there are many sensors having different spatial and temporal resolutions as well as a different spectral bands configuration.

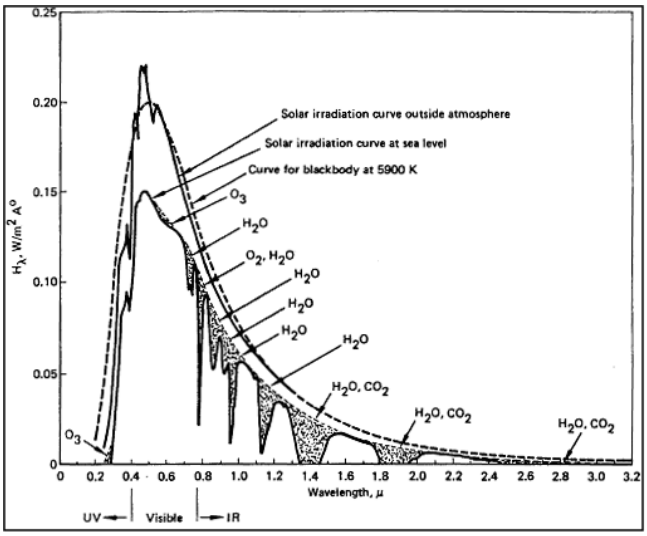

Figure 2.2. Solar irradiance curve on top of the atmosphere, at see level and blackbody emission. The principal atmospheric gases absorptions are also indicated. Source: http://msis.jsc.nasa.gov/.

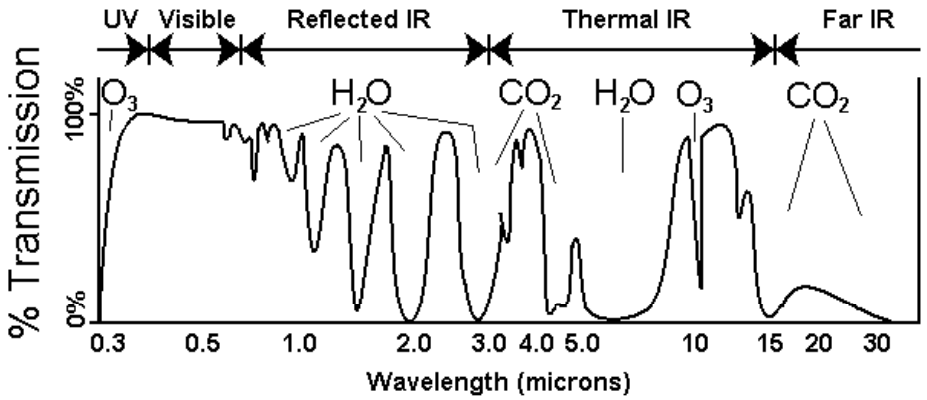

Figure 2.3. Atmosphere transmission. The spectral regions with a high transmission are the so-called atmospheric windows. The principal atmospheric gases absorptions are also indicated. Source: http://tncweeds.ucdavis.edu/.

2.3. Satellite and sensors characteristics.

As explained in **Chapter 1**, in this work we make use of LANDSAT-TM and ENVISAT-MERIS sensors. The basic characteristics of these instruments are resumed below.

LANDSAT/TM:

The NASA Landsat program (http://landsat.gsfc.nasa.gov/) has been providing earth observation data for more than 30 years. The first satellite of the family (Landsat-1) was launch in 1972 ant the most recent (Landsat-7) in 1999. Up to day there are two Landsat satellites operational: Landsat-5 (only TM instrument) and Landsat-7 (although in 2003 there was a failure of the Scan Line Corrector, SLC). The continuation of the program will be the Landsat Data Continuity Mission (LDCM).

Landsat-5 and Landsat-7 Orbital characteristics:

Orbit: Polar, sun-synchronous

Altitude: 705 Km

Repeat coverage: 16 days

Instruments:

Landsat-5: Thematic Mapper (TM), Multispectral Scanner (MSS)

Landsat-7: Enhanced Thematic Mapper Plus (ETM+)

Scene size:

Landsat-5 : 185km x172km

Landsat-7 : 183km x170km

The spectral bands and Instantaneous Field Of View (IFOV) of TM and ETM+ sensors are detailed in **Tables 2.1** and **2.2**.

Band Number	µm	Resolution (m)
1	0.45-0.52	30
2	0.52-0.60	30
3	0.63-0.69	30
4	0.76-0.90	30
5	1.55-1.75	30
6	10.4-12.5	120
7	2.08-2.35	30

Table 2.1. TM Bands. Band 5 is for termal infrared radiation, acquired at night.

Band Number	µm	Resolution (m)
1	0.45-0.515	30 m
2	0.525-0.605	30 m
3	0.63-0.69	30 m
4	0.75-0.90	30 m
5	1.55-1.75	30 m
6	10.4-12.5	60 m
7	2.09-2.35	30 m
8	0.52-0.9	15 m

Table 2.2. ETM+ Bands. New features on Landsat 7 are a panchromatic band with 15 m spatial resolution.

ENVISAT/MERIS:

ENVISAT satellite was launched in March 2002.

ENVISAT Orbital characteristics:

Source: http://www.esa.int/esaEO/SEMWYN2VQUD_index_0_m.html.

Orbit:	Sun synchronous
Mean Altitude:	800 km
Repeat cycle:	35 days.

Instruments:

ASAR	Advanced Synthetic Aperture Radar. C Band
GOMOS	Global Ozone Monitoring by Occultation of Stars
LRR	Laser Retroreflector (Passive array of corner cubes for satellite ranging)
MIPAS	Michelson Interferomter for Passive Atmospheric Sounding (measures stratospheric chemistry and cimatology)
MERIS	MEdium Resolution Imaging Spectrometer Instrument
MWR	Microwave Radiometer (measure the integrated atmospheric water vapour column and cloud liquid water content, as correction terms for the radar altimeter signal).
RA-2	Radar Altimeter.
AATSR	Advanced Along Track Scanning Radiometer. (Measures surface temperatures).
DORIS	Doppler Orbitography and Radioposition Integrated by Satellite. (Trackig ystem to provides orbit accuracy on order of centimeters).

SCIAMACHY SCanning IMaging Absorption SpectoMeter for Atmospheric CHartographY (measures traces gases in atmosphere).

In depth information can be found at ESA, 2006 http://envisat.esa.int/instruments/.

MERIS is a 68.5º field-of-view pushbroom imaging spectrometer that measures the solar radiation reflected by the Earth, in 15 spectral bands, in the visible and near infra-red. The bands are progamable in position, width and gain, but expect for particular experiments, the instrument is set to the bands shown in **Table 2.3**. In Full Resolution mode (FR), MERIS has an spatial resolution of 300 m, and in Reduced Resolution (RR) of 1200 m. MERIS allows global coverage of the Earth in 3 days. MERIS was designed for measuring ocean color.

Band Number	Band center (μm)	Bandwith (nm)
1	412.5	10
2	442.5	10
3	490	10
4	510	10
5	560	10
6	620	10
7	665	10
8	681.25	7.5
9	708.75	10
10	753.75	7.5
11	760.625	3.75
12	778.75	15
13	865	20
14	885	10
15	900	10

Table 2.3. MERIS spectral bands characteristics. (Source: : http://earth.esa.int/envisat/instruments/meris/descr/concept.html).

2.4. The atmospheric effect and its correction.

In the optical region of the electromagnetic spectrum, the constituents of the atmosphere affect both the downward radiation, coming from the sun, and the upward radiation reflected on the soil. A classical reference describing the atmospheric effect and its correction is Kaufman (1989). Atmospheric gases, aerosols and clouds absorb incoming radiation and scattered radiation, not coming from the observed target, into the sensor field of view. The surroundings of a target can contaminate the measured signal, as atmospheric diffuse radiation arrives to the sensor field of view. This phenomenon is known as adjacency effect or 'blurring' effect. As a consequence of adjacency, images losses part of its contrast: dark surfaces will appear brighter because photons from the surroundings arrive to the sensor field of view, while bright areas will appear darker as the photons that are diffuse out of the sensor field of view are not compensate by those coming from the surroundings. Adjacency effects are second order effects that depend on the target size, its homogeneity and its surroundings. The atmosphere turbidity and the surface heterogeneity will control the magnitude of this phenomenon. Effects are more important in homogeneous than in heterogeneous areas and in atmospheres with high aerosols concentration than in clear atmospheres. The spatial distance in which adjacency effects are important is considered to be about 1 km (Richter, 1997). At the spatial resolutions of sensors like MODIS (1Km pixel size) or MERIS Reduced Resolution (1.2 Km) adjacency can be neglected. At middle spatial resolutions like MERIS-FR (300m pixel size) adjacency may still have some impact. The effect will be more important at the high spatial resolution of Landsat or SPOT. Adjacency is generally modelled by means of spatial filters, for instance circulars spatial convolution filters (Tanré et al. 1981, Verhoef and Bach, 2003).

3-D radiative transfer modelling would be necessary for an accurate treatment of this phenomenon.

In respect to clouds the usual procedure consists on using a cloud detection method for masking all those pixels in the image affected by clouds. The main difficult is the detection of sub-pixel clouds.

The absorptions produced by gases depend on their molecular structure. They are very well characterised and their behaviour is invariant. Among all the gases in the atmosphere, the only one with an important spatial and temporal variation is water vapour.

Molecular scattering is described by Rayleigh theory. In this theory the contribution of the molecules to the optical path is described with an optical thickness τ that depends on λ^{-4}. The difficulties in the atmospheric correction come from aerosols and clouds, as both are variable in time. The effects of aerosols can be very different depending on the origin of the aerosol, its physical properties (size, shape and concentration) and its chemical composition. This high variability makes the quantification of aerosols effects difficult. A usual approach to simplify the description of aerosols is their classification into models (for instance, maritime, urban, rural or continental models). The Mie theory describes, for the case of homogeneous and spherical particles, the optical properties of an aerosol as a function of its physical properties. In a more general way the attenuation of the radiation produced by aerosols is characterized with the aerosols optical thickness (AOT). The physical properties of aerosols, such as the size distribution or concentration, can be inferred from the wavelength dependence on the aerosol optical thickness (Estelles et al., 2006).

There are several methods that have been adopted for atmospheric correction of remote sensing data. Some of them are empirical and consist in finding a linear relationship between ground measured spectra and the

corresponding spectra in the images. More accurate methods make use of radiative transfer theory to calculate the contribution of the atmosphere in a particular condition, and afterwards, invert the measured radiances to obtain surface reflectance. For computing this contribution it is necessary to characterise the atmosphere status at the image acquisition time (knowing the atmosphere parameters). The most frequently used radiative transfer atmospheric models for remote sensing atmospheric corrections are the MODTRAN code (Berk et al., 1999) and the Second Simulation of the Satellite Signal in the Solar Spectrum 6S code (Vermote et al., 1997).

Related to the atmospheric correction is the correction of topographic effects. The topographic correction is also known as "illumination correction". It consists on using a Digital Elevation Model from which the elevation of a pixel and the surrounding slopes can be obtained. This allows calculating the deviations between the astronomical solar zenith angle and the actual zenith angle for a given pixel. Illumination effects can be as important as atmospheric effects.

Many surfaces show anisotropic reflectance behaviour for off nadir viewing geometries. The way in which a surface reflects incident radiation in a particular direction is described by its bidirectional reflectance distribution function (BRDF). BRDF effects can be important for sensors with a large range of view angles. In general, for atmospheric corrections, it is sufficient to assume Lambertian (isotropic) behaviour.

The MERIS-FR Level 1b images used in this work have been atmospherically corrected using the method of L. Guanter specifically developed for hyperspectral/multispectral (Guanter et al., 2007) remote sensing data. This algorithm obtains the atmospheric parameters needed for the correction from the image itself and has been implemented using IDL (Interactive Data Language). The method has been validated using ground-

based measurements from the SPARC campaigns and also compared with aerosols and water vapour measurements from the Aerosol Robotic NETwork (AERONET) (Holben et al., 1998). It has also been applied to the atmospheric correction of the Compact High Resolution Imaging Spectrometer (CHRIS) data (Guanter et al., 2005).

The atmospheric correction methodology of Guanter involves the following phases:

a) Cloud masking. The method can use both the cloud mask algorithm implemented in the Basic ERS&ENVISAT (A)ATSR MERIS (BEAM) Toolbox (Fomferra and Brockmann, 2005) and a cloud detection method based on image thresholds. Cloud masking is important to avoid cloudy pixels being involved in the retrieval of AOT.
b) Retrieval of atmospheric parameters.
   - b1. AOT retrieval. For the derivation of the AOT, the atmosphere is considered invariant across 30 × 30 km windows, while the surface reflectance is allowed to vary from pixel to pixel, and it is assumed to be represented as a linear combination of two vegetation and soil end-members. An inversion of the top of atmosphere (TOA) radiances in 5 reference pixels is performed to obtain the aerosol optical thickness (AOT), and the proportions of vegetation and soil in the 5 pixels. For the inversion, TOA synthetic data are generated using MODTRAN-4 code. As MERIS data do not have enough information to estimate the aerosols model over land, the aerosol model is set to the standard rural model. A mid-latitude summer atmospheric profile and a lambertian

surface behaviour are assumed. MERIS bands 11 and 15 are not used in this inversion because they are affected by strong absorptions (water vapour and ozone) and might be sources of errors in the AOT retrieval.

- b2. Water vapour retrieval. It is based on the inversion of the ratio of MERIS bands 14 and 15.

For the topographic corrections the method uses the Global Earth Topography And Sea Surface Elevation at 30 arc second resolution (GETASSE30) Digital Elevation Model (DEM) that is included in the BEAM Toolbox.

c) Surface reflectance derivation. The estimated atmospheric component concentrations from the previous step are used to convert the measured TOA radiance to surface reflectance. Bands 11 and 15 are interpolated or extrapolated from the nearest bands. Finally adjacency effects correction is done with the simple approach of Vermote et al, 1997.

d) Geometrical correction. This is an optional step performed after the atmospheric correction. The geometrical correction makes use of the BEAM orthorectification algorithm.

Landsat images have been corrected using a simplification of the method previously described (steps b) and c)). Water vapour is inverted at the same time that AOT.

The MERIS instrument is a CCD camera. The spectral measurements of each pixel along an image line are made by a different set of CCD sensors. This causes small variations of the spectral wavelength of each pixel along the image, the so-called "smile effect". MERIS Level 2 data are smile corrected in

the ESA processing chain, but this is not the case for Level 1b data. Smiling correction can affect bands with strong gases absorptions (MERIS bands 11 and 15) but it is not critical for other bands. An algorithm for the smile correction algorithm can be found in D'Alba and Colagrande (2005). In this work, we have not performed any smiling correction of our images.

For the inversion of vegetation parameters from vegetation surface reflectances an atmospheric correction is necessary. The accuracy of this correction may have an impact in the quality of the retrieved biophysical parameters, mainly because a good atmospheric correction can remove part of the temporal noisy.

2.5. Vegetation reflectance and biophysical parameters.

2.5.1. Leaf optical properties.

Leaves are the elements of a plant where light is collected for making the photosynthesis, the chemical reaction in which CO_2 and water are transformed into sugar and used by the plant to live on. Optical remote sensing provides non-destructive methods to obtain information on the photosynthetic characteristics of a plant, its biochemical constituents and plant status, which are needed to support the modelling of photosynthesis and crop growth monitoring. Those methods are based on the optical properties of the vegetation. When light interacts with a leaf, different mechanisms of reflection, absorption and scattering happen. These will determine the optical properties of the leaf: reflectance, transmittance and absorption. Part of the absorbed light can be re-emitted at longer wavelengths by fluorescence. The different leaf biochemical constituents carry out absorption. Absorption can be due to

electron transitions in the pigment molecules or to changes in the vibration and rotational states of the molecules as in the case of water. Scattering depends on the internal structure of the leaf. **Figure 2.4** shows schematically the internal structure of a leaf. The different elements that can be found are: cuticle (serves to prevent water looses), epidermis (layer of plate cells), mesophyll (contains the chloroplast and other photosynthetic cells), stoma (permit the exchange of water and carbon dioxide between the leaf and the atmosphere), guar cells (control the opening of the stoma), and vascular bundle (in which xylem serves to transport water and minerals from the roots and phloem transport the photosynthesis product). This structure varies for different species (see **Figure 2.5**).

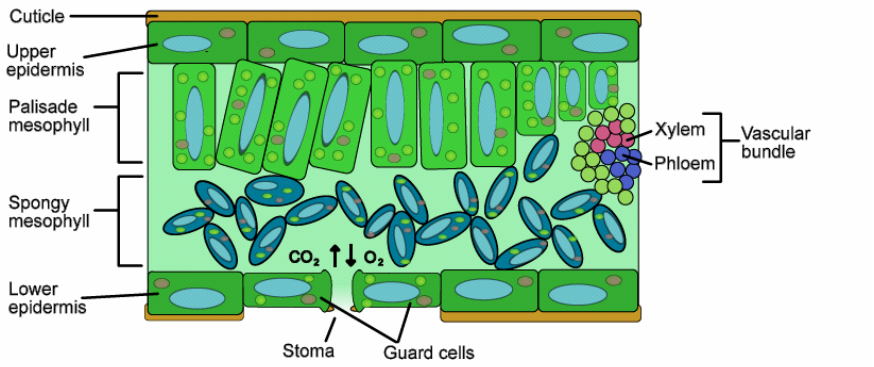

Figure 2.4. Scheme of the Leaf internal structure. Source wikipedia (copyright free).

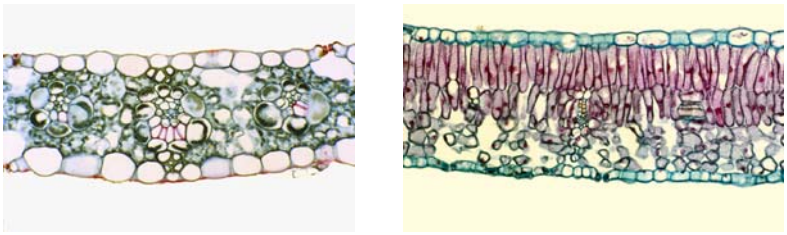

Figure 2.5. a) Zea leaf cross section b) Lilac leaf cross section. Images from: http://www3.baylor.edu/~Darrell_Vodopich/Botany%20Book%20Photos/

The reflectance and transmittance of a fresh leaf and a dry leaf are shown in **Figure 2.6**. The reflectance of a fresh green leaf is characterized by a strong absorption of the chlorophyll in the visible region, centered on 650 nm, a plateau of high reflectance in the near-infrared, around 850 nm, and water absorptions in the middle infrared region at 1450 nm and at 1950 nm. The transition from the strong chlorophyll absorption in the visible to the high reflectance in the near-infrared is known as red-edge. These spectral characteristics of the leaf are maintained at canopy level. The red-edge feature is the most important characteristic of vegetation, and it is the basis of many vegetation indexes. The point of maximum slope in the leaf reflectance, the inflexion point of the red-edge feature, occurs at wavelengths between 690 and 740 nm. The red-edge position and the red-edge slope have been shown to be correlated to chlorophyll concentration (Curran et al., 1990; Gitelson et al., 1997). When the leaf dries (see **Figure 2.6b**), it losses chlorophyll and the absorptions due to other leaf constituents such as lignin can be observed. A dry leaf absorbs much less radiation than a fresh leaf. **Table 2.4** resumes the most important spectral features in leaves.

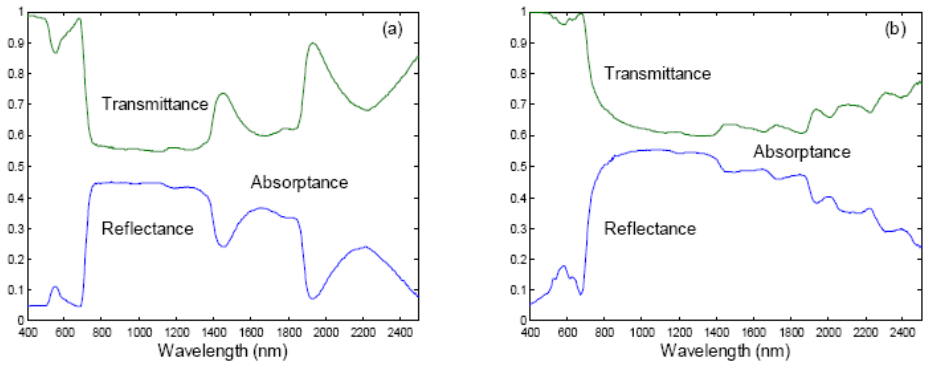

Figure 2.6. Reflectance and transmittance of a fresh and a dry leaf. From Jacquemoud et al., 2001.

Waveband	Waveband width (nm)	Characteristics
Ultraviolest/blue	350-500	Strong chlorophyll and carotene absorption
Green	500-600	Reduced level of pigment absorption
Red	600-700	Strong chlorophyll absorption
Red edge	700-740	Transition between strong absorption and strong reflectance
Near-infrared	740-1300	High vegetation reflectance
Middle-infrared	1300-2500	Water, cellulose and lignin absorption

Table 2.4. Characteristic spectral features of foliar biochemicals. (Table from Curran and Dash, 2005, MERIS ATBD: Chlorophyll Index).

In the visible electromagnetic region of the spectrum there are 4 types of pigments that absorb part of the incident radiation:

- Chlorophyll: this is the pigment that makes leaves look green, and it is fundamental for the photosynthesis. There are several types of chlorophyll, where chlorophyll a and chlorophyll b are the most important in leaves. Chlorophyll absorbs radiation in the range from 550-700 nm.
- Carotenoids: they give leaves the yellow or orange colours. They are always present in the leaf but only become visible when chlorophyll disappears. They absorb radiation in the region between 400-500 nm.
- Anthocyanins: they give leaves a red colour. They are not always present in the leaf. Xantophyll is an example of anthocyanin. They absorb radiation in the region from 530-620 nm. They protect the leaf from an excess of light.
- Tannins: they give leaves a brown colour. They are always present in the leaf but become visible when chlorophyll and carotenoids are not dominant. Tannins absorb radiation also in the infrared.

In the mid-infrared electromagnetic spectrum region absorbers are water, lignin, cellulose, proteins, sugar, etc. A complete list of the absorption features of foliar biochemical constituents can be found in Curran (1989).

2.5.2. Leaf models.

There are several models in the literature that describe the reflectance and transmittance of the leaf. Among them, the simplest models are the so-called plate models. They describe the leaf as a stack of several layers characterised by the refraction index and the absorption coefficient. Nowadays, the most commonly plate model used is the PROSPECT model (Jacquemoud and Baret 1990), in which the leaf absorption coefficient is expressed in terms of the leaf biochemical constituents. Another well known model, also on the basis of biochemistry, is LIBERTY (Leaf Incorporating Biochemistry Exhibiting Reflectance and Transmittance Yields) by Dawson et al., (1998) and LEAFMOD (Leaf Experimental Absorptivity Feasibility MODdel) by Ganapol et al., (1999). The particularity of LIBERTY is that it has been developed for needle-shaped leaves, and thus can be used for forestry applications. The advantage of those simple radiative transfer leaf models is that they are invertible.

Other theoretical approaches are ray tracing models such as RAYTRAN (Govaerts et al. 1996; Govaerts & Verstraete, 1998), or stochastic models like SLOP (Maier et al., 1999).

2.5.3. The PROSPECT model.

The PROSPECT model has been used to simulate the optical properties of the leaf. In this study, we used the '4 inputs' version, PROSPECT v. 3.01 (5 May 1998), which is available from http://teledetection.ipgp.jussieu.fr/opticleaf/models.htm. This version has been widely used in the literature: for instance Jacquemoud and Baret, 1990; Haboudane et al., 2004. The model was calibrated with the LOPEX dataset (Hosgood et al., 1995; Jacquemoud, et al., 1996).

PROSPECT simulates the reflectance and transmittance of a leaf in the region from 400 to 2500 nm. The model assumes that the leaf is a stack of N elementary layers separated by N-1 air spaces, and that the biochemical components are mixed homogeneously in the leaf. The absorption coefficient of the leaf $k(\lambda)$ is then given by the following equation:

$$k(\lambda) = k_0(\lambda) + \sum_i \frac{C_i k_i(\lambda)}{N} \qquad \text{[Eq. 2.4]}$$

where, N is the structural mesophyll parameter, λ is the wavelength, C_i the concentration of the constituent, k_i the specific absorption coefficient of the constituent and k_0 the absorption of an albino leaf under 500 nm (see **Figure 2.7**). The specific absorption coefficient of each constituent can be determined through calibration. The first studies that used PROSPECT proposed a relation between the N parameter and the SLW (specific leaf weight), but this relation was later discarded.

Inputs to the PROSPECT model are Leaf Chlorophyll Content (CC), Leaf Water Content (CW), Leaf Dry Matter Content (DM) and the Leaf Structural Parameter, N (see **Table 2.5**).

PROSPECT Inputs
Leaf Chlorophyll Content (CC)
Leaf Water Content (CW)
Leaf Dry Matter Content (DM)
Leaf Structural Parameter (N)

Table 2.5. Inputs to the PROSPECT model.

There is also a 5 inputs version of PROSPECT that includes the so-called brown pigments or senescent pigments concentration (Demarez et al., 1999 and Zhang et al., 2005). However this version of the model has not benefit from an extensive calibration.

The different pigments on a leaf have absorption coefficients, which are superposed. This makes the determination of the absorption coefficients difficult, and it is the origin of the existence of several versions of the model. Between distinct versions of PROSPECT the absorption coefficients may differ (see **Figure 2.7b** and **2.8**). The main difference between them is related to the dry matter in the NIR (see **Figure 2.9**).

Le Maire et al., (2004), found inaccuracies in the PROSPECT specific absorption coefficients. The work by Jackquemoud further analyzed these issues and proposed a new calibration of PROSPECT, which was recently published (Jacquemoud, 2008).

The assumptions made by the PROSPECT model can be summarized as follows:

- The internal structure of the leaf is simplified to a stack of plate layers, controlled by the parameter N that can change between species or leaf status.

- Later versions of the model only consider three biochemical absorbers: chlorophyll, water and dry matter. The specific absorption coefficients of these absorbers have been obtained from calibration.

- No distinction between adaxial side (upper side) and abaxial side (underside) of the leaf.

During this thesis work, some numerical inconsistencies were found in the model: erroneous values for the reflectances for some wavelengths are obtained when inputs have very high CW content and DM content. However, those values of CW and DM are not found in nature so this does not represent a problem for our posterior analysis.

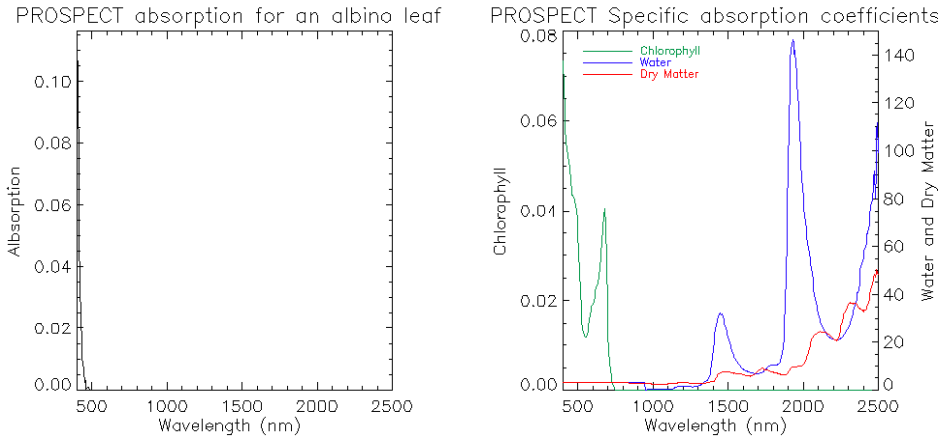

Figure 2.7. Absorption coefficients in the PROSPECT model of 4 inputs.

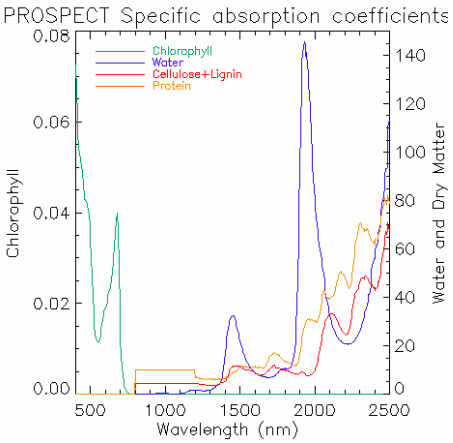

Figure 2.8. Absorption coefficients in the PROSPECT model of 5 inputs.

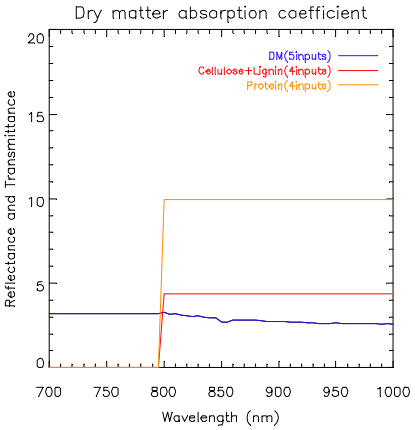

Figure 2.9. Zoom on the dry matter in the near infrared region for two versions of PROSPECT.

Effect on the reflectance of the PROSPECT model variables.

The effect of each one of the PROSPECT variables on the reflectance and transmittance of leaves is shown in **Figure 2.10**. Similarly, **Figure 2.11** displays the effect on the absorption. The N parameter has no impact in the absorption but it controls the level of reflectance and transmittance. Absorption in the visible depends in a non-linear way on the chlorophyll concentration. Absorption in the near infrared is only controlled by the DM content, and for wavelengths >900 nm. DM content and CW content have an effect in the absorption. Absorption due to water is highly non linear. At canopy level is the absorption which plays an important role.

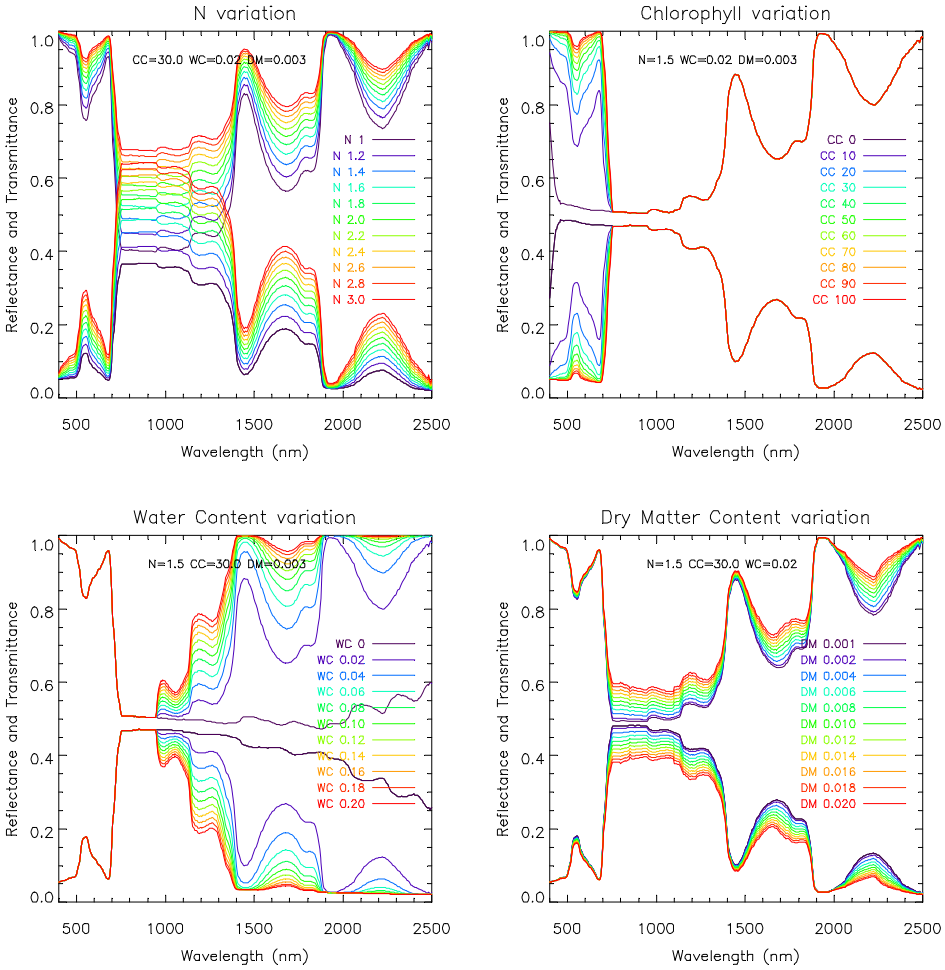

Figure 2.10. Reflectance and transmittance as a function of the PROSPECT variables: N (top left), Chlorophyll Concentration (top right), Water Content (bottom left) and Dry Matter Content (bottom right).

2.5.4. The SAIL model for canopy reflectance.

Radiative Transfer theory:

The interaction of electromagnetic radiation with a medium follows Maxwell's equations. When the medium is complex in terms of its structure, as it is for instance vegetation, Maxwell's equations are too complicated to be solved analytically and different approximations are needed. An alternative to study this electromagnetic problem is the Radiative Transfer (RT) theory. Radiative Tranfer is based on the principle of conservation of energy and describes how the energy propagates through a medium. RT was developed by astrophysicist at the beginning of 20th century but has applications in many different fields ranging from atmospheric sciences to nuclear physics.

The RT equation results from establishing the energy balance in an elementary element of length ds which can absorb, emit and scatter radiation. The equation shows the variation in the intensity I per unit of solid angle Ω (then $Wm^{-2}sr^{-1}$) of an electromagnetic wavelength in the point $\vec{r}$ along the direction $\vec{s}$. The integro-differential equation of the RT is thus:

$$\frac{dI(\vec{r},\vec{s})}{ds} = -\kappa_e I(\vec{r},\vec{s}) + \int \psi(\vec{s},\vec{i}) I(\vec{r},\vec{s}) \sin\theta d\theta d\phi + J_e(\vec{s}) \qquad \text{[Eq. 2.5]}$$

The first term represents the energy losses by absorption and scattering in the medium. Those losses are determined by the extinction coefficient κ_e. The extinction coefficients can be expressed as the sum of the absorption coefficient κ_a and the scattering coefficient, κ_s ($\kappa_e = \kappa_a + \kappa_s$). The second term of the RT equation is the energy scattered in the direction $\vec{s}$. This energy

depends on the phase function* ψ and the energy that comes from all the directions (thus the integral to the solid angle).

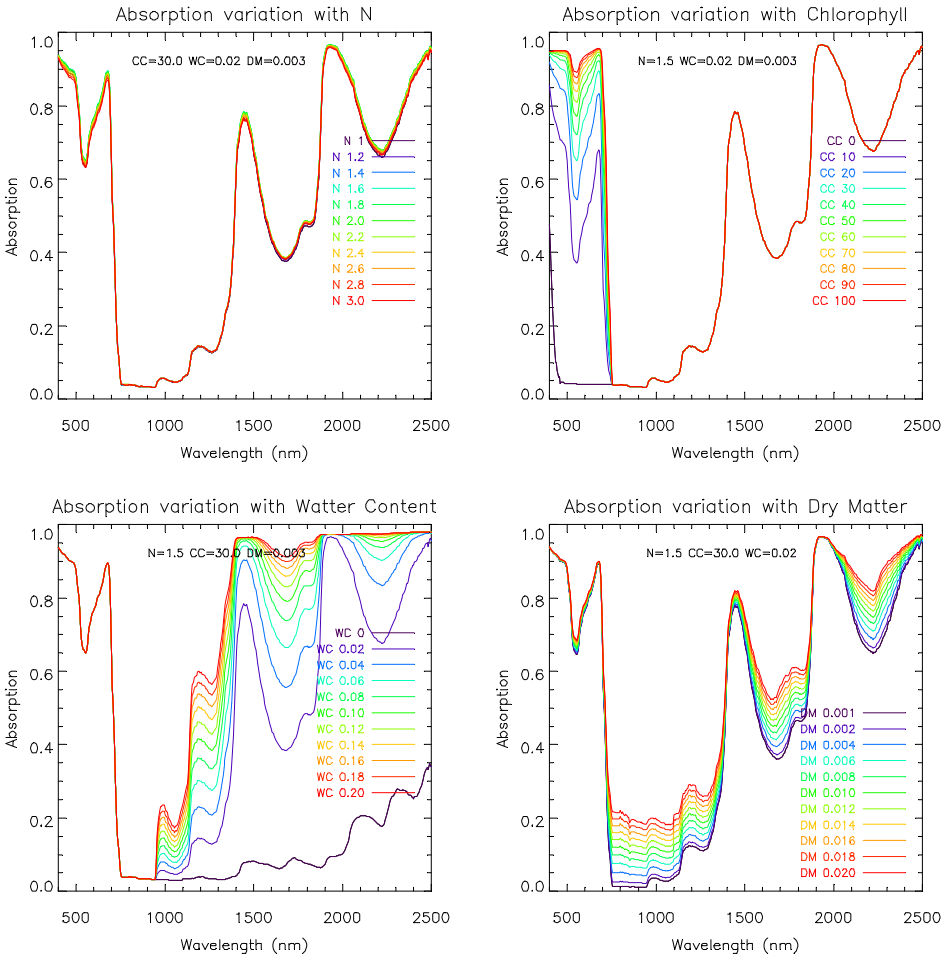

Figure 2.11. Absorption as a function of the PROSPECT variables: N (top left), Chlorophyll Concentration (top right), Water Content (bottom left) and Dry Matter Content (bottom right).

* Citing Goel, 1988 : *The name phase function has its origin in astronomy where it refers to lunar phases. It has no relation to the phase of a wave"*

The last term represents the thermal emission. RT theory can be applied to any region of the electromagnetic spectrum if certain hypothesis concerning the medium hold. RT theory cannot explain interferometric phenomena, as the phase of the electromagnetic field does not intervene in the formulation. That means that the elements in the medium must be spaced enough with respect to the wavelength to assure that electromagnetic fields are de-correlated. The elements should neither be distributed in a regular spatial pattern, which could generate interference patterns. In a vegetation medium, these assumptions correspond very well to the optical range (wavelength of μm) and it is less applicable to the radar case (wavelengths of cm or more). The RT equation in its integro-differential form has not an analytical solution. When applied to a particular wavelength range different approximations can be made in this equation. For instance in optical and radar remote sensing the thermal emission is neglected but in addition other approximations need to be done. The main difficulty to solve **Equation 2.5** is the calculation of the phase function and the extinction coefficient in terms of the properties of the vegetation. Different approximations based on the medium characteristics and wavelength are done (approximations regarding the orientation, spatial distribution and size relatively to the wavelength of the scatters in the canopy). RT models can be classified as homogeneous or heterogeneous depending on how the medium is described. In the homogeneous models, the canopy elements (leaves, stems, ears, branches, etc) are distributed uniformly in the horizontal plane, while in the heterogeneous models the canopy elements are distributed non-uniformly in a three dimensional space. Examples of homogeneous models are the SAIL model (Verhoef, 1984) or the model of Kuusk, (Kuusk, 1995). Non homogeneous models are for instance DART (Gastellu-Etchegorry et al., 2004). Although the assumption of homogeneity is sometimes too strong, homogeneous models (also referred to as turbid

models) depend on a small number of variables and they are easy to invert. For these reasons, in this work we use the SAIL model, described in a following section.

The second way of classifying RT models attends to the numerical method use to solve the equation (after doing the approximations relative to the medium). The most frequent methods are adding-doubling, discrete ordinates, ray tracing, successive approximations, etc.

Kubelka-Munk (KM) approximation for a parallel-plane medium.

The Kubelka-Munk approximation is a simplification of the RT equation is for a parallel-plane medium. This approximation is common in optical remote sensing. In the KM theory the light propagation is described with a limited number of ascending and descending fluxes. The diffuse radiation is in turn represented by an ascendant flux E_+, and a descending flux E_-. The direct radiation (collimated in a particular direction) is represented by an ascending flux F_+ and a descending flux F_-. The variations in those fluxes depend on: α and γ, which are the absorption and scattering coefficients for the diffuse flux, K, the absorption coefficient for the direct flux, and the two coefficients, Λ_1 and Λ_2, the scattering coefficient for the direct flux into the same direction and into the opposite direction respectively. Those scattering and absorption coefficients depend on the solar and viewing directions. The ratio between the upward radiation leaving the top of the canopy and the downward radiation constitutes the canopy reflectance. The KM approximation is then a set of linear differential equations:

$$\frac{dE_-}{d(-\tau)} = -(\alpha+\gamma)E_- + \gamma E_+ + \Lambda_1 F_- + \Lambda_2 F_+ \quad \text{[Eq. 2.6]}$$

$$\frac{dE_+}{d\tau} = -(\alpha+\gamma)E_+ + \gamma E_- + \Lambda_1 F_+ + \Lambda_2 F_- \quad \text{[Eq. 2.7]}$$

$$\frac{dF_-}{d(-\tau)} = -(\mathrm{K}+\Lambda_1+\Lambda_2)F_- \quad \text{[Eq. 2.8]}$$

$$\frac{dF_+}{d\tau} = -(\mathrm{K}+\Lambda_1+\Lambda_2)F_+ \quad \text{[Eq. 2.9]}$$

In **Equation 2.6** to **Equation 2.9** τ is the optical path in the z direction. This optical distance is related to the density of the canopy (LAI or biomass). The **Equations 2.6** to **2.9** mean that the descending diffuse flux decreases along an optical path due to the absorption and scattering produced by the medium, and it is increased with the scattered ascending diffuse flux and the scattered ascending and descending direct fluxes.

The evolution of the SAIL model.

The original SAIL (Verhoef, 1984) was a turbid-medium vegetation reflectance model that consisted in an improvement of the Suits model (Suits, 1972). In the Suits model, leaves could only be distributed vertically or horizontally. The improvement in the first version of SAIL consisted in the possibility of any inclination distribution. The SAIL model is based in the approximation of Kubelka et Munk for the radiative transfer. Since the first formulation, SAIL has evolved dealing to several versions. SAILH (Verhoef, 1998) incorporated the hot spot effect following the theory of Kuusk. GeoSAIL (Bach, Verhoef and Schneider, 2001) was a 2 layers model in which a sub-model of soil reflectance was incorporated. In GeoSAIL it was possible to distinguish between green and brown leaves. The main characteristics of SAIL++ (Verhoef, 2002) were the improvements in the multiple scattering calculations using the N+2 stream method. The version called 4SAIL (Verhoef et al., 2007) is a one-layer version that was improved numerically and

computationally and also adapted to thermal applications. Up to date the most recent version of SAIL is the 4SAIL2 that is a 2 layers model and includes soil BRDF (Hapke type) and clumping effects (Begiebing and Bach, 2004).

Moreover different multi-layers/multi-elements modifications to the SAIL model can be found in the literature, for instance the SAIL-2 (Zhang et al., 2005), which accounts for stems and leaves) and the multi-layer version named 2M-SAIL (Weiss et al., 2001) that distinguish between leaves, ears and stems of wheat. There are also 2-Dimensional versions of SAIL (Major et al., 1992).

In the SAIL model, the contributions due to single scattered solar radiation and multiple scattered fluxes are separated. Since SAILH, the single scattering contribution takes into account the hot spot and thus does not follows strictly the turbid model approximation. The contribution due to multiple scattering follows a turbid medium approach. Thus, although SAIL is not "rigorously" a turbid medium model, many authors refer to it as a turbid medium model with the inclusion of hot spot or also as a hybrid model.

The SAIL version available for this study is the 4SAIL developed by Verhoef et al., (2007). available for the FluorMod project (Miller et al., 2004). A version of FluorMod is available from: http://www.ias.csic.es/fluormod/. 4SAIL is a version of the original SAIL model (Verhoef, 1984), which includes the hot spot effect and has been improved numerically and computationally with respect to previous versions.

Variables in the SAIL model and their effect in the reflectance.

Inputs to the SAIL model are structural parameters that include LAI, *a*, and *b*, two parameters that describe the Leaf Angle Distribution (LAD), as explained in Verhoef, 2002, the Hot Spot parameter, *h*, the background soil

spectrum and the geometry of observation. Both, parameter *a* and parameter *b* can vary between -1 and 1, but the sum of their absolute values has to be always less than or equal to 1. Parameter *a* controls the average leaf inclination angle (ALA), which in the SAIL model can range from 8.52 degrees (*a*=1) to 81.48 degreess (*a*=-1). Parameter *b* characterises the bimodality of the LAD. High values of *b* correspond to a high frequency of both horizontal and vertical leaves (Verhoef, 2002). **Figure 2.12** and **Figure 2.13** show the effect on the reflectance of the variables to which the model is more sensitive. The following table (**Table 2.6**) summarizes the inputs to the SAIL model:

SAIL Inputs
Leaf Area Index (LAI)
Hot Spot parameter (*h*)
Leaf Angle Distribution (*a*, *b*)
Solar zenith angle (θ_{solar})
Solar azimuth angle (ϕ_{solar})
Relative azimuth ($\phi_{relative}$)
Background soil spectrum (ρ_{soil})

Table 2.6. Inputs to the SAIL model.

2.5.5. Model inversion.

In remote sensing, RT is used to relate the physical magnitudes measured by the sensor (i.e. radiance, brightness temperature, power) to the physical properties of the observed surface (i.e. extinction coefficient, emissivity, temperature, dielectric constant). Those physical properties are in turn related to other physical magnitudes or variables that describe the current status of the surface (LAI, height, temperature, moisture, etc) and are the inputs to the RT models. In addition, depending on the wavelength, the RT also needs to be applied to the atmosphere.

The forward modelling consist of simulate the sensor measurements, while the inverse modelling consists of predicting the vegetation characteristics that correspond to the sensor measurements (**Figure 2.14**). For instance, when the SAIL model is used in the forward modelling, the reflectance is calculated as a function of its inputs (LAI, hot spot, etc.). The inverse modelling can be considered as the opposite of forward modelling. By measuring the reflectance and by using the inverse scheme it is possible to obtain the estimations of the inputs of the model.

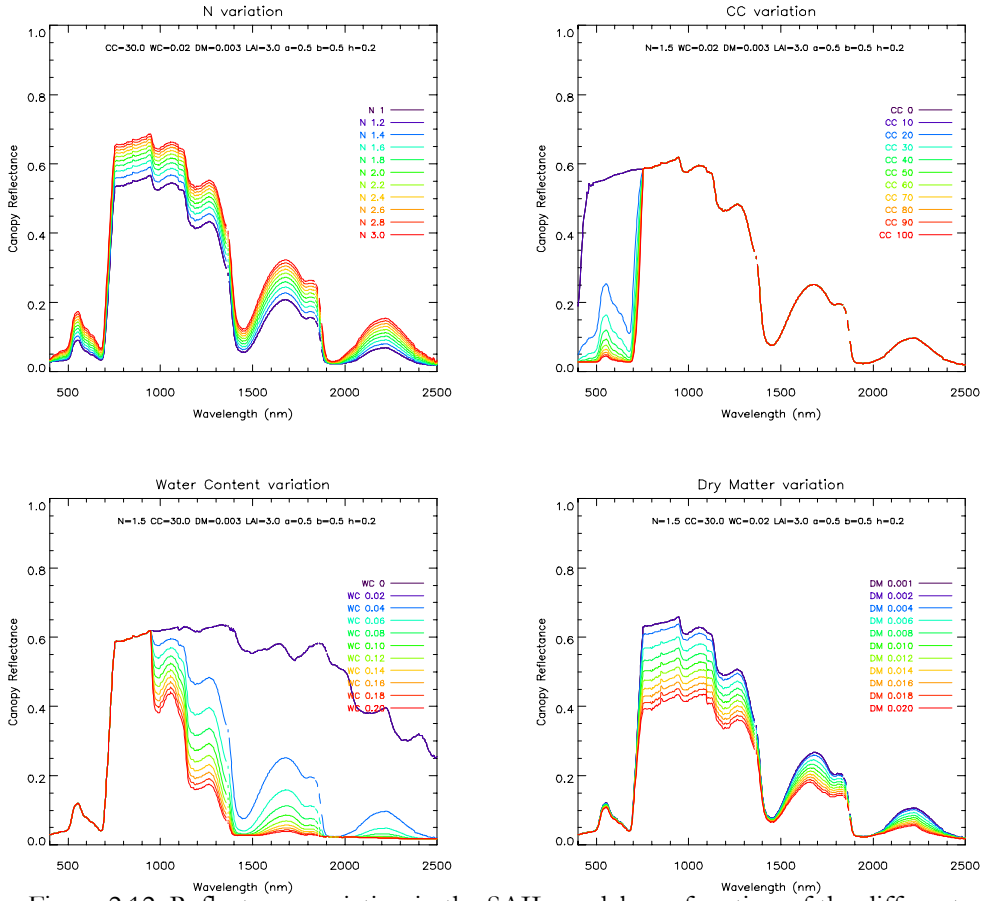

Figure 2.12. Reflectance variation in the SAIL model as a function of the different parameters: a) variation with N parameter, b) variation with CC, c) variation with WC content and d) variation with DM content.

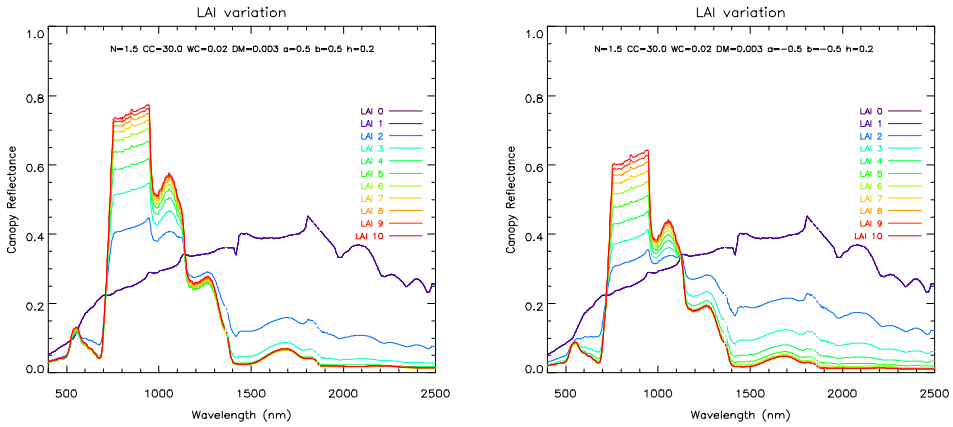

Figure 2.13. Reflectance variation with LAI according to the SAIL model for two different cases of Leaf Angle Distribution functions.

Due to its complexity, RT models cannot be inverted by means of an analytical expression. Thus, in practice, the solution of the inverse problem relies on different numerical techniques, such as the minimization between the simulated reflectances and the sensor measurements. The inverse solution can also be searched among pre-defined solutions implemented in the form of look-Up Tables. Other techniques very common in the model inversions are for instance Neural Networks or genetic algorithms. In general numerical methods are time consuming because a large space of possible solutions is explored. A review of bibliography concerning the approaches used for the retrieval of LAI and Chlorophyll are given in **Section 2.6**.

The problem of inverting a RT model is not usually a simple task. The reason is that the problem is, in general, ill-posed. On one hand, it may happen that several combinations of the inputs to the model gave the same solution. On the other hand, because of the non-linearity of the problem, small variations of the reflectances may result in a low precision of the desired

parameter. Several approaches can be used to overcome the ill-posed problem, such as the use of a-priori information or temporal constraints.

In this study, to approaches have been used for the inversion of the PROSPECT+SAIL model. In the first approach, presented in **Chapter 3**, the LAI is inverted by using Look-Up Tables and a-priori information. In the second approach, presented in **Chapter 4**, the inversion of LAI and Chlorophyll is investigated by using a numerical inversion method and temporal constraints.

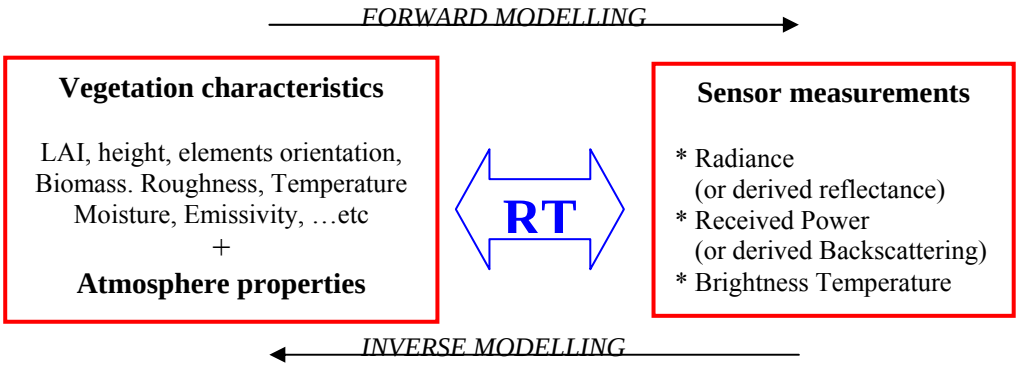

Figure 2.14. Radiative Transfer applied to Remote Sensing.

2.6 Current capabilities to retrieve biophysical parameters.

To conclude this chapter a review of bibliography concerning the retrieval of biophysical parameters using remote sensing data is done. As the objective of this PhD focuses on LAI and Chlorophyll only those two parameters are addressed.

LAI:

In recent decades, a large amount of studies on the derivation of LAI and other biophysical parameters (for example, fraction of photosynthetically active radiation, chlorophyll content and water content) from optical data have been published. Two main approaches have been used: empirical and physically-based approaches.

The empirical approaches are based on the experimental relationships between combinations of reflectances in different spectral bands (indices) and the parameter to be retrieved. This approach has been frequently applied to various satellite data to calculate the LAI of large classes or categories of vegetation. In particular, Turner et al. (1999) used Landsat data with empirical relationships to derive the LAI of grassland, shrubland, hardwood and coniferous forest; Chen et al. (2002) used AVHRR, SPOT VGT and Landsat data to retrieve the LAI of forests and crops. In a similar way, this approach was applied to particular crop types, such as wheat, with Landsat-TM data (Duchemin et al., 2006) and with SPOT HRV data (Clevers et al., 2002a, among others).

A drawback is that the general applicability of these empirical approaches is reduced because the vegetation indices (VI) are affected by many factors, including atmospheric effects, leaf structure, canopy geometry, vegetation developmental stage, geometry of observation, understory vegetation and soil conditions (Baret and Guyot, 1991; Turner et al., 1999; Gitelson et al., 2005; Boegh et al., 2002).

Physically-based approaches (e. g. Kimes et al., 2000) are based on the application of Radiative Transfer models. These models describe the physical processes of radiative transfer in the soil vegetation system, connecting the canopy biophysical variables and the canopy reflectance. These approaches, though more complex, are more general in application because they can

account for the different sources of variability, although in many cases the information needed to constrain model inputs is not available.

Among physically-based approaches, the most widely used consists of the inversion of a simple canopy radiative transfer model coupled with a leaf model. Regarding inversion techniques different approaches have been used: a) direct numerical inversion (Gao and Lesht 1997; Bicheron and Leroy, 1999), b) Look Up Tables (Weiss et al. 2000; Combal et al, 2002(a)), c) neural network techniques (Weiss and Baret, 1999; Qi et al., 2000; Fang and Liang, 2003) and d) genetic algorithms (Fang et al., 2003).

The retrieval of LAI in agricultural areas has been the subject of many studies. However, these studies have not often shown the applications of LAI retrieval methods for a variety of crops, along a complete season and in extensive agricultural areas. This study has the objective of assessing the applicability and accuracy of LAI inversion over a complex agricultural landscape. To this aim, a physically-based model has been preferred, because in-situ measurements were available and can be used to constrain the inputs of the model. The PROSPECT+SAIL models are thus used to generate Look Up Tables (LUTs). Those LUTs are subsequently used to invert Landsat-TM and Landsat-ETM+ images. The research dealing with the retrieval of LAI will be presented in the next chapter of this manuscript.

Chlorophyll:

As it was discussed in **Chapter 1**, the information of biophysical parameters, like LAI, biomass or chlorophyll, is very useful for the monitoring of crop growth. The chlorophyll content of the plant is related to its nitrogen content (Yoder and Pettigrew-Crosby, 1995), which is a limiting factor for crop growth. Furthermore, the total chlorophyll in the canopy, which can be

estimated by the product of the chlorophyll content in the upper leaves multiplied by the LAI, is closely related to the gross primary production (Gitelson et al., 2006). Thus, the research on the retrieval of chlorophyll content is of high interest for crop studies.

As it was already commented in this chapter, the chlorophyll content of the leaf is linked to its reflectance. This relationship is established through spectral indices, and spectral derivatives, mainly in the red edge spectral region (Curran et al., 1990; Clevers et al., 2002b; Cho and Skidmore, 2006).

As it is done for LAI, spectral indices (Yoder and Pettigrew-Crosby, 1995) and the inversion of radiative transfer models (Demarez et al., 1999; Weiss et al., 2000; Jacquemoud et al., 2000) are the main methodologies used to estimate the chlorophyll content. There is a long list of indices for the derivation of the chlorophyll content. A review of the most common chlorophyll indices can be found in Bannari et al., (2007). The same indices that were developed for the estimation of chlorophyll at the leaf level are sometimes used to derivate chlorophyll at canopy level (Gitelson and Merzylak, 1997), but there are also indices specifically derived for the canopy cover, like MCARI, OSAVI, etc., (Broge and Leblanc, 2001; Haboudane et al., 2002).

In the physically-based approach, leaf reflectance and transmittance are simulated using a leaf reflectance model, which is later used as input to the model of canopy reflectance. The advantage of this approach is that it is more general than the spectral indices. The drawback is that the models do simplifications in the number of pigments present in the leaves. In addition, changes in the specific absorption coefficients along the crop cycle (from emergence to senescence stage) are not usually taken into account. This approach was applied using field spectrometry data (Jacquemoud et al., 1995), simulated data (Jacquemod, 1993; Weiss et al., 2000; Demarez et al., 1999), AVHRR, and VEGETATION/SPOT data (Weiss and Baret 1999).

Many of the previous studies agree in that, without a-priori information, it is not possible to invert the PROSPECT+SAIL model to obtain, at the same time, several variables with accuracy. These studies also paid attention to the compensations between the variables. The inversion of both LAI and chorophyll appears to be particularly difficult (Combal et al, 2002a). Recent studies, inverted the product of LAI and chlorophyll from TOA MERIS, using neural networks (Bacour et al., 2006).

The multi-temporal aspect has not been much explored in the context of the inversion of biophysical parameters. One of the few studies that investigates this issue is Koetz et al., (2005), who proposed a multi-temporal method for the retrieval of LAI. This method is based on the coupling of a RT model and a semi-mechanistic canopy structure dynamic model. In their approach, the semi-mechanistic model is used to fit the results of the RT inversion, and, later, this result is used as the initial conditions of a new inversion.

Most of the literature related to the estimation of chlorophyll content reports results for forest (Zarco-Tejada et al., 2004) or for a particular crop, mainly corn (Daughty et al., 2000), wheat (Wang et al., 2004) or soybean (Gitelson et al. 2005), and using a limited number of datasets. Few studies report results on several crops. Thus, the inversion of chlorophyll content in agricultural areas requires further studies.

In **Chapter 6**, the possibilities of using the multi-temporal dimension, in order to invert at the same time, LAI and Chlorophyll are investigated. The analysis is done in the agricultural area of Barrax (Spain) and focuses on small grain cereal fields.

[…] Por esta Mancha-prados, viñedos y molinos –
que so el igual del cielo iguala sus caminos […]
por este seco llano de sol y lejanía,
en donde un ojo alcanza su pleno mediodía […]
por esta tierra, lejos del mar y la montaña,
el ancho reverbero del claro sol de España,
anduvo un pobre hidalgo ciego de amor un día […]

Antonio Machado, Campos de Castilla (1907-1917)

CHAPTER 3: SEASONAL VARIATIONS OF LEAF AREA INDEX OF AGRICULTURAL FIELDS RETRIEVED FROM LANDSAT DATA [#].

This chapter is dedicated to the assessment of a LAI model inversion approach applied to multitemporal LANDSAT-TM data. The method has been applied over the agricultural region of Barrax. The chapter is organised as follows: first, the study area, ground measurements and satellite dataset used in this work are described. Second, the methodology, which includes the derivation of a land use map and an inversion of the selected model, is described. Finally results and validation are presented followed by a discussion.

[#] The contents of this chapter have been published in the following paper: González-Sanpedro, M. C., Le Toan T., Moreno, J., Kergoat L. and E. Rubio. Seasonal variations of leaf area index of agricultural fields retrieved from Landsat data. Remote Sensing of Environment 112, (2008), 810-824, doi:10.1016/j.rse.2007.06.018.

3.1. Introduction.

Monitoring agricultural crops during the growing season becomes increasingly important in order to adjust the management (e.g. irrigation, fertilizers) and to provide information for obtaining yield predictions before harvest time. Crop growth models and soil-vegetation-atmosphere process models are more and more used for such monitoring activities. However, it is difficult for the models to account for the spatial heterogeneity in vegetation and soil conditions as well as the inherent difficulties of phenology modelling. One solution consists in calibrating the models using measurements of biophysical parameters (e.g. Brisson et al., 1998; Bondeau et al., 1999; Launay and Guerif, 2005; Spitters et al.; 1989).

For calibrating crop growth models, a key variable is the leaf area index (LAI), which accounts for the leaf surface intercepting in-coming radiation. LAI stands out because it takes part in functioning processes through the allocation of carbon to leaves. LAI is also involved in the description of soil-vegetation-atmosphere exchanges like evapotranspiration, photosynthesis and biogenic emissions. For instance, in irrigation management, LAI is required to model the surface resistance when calculating evapotranspiration (ET) by direct application of the Penman-Monteith's equation (Allen, 2000). ET models based on surface energy balance and hydrological models that take into account the role of vegetation also require LAI as input for partitioning ET into evaporation and transpiration (Montaldo and Albertson, 2003; Norman et al., 1995; see also Hadria et al., 2006).

In crop monitoring studies conducted in recent years in the region of Barrax, Spain (Berger et al., 2001; Moreno et al., 2004), in situ LAI measurements have been performed during specific remote sensing experiments and can be used to calibrate crop growth models and coupled

vegetation and hydrological models. However, given the large number of crop types, the large differences in crop calendar and the diversity of field management in the region, in situ LAI measurements appeared insufficient, as they are usually available for only a limited number of fields and dates.

Multitemporal high resolution optical remote sensing is considered an advantageous alternative to infer both spatial and temporal LAI, provided that the retrieval of LAI from satellite data is effective for the diversity of crop types in the region.

Methodologies to derive LAI from satellite optical data have been the subject of a large amount of work. In contrast, few papers have addressed the effective model inversion of high resolution satellite images for a complete temporal series of data for various crop types in a given region. The crop types present in the region of Barrax include: cereals, corn, alfalfa, sugar beet, onion, garlic, papaver. Some of the crop types (onion, garlic, papaver) have not been addressed in previous studies.

In the present study, we focused on the assessment of a LAI model inversion approach applied to multitemporal optical data over the region of Barrax. Both the inversion approach and data sources are chosen because of their wide use: the inversion makes use of the PROSPECT+SAIL model and the satellite data are LANDSAT images. First, the PROSPECT+SAIL model benefits from in situ measurements of crop biophysical properties used as constraints on the model parameters; second, we use a model inversion technique consisting of a Look Up Table to invert a complete time series of Landsat-TM and ETM+ scenes acquired all along the crop growth period in the Barrax area (i.e. from March to September). The image data used here consisted of twelve Landsat-TM and ETM+ scenes. Our objective is to obtain temporal LAI curves for the diversity of crops in the area of Barrax.

3.2. Site description and datasets.

3.2.1. Site description.

The area of Barrax (Castilla-La Mancha, Albacete, Spain) is located on a central plateau at 700 m above sea level. Relevant characteristics of this region are its flat topography and the presence of large uniform land-use units. Castilla-La Mancha is one of the driest regions of Europe with mean annual precipitation of about 400 mm, which is mostly concentrated in spring and autumn. The study site covers an area of 51 km × 38 km. Vegetation in this site is representative of the crop types and agricultural practices of Castilla-La Mancha. Two thirds of the study area is dry land with dominant winter/spring cereals (60%) and bare soil/fallow land (30%), and the rest is irrigated land cropped with corn, wheat, barley, sunflower, alfalfa, onion and vegetables.

3.2.2. Ground biophysical measurements.

Biophysical parameters and ground information used in this work were collected in the 2003 growing season in the framework of two different activities: the experimental campaigns of ESA/SPARC-2003 (Moreno, et al., 2004), and the field activities planned in the DEMETER project (Jochum and Calera, 2006).

Intensive field measurements of biophysical properties were collected during the period 11-15 July 2003. These measurements were concentrated in a 10 km × 10 km site within the "Las Tiesas" experimental facilities of the Diputación Provincial de Albacete. The measured biophysical parameters comprised the following: LAI, Leaf Chlorophyll content CC, Leaf Water Content WC Leaf Dry Matter DM and Fraction of Vegetation Cover FVC. The measurements were taken in fields of alfalfa (Medicago sativa L.), corn

(Zea mays L.), garlic (Allium sativum L.), onion (Allium cepa L.), papaver (Papaver somniferum L.), potato (Solanum tuberosum L.) and sugar beet (Beta Vulgaris L.). The Leaf Chlorophyll Content was measured using the CCM-200 Chlorophyll Content Meter, which was calibrated through laboratory analysis of specific samples (Gandía et al., 2004). Leaf Water Content and Leaf Dry Matter were determined by weighing the wet and dry samples and by estimating the leaf area through the analysis of digital pictures. LAI measurements were made using the Plant Canopy Analyser, LAI-2000 (LI-COR Inc., Lincoln, NE, USA). LAI measurements were carried out under uniform clear diffuse skies at low solar elevation to prevent the effects of direct sunlight on the sensor. The fraction of vegetation cover was measured using directional hemispherical photographs (DHP), (Martínez et al., 2005) **Figure 3.1** shows a Landsat close-up of the "Las Tiesas" site with the measured fields highlighted in colour, and the location of the individual samples that were collected. In this figure, the circular fields have diameters that range between 300 m and almost 2 km. These circular fields correspond to irrigation units known as "pivot". The figure shows that a large part of the image is not covered by vegetation at the date of July 15. The non vegetated areas include mainly harvested cereal fields with variable reflectances, whereas bare soil surfaces have higher reflectance. The nomenclature chosen in this paper for the fields is Fn, where F is a letter denoting the field type (A stands for Alfalfa, C for Corn, G for Garlic, ON for Onion, P for Potato, PA for Papaver and SB for Sugar Beet) and n is a digit corresponding to the field number. For consistency with other analyses using the same datasets (Moreno et al., 2004), the numbering of the fields from the original dataset is maintained. **Table 3.1** lists the mean and standard deviation values of DM, WC, CC and FVC measured for each crop. LAI measurements for each individual field are given in **Table 3.2**. Here, an average value was calculated for each individual field

from the sets of measurements performed on the various samples measured within every given field. For a more detailed description of the ground data-set of the SPARC-2003 campaign, see Moreno et al. (2004). The different parameters in **Tables 3.1 and 3.2** were found weakly correlated (with r2 of the order of r2~0.25), except LAI and Dry Matter Content (r2 ~0.5) (Gandía et al., 2004). In particular, for the same Fraction of Vegetation Cover, e.g. 0.6 for corn, onion and alfalfa in **Table 3.1**, additional information is contained in LAI, e.g LAI values range from 1.4 to 3.5 in **Table 3.2**. Phenology observations (e.g. on potato and onion) made by the Irrigation Advisory Service (IAS) of ITAP (Instituto Técnico Agronómico Provincial) were also available.

Spatial sampling strategy:

The spatial sampling strategy was designed to represent the variability of the fields in the area. Following this criterion, several sampling units were selected inside the fields. Each sampling unit had a size of 20 m x 20 m. The position of the sampling units was georeferenced by using a portable GPS. For LAI measurements, 60 statistically representative sampling units were measured. The exact number of sampling units inside each field was: A1 (4 points), A9 (4 points), A10 (3 points), C2 (4 points), C3 (3 points), C6 (3 points), C7 (3 points), G1 (7 points), ON1 (6 points), ON2 (3 points), PA1 (4 points), P1 (11 points), SB2 (5 points). For each one of these sampling units the LAI-2000 measurements result from averaging three replications consisting of one measurement above and eight below the canopy. The replications were distributed randomly within the area (Martinez et al., 2005).

The sampling strategy for the photographs used for calculating the FVC was adopted from the VALERI methodology (Baret et al., submitted). A total number of 53 sampling units were selected for the measurement of the

FVC. The mean value for each sampling unit was the average of 12 DHP distributed according two different schemes depending on the canopy spatial distribution. For homogeneous crops the 12 DHP were distributed in a pseudo regular grid inside the unit, while for row crops, they were distributed following a diagonal transect (Martinez et al., 2005).

Crop	Dry Matter (DM) ($g\ m^{-2}$)	Water Content (WC) ($g\ m^{-2}$)	Chlorophyll Content CC) ($mg\ cm^{-2}$)	Fraction of Vegetation Cover (FVC)
Corn	61±6	180±18	50.6±0.8	0.63±0.08
Potato	43±3	223±21	35.6±0.5	0.96±0.04
Sugar beet	72±11	400±120	44.3±1.4	0.94±0.02
Garlic	130±30	600±140	15±2	0.12±0.09
Onion	83±7	680±150	20±2	0.64±0.05
Alfalfa	89±23	140±70	48.5±1.2	0.59±0.04
Alfalfa	65±19	130±50	48.5±1.2	0.59±0.04
Sunflower	77±5	390±50	42.7±0.4	0.16±0.05
Vine	90±10	190±30	34.6±0.7	NA

Table 3.1. Mean and standard deviation values of the Leaf Dry Matter (DM), Leaf Water Content (WC), Chlorophyll content (CC) and Fraction of Vegetation Cover (FVC) measured during the field campaigns for each crop. Data correspond to the SPARC-2003 campaign except for sunflower and vine that were measured in SPARC-2004 campaign. Chlorophyll content and FVC of alfalfa fields was assigned the same as it was measured only once.

3.2.3. Remote sensing data.

Table 3.3 lists the twelve Landsat 5 and 7 acquisition dates and the illumination geometries. Pre-processing of the Landsat images comprised first their geo-coding, then calibration and finally the atmospheric correction providing surface reflectance images. The geo-coding of the twelve images was performed by using a total of more than 100 ground control points (GCPs) distributed over the Landsat scenes and measured in-situ with GPS. The images were first rectified using a polynomial transformation with an error lower than 1 pixel, and then resampled at 30 m spatial resolution by using the nearest neighbour algorithm. The images were subsequently calibrated by calculating the at-sensor radiance, and the surface reflectances were retrieved by performing the atmospheric correction following Guanter et al. (2007). In this step, the atmosphere is considered invariant across 30 × 30 km windows, while the surface reflectance is allowed to vary from pixel to pixel, and it is assumed to be represented as a linear combination of two vegetation and soil endmembers. An inversion of the top of atmosphere (TOA) radiances in 5 reference pixels is performed to obtain aerosol optical thickness (AOT), water vapor and the proportions of vegetation and soil in the 5 pixels. The estimated atmospheric component concentrations are then used to convert the TOA radiances to surface reflectances. This atmospheric correction method has been validated with MERIS and sun-photometer data (Guanter et al., 2007).

CROP/ID		LAI
Alfalfa	A1	1.36±0.13
Alfalfa	A9	2.99±0.16
Alfalfa	A10	1.90±0.08
Corn	C2	3.5±0.4
Corn	C3	3.3±0.3
Corn	C6	3.85±0.13
Corn	C7	3.3±0.6
Garlic	G1	0.56±0.10
Onion	ON1	1.8±0.3
Onion	ON2	1.7±0.2
Papaver	PA1	1.6±0.2
Potato	P1	5.4±0.4
Sugar beet	SB2	4.2±0.4

Table 3.2. Mean LAI-2000 measurements during the SPARC-2003 for each measured field. Spatial distribution of the measurements is shown in **Figure 3.1**.

Date	DOY	Satellite	Solar zenith	Solar zenith used in the LUT	LUT reference
10/03	69	Landsat-7	49.20	49.00	1
27/04	117	Landsat-7	32.05	32.00	2
20/05	140	Landsat-7	26.97	27.00	3
29/05	149	Landsat-7	25.88	27.00	3
29/06	180	Landsat-5	28.00	29.00	4
08/07	189	Landsat-5	29.00	29.00	4
15/07	196	Landsat-5	29.00	29.00	4
24/07	205	Landsat-5	31.00	32.00	5
31/07	212	Landsat-5	32.00	32.00	5
09/08	221	Landsat-5	33.00	32.00	5
25/08	237	Landsat-5	37.00	37.00	6
17/09	260	Landsat-5	42.72	43.00	7

Table 3.3. List of Landsat-7 & Landsat-5 data acquisitions, solar zenith angle (degrees) at satellite pass time and solar zenith angle (degrees) used as input of SAIL for generating the LUTs. A total number of 7 Look Up Tables were generated (for each crop).

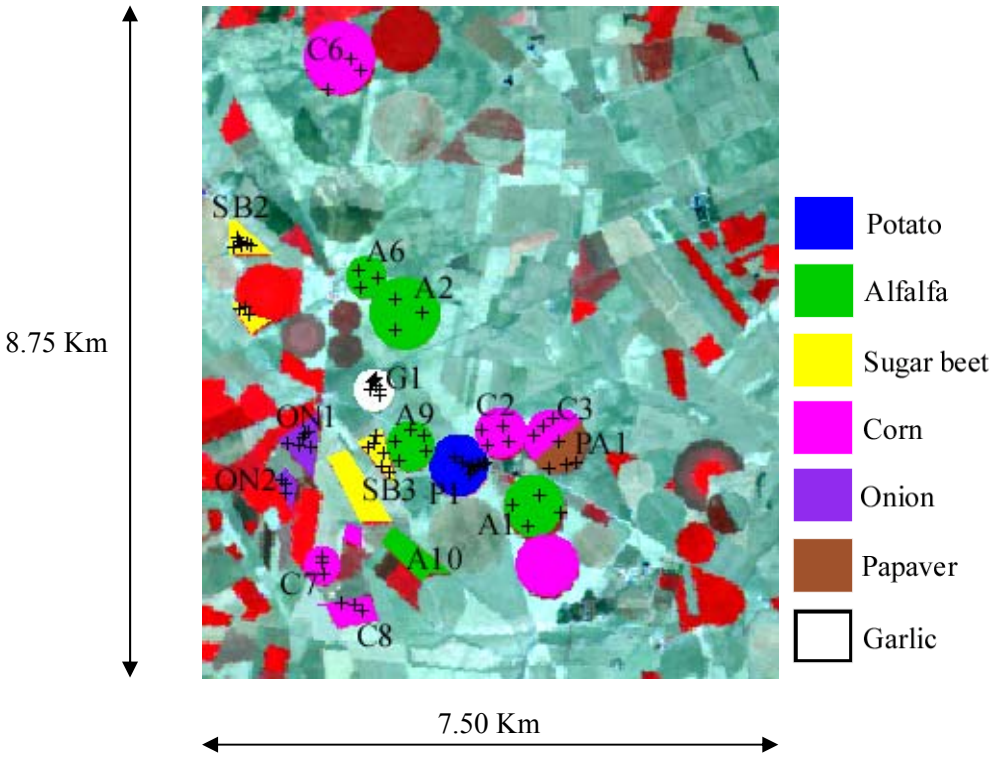

Figure 3.1. Landsat false colour (15 July 2003) close-up of "Las Tiesas" experimental facilities site with the location of the monitored fields (highlighted in colours) and the points where individual samples were measured.

3.3. Methodology.

Land use map:

The time series of Landsat images was first used to generate a land use map of the area. The classification method was based on a multitemporal supervised algorithm that takes advantage of the different phenological development of the crops in the area. The resulting classification has eleven general classes initially defined for irrigation management purposes. Apart

from urban areas and water/wet areas, the land use and land cover classes include: Natural vegetation, Spring irrigated crops (mostly small grain cereals), Summer irrigated crops (mostly corn and sugar beet, locally other crops), Double harvest (cereals in spring followed by irrigated summer crops), Alfalfa, Fallow/Bare Soil (in this area fallow is equivalent to bare soil), Dry crops (mainly non irrigated cereals), Other crops (unknown), Vineyard (*Vitis vinifera Lin.*)/Fruit trees. The validation was done with 519 plots. The Kappa coefficient, K, which is an indicator of the overall accuracy of the classification was K=0.92. The producer's accuracy is respectively of 80% for Natural Vegetation, 100% for Spring irrigated crops, 98% for Summer irrigated crops, 79% for Double harvest, 100% for Alfalfa, 100% for Fallow/Bare Soil, 88% for Dry crops and 83% for Vineyard. A further classification step has been done, based on more detailed information that was available for some fields through field survey, to partition the land use/land cover classes into crop types. This information was overlaid to the general classification giving refined classes for corn, sugar beet, wheat (*Triticum L.*), barley (*Hordeum vulgare L.*), onion, garlic, sunflower (*Helianthus annuus* L.), peas (*Pisum sativum L.*), potatoes, oat (*Avena sativa L.*), pepper (*Capsicum annuum*), rye-grass (*Lolium L.*), kenaf (*Hibiscus cannabinus L.*) and papaver fields. **Figure 3.2** shows the final land use map of the study area. Therefore, the classification of **Figure 3.2** contains general classes (class 1 to class 11) and detail classes for a subset of fields (class 12 to class 21). For purposes of LAI retrieval, some categories such as Urban areas, Water/wet areas and Fallow fields, were masked in the Landsat images prior to inversion.

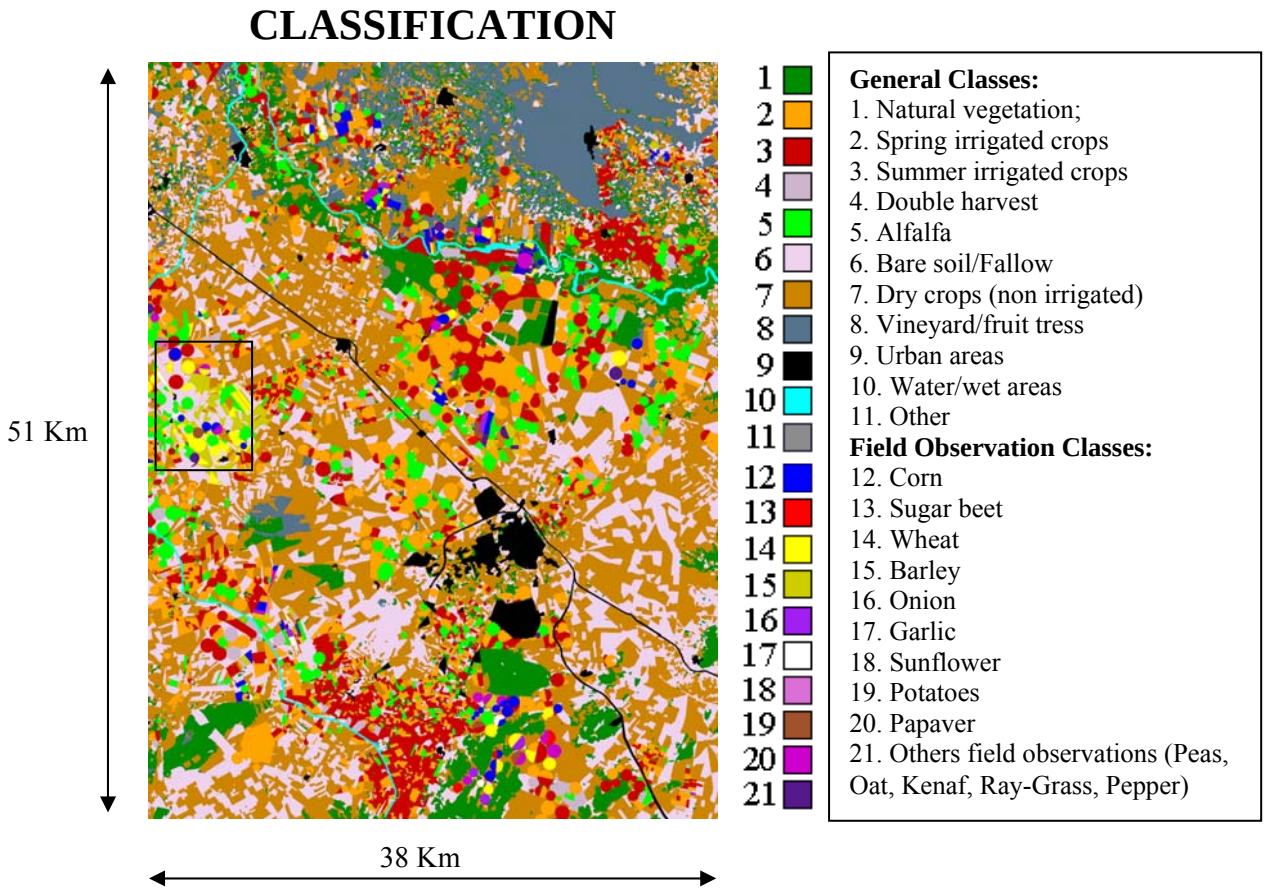

Figure 3.2. Land use map of the study area. Classes 12 to 21 are local refinements of classes 2 to 7. The black rectangle corresponds to Figure 3.1.

Choice of the models and approach:

A discussion about the advantages and disadvantages of physically-based approaches and semi-empirical approaches has been done in **Section 2.6** of **Chapter 2**. For the objective of this study, which is to investigate the applicability and accuracy of LAI inversion over a complex agricultural landscape, we retain a physically-based approach, taking the benefit of having experimental data to be used as model constraints. Nevertheless, we will compare the results from a physically-based approach to those obtained using an empirical approach.

Among the available models and inversion techniques, we retained models which have been widely applied and an inversion technique which is easy to implement: the model is PROSPECT+SAIL and the inversion is based on Look Up Tables (LUTs). The models have been described in **Section 2.5.3** and 2.5.4 of **Chapter 2**.

Description of the chosen inversion approach:

Even in the case of simple radiative transfer models, the estimation of LAI through inversion of reflectance data is an ill-posed problem, as the number of unknown parameters is higher than the spectral information. The problem can be solved by using a-priori information (Combal et al., 2002b), for instance using in-situ measurements to limit the range of parameters values. Thus, taking advantage of the vegetation biophysical measurements that were acquired for our study area, the more general physically-based approached has been preferred to a semi-empirical approach.

In a probabilistic description of the inverse problem (Tarantola, 2005), the cost function K describing the discrepancies between the simulations and the measurements will be proportional to the term:

$$K \propto \left(\vec{\rho}^{LANDSAT} - \vec{\rho}^{LUT}\right)^T C^{-1} \left(\vec{\rho}^{LANDSAT} - \vec{\rho}^{LUT}\right) \qquad \text{[Eq. 3.1]}$$

where, C is the covariance matrix of the measurements accounting for measurement errors. The elements off-diagonal are not null when errors are correlated between bands. Usually, correlations are unknown, and a first approximation to the problem consists in neglecting them. The inversion of our Look Up Tables consisted in finding which spectrum from the Look Up Table minimizes the following expression:

$$\mathrm{K} = \sum_{b=1}^{6} \left(\rho_b^{LANDSAT} - \rho_b^{LUT}\right)^2 \qquad \text{[Eq. 3.2]}$$

The latter equation implies that measurement errors are assumed equal (as the same weight has been given to all bands) and without correlations (elements off-diagonal are zero).

Due to the lack of information to quantify the covariance matrix, it has been chosen to give the same weight to all bands. Moreover, in this sort of methodology, measured reflectances are compared with "ideal" simulated reflectances, as it is assumed that the model has no errors. Errors in the model are indeed very difficult to quantify, also they may be comparable or even higher than measurements errors.

The inversion following **Equation 3.2** is applied to each of the Landsat images, on a pixel by pixel basis, for each specific crop type according to the land use map (see **Figure 3.2).**

The inversion method consists in using crop-specific Look Up Tables (LUTs) which have been created using the outputs of PROSPECT+SAIL models. The PROSPECT model computes the leaf reflectance and transmittance needed for running the SAIL model.

Both PROSPECT and SAIL models were run by steps of 2.5 nm wavelength. To simulate Landsat-like spectra, the SAIL model was run in the

range 400 to 2500 nm. The atmospheric parameters needed for this version of SAIL (extraterrestrial solar irradiance, direct solar transmittance, atmospheric spherical albedo and diffuse solar transmittance) were calculated in the full range from 400 nm to 2500 nm using MODTRAN-4. The 2.5 nm step simulated hyperspectral reflectance is then aggregated using Landsat sensor filters to give a 6 bands spectrum. Look Up Tables adapted to solar zenith angle for each Landsat date (see **Table 3.3**) were generated for alfalfa, corn, garlic, onion, sugar beet, potato, sunflower, vineyard/fruit trees, wheat/barley and natural vegetation. In addition, a general LUT was created for the rest of crops (peas, pepper, etc).

Inputs to the PROSPECT+SAIL models are experimental data, when available, completed by information from literature. The structural parameters *a* and *b* are established based on our knowledge of the plant structure (erectophile, planophile, extremophile …) and the related LAD parameterisation values in SAIL. **Table 3.4** and **Table 3.5** list these parameters and their ranges of values. In a first approximation, the ranges of values centered on in situ measurements collected in July 2003 (and also in July 2004) were applied to the whole season assuming that the ranges measured at these dates are sufficiently large to cover all plausible values. One exception concerns chlorophyll content, which commonly varies within the plant cycle. The distribution of chlorophyll has been widened for dates other than June 29 to July 15. To run the models, we choose to give discrete values within the interval with a regular step. The exact number of steps used for each crop is indicated in **Tables 3.4** and **3.5**. Typical values in the LUT are at 5 μg.cm-2 steps for CC; 100 μg.m-2 for CW; 10 mg.cm-2 for DM; and 0.1 steps for a, h and LAI. The LAI range is between 0.1 and 6.0 for all crops except for vineyards which varies from 0.1 to 2.5. Vineyard in the region has low fractional cover (<5%), (Lanjeri et al., 2001) and low LAI. For the LAD

parameter b, and the leaf structural parameter N, a unique value was given for each crop type, as it is frequently done in literature (e.g., Combal et al., 2002(a); Jacquemoud et al., 1995; Haboudane et al., 2004).

We use as input to SAIL, the soil spectrum extracted from a HyMAP airborne hyperspectral sensor image at nadir, acquired simultaneously to the SPARC campaign in Barrax, in July 2003. The spectrum has been chosen to have finer spectral resolution than Landsat: 2.5nm wavelength resolution interpolated from the original spectrum. The Hymap spectrum is found very close to the mean spectrum derived from bare soil/fallow class in the Landsat July image (**Table 3.6**). We use a fixed soil spectrum in the SAIL model, because the Barrax study site is a dry area, with low variability in soil type. This assumption may not hold for irrigated fields. However, since the evapotranspiration rates are high, we consider that the effect of irrigation is not resilient. The effect will be important for crops that have been irrigated a few hours prior to the image acquisition, and at low stage development (crops with low FCV).

3.4. Results and validation.

LAI mapping:

A map of LAI was generated for every Landsat image, which are listed in **Table 3.3**. **Figure 3.3** shows the LAI map for July 15. For this date, non vegetated pixels (bare soil/fallow fields, and already harvested small grain cereal fields) have been masked out. LAI values range from 0.1 to 6. The lowest LAI values (in light pink colour) correspond mainly to vineyards, and the highest LAI values (dark violet and black colour) to summer-irrigated crops (sugar beet, corn, potatoes) and alfalfa. The mean value of LAI for vegetated pixels is 1.1, and the standard deviation (STD) is 1.2. The LAI distribution is as follows: 80% of the vegetation pixels have LAI<2, 16% have a LAI in the

range [2-4] and 4% of the pixels have LAI>4. If we exclude vineyard and natural vegetation, the mean LAI value for crops is LAI=1.8 with a STD=1.4, with 59% of the pixels having LAI<2, 33% in the range [2-4] and 7% having LAI>4. The low mean value of LAI, and the large LAI range (0.1 to 6) are typical of semi arid agricultural regions where irrigation allows sustained growth despite a rather dry climate. The twelve LAI images denote a dynamic patchy landscape with high contrasts among three vegetation categories (natural vegetation, spring crops and summer crops) and bare soil surfaces. It can be foreseen that the temporal monitoring of crops in such a region is difficult to be done with low resolution data (e.g. MODIS or MERIS), for which a pixel can contain several fields.

LANDSAT BANDS	LANDSAT	HyMAP filtered reflectance
B1	0.12 ± 0.03	0.07
B2	0.20 ± 0.04	0.17
B3	0.27 ± 0.05	0.25
B4	0.37 ± 0.06	0.31
B5	0.48 ± 0.06	0.49
B7	0.42 ± 0.07	0.38

Table 3.6. Average soil spectrum reflectance and standard deviation in the image of July the 15th and the HyMAP soil spectrum used in the LUTs filtered to the LANDSAT bands for comparison.

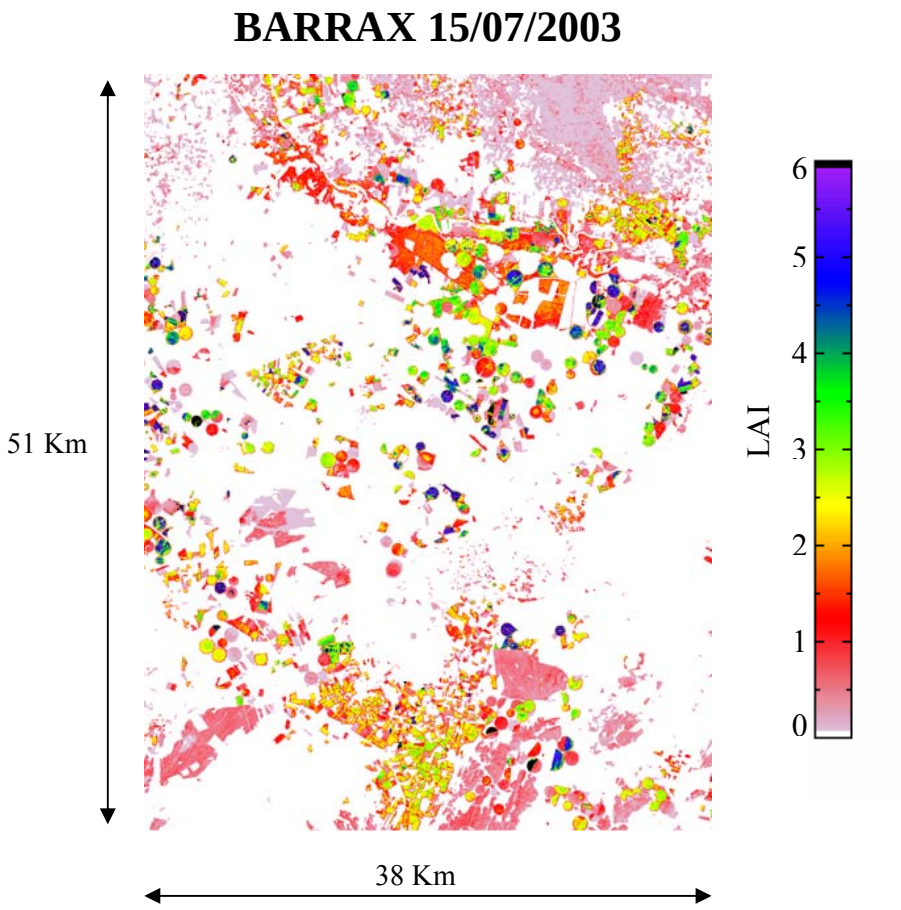

Figure 3.3. Landsat derived LAI map in July the 15th, showing contrast between crops.

	N	CC (μg cm^{-2})	WC (g m^{-2})	DM (g m^{-2})	LAI	a	b	h
CORN	1.6	50.0	[100, 200] *i*=3	[50, 70] *i*=3	[0.1, 6.0] *i*=60	[-0.4, -0.6] *i*=3	-0.4	[0.1, 0.3] *i*=5
SUGAR BEET	1.6	44.0	[300, 600] *i*=4	[50, 80] *i*=7	[0.1, 6.0] *i*=60	[-0.2, 0.0] *i*=3	0.8	[0.3, 0.6] *i*=7
POTATO	1.6	36.0	[200, 300] *i*=3	[40, 50] *i*=3	[0.1, 6.0] *i*=60	Spherical		[0.1, 0.2] *i*=3
SUNFLOWER	1.6	43.0	[300, 600] *i*=7	[60, 90] *i*=7	[0.1, 6.0] *i*=60	[0.7, 0.9] *i*=3	0.0	[0.1, 0.25] *i*=4
ALFALFA	1.7	49.0	[120, 160] *i*=5	[30, 80] *i*=6	[0.1, 6.0] *i*=60	[0.8, 1.0] *i*=3	0.0	[0.05, 0.12] *i*=8
GARLIC	1.6	15.0	[500, 700] *i*=5	[50, 200] *i*=4	[0.1, 6.0] *i*=60	[-0.1, 0.1] *i*=3	0.5	[0.05, 0.07] *i*=3
ONION	1.6	20.0	[500, 800] *i*=4	[50, 90] *i*=5	[0.1, 6.0] *i*=60	[-0.1, 0.1] *i*=3	0.5	[0.05, 0.07] *i*=3
NATURAL VEGETATION	1.5	[20.0, 50.0] *i*=4	[50, 200] *i*=4	[10, 90] *i*=5	[0.1, 6.0] i=60	Spherical		[0.05, 0.15] *i*=3
VINEYARD-FRUIT TREES	1.6	36.0	[150, 250] *i*=3	[80, 100] *i*=3	[0.1, 2.5] *i*=25	Spherical		[0.08, 0.12] *i*=5
OTHERS	1.6	[10.0, 50.0] *i*=5	[100, 800] i=8	[40, 200] *i*=17	[0.1, 6.0] *i*=60	Spherical		[0.01, 0.10] *i*=10

Table 3.4. Range of values and number of values inside this range (*i*) that have been used in the Landsat Look Up Table generation for each crop on June the 29th, July the 8th and July the 15t

	N	CC (µg cm^{-2})	WC (g m^{-2})	DM (g m^{-2})	LAI	a	b	h
CORN [(b)]	1.6 [(11)]	[35, 60] [(1)] *i*=6	[100, 200] *i*=3	[50, 70] *i*=3	[0.1, 6.0] *i*=60	[-0.4, -0.6] [(11)] *i*=3	-0.4	[0.1, 0.3] [(4), (5), (12)] *i*=5
SUGAR BEET [(b)]	1.6	[40, 50] *i*=3	[300, 600] [(9)] i=4	[50, 80] *i*=7	[0.1, 6.0] *i*=60	[-0.2, 0.0] [(13)] *i*=3	0.8	[0.3, 0.6] [(7)] *i*=7
POTATO [(b)]	1.6	[25, 45] *i*=5	[200, 300] *i*=3	[40, 50] *i*=3	[0.1, 6.0] *i*=60	Spherical		[0.1, 0.2] *i*=3
SUNFLOWER [(b)]	1.6	[38, 48] *i*=3	[300, 600] *i*=7	[60, 90] *i*=7	[0.1, 6.0] *i*=60	[0.7, 0.9] *i*=3	0.0	[0.10, 0.25] *i*=4
ALFALFA	1.7	[45, 55] *i*=3	[120, 160] *i*=5	[30, 80] *i*=6	[0.1, 6.0] [(10)] *i*=60	[0.8, 1] *i*=3	0.0	[0.05, 0.12] *i*=8
GARLIC [(b)]	1.6	[15, 55] *i*=3	[500, 700] *i*=5	[50, 200] *i*=4	[0.1, 6.0] *i*=60	[-0.1, 0.1] *i*=3	0.5	[0.05, 0.07] *i*=3
ONION [(b)]	1.6	[10, 20] *i*=3	[500, 800] *i*=4	[50, 90] *i*=5	[0.1, 6.0] *i*=60	[-0.1, 0.1] *i*=3	0.5	[0.05, 0.07] *i*=3
NATURAL VEGETATION	1.5	[20, 50] *i*=4	[50, 200] [(14)] *i*=4	[10, 90][(14)] *i*=5	[0.1, 6.0] *i*=60	Spherical [(2), (3)]		[0.05, 0.15] *i*=3
VINEYARD-FRUIT TREES	1.6	[25, 45] *i*=5	[150, 250] [(15)] *i*=3	[80, 100] *i*=3	[0.1, 2.5] *i*=25	Spherical		[0.08, 0.12] *i*=5
OTHERS	1.6	[10.0, 50.0] *i*=5	[100, 800] *i*=8	[40, 200] *i*=17	[0.1, 6.0] *i*=60	Spherical		[0.01, 0.10] *i*=10
WHEAT, BARLEY [(a)]	1.6	[5, 50][(8)] *i*=10	[100, 500] *i*=5	[40, 60][(6)] *i*=3	[0.1, 6.0] *i*=60	[-0.3, 0.3] *i*=7	-0.4	[0.01, 0.03] [(4)] *i*=3

Table 3.5. Range of values and number of values inside this range (*i*) that have been used in the Landsat Look Up Table generation for each crop for dates others than June the 29th, July the 8th and July the 15th. a) Applied from March the 10th to May the 29th.b) Applied from June the 29th to September the 17th. [(1)] Viña et al. 2004 ; [(2)] Fang et al., 2003 ; [(3)] Fang and Liang, 2003 ; [(4)], Qin et al., 2002 ; [(5)], España et al., 1999 ; [(6)] Verhoef & Bach, 2003 ; [(7)] Andrieu et al., 1997 ; [(8)] Kneubühler, 2002 ; [(9)] Combal et al, 2002(a), [(10)] Confalonieri & Bechini, 2004 ; [(11)] Koetz et al., 2005 ; [(12)] Combal et al, 2002(b), [(13)] Duke and Guérif, 1998, [(14)] Weiss & Baret., 1999, [(15)] Fourty, 1996.

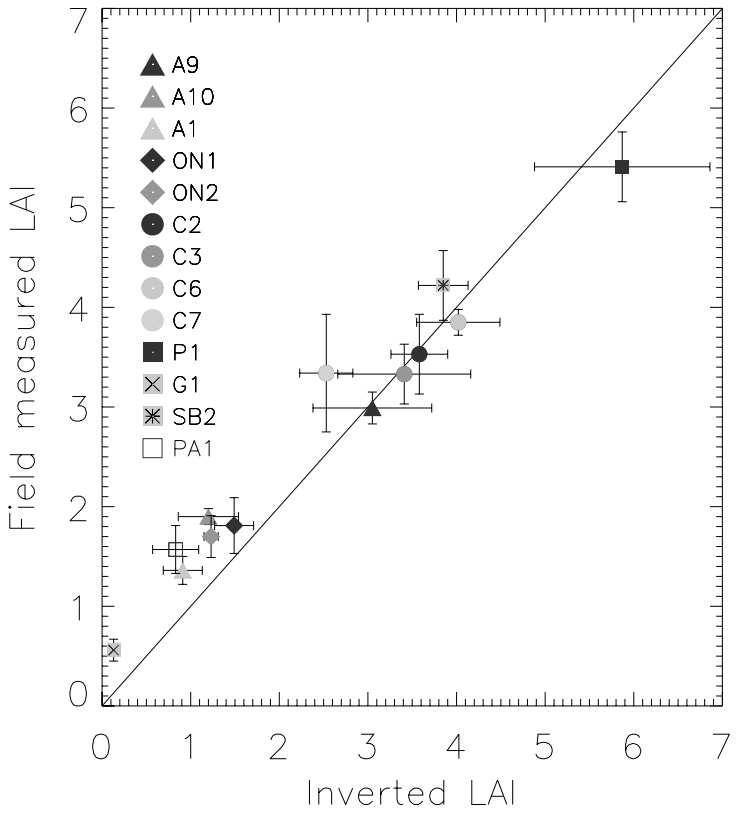

Figure 3.4. Validation of Landsat derived LAI with LAI-2000 measurements. A stands for Alfalfa, C for Corn, G for Garlic, ON for Onion, P for Potato, PA for Papaver and SB for Sugar Beet.

Validation using ground data:

The LAI values retrieved for July 8 and July 15 were validated against in-situ LAI measurements, which were both averaged over the fields where ground data have been collected (**Cf. fig.1**). Ground measurements were taken during 5 consecutive days (11 to 15 July), thus the retrieved LAI values were interpolated between the two image dates. **Figure 3.4** presents the comparison for the 13 fields of different crop types. LAI-retrieved error bars correspond to

the standard deviation of the pixels in the field. Ground data error bars correspond to the standard deviation of the point measurements in each field (around 5).

The comparison shows a high linear correlation (r2=0.97) for the 13 data points of 7 crop types, being: $LAI_{retrieved}=0.83*LAI_{observed}+0.70$. The results do not show any saturation in the whole LAI range (0 to 6), although these results, obtained using only one field with LAI>4 (potato), do not prove that saturation does not exist in the range (4-6). The standard deviation of the inverted LAI ranges from 1% (alfalfa field A2) to 30% (garlic field G1 and papaver field PA1) reflecting field heterogeneity.

A similar agreement is obtained for the July validation when using the LUTs designed for the inversion along the season (larger chlorophyll range).

LAI temporal monitoring:

Temporal curves of the retrieved LAI for different crop types were analysed with respect to their development and phenological stages to assess the performance of the LAI estimations throughout the crop cycles. **Figures 3.5** through **3.10** present examples of temporal LAI curves for fields of different crop types. When available, the phenology observations and LAI-2000 measurements for the same field are also displayed.

Figure 3.5 shows the results for two potato fields with shifted calendars and different cycle length. P2 has a longer cycle than P3: emergence is two weeks earlier and harvest is two months later. The retrieved temporal LAI variation follows well the observed phenology. It can also be noted in **Figure 3.5** that the standard deviation is large during period from flowering to

potato growing. This may result from the heterogeneity of the field during this fast varying period.

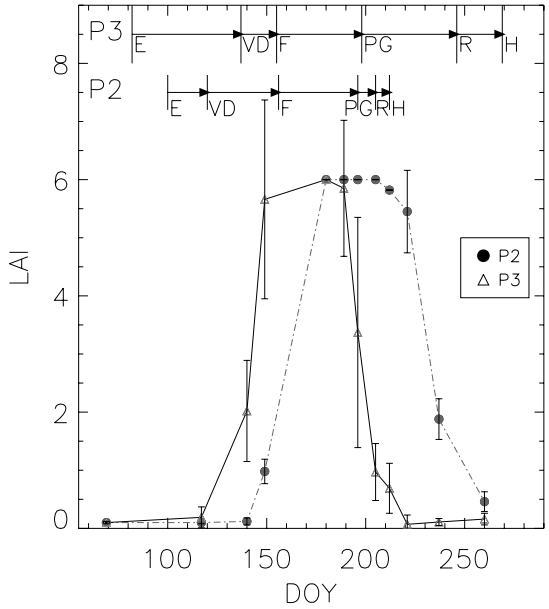

Figure 3.5. Retrieved LAI for two potato fields (P2 and P3) with different calendar. Phenological observations are indicated on top. P2 has a longer cycle than P3: emergence is earlier and harvest is later than for P2. E stands for Emergence, VD for Vegetation Development, F for Flowering, PG for Potato Growing, R for Ripening an H for Harvest.

Figure 3.6 shows the temporal LAI curve for an onion field, which also shows consistency with the in situ observed phenology. **Figure 3.7** presents the temporal LAI curves for two alfalfa fields. The curves clearly reveal at least two cuts (field A10) and 3 cuts (field A9) between March and September 2003, which are consistent with standard practices in the region.

Figure 3.8 presents the temporal curves for two corn fields from June 29 (no Landsat data was available during the first part of the development stage which

is from end of May to mid July). The temporal variation does not appear very consistent with respect to the development stage. Field C7 has unexpectedly low LAI for a standard corn crop, but it would be more consistent with a sweet corn which usually has low LAI values in the region. Unfortunately additional ground information that could be used to verify this hypothesis was not available. Field C2 (but also for fields C3 and C6, not presented) has large fluctuations during the reproductive phase, where LAI is expected to be the highest. Similar fluctuations have also been observed with sugar beet fields during the peak period. As a consequence, the inversion for those summer irrigated fields with high LAI will need further studies. **Figures 3.9 and 3.10** show the temporal curves for papaver and garlic fields. Although few data have been acquired during the key development stage of the crops, the temporal variation appears smooth. In addition, for these crops with low fractional vegetation cover (onion, garlic and papaver), the changes in soil conditions (mainly soil moisture) can affect the retrieval results. The smooth behaviour is consistent with the approximation of not considering soil moisture variations in our study area.

In summary, the inversion results shown in **Figures 3.5 to 3.10** indicate the following: a) the results seem correct except for corn and sugar beet, b) the retrieved values are consistent with specific LAI values for each crop; c) the temporal variation of the retrieved LAI is smooth, meaning that the date by date retrieval is consistent.

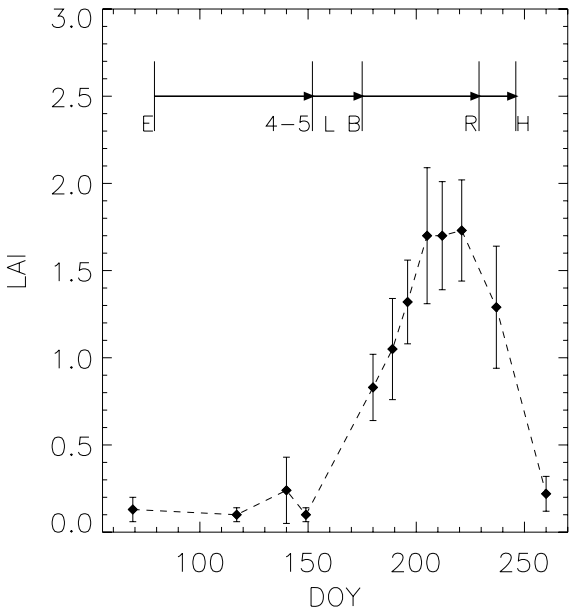

Figure 3.6. Retrieved LAI for an onion field. Error bars correspond to the standard deviation for the pixels in the field. Phenological observations for this field are indicated on top: E stands for Emergence, 4-5L for 4-5 leaves, B for bulb growing, R for Ripening and H for Harvest.

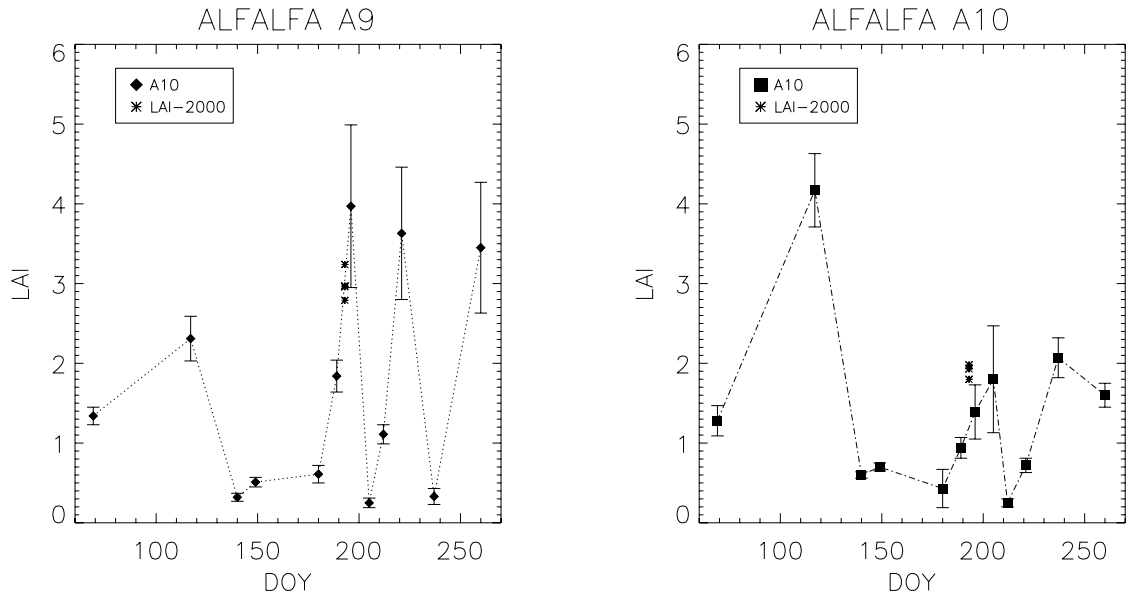

Figure 3.7. LAI curves for alfalfa field A9 and field A10. Ground measurements with LAI-2000 instrument are also displayed. Regular cuts of alfalfa are clear. Field A10 had one less cut than field A9 during year 2003.

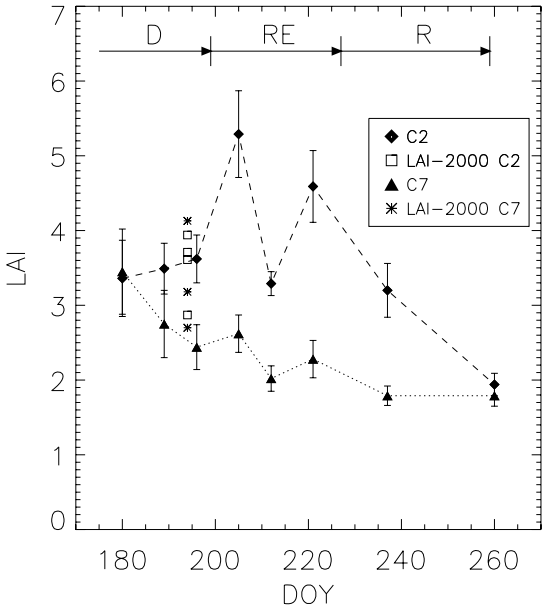

Figure 3.8. Retrieved LAI for two corn fields (C2 and C7). The average phenology of corn in the region is indicated on top: D stands for Development, RE for Reproduction and R for Ripening.

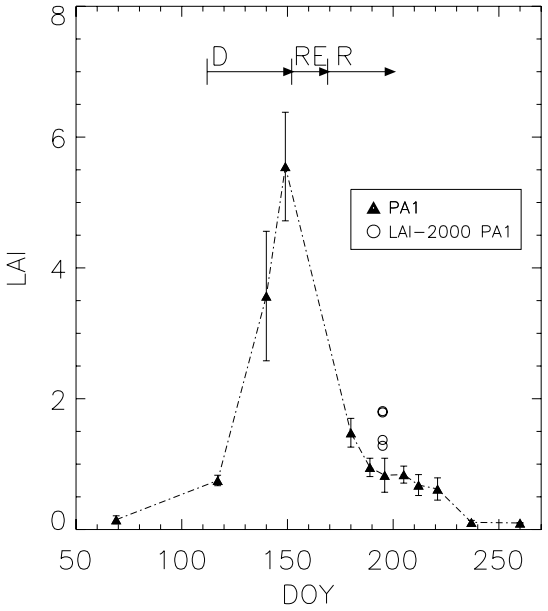

Figure 3.9. Retrieved LAI for a papaver field. Phenology for papaver in the region is indicated on top: D stands for development, RE for reproduction and R for Ripening.

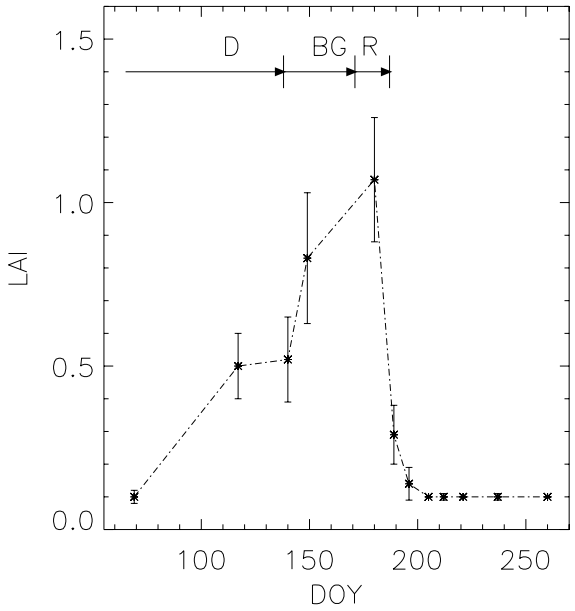

Figure 3.10. Retrieved LAI for a garlic field. Phenological observations for this field are indicated on top: D stands for development, BG for bulb growing and R for Ripening.

To better understand these results, we examine the different sources of errors in the methodology. Those include:

a) Radiometric quality of the satellite data (due to absolute miscalibration or temporal radiometric calibration instability, radiometric sensitivity and residual errors after atmospheric corrections). This problem is more important in NIR-SWIR for which temporal instability in the case of Landsat is higher (sinusoidal variation of the calibration coefficients). NIR is the part of the spectra which is the most sensitive to LAI. Crops with high vegetation density, such as corn, require accurate calibration in all bands as

LAI retrievals are also affected by total canopy water content. The poor results obtained with corn and sugar beet could be explained by the radiometric quality of the data.

b) Error and uncertainties linked to the a-priori parameters for crop characteristics used in LUT generation. The small retrieval errors as compared to in situ LAI (**Figure 3.4**) can be explained by the use of in situ crop parameters measured at the same date to create the LUT. Greater errors are expected for the other dates where input parameters are not measured, as the parameters space is under-sampled.

c) Limitation of the inversion method. Even though we have reduced the space of possible solutions when constructing the LUTs with a limited range of variation in the parameters, the inversion problem may still be ill-posed. For instance compensation between LAI and other parameters can bias LAI retrievals. This may occur in the inversion for corn and sugar beet. In this study, solutions for individual pixels in a field have been averaged to reduce the error. Further improvement could be to use the temporal dimension for the search of a better solution, adding a temporal dependent term (a temporal constraint) in the merit function to be minimized. The work of Koetz et al., (2005) showed improvements in corn LAI retrievals when taking into account the temporal dimension by using the phenological LAI dynamics to better define the a-priori information in a refined LUT based inversion method. Other studies also explored the spatial aspects (Atzberger, 2004) and both temporal and spatial dimension (Lauvernet and Baret, 2005).

d) Model limitations. Both PROSPECT and SAIL models apply to "average" vegetation properties, some particularities of crop canopies not being taken into account. For instance a 1-D model like SAIL can not describe

accurately structural differences in crops (foliage clumping, row effects). PROSPECT, on the other hand, considers cumulative spectral responses of different leaf pigments (absorbers), which are assumed to be invariable from one leaf to another. This may explain the differences in the results of different crop types. The work by Le Maire et al., 2004, discusses the necessity of re-calibration of PROSPECT. It could be interesting to re-calibrate PROSPECT specifically for agricultural crop leaves or for each crop type in our study at the expense of generality of the method.

e) The specific crop parameters used in the LUTs: the LUT inversion requires knowledge of crop parameters ranges in the area under study. When applying this methodology to other regions, the question is whether these parameters should be adapted locally. In the literature, there is a lack of documentation about the parameters that have been used in the PROSPECT+SAIL models for LAI inversions. In particular, dry matter content is often poorly documented. Surprisingly the largest uncertainties were found in well-studied crops like corn, rather than crops like onion or garlic. For these last crops, a priori parameters are readily different (e.g. large leaf water content) but the inversions are correct. Further field work could help to properly characterize crop parameters and their temporal variation to be used as a-priori in simple RT modelling inversion.

f) Soil variability (soil type and soil moisture). When a single soil spectrum is used, the soil variability caused by soil type or soil irrigation can give errors in the simulated vegetation spectra, propagating to errors in LAI inversion. Simulations show that the effect of soil background is more important for erectophile than for planophile vegetation, at lower fraction cover than at higher fraction cover (not shown). Also, a brighter soil reduces

the dynamic range of reflectance in the NIR as a function of LAI. This case is less favourable to LAI inversions. However, as the reflectance variation with LAI is different with the wavelength, it is not clear how this could actually affect the inversions using the full spectra. To quantify the background effect on the inversion, we used two soil spectra, the fixed spectrum used in the LUT multiplied by brightness factor 1.1 and 0.9 (+/- 10%) for LAI retrieved from date 29/06 to date 09/08 in the inversion of alfalfa and corn surfaces. We found that the effect on alfalfa was negligible, whereas the retrieved LAI of corn field differs by +/- 0.3. For the Barrax region, the effect of soil background variability does not appear to be a major source of error. The particular cases of recent rainfall and recently irrigated fields could not be taken into account in this study, except through the a posteriori examination of the time profiles.

3.5. Discussion.

In this study, we have retrieved LAI from Landsat data, on a pixel basis, for 12 images from March to September 2003 in the agricultural region of Barrax, a semi arid region with a diversity of crop types and crop growth cycles.

The results are compared with in situ LAI measurements available in mid July, with very good agreement but a slight bias. The LAI temporal variation of the analysed fields shows consistency with the crop phenological stages for most crop types with the exception of corn and sugar beet fields where some fluctuations in the retrieved LAI are found during a period when LAI is typically high.

Several issues are discussed below in a broader context:

- Effective LAI:

Green LAI is defined for flat leaves as the sum of the one-sided green leaf area per unit ground area (Chen and Black, 1992). In plants, leaves are usually grouped together rather than distributed uniformly: this is known as the foliar clumping. The LAI (also called true-LAI) is the "effective" LAI corrected for clumping (Chen, 1996; Lacaze et al., 2002). The LAI "seen" by optical instruments (i.e. LANDSAT and LAI-2000) is the effective LAI. The scope of this work is to give an estimation of the effective green LAI. Furthermore, optical instruments, which measurements are based on light absorption, are sensitive not only to leaves but also to other plant elements (stems). Thus we have been abusively using LAI in place of plant area index (Bréda, 2003).

When comparing total LAI destructive measurements with optically-retrieved LAI, discrepancies will be found, in particular for canopy with high LAI. This is due to the clumping effect, and due to the physical saturation of the reflectances in the optical region. The effective LAI is directly linked to the light absorption processes, photosynthesis and evapotranspiration, whereas true LAI is related to carbon allocation and growth processes.

- Empirical relationships (NDVI-LAI) versus model inversion:

To assess the possibility to retrieve LAI using empirical relationships between LAI and vegetation indices, e.g. NDVI, LAI for different fields retrieved at different dates are analysed against NDVI derived from the Landsat images. **Figure 3.11a** shows the retrieved LAI as a function of NDVI for different fields and **Figure 3.11b** shows the curves fitted for a few crop types, together with the LAI-2000 measurements. **Figure 3.12** shows the NDVI-in situ LAI relationships (all data). **Figures 3.11** and **3.12** confirm that

a) the NDVI-LAI relationships are dependent on crop type, because the relationships between reflectances and LAI are affected by the plant structure and leaf properties

b) for a given crop, the sensitivity of NDVI to LAI decreases significantly when LAI exceeds 2 or 3.

Secondly, in the NIR band, the vegetation spectra are affected by other vegetation parameters such as leaf dry matter content, leaf angle distribution and other factors (i.e. soil background, angular configuration) causing large uncertainties to the retrieval. Using a model with sufficient spectral bands, we may preserve the sensitivity to LAI of NIR band to access to higher values of LAI compared to NDVI, and separate the effects of different parameters to reduce uncertainties in the retrieval.

The graphs indicate that large uncertainties can be expected when deriving LAI from NDVI using a non crop-specific relationship, especially at high values of NDVI (0.6 to 0.8).

The main advantage of model inversion in comparison with empirical NDVI-LAI relationship is that LAI can be inverted in a higher range (**Figure 3.4** and **Figure 3.12**). This is important for agriculture as crops can reach high LAI values (**Table 3.2**). One possibility to combine the two approaches is to use the crop-specific NDVI-LAI relationships derived from model simulations (such as in **Figure 3.11**.) for a given region. The approach would benefit from the prior crop classification using the time series of satellite data. For our study site, the simulated NDVI-LAI relationships need to be further validated for the whole growth cycle and for their inter-annual variation, before their use in such a semi-empirical retrieval scheme.

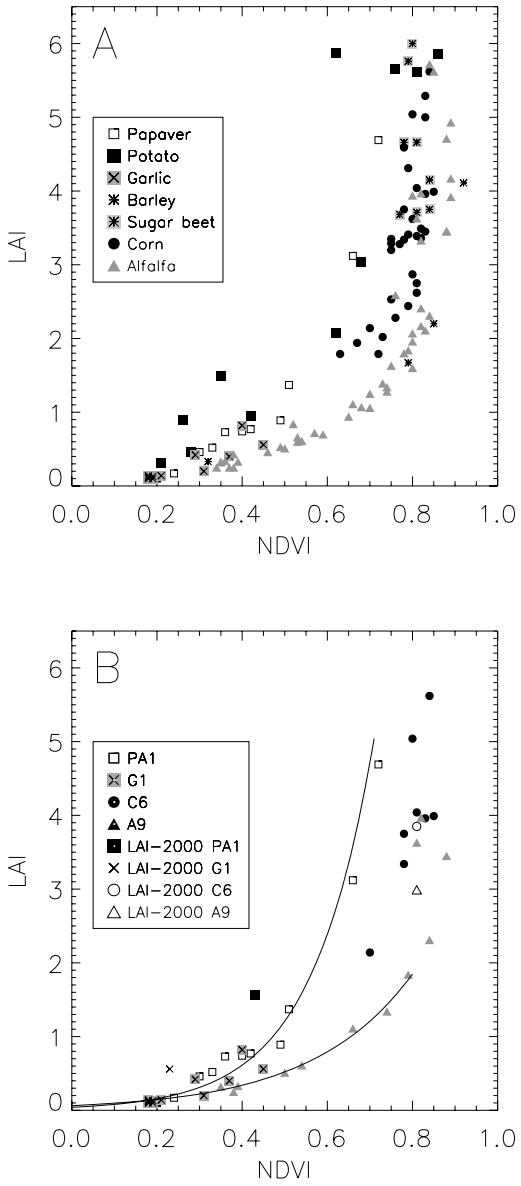

Figure 3.11. a) NDVI-LAI relationships for several crops. LAI is the Landsat derived LAI. b) Crop-specific NDVI-LAI relationships derived from model simulations for some crops and in-situ LAI measurements.

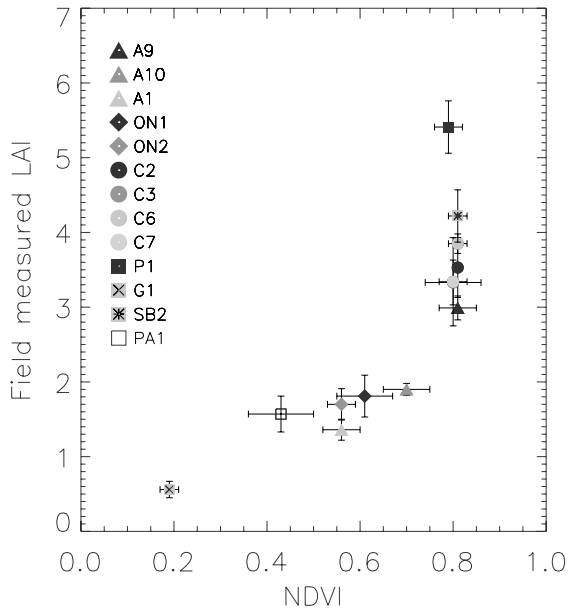

Figure 3.12. Relationship between NDVI and in-situ LAI. A stands for Alfalfa; C stands for Corn; G stands for Garlic; ON stands for Onion; P stands for Potato; PA stands for Papaver and SB stands for Sugar Beet.

-Instrument requirements:

To benefit from the whole potential of model inversion techniques, a sufficient number of appropriate spectral bands (i.e. with appropriate central wavelengths and narrow bandwidths) are necessary. The information provided by these bands has to be radiometrically accurate and as much spectrally uncorrelated as possible. The spectral information should be sufficient for aerosol correction and for decoupling the contribution of chlorophyll and water content. This means that the performance of the model inversion techniques would also depend on the satellite data used. Other current sensors with more and narrower bands (i.e. MODIS or MERIS) have, in return, the problem of spectral signal mixing due to their lower spatial resolution over

most agricultural mosaics (heterogeneous landscapes). They may be used to monitor the largest fields but will have a majority of mixed pixels at the regional scale. As the relationship between reflectance and LAI is non-linear, inversions using coarse resolution data under the assumption of spatially homogeneous pixel will introduce a bias on the LAI (Tian et al., 2003; Garrigues et al., 2006). The spatial resolution of Landsat (30m) is adequate enough to ensure accurate retrievals of LAI in our study area.

For the type of heterogeneous landscape we studied, high spatial resolution is necessary to avoid mixed pixels. Higher temporal frequency is also necessary in the period of fast development of the plants. For instance, in our dataset, a critical period (beginning of May) was missed. The presence of clouds ultimately represents a major limitation for multitemporal studies. A higher frequency of acquisitions for optical data to compensate for potential loss of images due to cloudiness would have a major impact on the applicability of the methodology described in this paper.

In particular, this methodology can be suitable for future missions (GMES Sentinel-2, FORMOSAT-2, VENUS, etc…) which will have better radiometric stability and narrower bands than Landsat but, more importantly, will ensure both the high spatial and temporal resolution necessary for most agricultural landscapes.

CHAPTER 4:
LAI AND CHLOROPHYLL RETRIEVAL USING MULTITEMPORAL MERIS DATA

In **Chapter 3** the LAI was obtained by applying a simple inversion method to the PROSPECT+SAIL model and LANDSAT-TM data, with good results. As it was discussed the use of the temporal dimension could be a further improvement in the retrievals. The objective of this chapter is to investigate the possibilities of retrieving, jointly, LAI and Leaf Chlorophyll content in agricultural fields, taking profit as much as possible, of the information contained in multi-temporal data. This is done, by adding a temporal constraint in the inversion procedure. Among the possible inversion methods, a direct search numerical method was selected because the temporal constraint was easy to implement in such a method. ENVISAT-MERIS data were preferred to other data like LANDSAT-TM because of its higher temporal frequency in spite of its lower spatial resolution. The method is applied to the area of Barrax (Spain) with a focus on small grain cereal fields.

4.1. Description of the methodology with multi-temporal constraints.

Formalism of the approach:

The methodology developed in this chapter consists of introducing temporal constraints on the parameters to be inverted. A temporal constraint is an additional condition in time that the inverted variables must follow to be considered as a valid inversion result. In this way, the use of the temporal dimension is done during the inversion procedure. This approach is different of Koetz et al., (2005). In their approach, the temporal constraint (a semi-mechanistic model of LAI) is applied as a refinement of the inversion of the radiative transfer model.

In the case of LAI the constraint that was adopted is a curve that is a function of the date of the year (DOY) and five parameters (**Figure 4.1**):

$$LAI = p_1\left(\frac{1}{1+e^{p_2(DOY-p_3)}} - \frac{1}{1+e^{p_4(DOY-p_5)}}\right) \qquad \text{[Eq. 4.1]}$$

Similar LAI curves have been used by Koetz et al., (2005) but as a function of the degree-day instead of the DOY. Analogously to the LAI case, other temporal curves can be used for the rest of variables to invert.

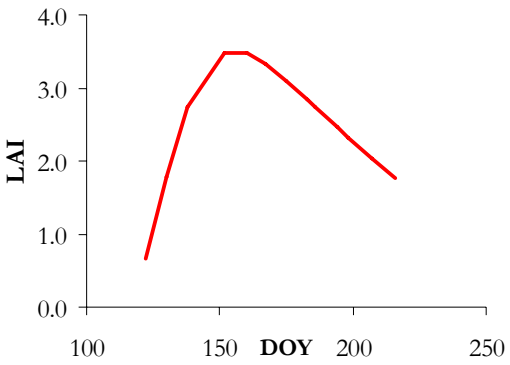

Figure 4.1. LAI typical curve

In the multi-temporal

approach, a merit function (cost function) is constructed using all the MERIS spectra acquired along the season. For instance, if the temporal constraint is only applied to LAI, this would result in the following merit function, K (the function to minimize during the inversion):

$$K = \sum_{i=1}^{n} \sum_{\lambda=1}^{11} (\rho_{i\lambda}^{MODEL} - \rho_{i\lambda}^{MERIS}) \qquad \text{[Eq. 4.2]}$$

where $\rho_{i\lambda}^{MODEL} = f(N_i, c_{m_i}, c_{w_i}, Chl_i, p_1, p_2, p_3, p_4, p_5, DOY)$

In **Equation 4.2**, the sum in i is done for the number of dates, and the sum in λ is done for the MERIS bands. Only 11 of the 15 MERIS bands were used, rejecting those bands that are less accurate because of noise. **Equation 4.2** shows explicitly that with the inclusion of the constraint, instead of inverting a LAI value for each date, the inversion is done for the 5 parameters that determine the curve followed by the LAI during the crop season.

The last part of the methodology consists in a minimization of the merit function of **Equation 4.2** using a numerical algorithm. In this study, the Powell's algorithm, described afterwards, was used.

The use of a temporal constraint is justified for LAI and Chlorophyll, as both variables show a smooth temporal behaviour (**Figures 4.2** and **4.3**).

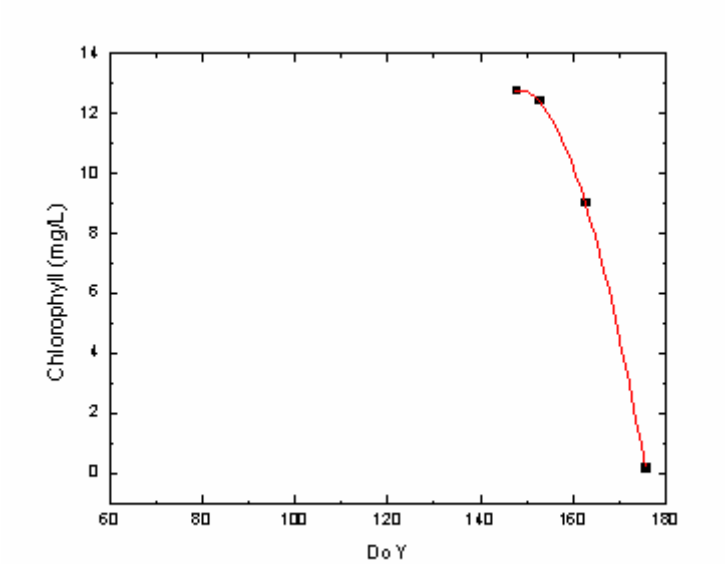

Figure 4.2. Leaf Chlorophyll content of wheat at Barrax in 2003 (Eva Rubio et al., unpublished data)

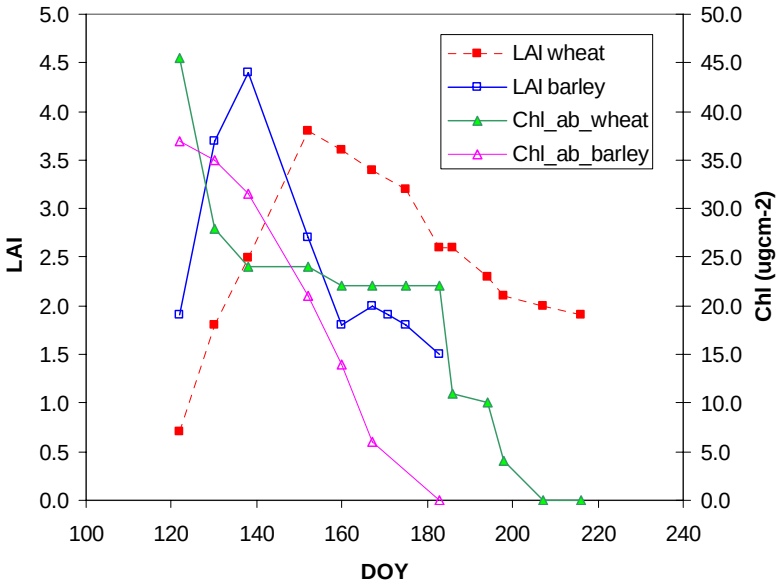

Figure 4.3. LAI and Leaf Chlorophyll measurements in a wheat and barley field (Kneubühler, 2002).

Selected numerical inversion method:

Iterative numerical techniques have been widely used in remote sensing (Privette et al., 1996; Pinty et al., 1990; Bacour et al, 2002). The most commonly used methods are the downhill simplex method or AMOEBA (Press et al., 1992), the conjugate direction set method, or Powell's method (Press et al., 1992) and the quasi-Newton method from the NAG algorithm (Numerical Algorithm's Group 1990). Those methods are relatively easy to implement and do not require any additional training as for instance needed in Neural Networks. The disadvantages are that these methods are time consuming and thus not very convenient for operational implementation. Also, depending on the initial conditions, these algorithms may find a local minimal, instead of the global minimum.

Among the direct-search methods, we have chosen the Powell method as it is said to have a fast convergence and allows for minimization of a high number of variables. The Powell's method searches for the minimum of a function in N dimensions through successive minimization. The basic idea behind Powell's method is to threat the N dimensional minimization as separate one-dimensional minimization problems. The minimization of the N dimensional function is done in one dimension at a time using a method of one-dimensional minimization, such as Brent's Method. Powell's minimization method starts from a set of directions in the multidimensional space, finds the minimum in each direction and evaluates the good performance of each direction. Then, starting from the minimum found in the previous direction, it chooses new search directions. An adjustable parameter in Powell's method is the fractional tolerance, τ. This parameter determines the convergence criteria: failure to decrease the gradient by the fractional tolerance the algorithm will

stop. Setting the fractional tolerance to a very small value can extremely increase the computation time without improving the results. The appropriate τ will depend on each problem.

4.2. Test with simulated data.

The methodology was tested first with synthetic data, previously to the application to MERIS data. In this section the results corresponding to a particular case are shown as an example. Synthetic data were generated using the LAI and Chlorophyll profiles **from Figure 4.2** and **Figure 4.3**, generating 13 dates of MERIS-like spectra (**Figure 4.4**). Inversions were done in the following way:

- A temporal constraint for LAI is assumed.
- No temporal constraint is applied to the Chlorophyll.
- All the other variables of the PROSPECT+SAIL model were fixed.
- Two cases or initial conditions were chosen for LAI, named IC-1 and IC-2. The case IC-1 corresponds to an unfavourable situation (IC far from the solution), while the case IC-2 is closer to the real solution.
- Initial conditions (IC) for Chlorophyll were set to Chl=40 for all dates.

A total number of 18 variables were inverted (5 from LAI curve, and 13 for Leaf Chlorophyll Content) using 13x11=148 MERIS spectral bands. Results are displayed in **Figure 4.5**.

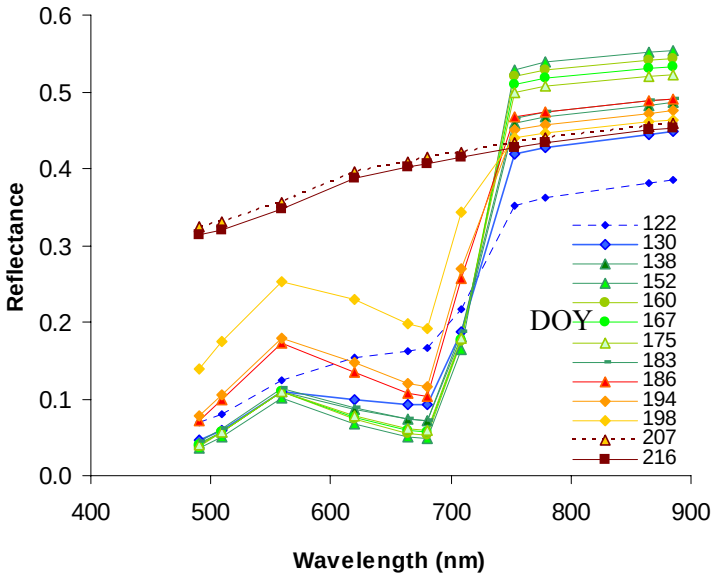

Figure 4.4. Simulated spectra using measurements of LAI and Leaf Chlorophyll Content.

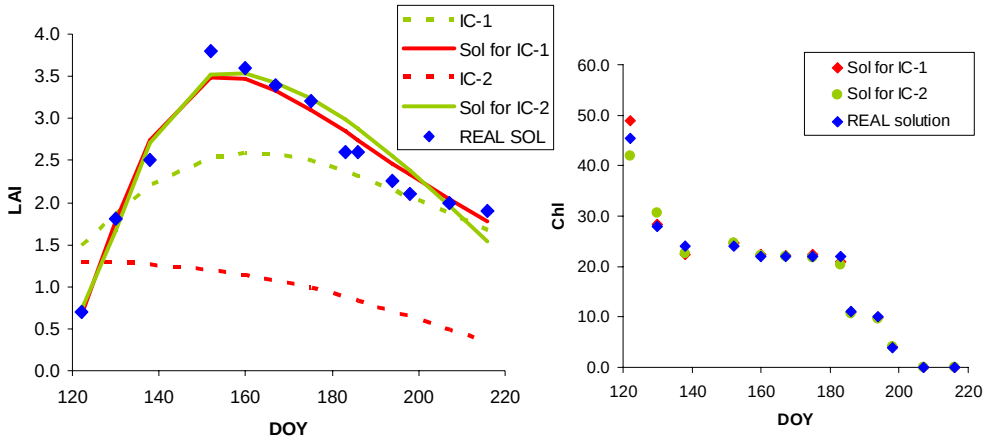

Figure 4.5. LAI curves and Chlorophyll values at each date inverted from MERIS-like simulated spectra, assuming a temporal constraint for LAI.

In the ideal case, the method performed very well. The 18 variables are well retrieved, even in the case in which initial conditions were far for the solution.

In order to test the sensitivity of the method to possible perturbations, the same example was analysed adding noise to the data. A 10% of Gaussian noise was added to the data, both in an additive and multiplicative way. Those two noise terms were correlated. This corresponds to a very unfavourable situation (see **Figure 4.6** in comparison with **Figure 4.4**).

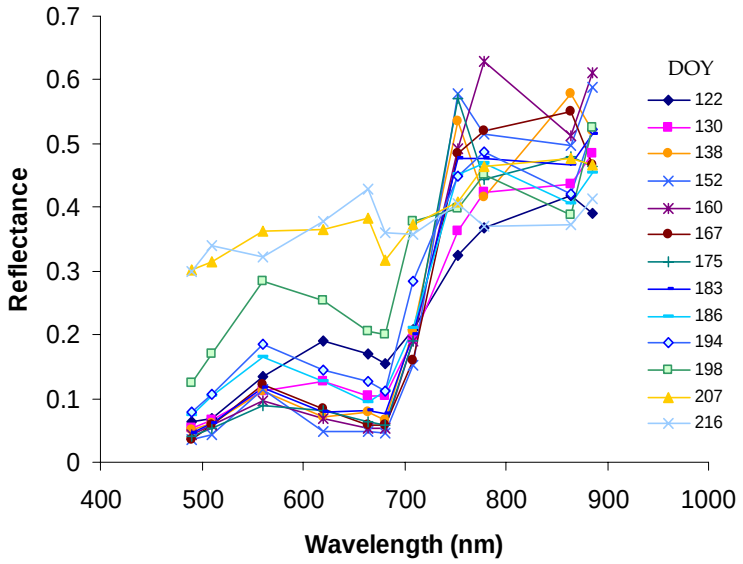

Figure 4.6. Simulated noisy spectra to be inverted.

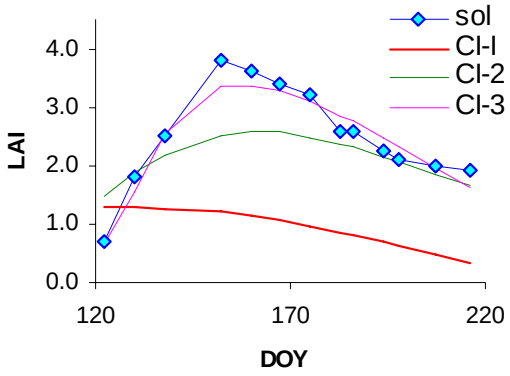

Figure 4.7. Three initial conditions (CI-1, CI-2, C1-3) and real solution (soil) corresponding to the simulation with noisy data.

Inversions were done with a constraint on the LAI and without constraint for the Chlorophyll, as in the example without noise. The initial conditions for the Chlorophyll were set to 40ug/cm2 for all dates. Three cases of LAI initial conditions (those shown on **Figure 4.7**) were tested. **Figure 4.7**. **Figure 4.8** presents the obtained results. In **Figure 4.8** Chlorophyll is well retrieved with a very good accuracy, with the exception of the fist date, and for the three tested cases of LAI IC. LAI curves are also well retrieved, but the results are more influenced by the LAI IC than Chlorophyll does.

This analysis using synthetic data has permitted to test the methodology. Two main conclusions can be given: first, the method appears to be robust to the presence of noise. The second conclusion is that with noisy data the choice of initial conditions may affect the results, although the results obtained with a very unfavourable situation were still satisfactory. In summary the results for LAI and Chlorophyll retrievals using simulated data, were encouraging.

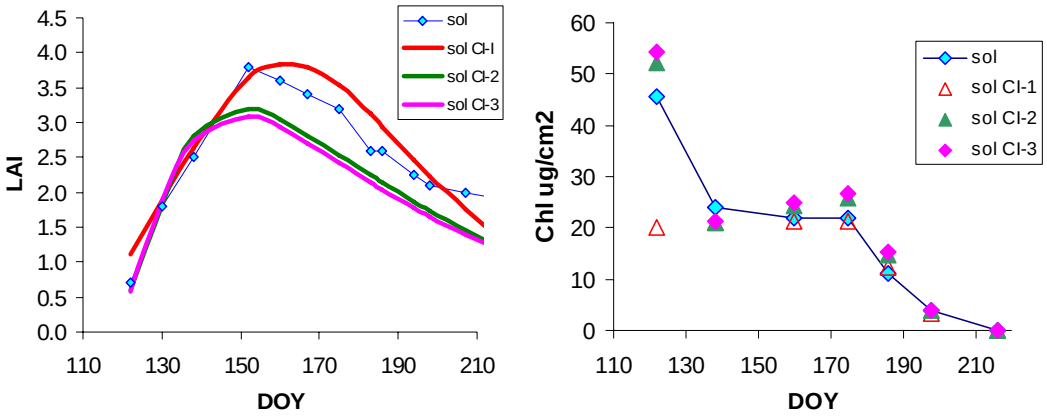

Figure 4.8. LAI curves and Chlorophyll values at each date inverted from nosy simulated spectra, assuming a temporal constraint for LAI.

4.3. Analysis of the first results with MERIS data.

In this section results using MERIS data are presented. **Table 4.1** lists the complete series of MERIS-FR images used in this study. Results with the multi-temporal method are compared to date-to-date inversions.

4.3.1 Selection of "pure" vegetation pixels.

For the application of the method we need to detect homogeneous pixels corresponding to agricultural fields. Even though in the area of Barrax the fields have a dimension of more that 1Km long, co-registration errors made difficult to find pixels that could be considered homogeneous. MERIS spectra to be inverted were selected on the basis of the NDVI. Only pixels that showed a smooth NDVI profile were analysed. Some examples are shown in

Figure 4.9 together with the corresponding Landsat NDVI profile from the same field.

Date	DOY	Date	DOY
12/03/2003	71	17/07/2003	198
06/04/2003	96	26/07/2003	207
13/04/2003	103	30/07/2003	211
02/05/2003	122	08/08/2003	220
12/05/2003	132	09/08/2003	221
14/05/2003	134	12/08/2003	224
27/05/2003	147	14/08/2003	226
31/05/2003	151	18/08/2003	230
12/06/2003	163	25/08/2003	237
18/06/2003	169	31/08/2003	243
19/06/2003	170	12/09/2003	255
01/07/2003	182	16/09/2003	259
05/07/2003	186	18/09/2003	261
11/07/2003	192	05/10/2003	278
14/07/2003	195		

Table 4.1. List of MERIS-FR data used in this study.

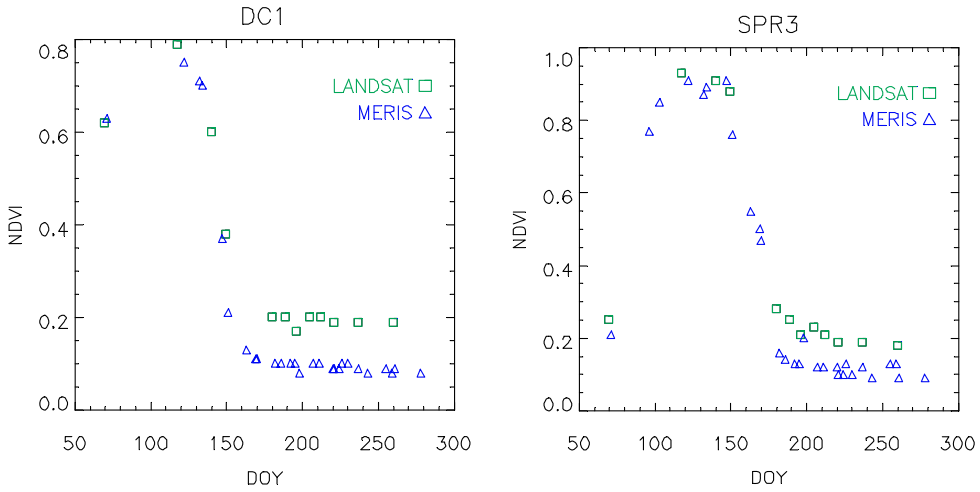

Figure 4.9. Examples of MERIS NDVI profiles. MERIS spectra to be inverted have been have been selected with the criteria of smooth NDVI profiles. Landsat NDVI for the same field is also plotted for comparison. DC is a non irrigated small grain cereal and SPR is a spring irrigated small grain cereal.

4.3.2 Background soils.

The geometry of observation for MERIS acquisitions can be very different from date to date, thus angular effects in the reflectance can be very important (**Figure 4.10**). The phase angle (sun-observation) explains the biggest part of the variability of the reflectance along the year. Variations in surface reflectance from one date to another can be due to changes in roughness, soil moisture and pixel miss-registration. In order to take into account these possible changes in the image brightness, which is due to the different geometries of acquisitions, a soil spectrum was extracted from a MERIS image at each date. These spectra are used as background soil in SAIL model (**Figure 4.11**).

A more accurate treatment for the changes on brightness of the soil background, would be to couple a BRDF soil model, for instance the Hapke or Minaert models. However, as we have seen in **Chapter 3**, a soil spectrum extracted for each image is still a good approximation in this region.

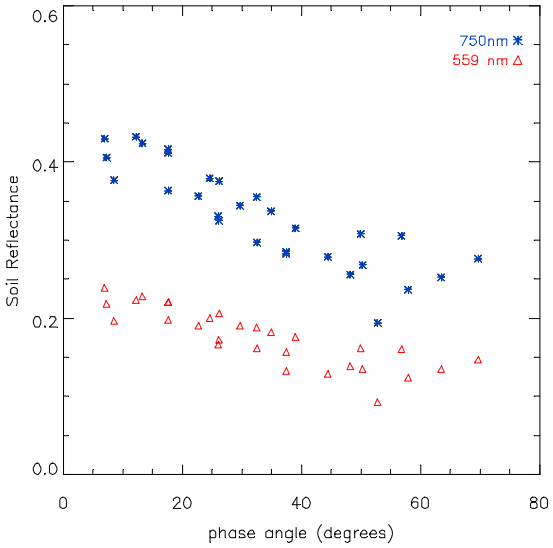

Figure 4.10. Reflectance as a function of the phase angle (angle sun-observation) for a MERIS soil pixel for two wavelength (750 nm and 659 nm).

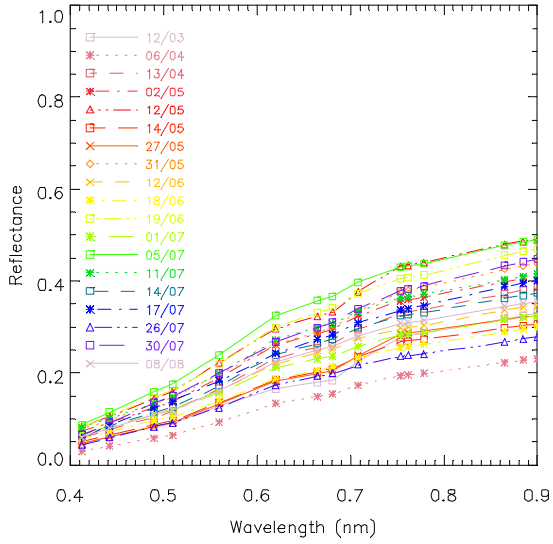

Figure 4.11. MERIS spectra used as soil background in the inversions.

4.3.3 Date-by-date inversions.

In order to compare with the multi-temporal inversions, date-by-date inversions were also done. In this section we present some examples. Additionally, those date-by-date inversions are used to illustrate the problems related to variable compensations. An example corresponding to a spring irrigated small cereal crop (named SPR1) is shown. Inversions were done in this way:

- Inversion is done for LAI and Chlorophyll using 11 MERIS bands. The rest of the model parameters have been fixed to the following variables: N=2.0, dm=0.005, h=0.02, LAD is assumed spherical. Leaf water content does not have any influence in the wavelength range of MERIS so it was fixed to an arbitrary value.
- LAI maximum value is fixed to 6 and Chlorophyll maximum value is fixed to 60ug/cm2. This was implemented by adding a penalty in the merit function.
- Tolerance in Powell was fixed to τ=10-06. An τ=10-03 was also tested giving similar results.
- The initial directions in Powell method were set to the unit directions. Several initial conditions where tested giving the same results for LAI (**Figure 4.12**). Chlorophyll retrievals appeared dependent on the initial conditions only for the first date, where LAI values are very low.

The temporal evolution of LAI obtained form the date-by-date inversion has the expected behaviour, but the Chlorophyll retrievals do not appear to have the appropriate temporal evolution (**Figure 4.12**). Also, LAI

shows saturation for DOY 122 to 134 4, as well as Chlorophyll for many of dates after DOY 150.

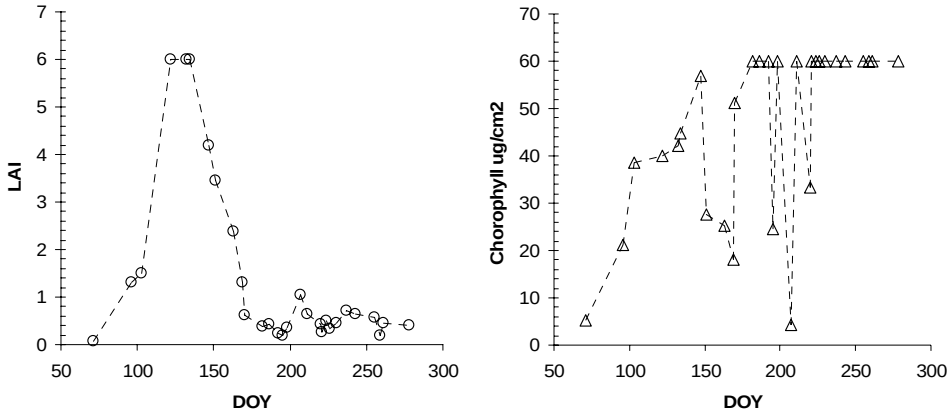

Figure 4.12. Date by date inversion for LAI and Chlorophyll. N=2.0, dm=0.005, h=0.02, LAD is assumed spherical.

Effect of parameter N:

The same inversion was done changing the N parameter from 2.0 to 1.5. Contrary to the findings of Jacquemoud et al., (1995), Chlorophyll retrievals are affected by changes in N parameter. However LAI is not very sensitive to those changes (see **Figure 4.13**). Another observation is that the compensation between LAI and Chlorophyll shows up. For days 4 to 7 is not as evident as LAI is saturated to the maximum value of 6.

Effect of Dry Matter:

Dry matter was changed from 0.005 mg/cm2 to 0.004 mg/cm2. Small changes in dry matter may affect specially the inversions of LAI in the medium range of LAI values (**Figure 4.14**).

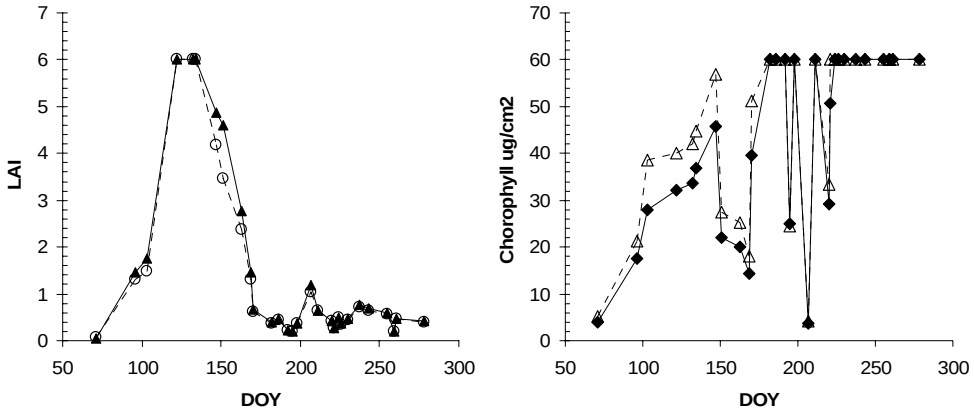

Figure 4.13. Date by date inversion for LAI and Chlorophyll. Solid line corresponds to N=1.5, dashed line to N=2.0. Dm=0.005, h=0.02, and LAD is assumed spherical.

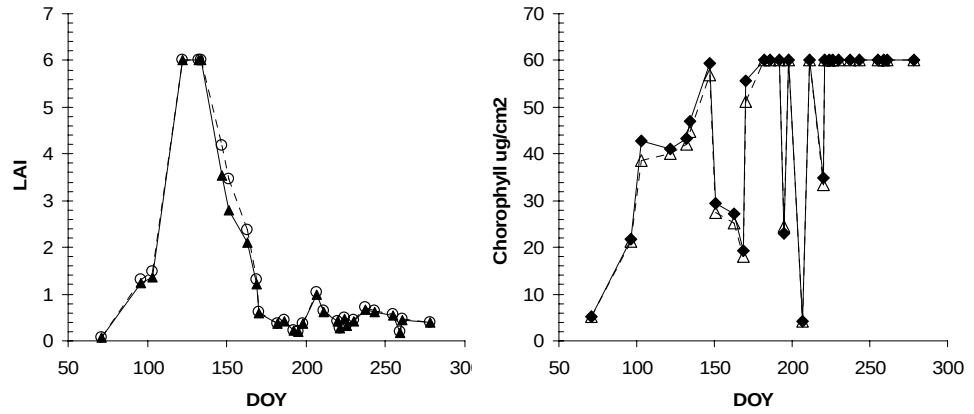

Figure 4.14. Date by date inversion for LAI and Chlorophyll. Solid line corresponds to dm=0.004 mg/cm2, dashed line to dm=0.005 mg/cm2. N=2, h=0.02, and LAD is assumed spherical.

Effect of Leaf Angle Distribution Function parameters:

Finally, the effect of LAD function was analysed, comparing with the moderate planophile and erectophile cases (a=0.5, and a=-0.5 respectively).

LAD is the parameter that has the most important effect on LAI and Chlorophyll inversions (**Figure 4.15**).

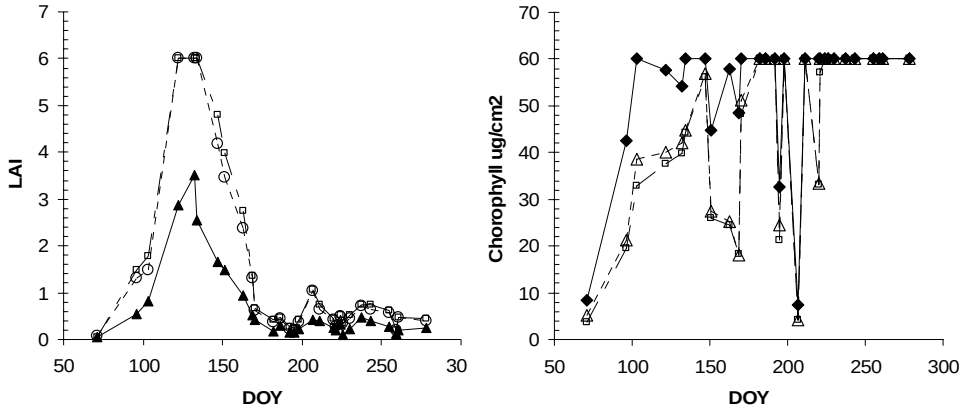

Figure 4.15. Date-by-date inversion for LAI and Chlorophyll. Solid line corresponds to parameter a=0.5, dashed line (triangle symbol) to a spherical LAD and dashed (square symbol) to parameter a=-0.5. N=2, h=0.02.

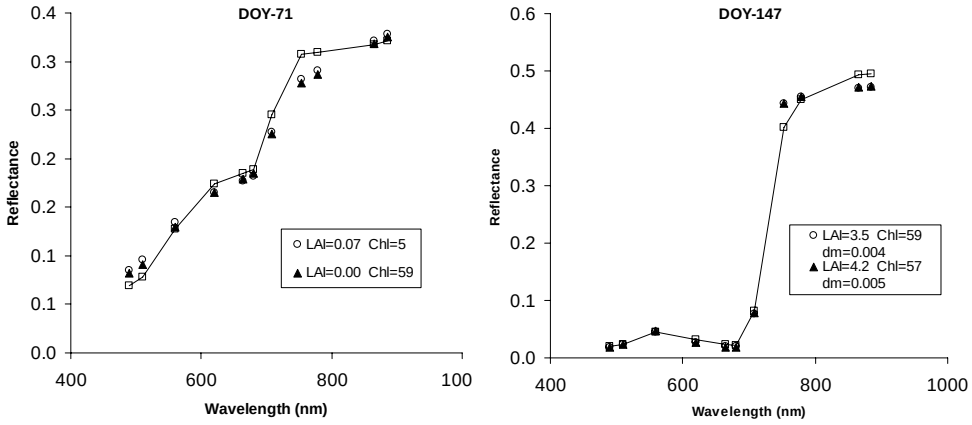

Figure 4.16. Examples of different solutions found during the inversions. Solid line is MERIS spectrum, the other two spectra the solutions found during the inversion.

Main difficulties in the inversions are found at early dates. For very low LAI values, the sensitivity of the reflectance to Chlorophyll is very low:

high Chlorophyll concentrations or very low Chlorophyll concentrations give almost the same spectrum (see **Figure 4.16**). An example of compensation between dry matter and LAI is shown in **Figure 4.16b** and effect of LAD is shown in **Figure 4.17**.

It is noticeable that the model does not seem to be able to properly simulate reflectance in the 753 nm band (red-edge), as can be observed in **Figures 4.16** and **Figure 4.17**.

Finally, for comparison with the next section, an inversion case for field DC1 is presented in **Figure 4.18.**

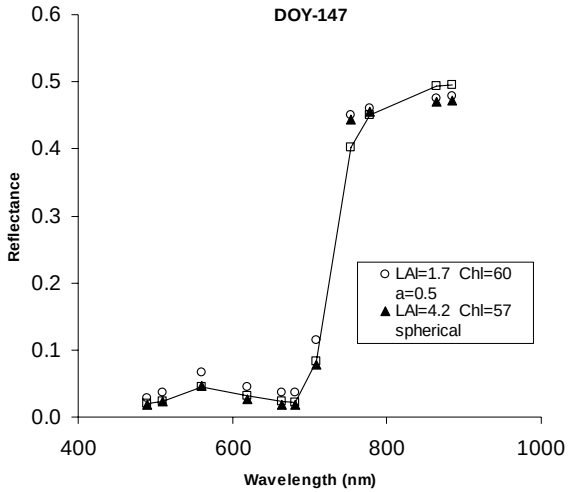

Figure 4.17. Examples of different solutions found during the inversions for different LAD distributions. Solid line is MERIS spectrum, the other two spectra found as solutions.

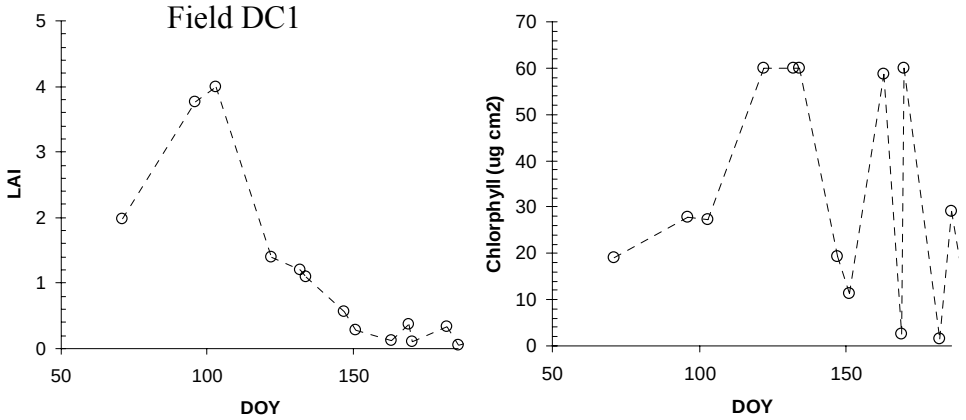

Figure 4.18. Date by date inversion for LAI and Chlorophyll for field DC1. N=2.0, dm=0.005, h=0.02, LAD is assumed spherical.

4.3.4 Results with the multi-temporal method.

Temporal constraint for LAI and Chlorophyll:

A temporal constraint of the type showed in **Equation 4.1** was forced for LAI and for Chlorophyll. All the other parameters of the model were fixed to N=2.0, dm=0.005, h=0.02. The number of variables to invert was 10. Inversions were done for DOY 71 to 186 (13 dates). Tolerance in Powell was fixed to τ=10-06. The initial directions in Powell method were set to the unit directions.

Dependence with LAD:

Six different cases of LAD functions, as shown in **Table 4.2** have been analysed.

	LAD	a
Case 1	27°	0.5
Case 2	63°	-0.5
Case 3	Spherical	
Case 4	56°	-0.3
Case 5	34°	0.3
Case 6	45°	0

Table 4.2. Different LAD used for the inversions

Results are shown for a non-irrigated field of small grain cereal (named DC-1) and 1 spring irrigated field of small grain cereal (named SPR1). Inverted LAI and Chlorophyll are shown in **Figure 4.19**, and the product of both variables is shown in **Figure 4.20**. In those figures, and the following, the initial conditions used are also plotted as well as the LAI inversions from Landsat LUT.

In comparison with the date-by-date inversion (cf. **Figure 4.12** and **Figure 4.18**) we conclude the following:

- in the case of LAI results are not significantly improved. The date of **maximum LAI** is always well identified. For irrigated cereals it is around DOY 130 (end of tillering, in agreement with phenology observations of the area).
- in the case of Chlorophyll, the fact of adding the temporal constraint avoids the divergences that occurred for field DC1 (DOY 163 and 170) and SPR1 (DOY 172 to 186). However, it seems that the obtained values in the senescence period are still overestimated.

The beginning of the cycles is not well described for Chlorophyll case. This can be due to the small number of images in that part of the cycle.

Probably another type of curve would be better for describing the Chlorophyll behaviour. A logarithm type and polynomials of different degrees (from 3 to 5) were tested but results were not improved. Polynomials were found not to be stable for being inverted, as coefficients tend to correlate among them.

Table 4.3 gives the values of the merit function for the solution. It can be seen that the problem is ill-posed as differences in the merit functions are very small.

LAI and Chlorophyll inversion are very dependent on the LAD. The compensation effect between LAI and Chlorophyll is very clear in **Figure 4.19**. The product LAIxChlorophyll is then more stable (**Figure 4.20**) but changes in LAD still affected the results.

		DC	SPR1
	LAD	**Function value**	**Function value**
Case 1	27°	0.517720	**0.353249**
Case 2	63°	***0.468370***	0.381167
Case 3	Spherical	**0.472978**	0.377690
Case 4	56°	**0.475671**	0.358981
Case 5	34°	0.497038	***0.353221***
Case 6	45°	0.486375	**0.354048**

Table 4.3. Values of the Merit Function

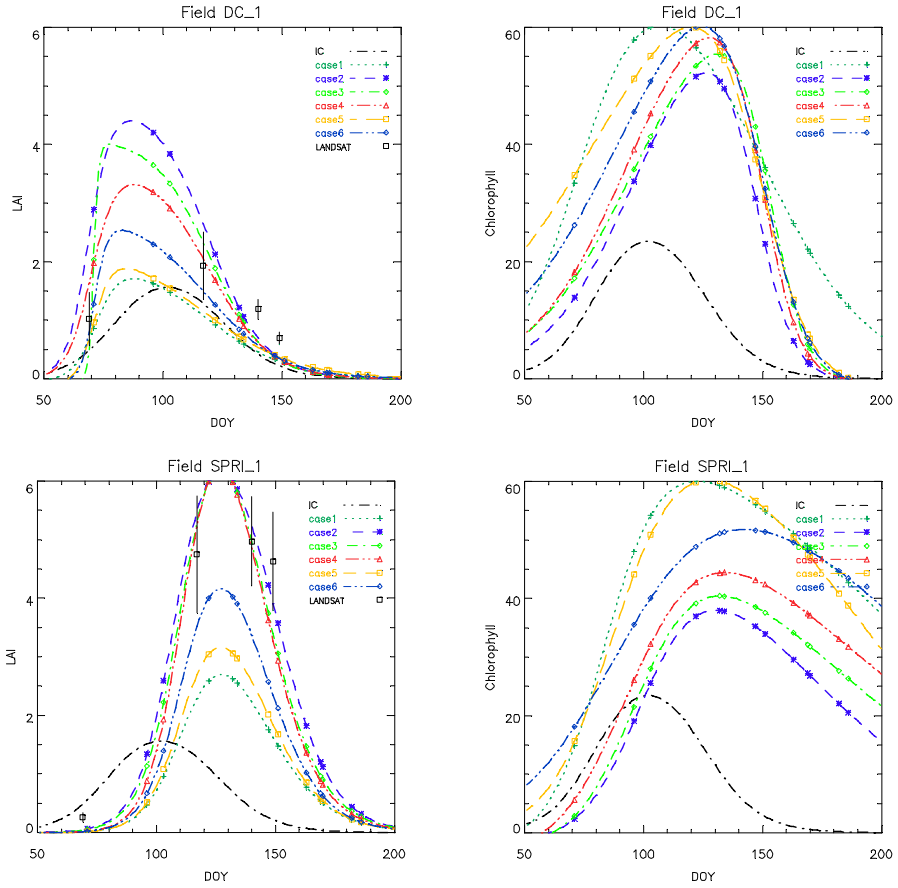

Figure 4.19. Multi-temporal inversions for different LAD functions.

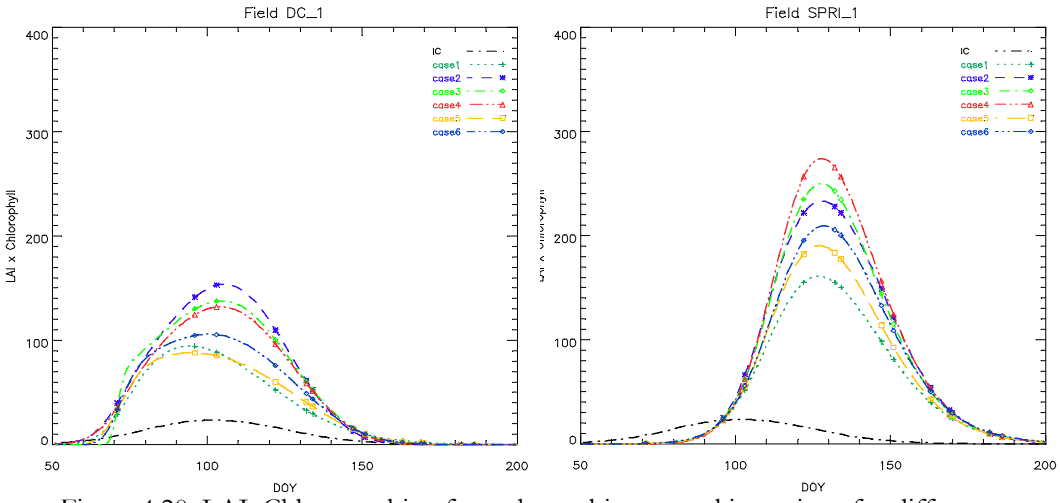

Figure 4.20. LAIxChl as resulting from the multi-temporal inversions for different LAD functions.

For the case of a spherical LAD we have also analysed the effect of, dry matter, the N parameter and the hot spot parameter

The results for the inversions in two fields, DC-1 and SPR-1, are shown in **Figures 4.21** to **Figure 4.24**. The results are compared to the LAI inversion (at four dates) obtained for the same field with the methodology of **Chapter 3**.

Temporal constraint for LAI and LAIxChl:

As it is difficult to choose a temporal constraint for Chlorophyll, it was preferred to apply a temporal constraint for the product LAI x Chlorophyll. That means that the inversion is done for two variables: LAI and LAI x Chlorophyll. A number of ten dates were used for the inversions.

Figure 4.25 shows the results obtained for this multi-temporal inversion on LAI and LAIxChl. The Chlorophyll was obtained dividing LAI x Chl and LAI. For dates before DOY 71 (first image acquisition) results should not be taken into account as they are extrapolated.

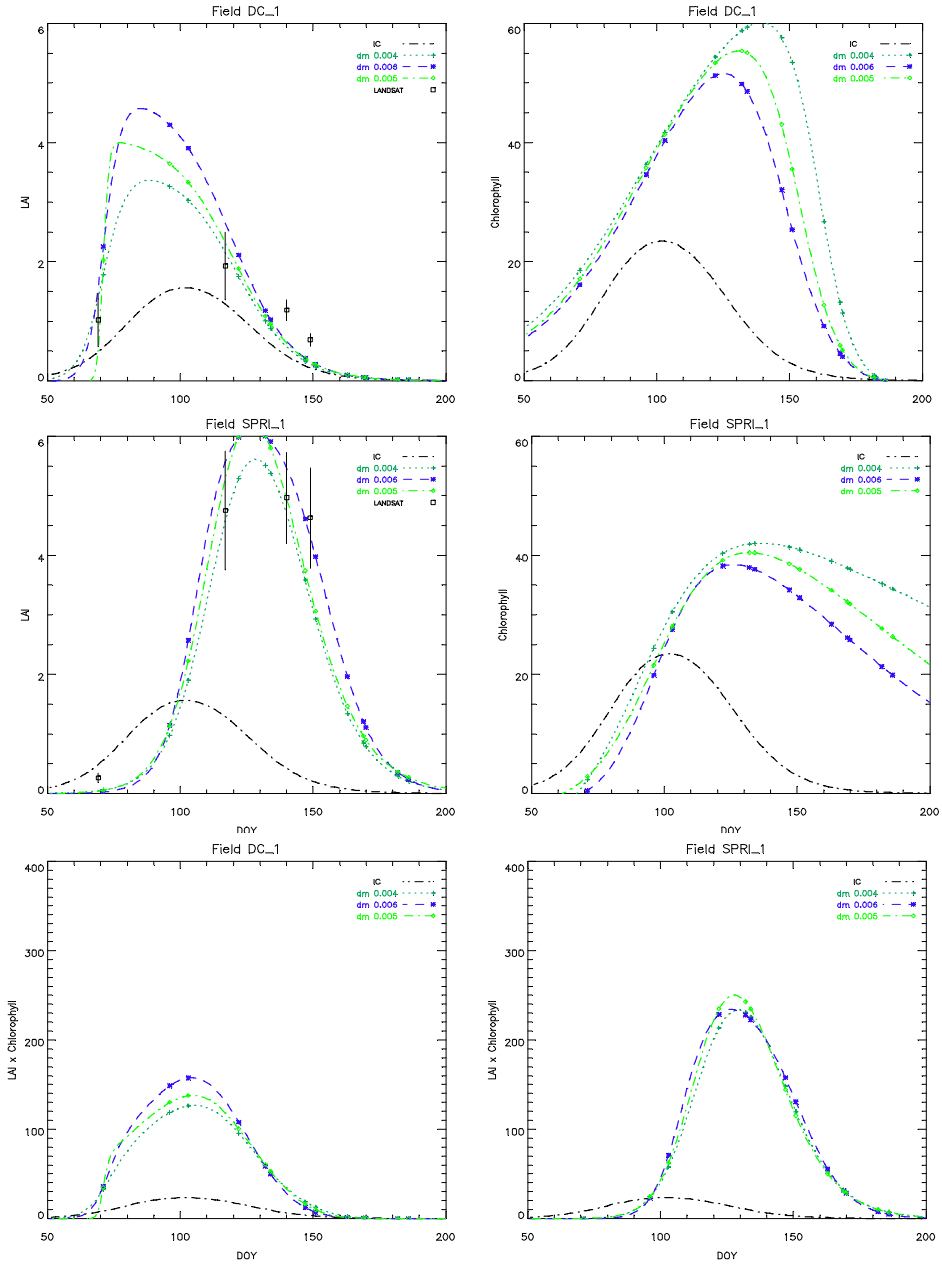

Figure 4.21. Efect of dry matter changes in the LAI, Chlorophyll and LAIxChlorophyll inversions.

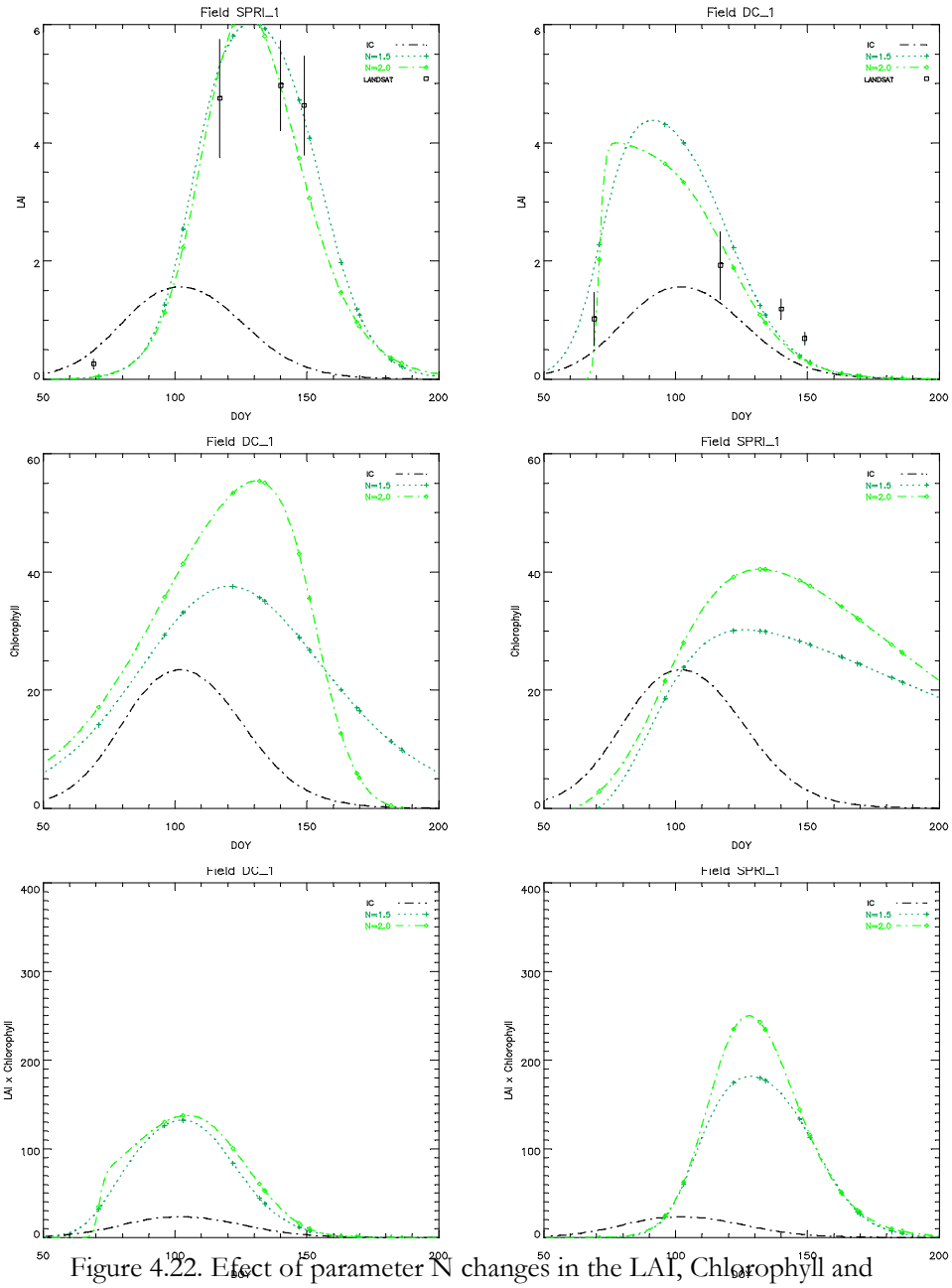

Figure 4.22. Effect of parameter N changes in the LAI, Chlorophyll and LAIxChlorophyll inversions.

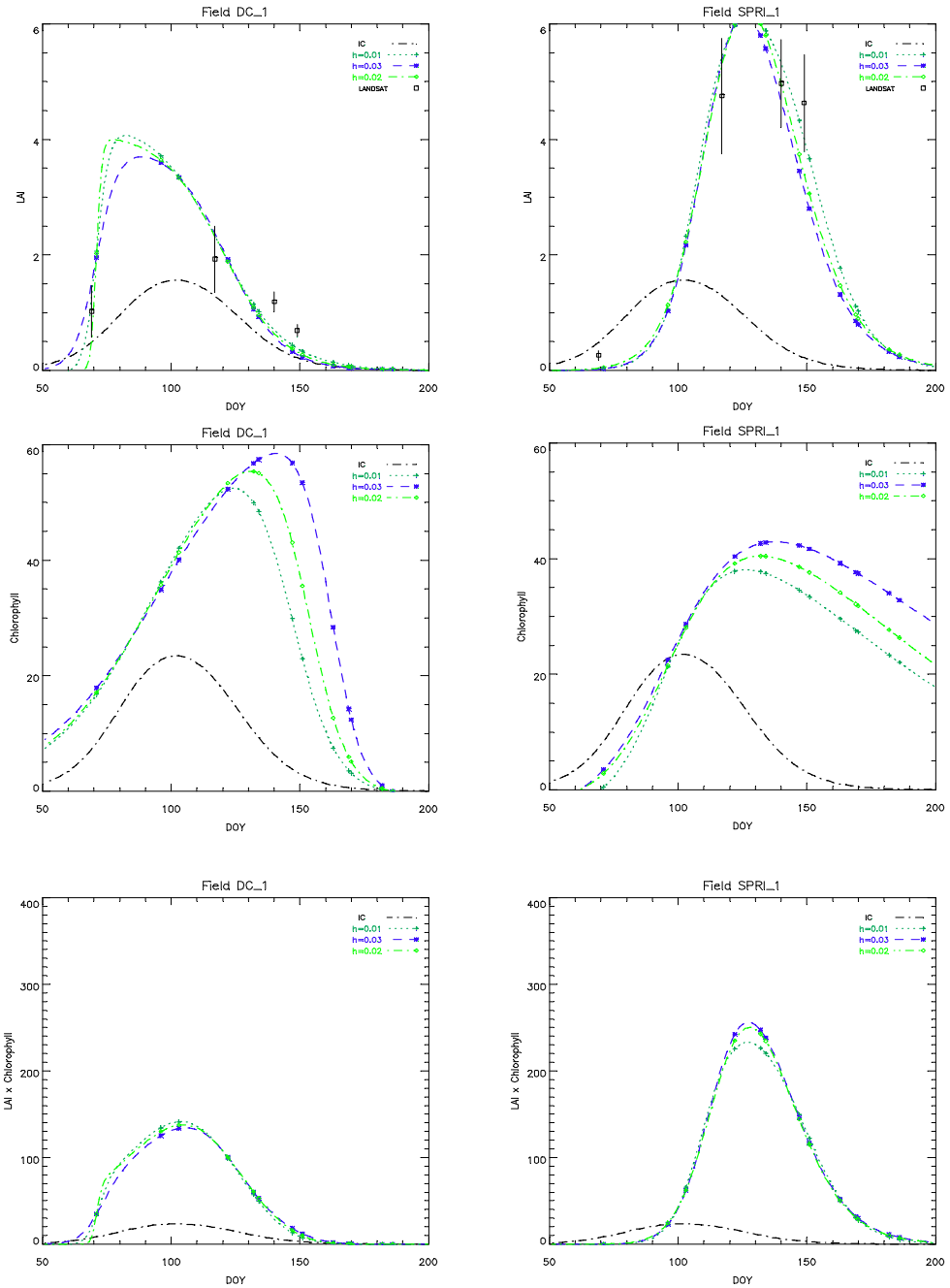

Figure 4.23. Efect of hot spot parameter changes in the LAI, Chlorophyll and LAIxChlorophyll inversions.

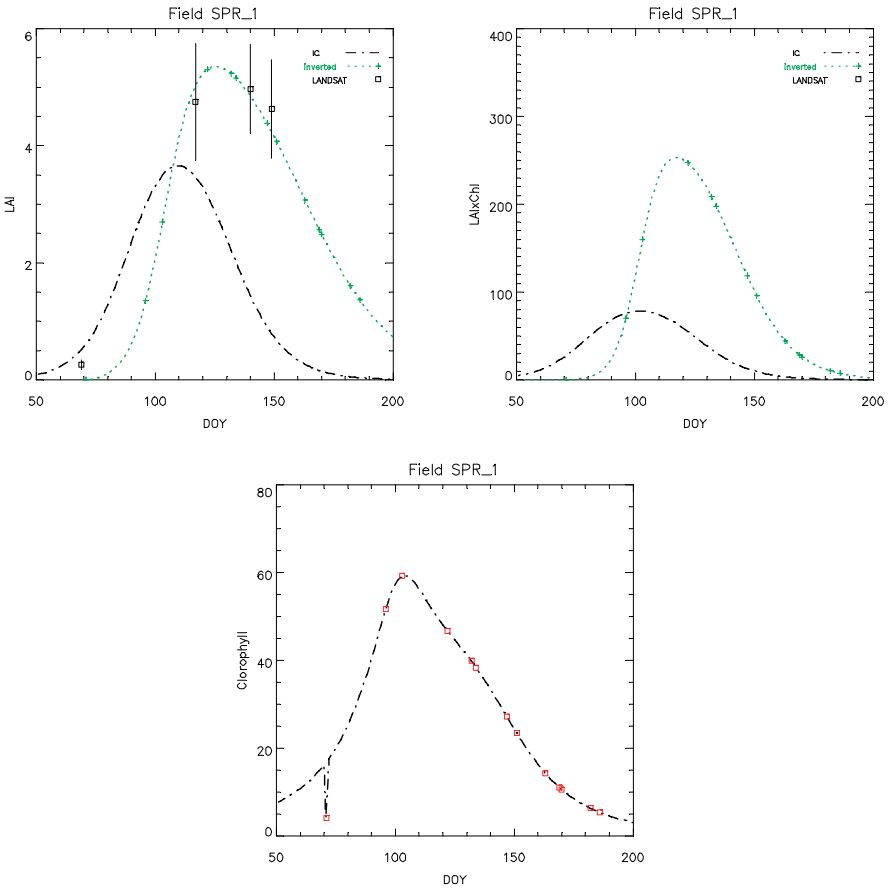

Figure 4.24. Inversion using LAI and LAIXChlorophyll constraint for a summer irrigated spring cereal.

In summary, the results obtained with the multi-temporal method were better than those obtained by the date-by-date inversions. However, at early dates Chlorophyll still seems underestimated. With a higher temporal frequency on that part of the cycle the results would be probably improved. Inversions could be dependent on the initial conditions (see **Figures 4.25** and **Figure 4.26**). For a better performance of the method, initial condition should not be very far from the final inverted value. For instance, initial conditions where LAI and LAI x Chlorophyll maxima are shifted should be avoided.

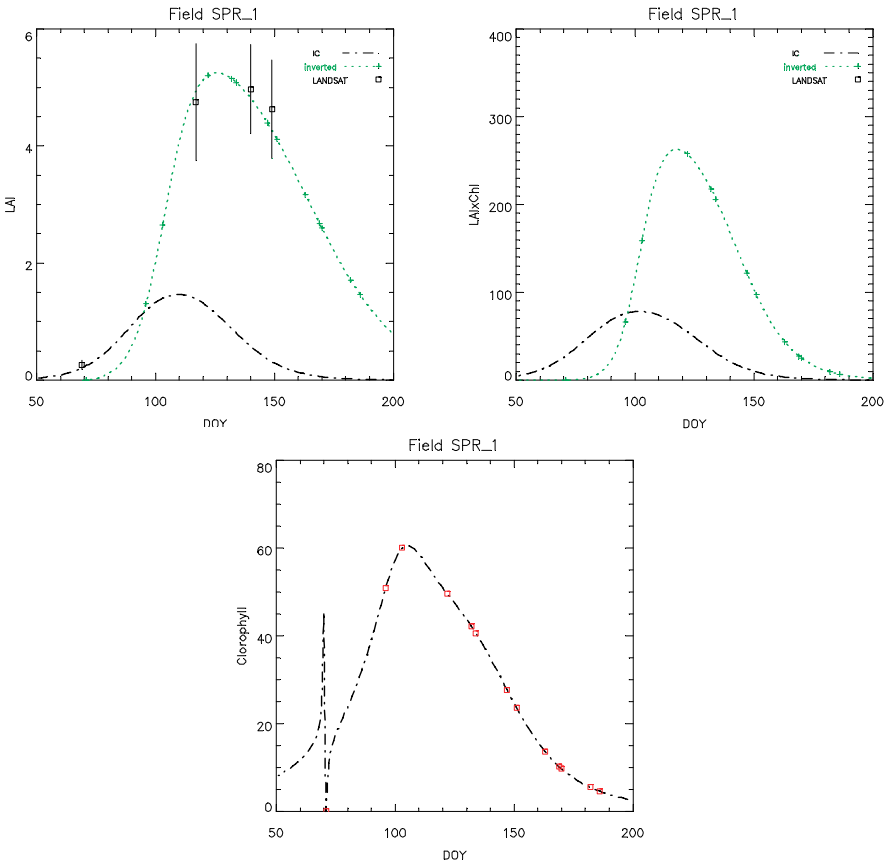

Figure 4.25. Inversion using LAI and LAIXChlorophyll constraint for a summer irrigated spring cereal for another set of initial conditions.

Another conclusion of this analysis is that the knowledge of the LAD parameter is very important. It has been shown that the LAD is the parameter that has the higher influence on the LAI and Chlorophyll inversions. The use of a priori information for characterising an appropriate value of this parameter of the PROSPECT+SAIL is strongly recommended. A better characterisation of this parameter would be of great value for reducing errors in the inversions".

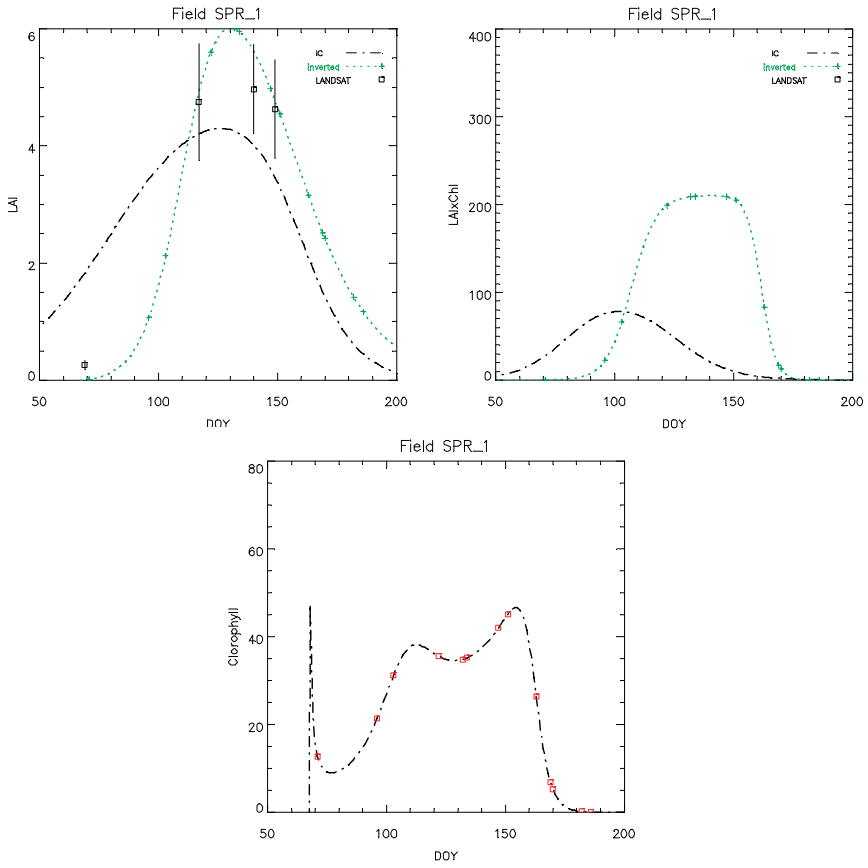

Figure 4.26. Inversion using LAI and LAI x Chlorophyll constraint for a summer irrigated spring cereal for a non-adapted set of initial conditions.

4.4 Discussion and perspectives.

The results on the use of a multi-temporal method to perform inversions of LAI and Chlorophyll are encouraging and present advantages in respect to date-by-date inversions. However, to improve this analysis, some issues related to the retrieval of biophysical parameters using medium-resolution need to be further investigated.

The first issue is related to pixel size. As it was already discussed in **Chapter 3**, the PROSPECT+SAIL model cannot take into account the inhomogeneities of the MERIS pixels. Although the SAIL model, by means of the leaf angle distribution function (LAD), takes into account the influence of the soil spectrum in the vegetation reflectance, this kind of treatment is not sufficient to describe a real MERIS pixel. For instance, it is not possible to take into account a situation in which the canopy covers only half of the pixel. At the resolution of MERIS, SAIL is not able to realistically simulate the spectral mixing between the soil and the vegetation. As a consequence, to be coherent with the assumptions of PROSPECT+SAIL, spectral un-mixing techniques should be applied before the inversions. If, prior to the inversion, the spectra have not been un-mixed, the results of the inversion should be corrected. In a first approximation, the correction could be done by means of the Fraction of Vegetation Cover (FVC) of the pixel. However, this second option would introduce additional errors, due to the non-linearity of the processes. In this study, the un-mixing problem was not addressed, nevertheless the pixels were selected to be as homogeneous as possible. Further research on the use of MERIS data acquired over agricultural areas more homogeneous than Barrax, would allow us to confirm the quality of the methodology, compared to date-by-date inversions.

In this study it was also seen that the co-registration of the images is an important source of noise in the methodology.

Even though the Powell method should be able to invert many variables, it was still necessary to fix the parameters of the model that were not inverted. As it was already discussed in **Chapter 4**, a better selection of the fixed parameters (N parameter, dry matter and LAD) would improve the

results. This could be done if detailed information coming from in-situ data is available.

A further improvement might be obtained by using a different inversion method, for instance, neural networks, even though it is not obvious how the temporal constraint would be introduced in such a method. However, the use other inversion methods would not significantly improve the results if the issues mentioned before, which are more important, are not solved first.

CHAPTER 5:
PHYSICAL BASIS OF ACTIVE RADAR REMOTE SENSING

This chapter gives a brief introduction to the fundamentals of radar remote sensing and to the concepts used in **Chapter 6** and **Chapter 7**.

5.1. Active Radar systems in Earth Observation.

Active Radar Remote sensing measurement:

The most important difference between an active radar remote sensing system (**Figure 5.1**) and an optical passive system (**Figure 2.1**) is that the source of energy is not the sun but a radar antenna placed in a satellite or airplane. Furthermore, the radars are coherent systems. Due to this coherent nature, the radar measurements are the result of constructive and destructive interferences between the signals scattered from individual elements within a resolution cell. As shown in **Figure 5.1** the radar instrument illuminates the observed surface with a radar beam, then the surface scatters the radiation in

many directions and part of it goes back to the radar antenna. Usually, radar systems are mono-static, meaning that the same antenna is used for emission and reception. The spaceborne and airborne systems used for Earth Observation use the aperture synthesis technique and are named SAR's (Synthetic Aperture Radar's). The advantage of the SAR technique, which is based on the Doppler effect, is that it is possible to obtain high spatial resolution in Earth Observation from satellite platforms without using very large antennas.

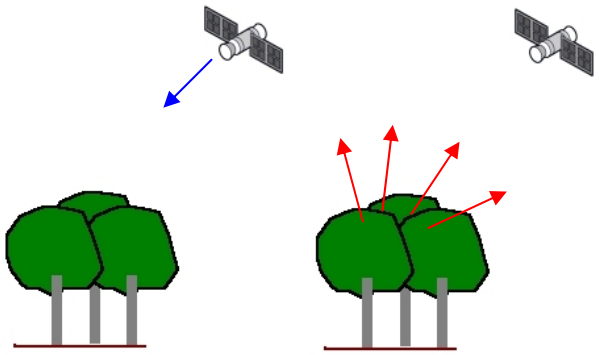

Figure 5.1. Active radar remote sensing system.

Radar frequency range:

Radar instruments transmit and receive radiation in the microwave electromagnetic spectrum region, which ranges approximately from 0,3 GHz to 100 GHz in frequency (**Figure 5.2**) or from 100 cm to 0.3 cm in wavelengths. Traditionally, the microwave region has been divided in frequency bands. The radar bands used in Earth Observation are the following: X (centred at around 9.4 GHz, 3.2 cm in wavelength), C (centred at around 5.3 GHz, 5.6 cm in wavelength), L (centred at around 1.25 GHz, 24 cm in wavelength) and P (centred at around 0.5 GHz, 60 cm in wavelength).

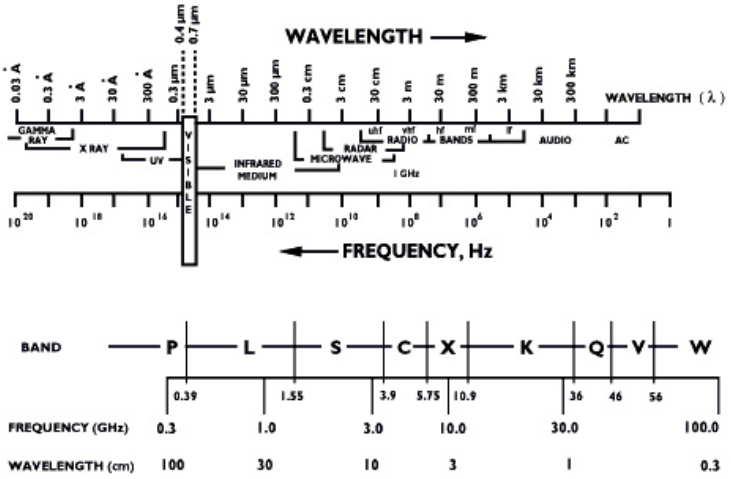

Figure 5.2. Electromagnetic spectrum and location of the microwave bands. (Source: http://earth.esa.int/).

Atmospheric effects:

An important difference between the optical and the microwave region is that, at microwave wavelengths the effects of the atmosphere can be usually neglected. Microwave radiation is insensitive to atmospheric aerosols and only weakly affected by atmospheric constituents, like water vapour. The presence of clouds or precipitation may also affect the microwave signal, depending on the frequency. In general, the effects of the atmosphere are not important for frequencies below the X band. This is an advantage of radar sensors compared to optical sensors: backscattering measurements are independent of weather conditions (clouds, rain) or changes in the characteristics of the atmosphere (aerosols variability or water vapour changes). However, atmospheric constituents have an effect on the phase of the signal, which is measured in radar interferometry.

Wave polarisation:

The polarisation is an important property of electromagnetic radiation, which influences scattering. To describe polarisation it is necessary to consider the vector nature of electromagnetic fields. Electromagnetic radiation consists of an electrical field, which is vibrating in a plane perpendicular to the direction of propagation, and a magnetic field, which is perpendicular to the electrical field. In a general case, when the electric vector of a plane wave is propagating in the $\vec{k}$ direction, the electrical field vector will lie in the X-Y plane perpendicular to $\vec{k}$. The propagating field therefore consists of two components: a X component and a Y component, and can be expressed as:

$$\vec{E}(k) = E_X(k)\vec{x} + E_Y(k)\vec{y} \qquad \text{[Eq. 5.1]}$$

The electrical field vector $\vec{E}(k,t)$ describes an ellipse in the X-Y plane while propagating. For certain values of E_X and E_Y the ellipse degenerates into a circle or a straight line. In these cases the polarisation is said to be circular or linear. Otherwise it is elliptical.

Linear and circular polarisations are the most used polarisation states in radar remote sensing. When the electric field is vibrating perpendicularly to the incidence plane (which is defined by the direction of propagation and a vector normal to the Earth's surface) the wave is said to be linear polarized in H polarisation. If the electric field is vibrating parallel to the incidence plane the wave is said to be linear polarized in V polarisation. In physical sciences, this fields were originally called parallel and perpendicular, but in remote sensing is it usual to use the terms vertical and horizontal. When the electric field is rotating clockwise, as seen by an observer towards whom the wave is

moving, the wave is said to be right-hand circularly polarized. If it is rotating counter-clockwise, it is left-hand circularly polarized (see **Figure 5.3**).

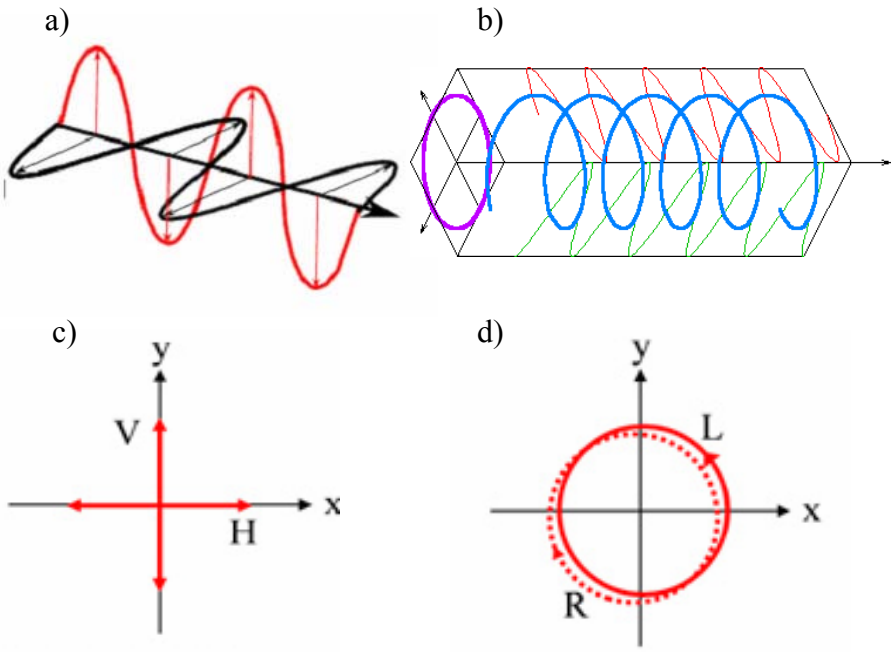

Figure 5.3 a) Propagation of a linear polarized wave b) Propagation of a Circular polarized wave c) Horizontal and vertical linear polarisations as seen by an observer placed perpendicularly to the direction of propagation d) Left and right circular polarisations as seen by an observer placed perpendicularly to the direction of propagation.

The polarisation state of a plane wave can be parameterised in a number of different ways, for instance using the geometric parameters of the ellipse described by the electrical field: the orientation angle, ψ and the ellipticity angle, χ (**Figure 5.4**).

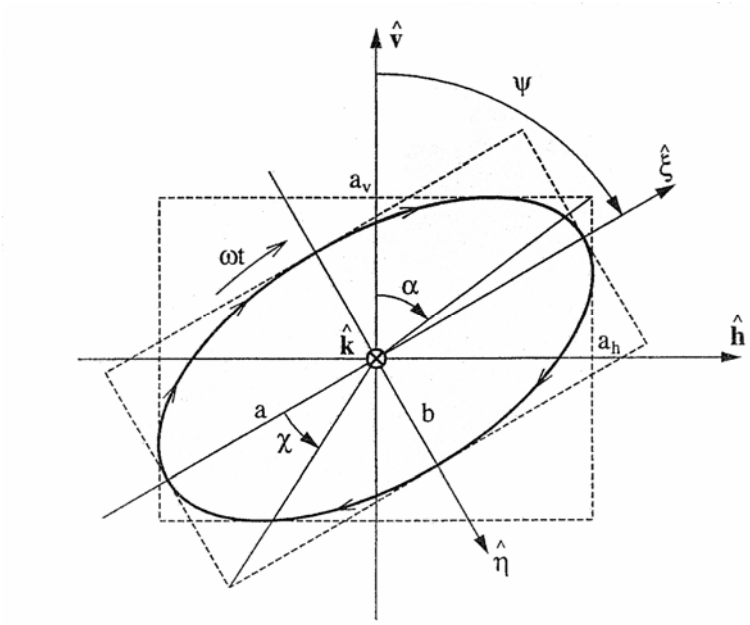

Figure 5.4. Polarisation ellipse.

An alternative representation of the polarisation state is the Stokes formulation, which is very common in optics and radar. The Stokes vector is defined as:

$$S = \begin{bmatrix} I \\ Q \\ U \\ V \end{bmatrix} = \begin{bmatrix} \left|E_H\right|^2 + \left|E_V\right|^2 \\ \left|E_H\right|^2 - \left|E_V\right|^2 \\ 2\Re\left(E_H E_V^*\right) \\ -2\Im\left(E_V E_V^*\right) \end{bmatrix} \qquad \text{[Eq. 5.2]}$$

where E_H and E_V are the components of the electric field in the $\vec{h}$ and $\vec{v}$ direction respectively.

Scattering matrix:

The polarisation state of a wave arriving to a surface, $\vec{E}^i$, and the polarisation state of the wave scattered by the surface, $\vec{E}^s$, can be related as follows:

$$\begin{pmatrix} E_H^s \\ E_V^s \end{pmatrix} = \begin{pmatrix} f_{11} & f_{12} \\ f_{21} & f_{22} \end{pmatrix} \begin{pmatrix} E_H^i \\ E_V^i \end{pmatrix} \qquad \text{[Eq. 5.3]}$$

The matrix relating the two states depends on the characteristics of the surface in the directions of incidence and scattering, as well as to the distance to the observer. For waves propagating in the far field, the electric field has the behaviour of a spherical wave and then, its dependence with the distance is of the form:

$$G(r) = \frac{e^{-ikr}}{kr} \qquad \text{[Eq. 5.4]}$$

Then, the previous equation can be expressed as:

$$\begin{pmatrix} E_H^s \\ E_V^s \end{pmatrix} = G(r) \begin{pmatrix} S_{HH} & S_{HV} \\ S_{VH} & S_{VV} \end{pmatrix} \begin{pmatrix} E_H^i \\ E_V^i \end{pmatrix} \qquad \text{[Eq. 5.5]}$$

The matrix of elements S_i is named scattering matrix. It is dimensionless and does not depend on the distance. It can also be expressed using the Stokes formulation. If the scattering matrix is known it is possible to compute the response of the target to any combination of incident and received polarisations. For instance, circular polarisations can be expressed as follows (Henderson, 1998):

$$S_{RR} = jS_{HV} + \frac{1}{2}(S_{HH} - S_{VV})$$
$$S_{LL} = jS_{HV} - \frac{1}{2}(S_{HH} - S_{VV}) \qquad \text{[Eq. 5.6]}$$
$$S_{RL} = \frac{j}{2}(S_{HH} + S_{VV})$$

Covariance matrix:

Different matrices can be derived from the scattering matrix, for example, the covariance or the coherency matrices. The covariance matrix, C, represents the average properties of a group of resolution elements. For a natural surface, reciprocity is applied, that is $S_{HV} = S_{VH}$, and then, the covariance matrix is defined as follows:

$$C = \begin{pmatrix} \langle S_{HH}S_{HH}^* \rangle & \langle S_{HH}S_{HV}^* \rangle & \langle S_{HH}S_{VV}^* \rangle \\ \langle S_{HV}S_{HH}^* \rangle & \langle S_{HV}S_{HV}^* \rangle & \langle S_{HV}S_{VV}^* \rangle \\ \langle S_{VV}S_{HH}^* \rangle & \langle S_{VV}S_{HV}^* \rangle & \langle S_{VV}S_{VV}^* \rangle \end{pmatrix} \qquad \text{[Eq. 5.7]}$$

In Eq. 5.7, the symbols $\langle\ \rangle$ denote averaging, and * denotes the complex conjugation. S_{mn} is the complex scattering amplitude for transmit polarisation m and receive polarisation n.

Coherency matrix:

The coherency matrix, T, results from a linear combination of the elements of the scattering matrix (Cloude and Pottier, 1997):

$$T = ww^H \qquad \text{[Eq. 5.8]}$$

where ^{H} denotes conjugate transpose, and w is:

$$w = (S_{HH} + S_{VV}, S_{HH} - S_{VV}, 2S_{HV}) \quad \text{[Eq. 5.9]}$$

The eigenvalues and eigenvectors of the coherency matrix are the basis of several polarimetric features: entropy (H), angle alfa (α), and anisotropy (A), which are not used in this study.

Frequency and polarisation in SAR systems.

A SAR is usually designed to transmit and receive horizontally or vertically polarized signals, combined as HH, VV or HV: the first refers to the polarisation state of the emitted wave and the second to the received wave. The case HV is also named as cross-polarisation. Non-fully polarimetric radars only measure the amplitude of the signal. Fully polarimetric radars receive and transmit SAR data in two orthogonal polarisation states and, at the same time, they measure the relative phase between the states. In this way fully polarimetric instruments measure the scattering matrix.

The amplitude and the phase, as it will be explained later, are a function of the dielectric and geometric properties of the scattering medium.

Until recently, radar satellites measured only single linear polarisation states (see **Table 5.1**). Polarimetric instruments were only available in airborne systems like JPL-AIRSAR.

Frequency is an important characteristic of the radar signal because scattering interactions depends on the relation between the wavelength, the scatters size and the number density of the scatters. Frequency also determines the penetration distance, longer wavelengths being more penetrating than shorter.

In vegetation studies, the choice of wavelength is done according to the dimensions of the observed scatters (leaves, branches, stalks) from which

information is to be retrieved. For example, to obtaine information on the biomass in trunks and branches of forest trees, L band (24 cm) and P band (60 cm) are used. X and C bands (3-5 cm wavelength) are more suitable than L and P bands for agricultural applications because the typical size of leaves and stems is of the order of several centimetres. As satellite X band was not available till 2007 (see **Table 5.1**) this sutdy focuses on the C-Band region.

SAR radar satellites:

Table 5.1 presents the frequency and polarisation characteristics of the present satellite systems as well as the mission nationality and dates. When the polarisation is not indicated it refers to a fully polarimetric system.

Mission	**Frequency-polarisation**	**Nationality/agency and mission dates**
PALSAR	L	Japan, January 2006
JERS-1	L-HH	Japan, 1992-1998
SIR-C	L	NASA, Apr & Oct 1994
ERS-1	C-VV	ESA, 1991-2000
ERS-2	C-VV	ESA, 1995-
Envisat/ASAR	C-dual pol.	ESA, 2002-
RADARSAT-1	C-HH	Canada, 1995-
RADARSAT-2	C	Canada, Dec 2007
SIR-C	C	NASA, Apr & Oct 1994
Sentinel-1	C	ESA Earth Watch, under development
TerraSAR-X	X	Germany, 2007-
Cosmo SkyMed	X	Italy, June 2007-
X-SAR	X-VV	Germany, Apr & Oct 1994 (with SIR-C)

Table 5.1. Major spatial SAR missions since 1990.

5.1.1 Concepts related to a SAR system.

The objective of this section is to give a simple overview of the most important concepts related to SAR systems. The detailed description of SAR signal processing and other technical information can be found in specific literature.

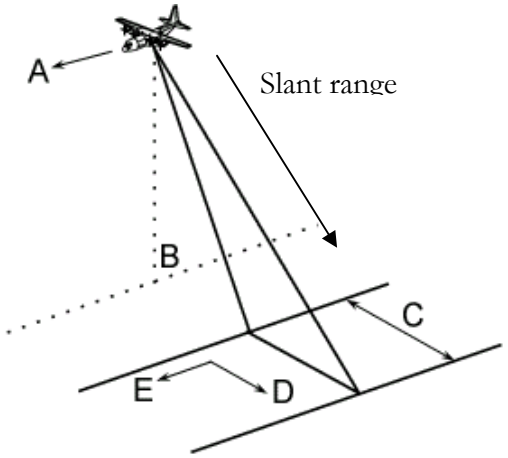

Figure 5.5. Geometry of radar observation.
Source:http :/envisat.esa.int/

Radar image acquisition:

The imaging geometry of a radar system is illustrated in **Figure 5.5**. The antenna is carried by a platform (airplane or satellite) that moves forward in the flight direction, following a trajectory, in the along-track or azimuth direction (A), being (B) de nadir. Radar instruments do not observe the nadir. The instrument is side looking: it transmits and receives obliquely at right angles to the direction of flight. With the movement of the platform, a two dimensional image is acquired. The portion of earth surface that is observed by the radar is the swath (C). The energy transmitted by the radar is pulsed, which means that it is confined to a very short interval of time (pulse time duration). A radar instrument measures the amount of energy scattered by the observed object, the phase, and distances. The radar measures the distances between the antenna and the observed object, this line determines the slant range image. The across-track dimension perpendicular to the flight direction is called range (D). Distances are measured as a function of the time that the signal travels

between the moment it is emitted and the moment it is received by the antenna. In order to be able to track the emitted pulse and the received signal, the radar instrument uses a sampling frequency, which provides sufficient time to an emitted pulse to return to the antenna before the next pulse is emitted.

The concepts of angle of incidence and local incidence angle are explained in **Figure 5.6** and **Figure 5.7**. The angle of incidence is the angle defined by the incident radar signal and the vertical. The incidence angle changes across the radar image swath, increasing from near range to far range. The near range is the portion of the image closest to the nadir, and the far range is the farthest from the nadir. The local incidence angle is the angle defined by the incident radar signal and the normal to the observed surface. If the surface is flat, both angles are the same. The ground range distances are the horizontal distances corresponding to each point measured in slant range.

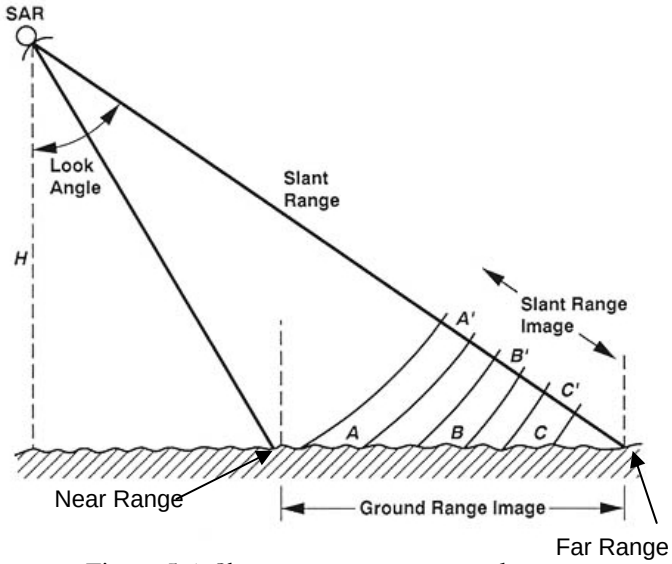

Figure 5.6. Slant range versus ground range.
Adapted from : http://history.nasa.gov/

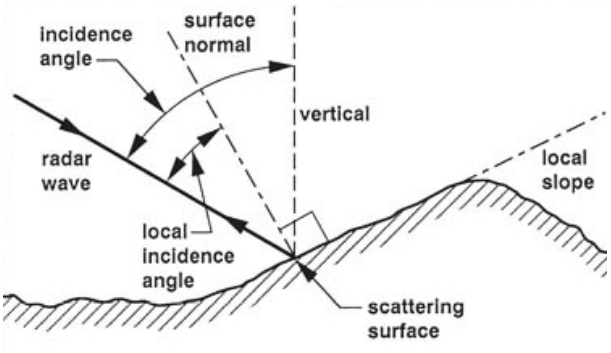

Figure 5.7. Incidence angle and local incidence angle.
Source: http://history.nasa.gov/

Synthetic Aperture Radar: concept and spatial resolution:

The Synthetic Aperture Radar uses a technique in which it is possible to achieve a longer aperture than the actual physical antenna. This technique consists in the integration of the backscattered signal over the entire time that a given surface target is viewed by the radar. In this way, higher azimuth resolutions are obtained.

The spatial resolution of a radar system indicates the ability of the radar instrument to distinguish between two point targets on the ground in the range or azimuth direction. The range resolution (see **Figure 5.6**) of a radar system depends on the duration of the radar pulse, τ, and the angle of incidence, θ. The range resolution R_r is:

$$R_r = \frac{c\tau}{2\sin\theta} \qquad \text{[Eq. 5.10]}$$

This range resolution can be improved by frequency modulations.

The SAR technique is based on the Doppler effect. Two targets separated in azimuth at any time have different speeds relative to the platform. Therefore the radar pulse backscattered from the two targets, has two distinct Doppler frequency shifts. The analysis of the Doppler frequency spectrum

allows resolving the two targets, even though the targets are at the same range and in the beam at the same time. The achievable azimuth resolution for a SAR system is:

$$R_{A,SAR} = \frac{L_a}{2} \qquad \text{[Eq. 5.11]}$$

With the SAR the achievable azimuth resolution only depends on the antenna length, L_a and it is independent of the wavelength, the satellite speed and the satellite altitude.

5.2. Radar equation, backscattering cross-section and backscattering coefficient.

The radar equation describes the relationship between the power transmitted, P_T, by an isotropic radiating radar antenna characterized with a gain G, and the power received by a radar antenna, P_R, from an isotropic scattering target. If the same antenna is used for transmission and reception (monostatic case) the radar equation is:

$$P_R = \frac{P_T G^2 \lambda^2 \sigma_c}{(4\pi)^3 R^4} \qquad \text{[Eq. 5.12]}$$

where, λ is the wavelength of the signal, R is the radial distance (range) from the antenna to a target with backscattering cross-section σ_c . The backscattering cross-section of a target is the area of that target that, if were considered as an isotropic scatter, would return the same amount of power as the target (which in reality is non isotropic).

The above equation can be generalized for an extended target as follows:

$$dP_R = \frac{P_T G^2 \lambda^2}{(4\pi)^3 R^4} d\sigma_c \qquad \text{[Eq. 5.13]}$$

The backscattering coefficient σ, or normalized radar cross section, is defined as the average backscattering cross section per unit area. It is a dimensionless quantity, and it is usually expressed in dB. The backscattering coefficient is a quantification of the ability of the target to scatter radiation. The study of vegetation using radar remote sensing is thus based in the relationships between the backscattering coefficient and biophysical properties.

The backscattering coefficient at polarisation pq can be obtained from the S_{pq} elements of the scattering matrix:

$$\sigma_{pq} = \left\langle S_{pq} S_{pq}^* \right\rangle \qquad \text{[Eq. 5.14]}$$

where $\langle\ \rangle$ denotes a spatial average and * denotes complex conjugate.

5.3. Backscattering measurements used to describe polarimetric properties.

Many polarimetric parameters can be derived from the covariance matrix. These parameters can be classified between those that require the phase relationships, present in polarimetric measurements (coherent parameters), and those that do not involve the phase information (non-coherent parameters or non-polarimetric). The most common incoherence parameters are the backscattering coefficients, which are spatially averaged: σ_{HH}, σ_{VV}, etc. Examples of coherent parameters are the entropy (H), angle alfa (α) or the correlation coefficient, ρ_{HH-VV}.

The following table summarises the parameters used in this work.

Feature	Definition
Backscattering coefficient	$\sigma_{pq} = \langle S_{pq} S_{pq}^* \rangle$, e.g. σ_{VV}, σ_{RL}
Polarisation ratio	$\frac{\sigma_{mn}}{\sigma_{pq}}$ e.g. $\frac{\sigma_{HH}}{\sigma_{VV}}, \frac{\sigma_{RR}}{\sigma_{RL}}$
Correlation coefficient	$\rho_{HH-VV} = \frac{\lvert \langle S_{HH} S_{VV}^* \rangle \rvert}{\sqrt{\langle S_{HH} S_{HH}^* \rangle \langle S_{VV} S_{VV}^* \rangle}}$

Table 5.2. Polarimetric parameters used in Chapter 6 and 7.

5.4. The speckle phenomenon in a SAR image.

The speckle is a phenomenon that results from the coherent nature of the radar measurement. When a coherent electromagnetic radiation interacts with a rough surface, the different scatters generate return signals with random phases, which interact with each other. The interferences are the cause of the grainy appearance of the generated image. As a consequence, the image of a homogenous surface shows pixels values with a high dispersion. These local variations of the amplitude make difficult for an observer to resolve the details of the image. In that sense, speckle is considered as noise, although physically it is not. The effect of speckle is illustrated in **Figure 5.8**. Individual pixels on a radar image are not direct measurements of the backscattering properties of the observed surface.

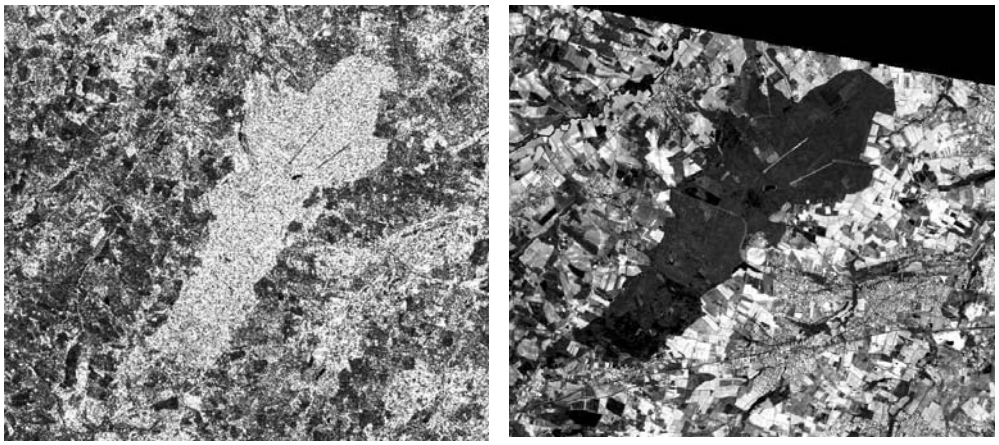

Figure 5.8. Example of speckle effect in an ENVISAT-ASAR image, VV polarisation, date 03/05/2003 (left image) compared to an optical SPOT-HVR image, band-4, date 23/05/2003 (right image), showing the forest of Bouconne, near Toulouse.

The problem of speckle can be overcome to some degree by producing multi-look images. During the SAR processing the signal is sampled to generate L looks. Each look represents an independent observation of the same scene. A limited number of looks, generally 3 or 4, are averaged incoherently. Thus, the image that is generated shows a reduction in speckle. The variance of the image is reduced by a factor L. The mean of L independent random variables with the same statistical distribution is the mean of the variables, and the variance is the variance of each variable divided by L. The multi-looking is usually done in azimuth.

The statistical properties of speckle in a SAR image:

The speckle is a source of variation in the pixel radiometry of a SAR image. In addition to the speckle, there are other variations related to the

nature of the surface. For instance, the image of an agricultural field, which can be considered as a relatively homogenous surface, shows an internal variability.

In the ideal case of an homogeneous area, the variability of the intensity image formed pixels of coordinates (x,y) can be described by a multiplicative model:

$$I(x,y) = A(x,y) \cdot \eta(x,y) \qquad \text{[Eq. 5.15]}$$

The variable $\eta(x,y)$ is a random variable, and it is assumed to be independent of the scene. Its mean value is equal to 1 and its variance is inversely related to the number of looks of the image, L. The natural distribution of the pixels in a SAR scene is not known. Therefore, several distributions have been used in the literature as approximations, for example, the gamma, the K or the Pearson distribution. The interest of knowing the distribution function of the pixels in a SAR image is that it allows to determine the uncertainties in the backscattering measurement.

Characterisation of the variability in a SAR image:

To characterize the variability in backscatter of a SAR image different parameters can be used for instance, the equivalent number of looks (ENL) or the spatial correlation. These parameters are usually unknown, and have to be estimated from the image itself. Selecting a homogenous region in the image, and calculating the mean and standard deviation can give an estimation of the equivalent number of looks:

$$ENL = \frac{\langle \mu \rangle^2}{std^2} \qquad \text{[Eq. 5.16]}$$

where $\langle \mu \rangle$ is the average value of the backscattering for the pixels in the region, and std is the standard deviation. As explained before, for non-

textured areas, the ENL will be the same as the uncorrelated looks used to generate the SAR image, provided that no other method to reduce the speckle in the image has been applied. The change in the ENL in a homogenous region is a good indicator of the improvement of the radiometric quality of an image after applying a speckle filter.

In order to reduce, even more, the speckle many filters have been developed which are based in the statistical properties of the SAR images. In this study, specific speckle filters have been applied to AIRSAR and ASAR images. The details are given in next chapters.

Reduction of speckle effects:

As explained before, due to the coherent addition of the signals coming from the many randomly distributed point scatters that constitute an observed target, the intensity measured by the radar is not a unique value, but follows a distribution function. Thus, the backscattering coefficient has a statistical uncertainty. The radiometric resolution of a SAR image is a measurement of its ability to distinguish between targets with different backscattering coefficient. A quantification of the radiometric resolution can be done using confidence intervals. The confidence intervals give the probability that the measurement lies between certain error bounds. Those confidence intervals can be calculated by integrating the probability density function of the measurements.

When increasing the ENL of an image, the distribution function narrows, thus, the radiometric resolution of the image increases. For many applications multi-looking is not sufficient to achieve the required radiometric resolution. For instance, in the case of ERS1 PRI products, generated with a

ENL=3, the confidence level for ±0.5 dB accuracy bounds is 15% (Bally and Fellah, 1995), which is very low.

Speckle filters can be used to improve the radiometric resolution. In general, the speckle filters can be classified in:

a) Mono-canal filters (Lee, 1986; Frost et al., 1982; Kuan et al., 1987). They are usually based on the averaging over the N pixels of a region, which reduce the uncertainties in the backscattering measurement of a target. This is based on the assumption that many of those pixels are uncorrelated.
b) Multi-temporal filters. In this study the series of ENVISAT images have been filtered with the multi-temporal speckle filter developed and described in Lopes et al., (1993), Beaudoin et al., (1994), Le Toan et al., (1997), Bruniquel and Lopes, (1997), Quegan et al., (2000), Quegan and Yu, (2001).
c) Polarimetric filters (Goze and Lopes, 1993; Lopes and Sery, 1997; Lee et al., 1999). The team of the University of Wageningen filtered AIRSAR images used in this study using the polarimetric filter of Shou and Skriver, 2001.

5.5 Scattering mechanisms in natural surfaces.

The scattering phenomenon is produced when radiation encounters changes in the media through its propagation. Scattering occurs inside a medium, like the vegetation, when radiation interacts with a particle that has a size similar or larger than the radiation wavelength. The density of the medium and the dielectric constant of the vegetation elements will affect the scattering.

The scattering also happens when radiation arrives to a boundary between two media. In this case, the scattering will depend on the differences between the dielectric constants of the two media. The larger the difference, the stronger the scattered field will be in comparison to the absorbed or transmitted field.

Thus, in general, in a natural surface it is possible to distinguish between two main types of scattering: surface and volume scattering. Surface scattering occurs on natural surfaces, such as, soil and water, while volume scattering occurs on vegetation and snow. The third type of scattering present in natural surfaces is the interaction between volume and surface, including double bounce scattering, which occurs in corner reflectors having perpendicular surfaces (tree trunks in flooded areas).

5.6 Surface scattering.

The roughness of the surface is the parameter that determines the types of surface scattering. Surface roughness can be characterised with statistical parameters that are measured in units of wavelengths. Thus, the same surface may appear rough for optical radiation and smooth for radar. The standard deviation of the surface height, m, is the most widely used parameter. Another common parameter is the surface correlation length, l, which is defined as the length in which the autocorrelation equals $1/e$.

When radiation interacts with a very smooth surface, specular reflection is produced. If the surface is perfectly smooth, the radiation is reflected forwards, with a reflection angle, θ_s, equal to the angle of incidence, θ_i, (Snell's law). The particular case is the nadir incidence for which radiation

is reflected backwards. The angular pattern of the perfect specular reflection is a delta function.

If the surface is not perfectly smooth diffuse reflection occurs. In this case, the scattered radiation has two components: a diffuse component and a specular component also referred as coherent component. The diffuse component consists on radiation scattered in all directions. The coherent component is only important for incidence angles close to the nadir. The reflection for a slightly rough surface is explained by the Fresnel equations. As the surface becomes rougher, the specular component decreases and almost all the scattered radiation is diffuse (**Figure 5.9**). A special case of rough surface, the Lambertian surface, is shown in Chapter 2.

According to this, the backscattering coefficient σ , measured in the radar direction, will be close to zero if the surface is very smooth, low if the surface is slightly rough and high if the surface is very rough. For the ideal lambertian case the backscattering coefficient is proportional to the cosine of the incident angle: $\sigma \propto \cos\theta$.

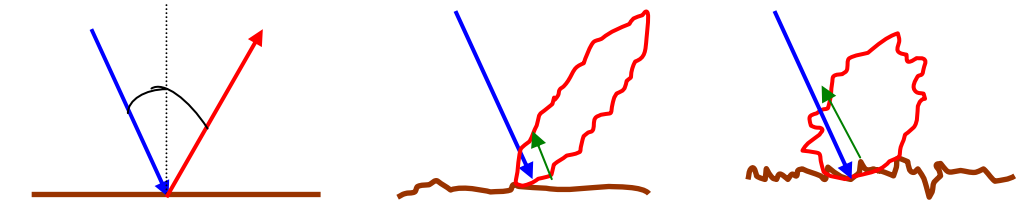

Figure 5.9. Scattering for different surface roughness conditions.

In addition to the surface roughness the second important parameter affecting surface scattering is the dielectric constant.

In this study there is an interest in the behaviour of natural soil surfaces observed by radar systems at C Band, as soils are the underlying surface under crop canopies. In general the backscattering from a bare soil includes also a contribution from volume scattering. However, if the penetration depth is not significant, only the scattering of the surface needs to be considered. The soil state will influence the backscattering measured in crop surfaces as will be explained in **Section 5.7**. In **Figure 5.9** and **5.10**, the backscattering dependency of soil surfaces with surface roughness and dielectric constant is illustrated.

Dependence of the soil backscattering coefficient on surface roughness:

In general, for smooth surfaces the backscattering coefficient decreases rapidly with increasing angle of incidence. The variation with the incidence angle in the case of rough surfaces is gentler. The effect of roughness in the backscattering can be illustrated with **Figure 5.10** (Ulaby et al., 1986).

Dependence on the dielectric constant:

The microwave dielectric constant of the soil has a strong dependence on soil moisture content and, in a lesser extent, on the soil type. The variation of the relative dielectric constant is illustrated in **Figure 5.11** (Ulaby et al., 1986) at C Band.

Soil backscattering models:

The problem of soil scattering is complex due to the diversity of conditions (texture, moisture, roughness) and high variability that are present in nature. The more precise solution of the problem can be obtained

numerically, by using the method of moments, but this method is not useful for practical applications, because of its complexity. The problem is usually approximated with more simple models. The disadvantage is that simple models are only valid at a certain range of roughness parameters. The most widely used of these simple models are the small perturbation model (SPM), the Physical Optics (PO) approximation and the Geometrical Optics (GO) approximation. The PO and GO are first order solutions and cannot be used to describe cross polarisation. A quite general solution for the soil backscattering is also is the Integral Equation Method (IEM) (Fung, 1994).

5.7 Volume scattering.

The type of scattering that occurs in a vegetation layer is the volume scattering, which is the scattering within a medium that contains several scattering elements. At radar wavelengths, the vegetation is seen as a volume formed by scatterers: branches, leaves, stems, etc. The signal returned comes from multiple scatterers and it is the result of the multiple bounces and reflections from the elements within the volume. The ratio between the scatterer dimension and the wavelength determines the contributions from the individual scatterers. When the scatter dimension is approximately the size of the wavelength the shape of the scatterer has an important role in the resulting backscattering and will also determine a particular polarimetric behaviour. When the dimensions of the scatterers are much smaller than the wavelength the scatterer shape is not important.

Inside the volume, there will be losses due to the scattering and the absorption. Thus, the radar signal suffers attenuation when passing through the volume (see **Figure 5.12**).

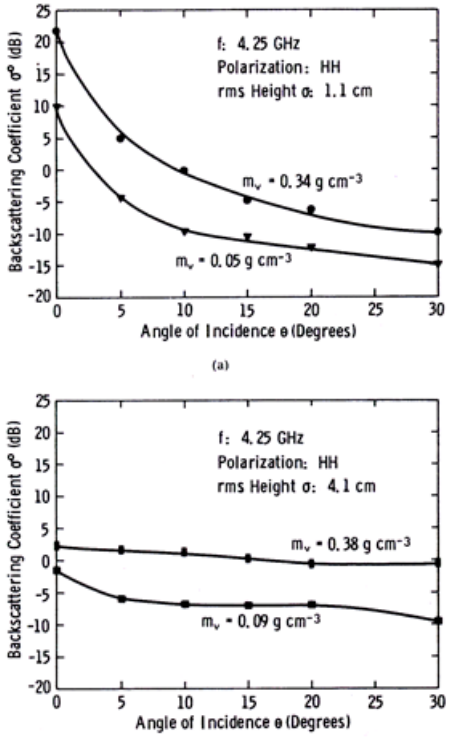

Figure 5.10. Backscattering coefficient behaviour at C Band as a function of the incident angle for a smooth surface (a) and a rought surface (b) and for two different volumetic moisture content.-

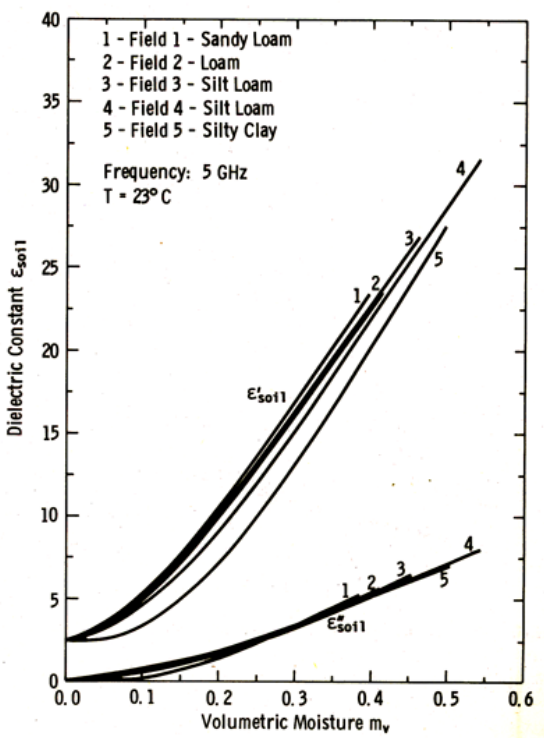

Figure 5.11. Backscattering coefficient measurements at C Band showing the relationship between the dielectric constant (imaginary and real part) of a soil and its volumetric moisture.

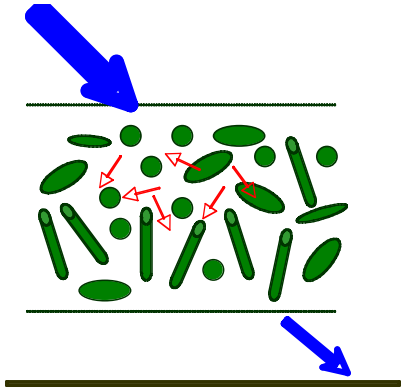

Figure 5.12 Attenuation of the signal produced by the vegetation volume.

The description of a vegetation medium involves the characterisation of all the scatterers. Due to the huge amount of scatterers in any vegetation media, in practise, it is not possible to obtain an exact description of the media, therefore electromagnetic models need to do approximations. One of those approximations consists on considering that the elements of vegetation have simple shapes: spheres, cylinders, discs or plate ellipsoids for instance. In general, the radar cross section of simple scatterers depends on the angle of the incident wave and the polarisation of the incident wave. The exact solution of the scattering for those simple scatterers is known, although its computation usually involves infinite series, and it is solved using numerical methods. The dimensions of the scaterers, their shape, orientation, position and dielectrical properties, determine the radar backscattering coming from a volume of scatterers. **Figure 5.13** shows the backscattering coefficient from a layer of cylinders randomly oriented. The figure clearly shows the dependence with the scatterer dimension to wavelength ratio.

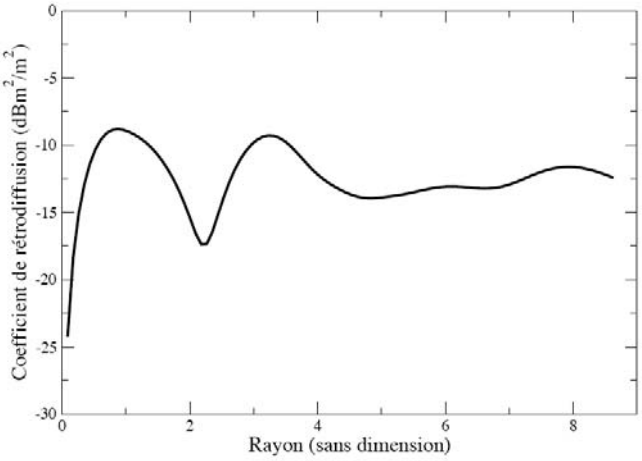

Figure 5.13. Backscattering from a half-infinite layer of cylinders randomly oriented as a function of the radius (more exactly as a function of the ratio between the perimeter and the wavelength inside the scatterers). (Figure extracted from Picard, 2002).

Finally, the distribution of shape and orientation of the scatterers will determine a polarimetric behaviour. Although the interaction of a polarized wave with a volume is complex, some statements can be made. For example, if the target is composed mainly of vertical components, the VV backscattering will be higher than HH. Another important characteristic of volume scattering is the depolarisation of the incident wavelength, which is much more important than in the surface scattering case (see **Figure 5.14**).

In conclusion, multipolarized radar measurements provide more information than single polarized measurements, and hence the high interest of polarimetry in agricultural studies.

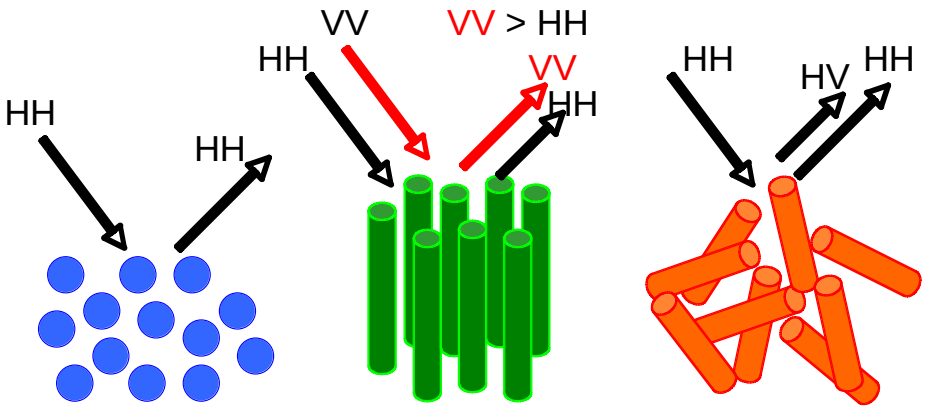

Figura 5.14. Depolarisation effects in volume scattering.

5.8 Scattering of agricultural crops.

In general, the signal backscattered from a cop canopy consists of three types of contributions, which are shown in **Figure 5.15**.

- Volume scattering from the plants
- Surface scattering from the underlying soil surface (this has crossed the vegetation layer twice before arriving to the sensor)
- Vegetation-Soil multiple scattering contributions

The magnitude of each of the contributions described on **Figure 5.15** depends on crop characteristics and radar characteristics. Both are detailed in next sections.

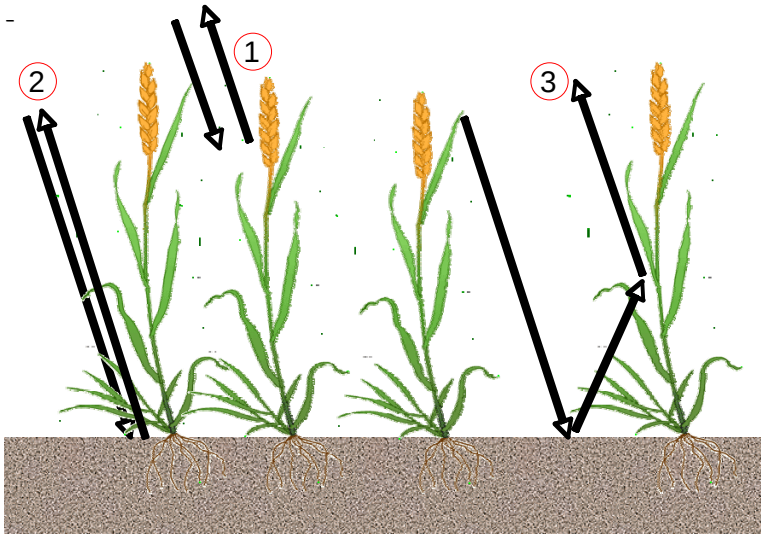

Figure 5.15. Sources of radar backscattering from a crop: 1) Volume scattering from the plants, 2) Surface scattering from the underlying soil moisture (two-ways attenuated) and 3) Vegetation-Soil interaction.

5.8.1. Radar characteristics affecting the scattering of crops.

The radar characteristics that will determine the backscattering measured from a crop surface are the frequency, the incident angle and the polarisation.

Frequency:

The penetration of the signal into the crops increases as frequency decreases. Thus, for higher frequencies like X Band the signal is dominated by canopy scattering while for lower frequencies like P or L Band the most significant contribution to the total backscattering will come from the soil. Also, when frequency decreases, the sizes of the crop scatterers (leaves, stems, etc) relative to the wavelength are smaller. As it has already been said, this

study is focused on the C band because the dimension of the elements present in crops is comparable to the wavelength signal in C band .

Angle of incidence:

At high incident angles, the path length through the crop is higher. Thus, the attenuation of the signal by vegetation will be higher at higher incident angles. The effects of the angle of incidence on the measured backscattering are illustrated in **Figure 5.16**. This figure shows VV backscattering measurements over an alfalfa canopy at two different stages of growth as a function of the incident angle and for a frequency or 13 GHz. The moisture conditions are very similar in both cases. Several observations can be made about the figure. First, it is shown that backscattering changes with the incident angle. Secondly, for the same crop type, this behaviour changes with the development stage. This is a consequence of the changes in the contributions of soil and vegetation. For the short canopy, the dominant term in the total signal is the soil contribution. When alfalfa is developed, vegetation maskes the underlying soil surface. The angular behaviour at C band for the same alfalfa field is expected to be different because the C band has a higher penetration. Thus, at C band, the contribution of the soil will still be important in a higher incident range than that shown in **Figure 5.16**.

The angular behaviour of other crops will be shown and interpreted in **Chapter 6**. This angular behaviour changes with the crop type and crop phenology.

Polarisation:

As has been discussed previously the polarimetric behaviour of a vegetation volume will depend on the shape and orientation of the different vegetation scatterers. An example of the polarisation response in agricultural crops is the different attenuation at HH and VV polarisation in a wheat canopy. This example is shown in **Figure 5.17** where changes with phenology and the angle of incidence can also be observed.

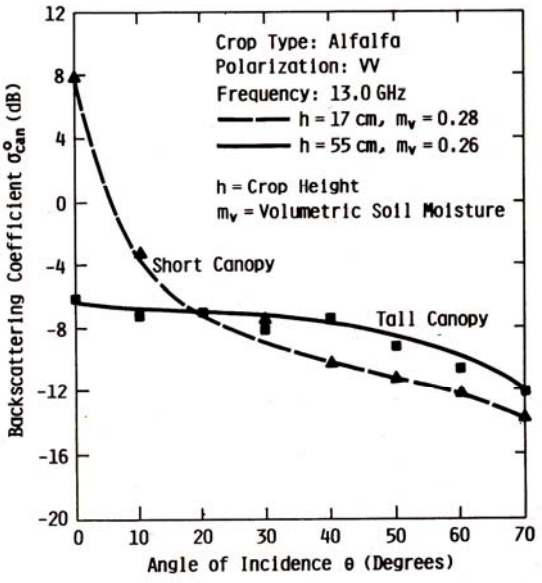

Figure 5.16. Measured backscattering coefficient of an alfalfa canopy at two stages of growth. (From Ulaby et al., 1986).

5.8.2. Characteristics of crops.

The characteristics of crops that affect the backscattering measured by a radar system can be listed as follows:

- The canopy density: density of plants, row direction, plant height.
- The canopy structure: size, shape and orientation of the plant elements.
- The water content of the plant (dielectric constant).
- The roughness and moisture (dielectric constant) of the underlying soil.

The first three elements vary with the crop type. Also, for a particular crop type they change with the growth stage (crop phenology) and development conditions.

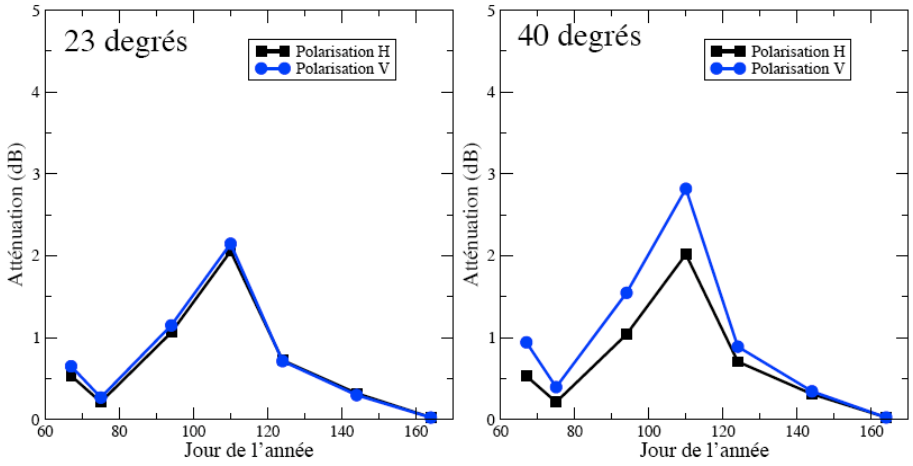

Figure 5.17. Model simulations of the attenuation of the signal produced by a wheat canopy, along the growing season, for the cases of vertical and horizontal polarisation at two incident angles, 23º and 40º. (From Picard, 2002).

Canopy Biomass

The amount of vegetation material of the canopy will determine the attenuation and absorption along the path. **Figure 5.18** shows an example of the one-way attenuation at 10.2 Ghz for a soybean canopy (Ulaby et al., 1986). The changes in the attenuation due to the phenology can be observed.

The amount of biomass in a medium can be characterised with the fractional volume, which is the ratio between the volume occupied by vegetation matter and the volume of the canopy. For instance a wheat canopy is much denser than a corn canopy.

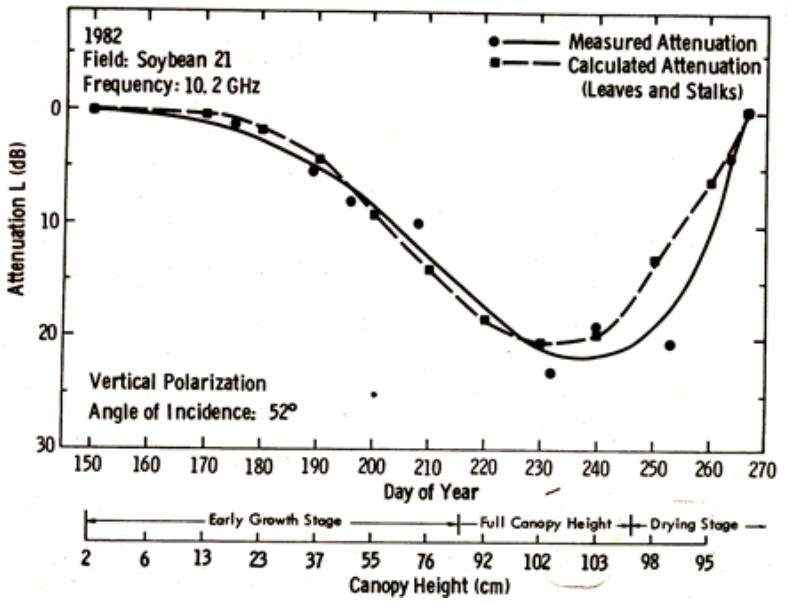

Figure 5.18. Temporal variation of the measure one-way attenuation for a soybean canopy. (From Ulaby et al., 1986).

The structure of vegetation:

The structure of vegetation influences the penetration of the wave into the canopy. The penetration increases with increasing wavelength and may

be dependent on polarisation if the canopy has components with specific orientations such as vertical needles, leaves or stalks (case of wheat and rice). For a particular wavelength, the attenuation coefficient depends on the fractional volume and the permittivity of the vegetation. Consequently, the penetration depth is, in general, more important in a forest canopy than in agricultural vegetation covers.

In some models, vegetation is considered as a multilayer media. Cereals are approached by a two-layer medium (soil + stalks) before heading, and a three-layer medium after heading (soil + stalks + heads).

The water content of the plant

The water content of the plant will affect the dielectric constant of the vegetation and thus the scattering and attenuation. The water content in the plant is mostly constant during the growing season, except in the senescence phase. When the plant is dry, it becomes almost transparent for the radar, producing very little attenuation.

Underlying soil

The characteristics of the soil depend on the cultural practices (irrigation, plough practices) and meteorology. For the same external conditions, the characteristics of the soil may differ with the soil type, particularly soil moisture. Examples describing the influence of soil roughness and soil moisture in the backscattering coefficient of bare soils have been shown in **Section 5.5**.

Conclusion:

In this chapter it has been explained how radar signal from a vegetation crop canopy depends on many factors. There are factors related to the radar instrument itself, frequency, polarisation and incident angle, and factors related to the vegetation canopy. The latter can be summarised as follows:

- canopy. dielectric constant, which depends on the biomass and plant water content
- plant elements structure: size, shape, orientation and number density of the elements
- canopy structure: row, plant number density
- underlying soil contribution, which mainly depends on the moisture and roughness.

All those factors are responsible of a particular polarimetric behaviour, which usually changes along the growing season. This thesis focuses on the study of the polarimetric backscatter of crops at C band as a function of the structural differences between the agricultural crop types. In **Chapter 6** polarimetric radar data are used for developing a method for classification of crops. In **Chapter 7** the possibility of retrieving wheat biomass by using the ratio between the HH and VV polarisation is investigated.

CHAPTER 6:
C BAND POLARISATION DATA FOR THE CLASSIFICATION OF CROPS.

As already discussed in **Chapter 1**, methods for the classification of crops using optical data are well established. However, in cloudy agricultural areas, like the North of Europe, there is a need of developing methods based on radar data.

In this chapter a crop classification method using C band polarimetic radar data is developed. In **Chapter 5** it was argued that C band data are more adapted to agriculture studies that other radar wavelengths. The choice of wavelength was also done in view of application to present satellite data (ENVISAT/ASAR, RADARSAT-2) and future satellite missions (SENTINEL-1).

A difficulty for the development of this kind of study is the lack of multi-temporal polarimetric C band satellite or airborne images together with a detailed crop map, necessary to the analysis and validation of the results. Consequently, the study has been performed on the NASA JPL- AIRSAR

airborne images acquired in 1991 July in Flevoland (The Netherlands), which constituted a complete dataset with corresponding ground data.

The first part of the chapter is dedicated to the analysis of AIRSAR data from the ERA-ORA database. The analysis results will be used to develop the classification method. Good results, shown in **Section 6.5**, have been obtained. Finally, AIRSAR data corresponding to the area of Barrax (Spain) have also been analysed in order to evaluate the performance of the algorithm rules in a different region.

6.1 SAR classification.

This Chapter treats the problem of determining the crop type of agricultural fields in a region using polarimetric radar data. Many authors have addressed the problem of classifying agricultural fields during the last decades, and several classification algorithms have been developed. Classification approaches are applied in a pixel basis or in an area basis. It is very common to perform image segmentation as a pre-processing step to classification. Segmentation algorithms (Lombardo et al., 2003; Dong et al., 2001) will divide the image into regions or objects with similar statistical properties that will be later classified. The problem in segmentation is that those regions can be found in an image at different scales, and it is not always possible to determine the correct scale of analysis (Arbiolo et al., 2006).

In general, the different classification algorithms can be divided in three main groups (Oliver and Quegan, 1998): Knowledge based approaches (Ferrazzoli et al., 1999; Pierce et al., 1994; Skriver et al., 2005), statistical methods and classification by scattering mechanisms. In the classification by

scattering mechanisms (van Zyl, 1989; Freeman and Durden, 1998) the data are classified according to their resemblance to the dominant scattering mechanism that occur in natural media, like double-bounce. The objective of the knowledge-based approaches is to classify the image into a several broad classes such as bare soil, water, urban areas, etc. The classification is based on the scattering properties of these classes. These scattering properties are used to define the classification rules of the algorithm. One of the most important works in this type of classifiers is the work of Ferrazzoli et al., 1999, which study the classification of crops using C, L and P band AIRSAR data several agricultural sites: Montespertory (Italy) and Flevoland (The Netherlands). The different crops were classified as belonging to broad classes defined by its structure and biomass, for instance, small stem crops. The statistical approaches cover a high variety of methods that make use of the maximum likehood (ML), (Hoekman and Quinones, 2000; Ranson and Suan, 2000), the ML based on the Wishart distrubution (Lee et al., 1994; Dong et al., 2001), polarimetric decomposition (Cloude and Pottier, 1997) or neural networks (Chen et al., 1996) among others.

The advantage of statistical approaches such as neural network is that they can be applied in cases where there is no knowledge about the scattering properties of the surface to be classified. The number of classes that can be determined using knowledge based approaches is usually smaller than when using statistical methods. On the other hand, the statistical methods are usually well adapted to a specific dataset but they are difficult to adapt to other datasets (Skriver, 2007). Knowledge based approaches are thus more robust and can be easily adapted to different regions. Furthermore the knowledge based approaches are appealing because they are based in the physics of the

scattering mechanisms. In this study a knowledge based classification algorithm is proposed for the classification of C-Band polarimetric data.

6.2 Test site and dataset.

6.2.1 Test site.

The test site is located in Southern Flevoland (The Netherlands), a polder reclaimed from lake Ijssel in 1966. The land surface is flat and lies ±3 m below sea level. The soil is homogeneous over the large area. The site has rectangular-shaped parcels of ±80 hectares. Farmers have subdivided these parcels into smaller fields, growing mainly sugar beets, potato and wheat. Secondary crops include barley, pea, onion, grass and corn. Some parcels in the area, belong to the "Directie Flevoland" who originally cultivated the polder, these are not subdivided, and have rapeseed, stem bean, flax and barley as the most common crops.

6.2.2 Ground data.

The acquisition of ground data at Flevoland was coordinated by ESA. Quantitative ground data include crop cover (%), crop height and plant number density on a limited number of fields of wheat, corn, potato and sugar beet. Soil moisture was also measured for some fields. **Figure 6.1** shows the mean crop cover and crop height at 4 dates. The figure indicates that on June 15, sugar beet and corn were in early stages of growth, and corn exhibits significant change during the last 2 weeks in July.

6.2.3 SAR images.

In the framework of the ESA MAC-Europe project, airborne campaigns using the multifrequency polarimetric NASA/JPL AIRSAR were conducted over selected test sites in Europe. In 1991, the campaign was planned for a six-week period on a multi-temporal basis starting on the last week of June until last week of July. The period coincided with a substantial part of the growing season. The Flevoland site was visited four times (June 15, July 3, July 12, and July 28). A C-band AIRSAR image from the 12th of July of the Flevoland site is shown in **Figure 6.2** (RGB: σ_{HH} , σ_{VV} and σ_{HV}).

The SAR data under study are C-band single look complex data at incidence angle from 26° to 65°. The images analysed in this study were obtained from the University of Wageningen (Dr. Hoekman).

6.2.4 ERA-ORA database.

The Flevoland/AIRSAR database was available through the Concerted Action European project ERA-ORA, co-ordinated by the University of Tor Vergata (Prof. Solimini). The data were covariance matrices, calculated on a per field basis, available for the following crop types:

- potato (406 fields)
- wheat (394 fields)
- sugar beet (317 fields)
- grass (186 fields)
- barley (101 fields)

- small numbers of fields of oats, maize, rapeseed, beans peas, alfalfa, oat, onion, flax, grass and fruit trees.

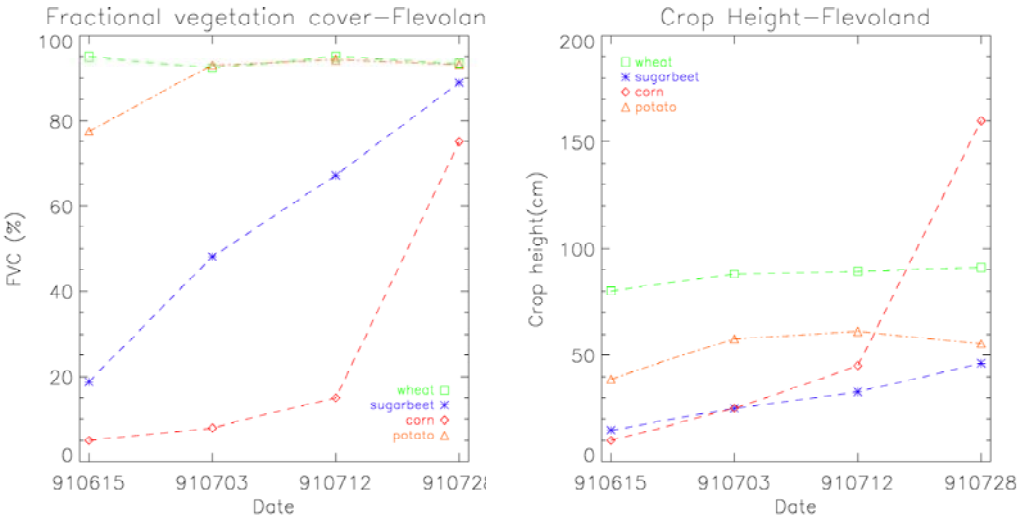

Figure 6.1. Average Fraction of vegetation cover (left) and average crop height (right) of the main crops in Flevoland.

The Flevoland dataset has a large number of crop types and fields of large size, distributed in a large range of incidence angle. The dataset is suitable for analysis of the frequency, angular, polarimetric and temporal behaviour of crop types prevailing in North Europe. The dataset is suitable for studying the temporal change during the peak period in June and July of the growing season, and less suitable for defining a classification scheme to be applied to a monthly temporal series of future satellite data. The weakness of the databases is the lack of biomass and structure information of the plants for quantitative interpretation and modelling work.

Figure 6.2 Flevoland study area. RGB composite using the three bands (HH, VV and HV) of C-Band AIRSAR data in July 12.

6.3 Angular variation of polarisation features.

This section is dedicated to analyse the variation of backscattering features with the incident angle. The database contains a sufficient number of fields for only four crop types: wheat, barley, sugar beet, potato and grass fields.

As explained in **Chapter 5**, the dominant scattering mechanisms in an agricultural field depends on the crop type and crop stage. The scattering mechanisms will determine different angular behaviours.

6.3.1 Single intensity measurements (HH, VV and HV).

a) If the volume scattering from the vegetation layer is the prevailing interaction mechanism, the angular variation is of type $\cos\theta$. This is the case for:
   - σ_{HV} at dates when the crops are well developed crops (July dates at Flevoland). Clear examples are sugar beet and potatoes (**Figure 6.3c, d**).
   - For σ_{VV} and σ_{HH} when crops are well developed and the soil contribution is small. This occurs for instance for potato and sugar beet (see **Figure 6.3a, b**).

b) When the soil backscatter is dominant (at early and late stages), the attenuation by the crop goes as $1/\cos\theta$, but the overall variation depends on the soil backscatter angular variation, which depends on surface roughness. This is the case for potato at C band in June, when two types of angular variation are observed, depending on the look angle with respect to the row direction (**Figure 6.3b**) or sugar beet at C in June (**Figure 6.3a**), with large dispersion in the angular variation, depending on the soil contribution in the backscatter.

c) When the soil-vegetation interaction is important, the angular variation may display quite different behaviour. This is the case for wheat and barley at C band σ_{VV} where the signal increases at incidence angles greater than 45° (**Figure 6.4a, b**).

d) When the crop class is not defined by the same interaction mechanisms, because of inter-field variability in phenological stage or because the class taxonomy corresponds to different canopy types, very large dispersions in inter-field backscatter can be observed. This

is true for most crops in June, when the growth rate is high and there is field-to-field variability in scattering mechanisms, resulting in large data dispersion. It is also the case for "grass" fields (**Figure 6.5**), which are herbaceous areas having a large range of height and plant number density. In these cases, the large class variance will be against the generality and robustness of any classification procedure.

6.3.2 Polarisation ratios of single intensity measurements (HH, VV and HV).

The angular behaviour of the polarisation ratios HH/VV, HV/VV and HV/HH is very different for small stem cereals (wheat and barley) and broad leaf crops (sugar beet and potatoes).

As seen before, for well-developed broad leaf crops (sugar beet and potatoes) the volume scattering is dominant for both HH, VV and HV which results in little angular variation of the single intensity polarisation ratios (**Figure 6.6a, b**). In addition, the data show little dispersion, indicating that the interaction mechanism is well defined. Row effects may cause the wave shape in the HH/VV for the potato case (**Figure 6.6a**).

In contrast, small stem cereals show a decreasing angular variation for HH/VV and HV/VV (**Figure 6.6c, d**). A higher dispersion is observed among the different fields. For the HV/HH case, the scattering is too high to conclude about a variation trend. Due to this high dispersion it is difficult to apply the inversion methodologies.

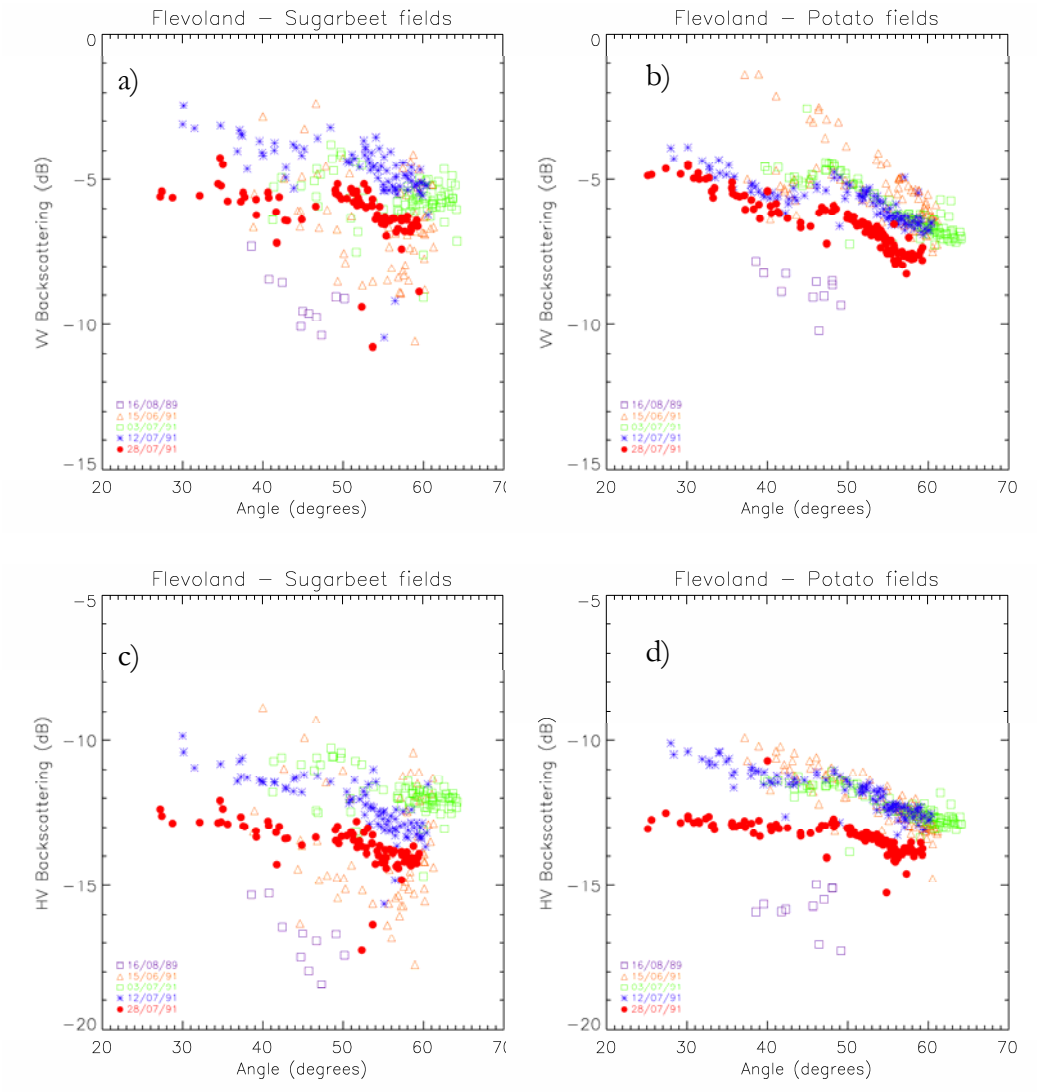

Figure 6.3. Angular Behaviour for sugar beet (left column) and potato (right column) at VV, VV and HH polarisations

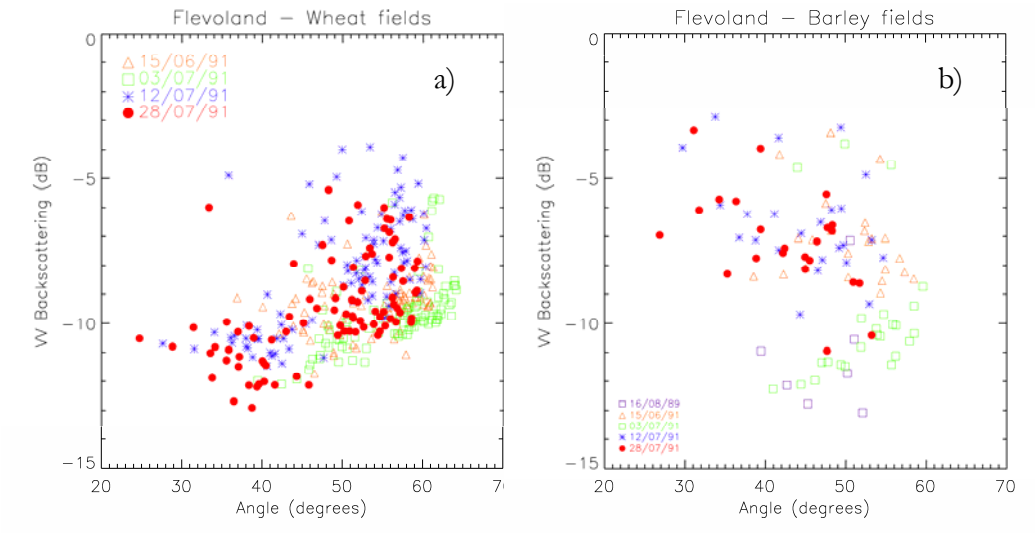

b)

Figure 6.4 Angular Behaviour for wheat (left column) and barley (right column) at VV, HV and HH polarisations.

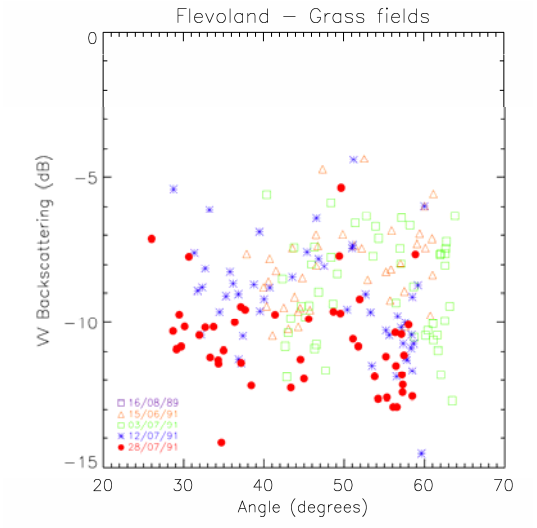

Figure 6.5. Angular Behaviour grass at VV polarisation.

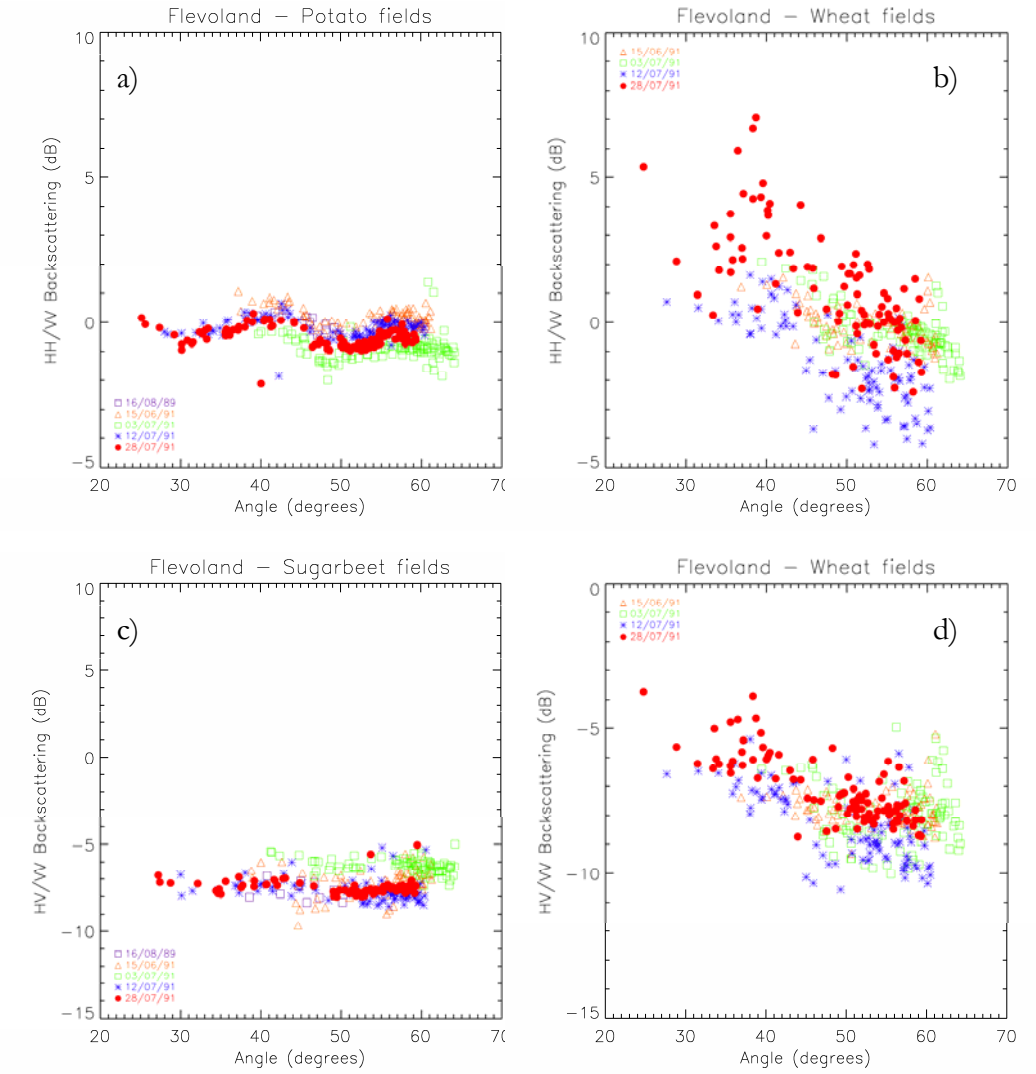

Figure 6.6. Angular behaviour of polarisation ratios for broad leaf crops (left) and small stem crops (right).

6.3.3 Circular Polarisation (RR and LL).

The angular behaviour of RL and LL (not shown) was found very similar to that of VV and HH. The ratio RR/RL do not show variation with the incident angle, except for the case of potato at beginning and mid-July. In general, the RR/RL angular behaviour was found very similar to that of HV/VV.

6.3.4 HHVV correlation.

The angular behaviour of the HH_VV correlation (not shown) was found inversely correlated to that of RR/RL.

6.3.5 The issue of the angle of incidence.

The scattering mechanisms and their relative importance in the total backscattering change as a function of the incidence angle. This is observed for different measurements or combinations of measurements (**Figures 6.7** and **6.8**). **Figures 6.7** and **6.8** show that in passing from 35°-45° to 45-55° the scatterplots of σ_{RR} versus σ_{HV} or σ_{RR}/σ_{RL} versus σ_{HV}/σ_{VV} for barley, wheat, sugar beet, potatoes and grass can change noticeably. The same was observed for all four June-July dates. The difference is more noticeable where a lower range (<35°) is compared to a higher range of incidence (>55°).

In summary, $\gamma = \sigma/\cos\theta$ can be used to compensate for variations of the angle of incidence only for HV backscatter at C bands in July. For HH and VV, the incidence angle range should be restricted (for example, by excluding data at low (<30°) and high (>50°) incidence angles), or by experimentally

assessing the angular variations specific to the case where soil backscatter is significant.

a)

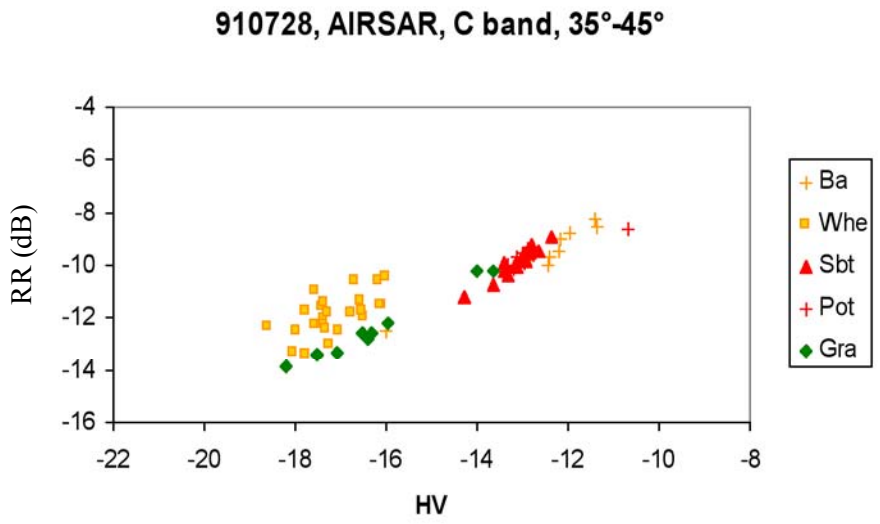

b)

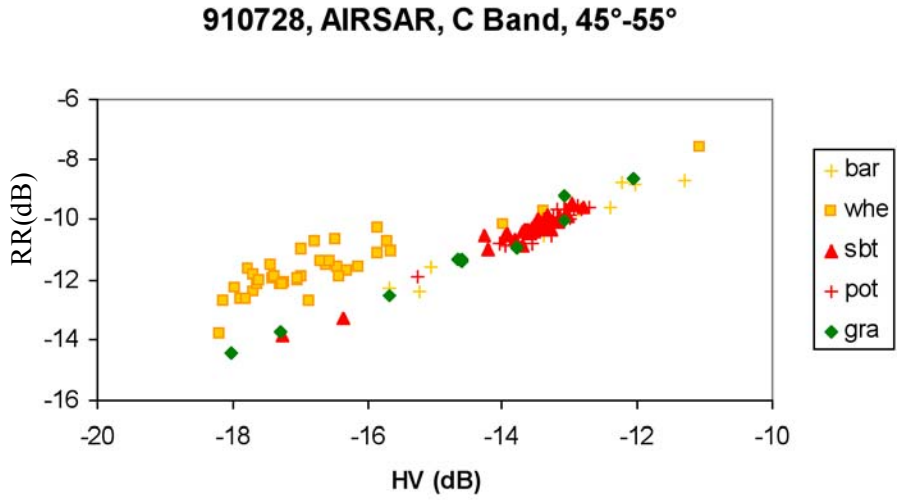

Figure 6.7. a) σ_{RR} versus σ_{HV} for the 35°-45° incidence angle range. b) Idem for the 45°-55° incidence angle range.

As a consequence, the data analysis and classification scheme should be applied over small ranges of incidence angle, i.e. 25-35°, 35-45°, 45-55° and >55°. A problem usually encountered with airborne data is that crop types are not evenly distributed across the incidence angle range. In the ERA-ORA database, many of the fields fall in the range 45-55°; few fields are available at near or far range.

In many studies, classification schemes were developed for this typical range of incidence. In Ferrazzoli et al. (1999), the data were at 50° of incidence (Montespertoli data at June 22, June 29, July 14, 1991) and at 40-50° range (Flevoland in August 1989). The applicability of the methods and algorithms derived from airborne datasets to future satellite datasets should be considered with care, since for polarimetric mode, incidence angles will be restricted to the lower range (polarimetric PALSAR mode onboard ALOS will be restricted to <28° of incidence).

6.4 Analysis of the backscatter measurements in view of crop classification.

This section presents an analysis of the backscatter measurements to be selected as classifiers. The Flevoland test area includes a large range of crop types and fruit trees. To reduce the confusion, which can be found at a single date, permanent cover type such as fruit trees (or grassland) can be masked out if a priori knowledge (map) is available. Multi temporal data can also be used to pre-classify such cover types. In Flevoland, grass may be distinguished from other crops in October-November, when the fields are bare soil. Fruit trees could be separated from the other crops by their stable temporal values. Thus,

in the following analysis, grass and fruit trees as well as other crops which are present in few fields (flax, oats) are not always included.

a)

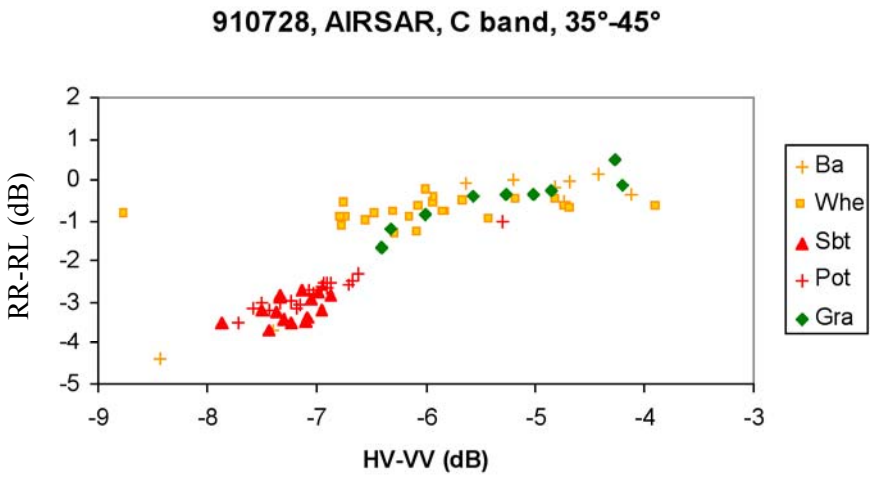

b)

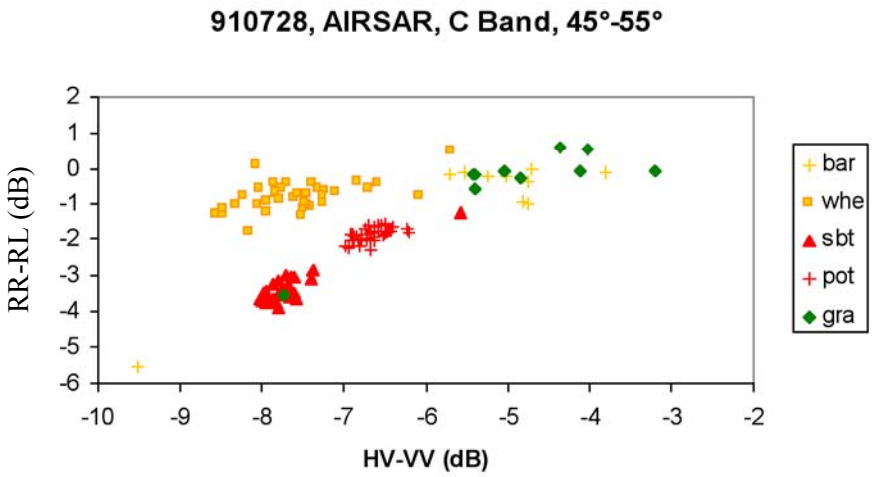

Figure 6.8. a) σ_{RR}/σ_{RL} versus σ_{HV}/σ_{VV} ratios for the 35°-45° incidence angle range. b) Idem for the 45º-55º incidence angle range.

6.4.1 HV versus VV.

It is interesting to analyse σ_{HV} and σ_{VV} (or σ_{HV} and σ_{HH}), which are available from ENVISAT/ASAR. **Figure 6.9** shows σ_{HV} o versus σ_{VV} for the four dates. This analysis includes data at all incident angles. As expected, σ_{HV} and σ_{VV} are correlated, but differences can be observed between crops and between dates.

a) Rapeseed has very high σ_{HV} and σ_{VV} backscatter except on July 28, caused by high volume scattering and probably by the high biomass of the pods. The backscatter decreases drastically on July 28, very likely due to harvesting.

b) Sugarbeet and potato exhibit large spreads in backscatter in June, due to the effect of soil backscatter, which varies among fields and across incidence angle ranges. On July 3, the two crops have the same σ_{HV} and σ_{VV} backscatter. On 12 July, they correspond to separate clusters, which become closer again on July 28.

c) Wheat and barley exhibit significant temporal change in their relative backscatter: closer on June 15 and July 3, and separated on July 12 and 28. On July 3, wheat and barley can be easily discriminated from sugarbeet and potato. On July 12, wheat has lower backscatter than barley, which also shows more spread in the data.

d) Corn fields have lower backscatter than sugarbeet and potato before July 12, and have similar backscatter at the end of July.

e) In general, beans have lower backscatter with large spread, probably because of different cultural practices and growth stage.

In summary, using σ_{HV} and σ_{VV}, wheat, barley, sugarbeet, potato, and rapeseed can be separated in July. It should be noted that the discrimination based on scattering mechanisms should take into account the significant variation of these mechanisms during July (early, mid and late July). Also, the crop development calendar may vary by +/- 2 weeks from one year to the next, depending on the weather.

6.4.2 HV versus Correlation between HH and VV.

Figure 6.10 shows σ_{HV} versus ρ_{HH-VV}. On June 15, large spread in the data and overlap in the clusters are observed, with the exception of rapeseed. On July 3, the clusters change drastically, with separation of potato/sugarbeet, corn, wheat/barley, and rapeseed. On July 12, wheat and barley, potato and sugarbeet form separate clusters. However, it should be difficult to identify barley and corn, which have large spread. A combination of July 3 and July 12 could be used to separate most crops. The July 28 data show more compact clusters, corresponding to a more homogeneous growth stage for spring crops. However, the clusters are close to one another.

6.4.3 HV/VV versus Correlation between HH and VV.

Results similar to those in the previous figures are observed: there is a large spread of data in June, there are distinctive clusters for wheat/barley and sugar beet/potato on July 3, and the clusters are less separated on July 28.

6.4.4 RR/RL versus HV/VV.

Figure 6.8 and 6.11 plots $\frac{\sigma_{RR}}{\sigma_{RL}}$ versus $\frac{\sigma_{HV}}{\sigma_{VV}}$. According to Ferrazzoli et al (1999), small stem crops can be separated from wide leaf crops using these measurements. This is observed at the later dates (July 12 and more clearly on July 28), whereas there is more confusion on June 15. Nevertheless, these parameters appear interesting for separating crops.

6.4.5 HH/VV versus HV/VV.

The analysis of $\frac{\sigma_{HH}}{\sigma_{VV}}$ versus $\frac{\sigma_{HV}}{\sigma_{VV}}$ is presented in **Figure 6.12**. For the date in June, there is an overlap of the clusters corresponding to each class. The day for which the clusters show the higher separation is July 3, on the HV/VV axis. At that day HH/VV could discriminate some of the barley fields from the wheat fields. In July 12 and July 28 there is also a high confusion between classes, but the most important observation is the different behaviour observed for wheat fields in the HH/VV axis. The ratio HH/VV increases significantly from most of the wheat fields from July 12 to July 28. This is interpreted as an effect of the vertical structure of wheat: VV is more attenuated than HH, and the attenuation is higher for higher biomass values. This property, and the possibility to relate the HH/VV ratio to the wheat biomass will be studied in **Chapter 7**.

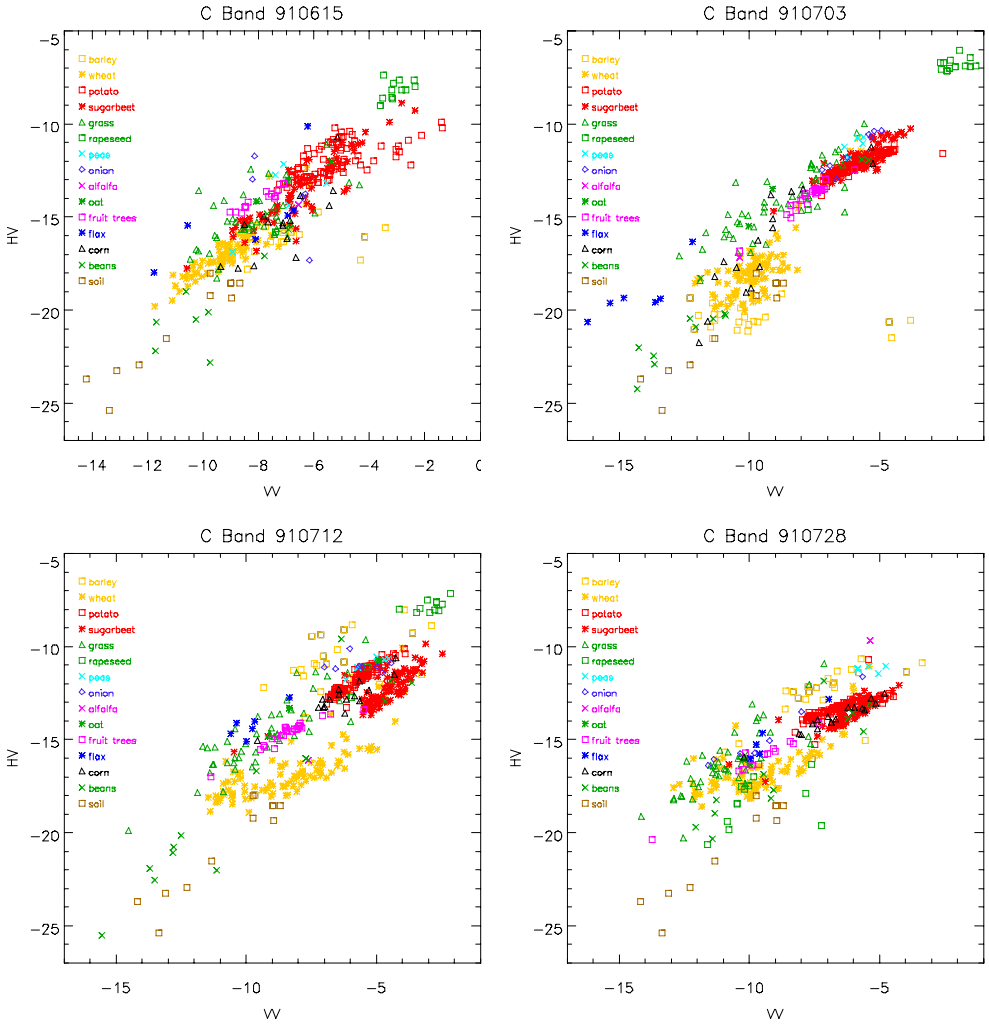

Figure 6.9. σ_{HV} versus σ_{VV} for the 4 dates of AIRSAR data in Flevoland.

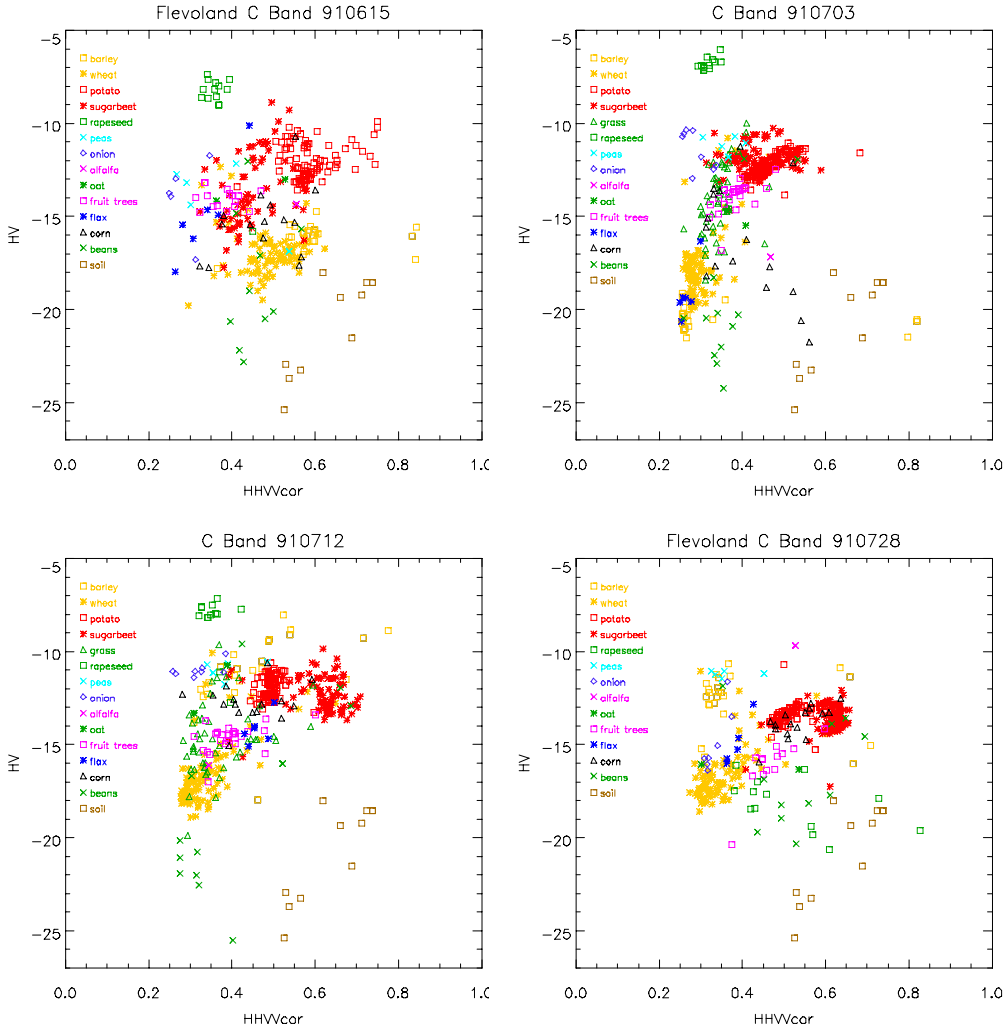

Figure 6.10. σ_{HV} versus ρ_{HH-VV} for the 4 dates of AIRSAR data in Flevoland.

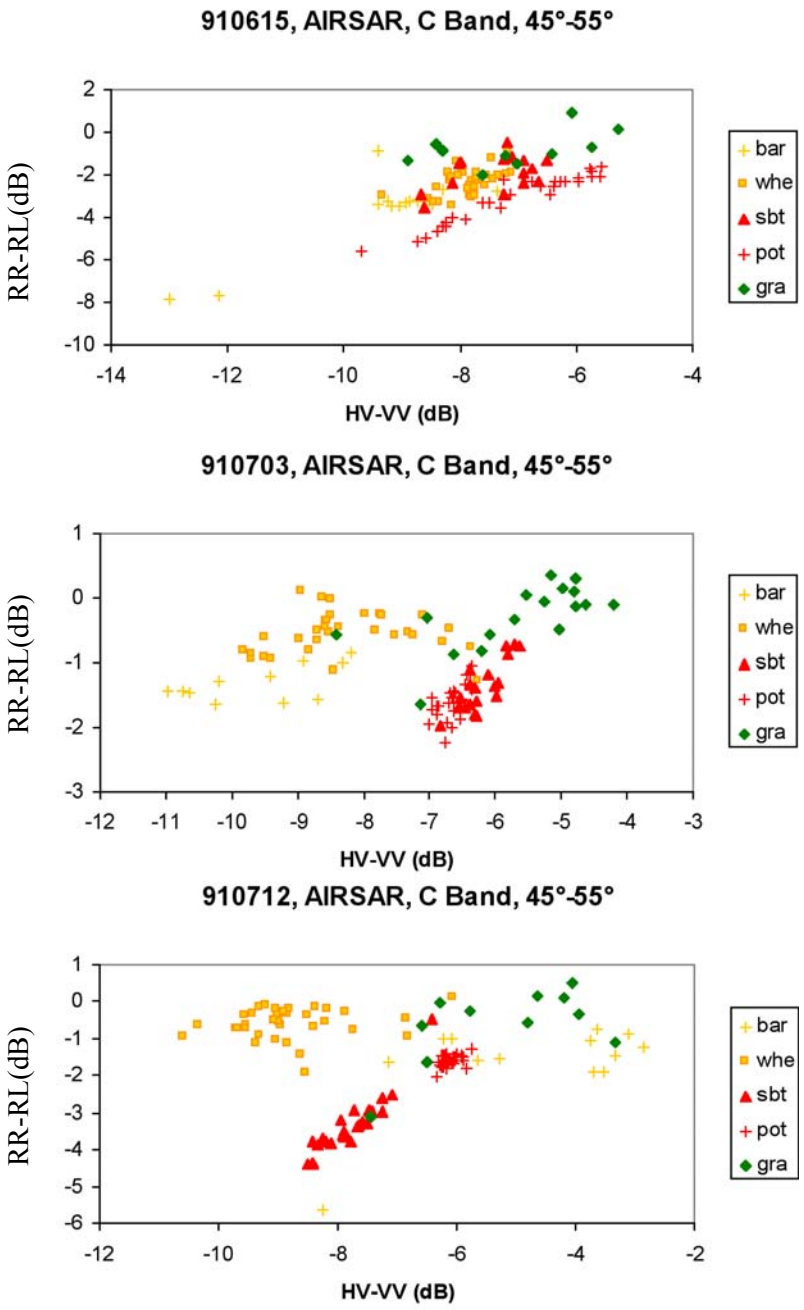

Figure 6.11. $\frac{\sigma_{RR}}{\sigma_{RL}}$ versus $\frac{\sigma_{HV}}{\sigma_{VV}}$ for three dates of AIRSAR data in Flevoland.

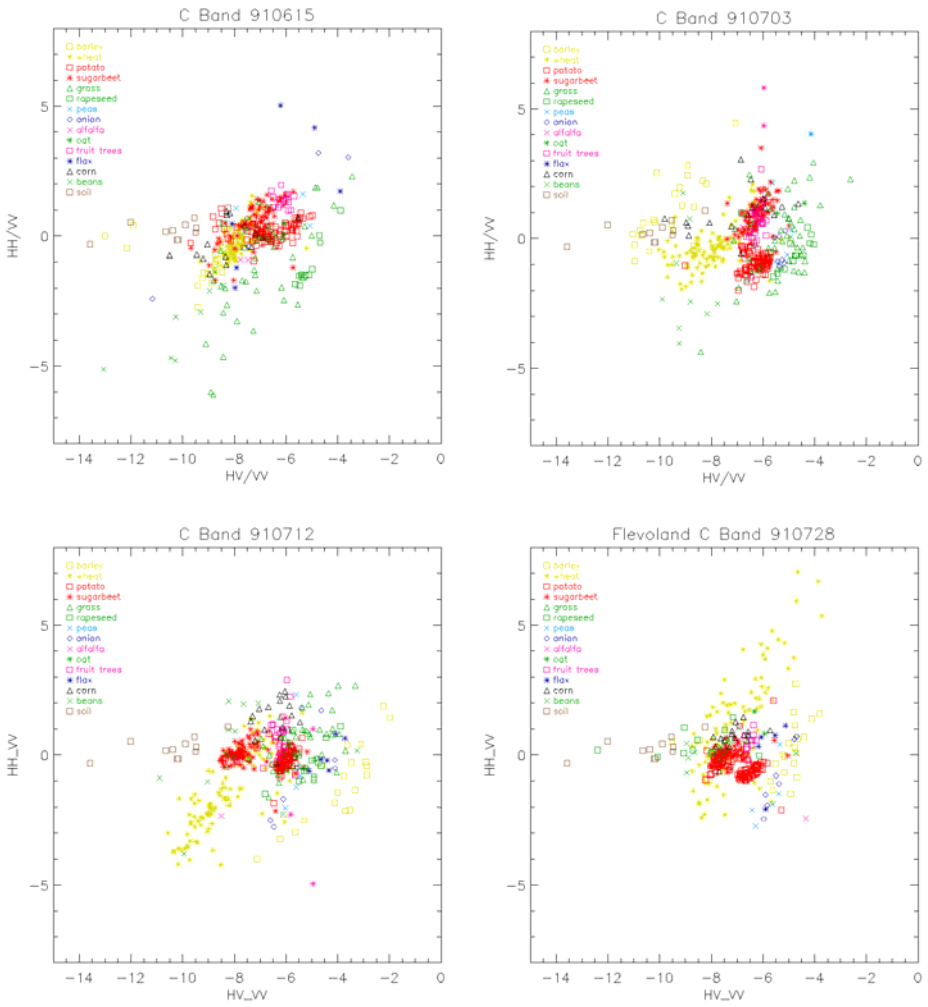

Figure 6.12. $\frac{\sigma_{HH}}{\sigma_{VV}}$ versus $\frac{\sigma_{HV}}{\sigma_{VV}}$ for the 4 dates of AIRSAR data in Flevoland.

6.5 Selection of backscatter measurements for crop classification.

6.5.1 Discrimination between vegetation and bare soils.

To reduce the confusion caused by responses of a large number of crops, spring and winter crops can be separated early in the growing season, based on the difference in surface and volume scattering. Late in the season, (e.g. late July for the test sites), harvested fields can be separated from non-harvested fields, also based on volume and surface scattering. Polarimetric parameters that are expected to have potential for discriminating between bare and vegetated fields are those, which maximise the difference between surface and volume scattering. These are:

a) The cross-polarized backscatter coefficient σ_{HV} , and the $\frac{\sigma_{HV}}{\sigma_{VV}}$ ratio (or $\frac{\sigma_{HV}}{\sigma_{HH}}$ ratio) , the latter having higher values for volume scattering than surface scattering. Ferrazzoli et al. (1999) propose the use of $\frac{\sigma_{HV}}{\sigma_{VV}}$ and $\frac{\sigma_{HV}}{\sigma_{HH}}$ for discriminating bare soils and vegetation.

b) The correlation coefficient between σ_{HH} and σ_{VV}, ρ_{HH-VV}, is high for a bare surface with roughness prevailing in agricultural fields for surface scattering. The correlation is low for vegetation, i.e., when:

- σ_{HH} and σ_{VV} result from differences in relative importance of interaction mechanisms (e.g. at C band for vertical crop structure, the dominant mechanism could be attenuated soil

scattering with σ_{HH} and canopy scattering with σ_{VV}),

- σ_{HH} and σ_{VV} result from the same mechanism but generated from different parts of the canopy. ρ_{HH-VV} is thus mainly affected by the plant structure.

6.5.2 Separation between broad leaf and small stem crops.

Ferrazzoli et al. (1999) showed in their simulations an appreciable difference between σ_{RR} and σ_{RL} backscatter when crops with small stem were compared with crops of wide leaves. The difference was interpreted as due to cylinder scattering compared with disc scattering. However, small stem crops, such as wheat and barley, have stems that are predominantly vertical, whereas broad leaf plants like sugar beet and potatoes contain more randomly oriented scatterers, and the difference may be due to the plant structure, in addition to the scatterer size and shape. **Figure 6.8** shows $\frac{\sigma_{RR}}{\sigma_{RL}}$ versus $\frac{\sigma_{HV}}{\sigma_{VV}}$ ratios (in dB) at the Flevoland site on July 28. Wheat, barley and grass have a limited range of σrr σrl, whereas potato and sugar beet have lower values. The separation is also clear on July 12 (**Figure 6.11c**), but less so on July 3 (**Figure 6.11b**) and not at all on June 15 (**Figure 6.11a**).

6.5.3 Separation of plants with different biomass levels.

σ_{HV} is a good discriminator of different biomass levels. At Flevoland, separation between rapeseed, barley, wheat and beans is possible with σ_{HV}. **Figure 6.10c** shows also that sugar beet and potato can be separated using ρ_{HH-VV} at this mid-July date.

6.6 Summary of the Flevoland database analysis.

The analysis carried out on the Flevoland dataset indicates the following:

a) The variation of the radar parameters with the angle of incidence is important and needs careful consideration when:

- Defining the optimum incidence angle for spaceborne SAR data,
- Applying classification methods to airborne SAR data, and
- Transferring conclusions based on airborne SAR data to spaceborne systems.

b) The various SAR parameters that can be derived from polarimetric SAR data vary significantly over intervals of 9-18 days in June-July. The temporal variations could be interpreted in terms of scattering mechanisms, using detailed crop and soil geometric and dielectric properties, if the relevant ground data were available. However, to derive robust classification methods based on scattering mechanisms, the crop calendar at a given test site must be known.

c) It may be possible to discriminate between broad leaf crops and small stem crops using acquisitions later in the growing season (mid to late July) using $\frac{\sigma_{RR}}{\sigma_{RL}}$.

d) Small stem crops with different biomass level can be discriminated uisng σ_{HV}.

e) An interesting observation was the high increase of the HH/VV ratio that occurs for wheat fields from July 12 to July 28, which is a

consequence of the vertical structure of wheat.

6.7 Physical based crop classification.

The analysis of the previous sections was based on field-averaged data. The study presented in this section makes use of pixel-based methods on Flevoland data. Because we are dealing with pixel data, but comparing with a ground cover map, some additional radiometric and geometric processing is necessary. In order to smooth the data, they were first filtered using methods developed at DTU (Technical University of Denmark), (Schou and Skriver, 2001). This MAP filter for multi-channel data introduces a bias into some of the covariance terms, which needs to be taken into account when setting thresholds based on field-averaged or unfiltered data. A geometrical correction was applied after the classification. Images were converted from slant to ground range geometry, and all the images were superposed by means of ground control points, using the image from July 12 as a reference. In order to validate the classifications, the crop map was scanned and superposed on the July 12 ground range image using ground control points. This digital map was then used for masking borders and all the parts of the images outside the ground truth map.

6.7.1 Proposed classification scheme.

The hierarchical classification method is based on the analysis of the Flevoland field-averaged database of the previous sections and on the work of Ferrazzoli et al., (1999). The algorithm, developed for the July 12 data, uses C-band and is described in **Figure 6.13**. The algorithm starts with a decision rule

that separates soil from vegetation. A second rule separates broad leaf and small stem crops using σ_{RR}/σ_{RL}. These two main classes are then separated into subclasses by using ρ_{HH_VV} for the broad leaves and σ_{HV} for the small stems. For the broad leaf class, two subclasses are defined: potatoes and sugar beets. For the small stem class, we define three subclasses: winter wheat, barley and rapeseed. The algorithm therefore contains five decisions rules, each of which requires the selection of a threshold, as indicated on **Figure 6.13**.

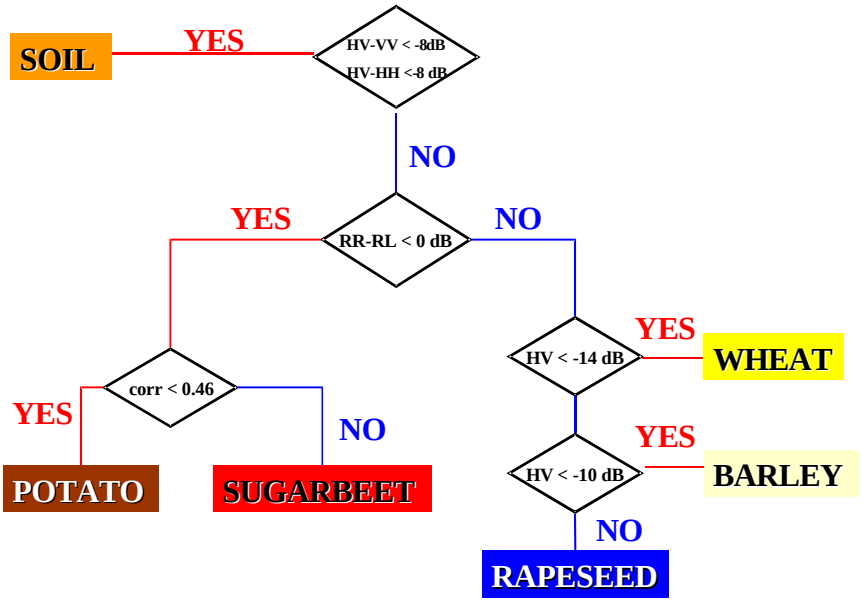

Figure 6.13. Hierarchical Classification Scheme of the proposed algorithm.

6.7.2 Results for July 12.

The effectiveness of the second decision in the algorithm, which uses σ_{RR}/σ_{RL} to separate broad leaf and small stem crops, is shown in **Figure 6.14.** The upper image shows broad leaf (red) and small stem (yellow) results while

the lower image displays the crop map with the 13 classes. It can be seen that potatoes and sugar beet are mainly assigned to the broad leaf class, while barley, wheat and rapeseed are labelled as small stem. Other fields, such as flax, are classified in the small stem class. Grass fields are labelled as broad leaf in the upper part of the image, but as small stem in the lower part. Alfalfa fields are also split between the two classes. **Table 6.1** summarises these results, and shows that 98% of the broad leaf fields and 95% of the small stem fields are correctly classified.

CROP/ID	No. of fields	No. of fields well classified
Small Stems	174	165 (95%)
Broad Leaves	217	212 (98%)

Table 6.1. Results of classifying the July 12 image into broad leaf and small stem classes

The classification of the July 12 image is shown in **Figure 6.15** (top), and should be compared with the crop map below it. Only a small number of pixels are assigned to the bare soil class, including those in one small barley field at the top of the image and some regions inside the biggest wheat fields. An effective way to visualise the spatial structure of the classification errors is by displaying the omission and commission errors for each class, where the omission errors for a given class are those pixels that belong to the class but are not assigned to it, and the commission errors are those pixels that do not belong to the class but are assigned to it. **Figure 6.16** and **6.17** respectively show, in white, the omission and commission errors for each class and for the five classes together. These figures indicate that there are no large-scale misclassifications of any of the crop types. Regarding systematic errors, from the 'sugar beet' panel in **Figure 6.16b** and the 'potato' panel in **Figure 6.16c** it

can be seen that the boundaries of many of the sugar beet fields are misclassified as potatoes. Some barley fields at the top of the image are classified as rapeseed, and some sections of wheat fields together with one whole rapeseed field are assigned to the 'residual', i.e. bare soil class.

Summary statistics for the classification are given in terms of confusion matrices, accuracies and kappa coefficients, and overall omission and commission errors.

In the confusion matrix, columns correspond to the ground truth and rows to the assigned classes. Hence element (i, j) gives the number of pixels in ground class j that are assigned to class i. The omission error for class k is the sum of all the non-diagonal terms in column k divided by the column-sum. The commission error for class j is the sum of all the nondiagonal terms in row j divided by the row-sum.

Table 6.2 shows the confusion matrix in percentage. As inferred from **Figures 6.16b** and **6.16c,** many of the sugar beet (30.99 %) fields are confused with potato and only 62.10% of the sugar beet pixels are correctly classified. The main errors in the wheat class are due to assignment of 13.62% of the wheat pixels to potato (compare the 'wheat' panel of **Figure 6.16b** with the 'potato' panel of **Figures 6.16c**) and 12.37% to soil. The confusion matrix shows that, apart from potato, significant proportions (exceeding 12%) of each of the crops are assigned to one or more of the other crop types.

Overall commission and omission errors are shown in **Table 6.3.** Potato has the biggest commission error (36.40%), while the biggest error of omission corresponds to sugar beet (37.90%). This is because almost all misclassified sugar beet pixels are labelled as potato. The overall accuracy is 73%.

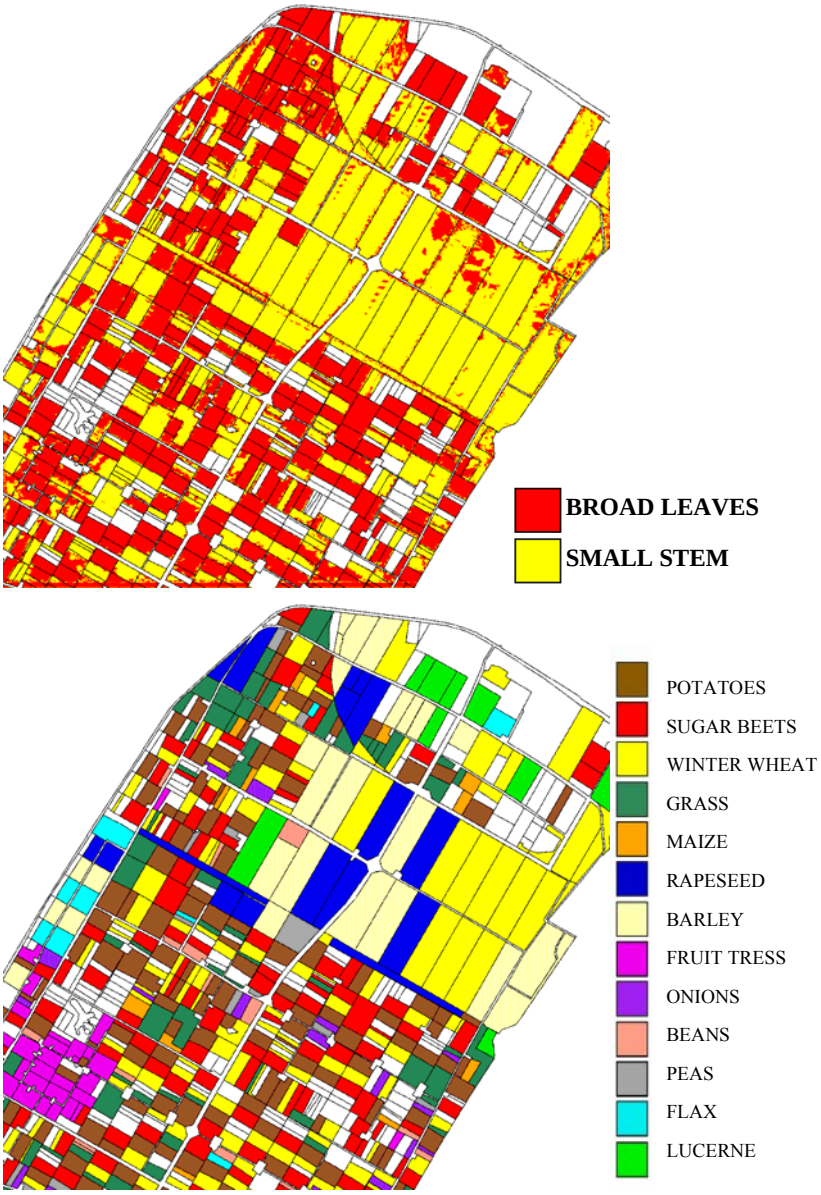

Figure 6.14. (Top) Broad leaf/small stem separation for the July 12 image. (Bottom) Crop map.

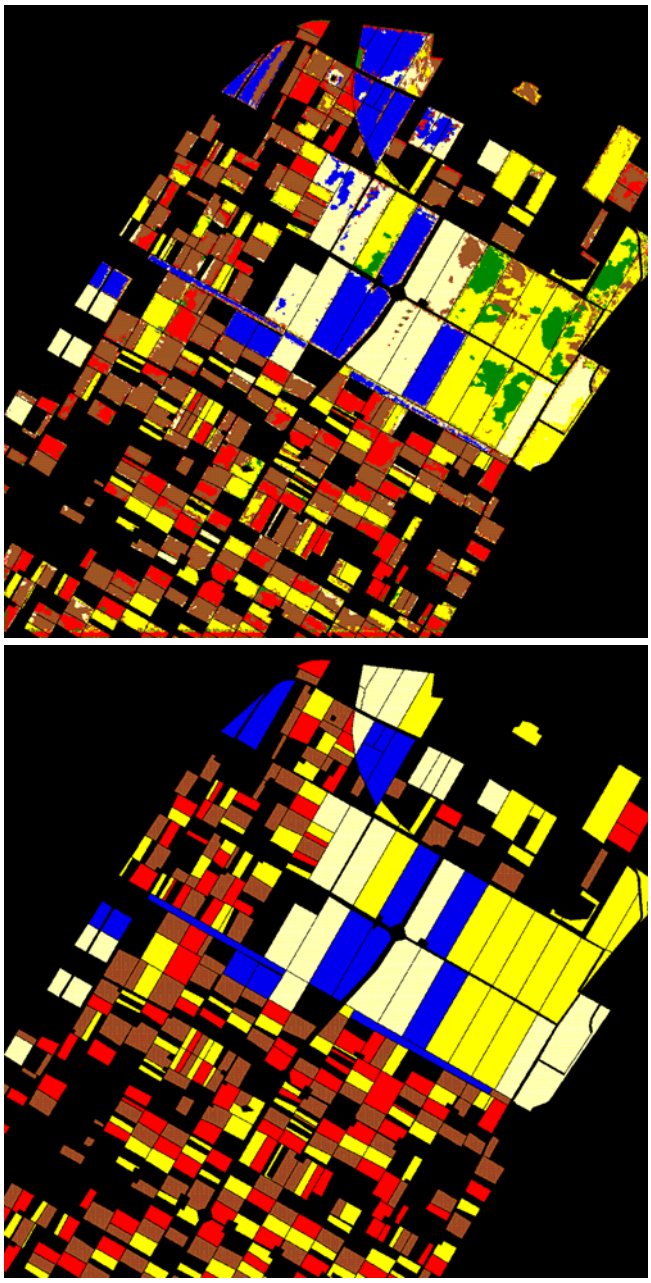

Figure 6.15. Classification results for July 12 (top) and ground truth (bottom). Six classes are distinguished: Potatoes (Siena), Sugar beets (Red), Rapeseed (Blue), Wheat (Yellow), Barley (Pale Yellow) and Bare Soil (Green). The other classes have been masked.

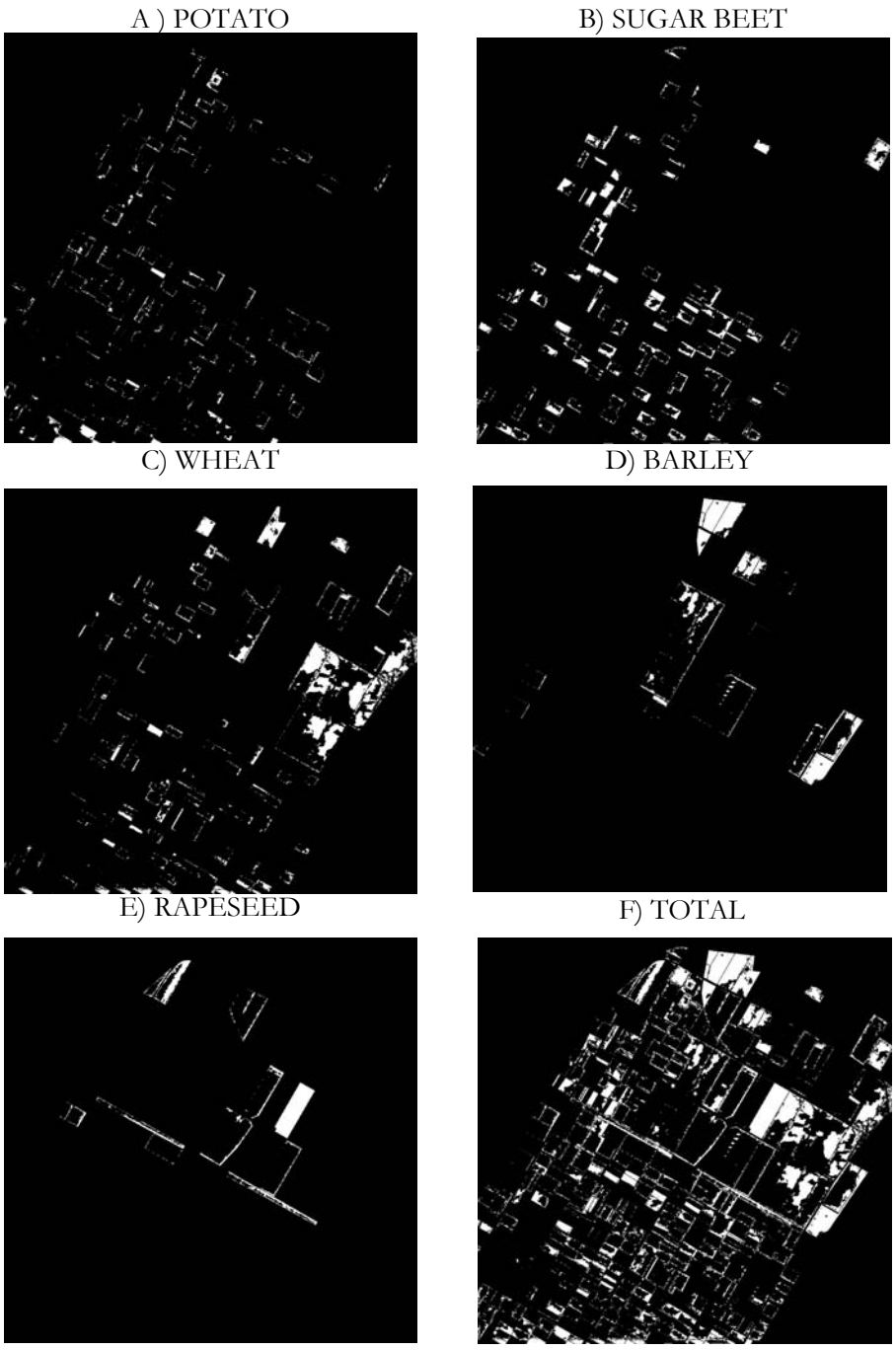

Figure 6.16. Error of omission for each class and total error for the July 12 image.

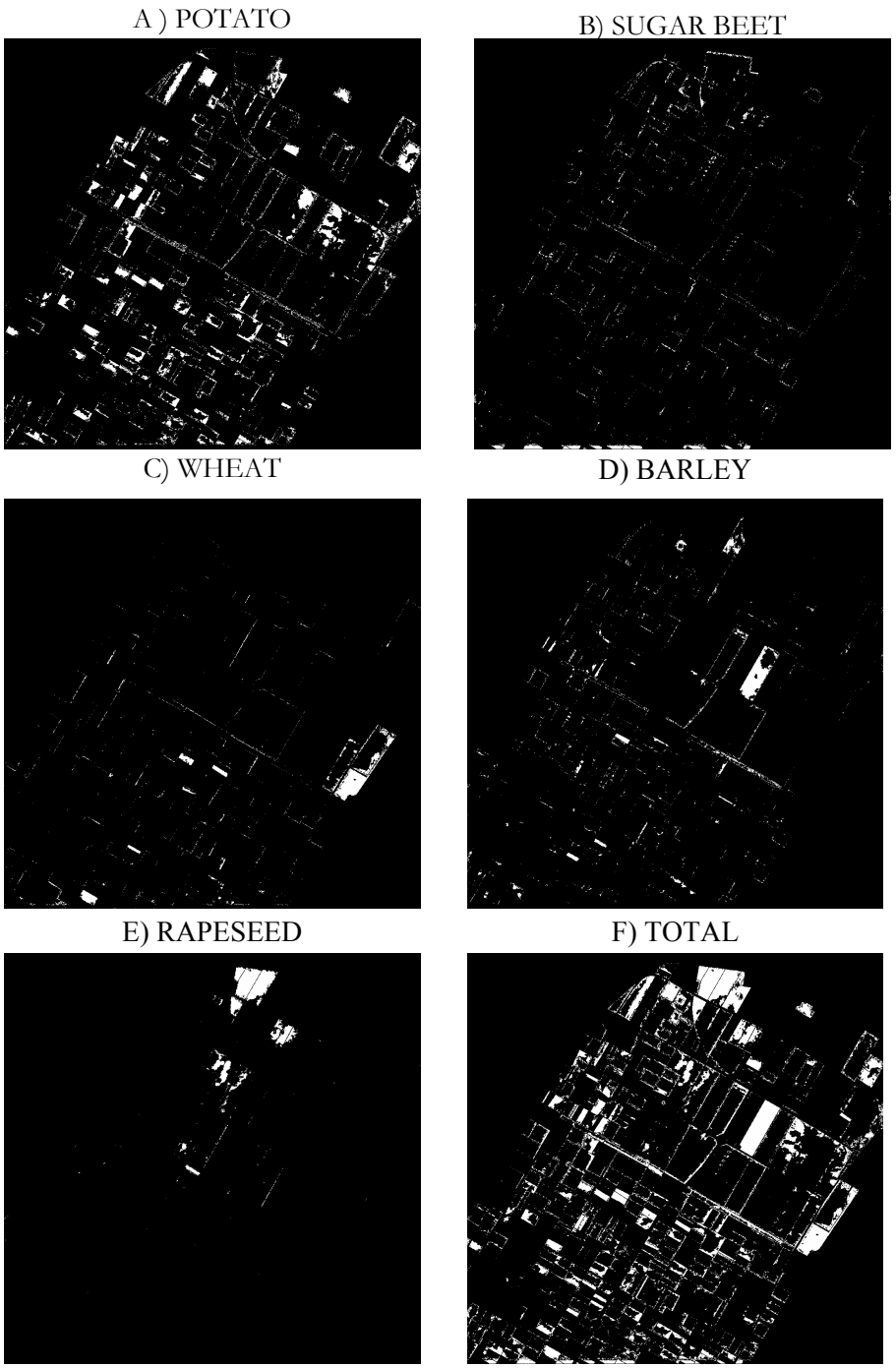

Figure 6.17. Error of commission for each class and total error for the July 12 image.

Overall accuracy: 72.92%, Kappa Coefficient: 0.66

	GROUND TRUTH (PERCENT)					
CLASS	**Potato**	**Sugar beet**	**Wheat**	**Barley**	**Rapeseed**	**Total**
Potato	87.03	30.99	13.62	2.70	13.18	31.85
Sugar beet	4.79	62.10	2.01	1.88	1.71	13.34
Wheat	3.10	2.12	69.79	7.69	0.89	23.65
Barley	4.44	1.12	2.18	72.11	13.45	16.02
Rapeseed	0.09	0.01	0.03	14.85	70.55	10.46
Soil	0.55	3.67	12.37	0.77	0.22	4.68
Total	100.00	100.00	100.00	100.00	100.00	100.00

Table 6.2. Confusion matrix for Algorithm 2 (July, 12) [%]

Class	Commission (%)	Omission (%)
Potato	36.40	12.97
Sugar beet	16.80	37.90
Wheat	10.77	30.21
Barley	21.14	27.89
Rapeseed	25.17	29.45

Table 6.3. Commission and omission errors for Algorithm 2 (July,12).

6.7.3 Results for July 28.

In this case the percentage of correctly classified fields is 98% for broad leaf and 63% for small stems **(Table 6.4)**.

CROP/ID	No. of fields	No. of fields well classified
Small Stems	166	105 (63%)
Broad Leaves	217	213 (98%)

Table 6.4. Results of classifying the July 28 image into broad leaf and small stem classes.

As it can be seen in **Figure 6.18**, on July 28 many of the rapeseed fields are labelled as bare soil. Others are classified as potato and sugar beet.

None of the fields is classified as rapeseed, although the class is considered in the algorithm. The ground truth map does not contain a bare soil class, so the confusion matrices have been constructed by equating soil with rapeseed. The confusion matrix (**Table 6.5** and **6.6**) shows that the percentage of well-classified potato fields is 73.73%, but 19.35% are confused with sugar beets. We can see in **Figure 6.20a** that this mainly occurs for fields located towards the top of the image. The lowest accuracy is for the soil class (0.73%). For barley, 62.18% of the pixels are well classified, with 29.83% being confused with wheat. The highest error of commission is 50.38% corresponding to potatoes, and the lowest 6.57% corresponding to barley. This is because 30.51% of the sugar beet pixels, 24.76% of wheat pixels and 37.43% of the rapeseed pixels are wrongly labelled as potato.

Class	Commission (%)	Omission (%)
Potato	50.38	26.27
Sugar beet	32.07	35.57
Wheat	25.03	36.00
Barley	6.57	37.82
Soil	37.31	43.78

Table 6.5. Commission and omission errors for Algorithm 2 (July,28).

Overall accuracy: 65.27%, Kappa Coefficient: 0.55

	GROUND TRUTH (PERCENT)					
CLASS	**Potato**	**Sugar beet**	**Wheat**	**Barley**	**Rapeseed**	**Total**
Potato	73.73	30.51	24.76	5.56	37.43	35.78
Sugar beet	19.35	64.43	0.63	1.17	3.39	16.90
Wheat	4.09	1.66	64.00	29.83	2.84	26.10
Barley	1.00	0.45	1.28	62.18	0.12	11.03
Rapeseed	1.11	2.43	9.15	1.01	5.22	9.82
Soil	0.73	0.52	0.18	0.25	0.00	0.37
Total	100.00	100.00	100.00	100.00	100.00	100.00

Table 6.6. Confusion matrix for Algorithm 2 (July, 28) [%]

6.7.4 Results for July 3.

The results for the direct hierarchical classification Algorithm 2 are given in **Table 6.7** and **Figure 6.8.** The classification and the total error are displayed in **Figure 6.19** and **6.20b**, respectively . They are clearly valueless: only rapeseed is well classified, while barley and sugar beet are lost as classes and many of the potato and wheat pixels are misclassified. This is exactly what was expected, given that the structuring of the data in the feature space is very different in early July compared to the later dates.

Overall accuracy: 65.27%, Kappa Coefficient: 0.55

	GROUND TRUTH (PERCENT)					
CLASS	**Potato**	**Sugar beet**	**Wheat**	**Barley**	**Rapeseed**	**Total**
Potato	62.02	79.63	4.75	2.09	3.56	29.97
Sugar beet	2.64	2.87	0.28	0.24	1.14	1.35
Wheat	6.27	3.50	49.04	11.67	0.87	19.12
Barley	27.39	12.04	1.11	0.49	1.91	8.93
Rapeseed	0.02	0.02	0.02	0.42	91.91	10.91
Soil	1.65	1.95	44.81	85.10	0.62	29.72
Total	100.00	100.00	100.00	100.00	100.00	100.00

Table 6.7. Confusion matrix for Algorithm 2 (July, 3) [%]

Class	Commission (%)	Omission (%)
Potato	53.05	37.98
Sugar beet	63.69	97.13
Wheat	22.10	50.96
Barley	99.02	99.51
Rapeseed	0.84	8.09

Table 6.8. Commission and omission errors for Algorithm 2 (July,3).

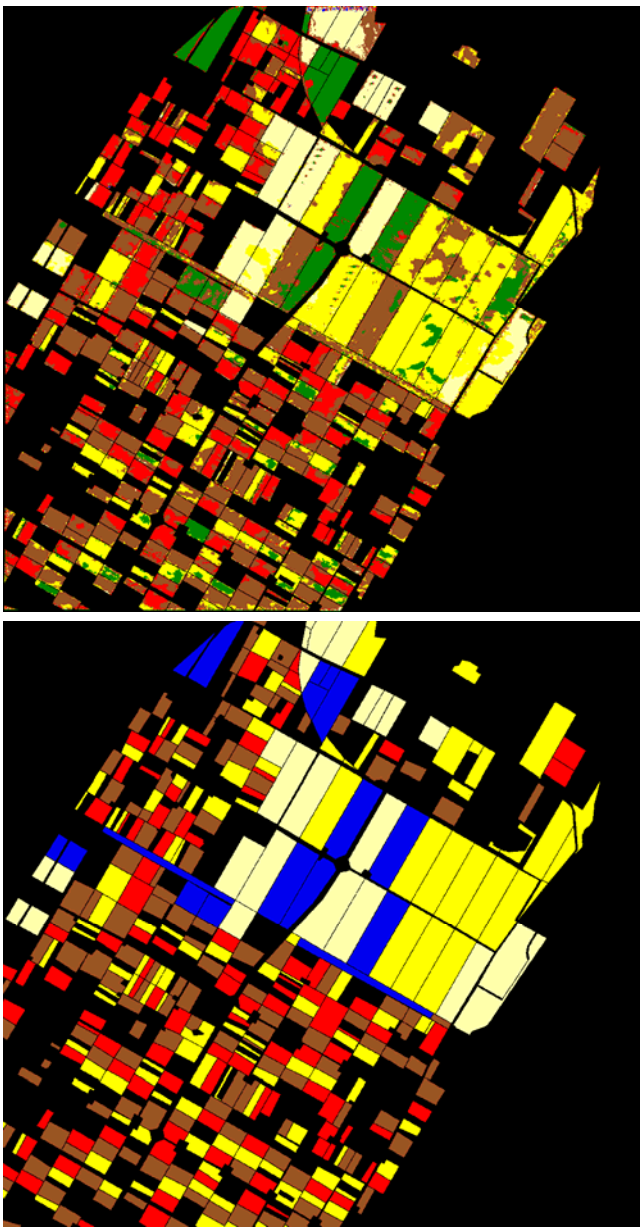

Figure 6.18. Classification results for the July 28 (top) and ground truth (bottom). Six classes are distinguished: Potatoes (Siena), Sugarbeets (Red), Rapeseed (Blue), Wheat (Yellow), Barley (Pale Yellow) and Bare Soil (Green). The other classes has been masked.

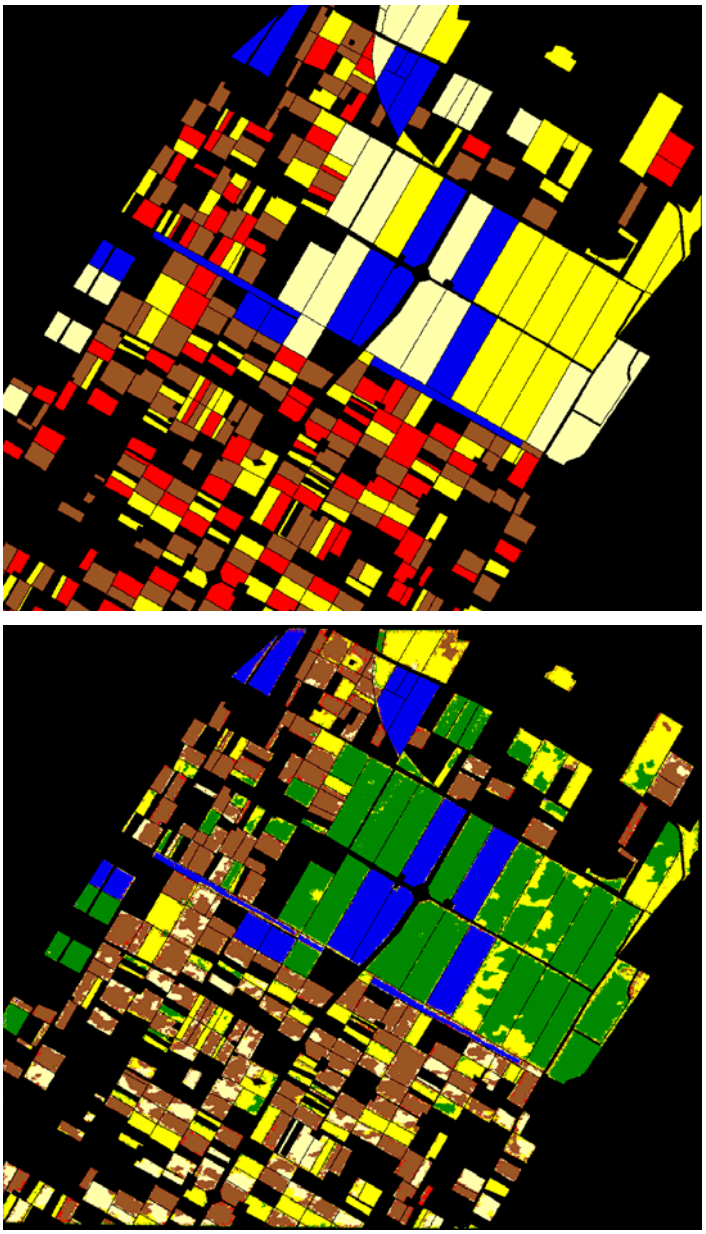

Figure 6.19. Classification results for the July 3 image (top) and ground truth (bottom). Six classes are distinguished: Potatoes (Siena), Sugar beets (Red), Rapeseed (Blue), Wheat (Yellow), Barley (Pale Yellow) and Bare Soil (Green). The other classes have been masked.

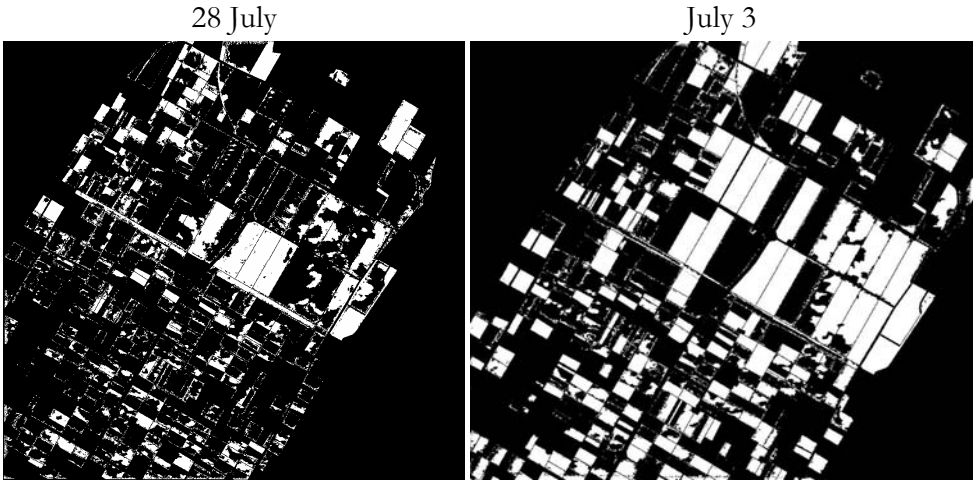

Figure 6.20. Total error for classification using algorithm 2 for a) July, 28 and b) July, 3.

Conclusions on the classification of the Flevoland fields:

Multi-temporal C-band polarimetric SAR data over Flevoland were analysed, with the aim to select optimum parameters for crop classification. The Flevoland dataset contains a large amount of measurements derived from AIRSAR data, acquired on June 15, and July 3, 12 and 28, 1991. The data analysis shows very strong temporal variation in the intensity and polarimetric measurements during June and July. Relatively invariant features for different dates in July appear to be the RR/RL ratio to discriminate crops with vertical from those with random structure, the correlation between HH and VV to separate structure in sugar beet and potatoes, HV to separate crops with different biomass levels, and the HH/HV ratio to separate vegetation from bare soil (or harvested fields).

6.8 Discrimination of crops using AIRSAR data in the area of Barrax.

This section presents an analysis of the AIRSAR data acquired in Barrax in order to evaluate the applicability or the proposed classification algorithm in a different area. The Barrax site was described in **Chapter 3**. AIRSAR data were acquired in the framework of the MAC-Europe campaign, at two dates: 19 June 14 July, in year 1991.

At mid-June, the small grain cereals (mainly wheat and barley) were in senescence stage and corn was at an early stage. The cereal fields were harvested between mid-June and mid-July. From mid-June to mid July the corn fields developed, but they were still far from the full development stage.

A field survey was conducted during the experiment to generate a crop field map (no-digital version available). These observations were used to identify the fields in the radar images, and extract the scattering signatures. Backscattering was averaged inside each field.

This dataset is not optimal for crop discrimination in the area using radar data, because at the current crop phenological situation (early stage for corn and senescence stage for cereals), the structural effects are hard to be detected. It would have been better to select dates at the beginning of May and beginning of August.

6.8.1 Data analysis.

The three steps of the classification algorithm developed for Flevoland were tested in the Barrax area.

Soil vegetation discrimination:

It was shown in **Section 6.4.1** that HV/HH and HV/VV ratios were able to discriminate between soil and vegetation. This ratios are interpreted as follows: the scattering of the vegetation volume gives high values of HV/HH and the scattering of the soil surface gives low values of HV/VV. A threshold of -8 dBs was found to be adequate for the Flevoland area.

The scatter plots comparing the HV/HH and the HV/VV ratios for June and July dates are shown in **Figure 6.21**. Small grain cereals (referred in the figure as cereals) and fallow have a large dispersion. For fallow fields, because of the dry conditions of the soils in the area, this spread is mainly due to differences in the surface roughness of the fields. From **Figure 6.21** it is deduced that, in June, this test is not able to discriminate the fallow fields from senescent cereals. Also many of the corn fields are confused. This result is not surprising because, during the senescent phase, cereals are almost transparent to radar signal in C band, especially if the soil is dry. The corn fields that are confused are probably in a very early phenological stage. The second observation that can be done is that the HV/HH, and HV/VV ratios allow us to detect cereal fields that were harvested in July (compare the two areas within squares in the two plots of **Figure 6.21**). In July, a threshold of -8dB/-9dB appears good for discriminating cereals and fallow fields from the rest of crops: corn, sunflower, garlic and alfalfa.

Similar results are obtained with the HH-VV correlation, ρ_{HH_VV}. **Figure 6.22** shows that in June cereal fields cannot be discriminated from fallow fields and as with the HV/HH, HV/VV ratios most of the corn fields are confused. It is interesting to compare **Figure 6.22b** with **Figure 6.10c** (12,

July Flevoland). In the Barrax region fallow fields present very high values of ρ_{HH_VV} (>0.7).

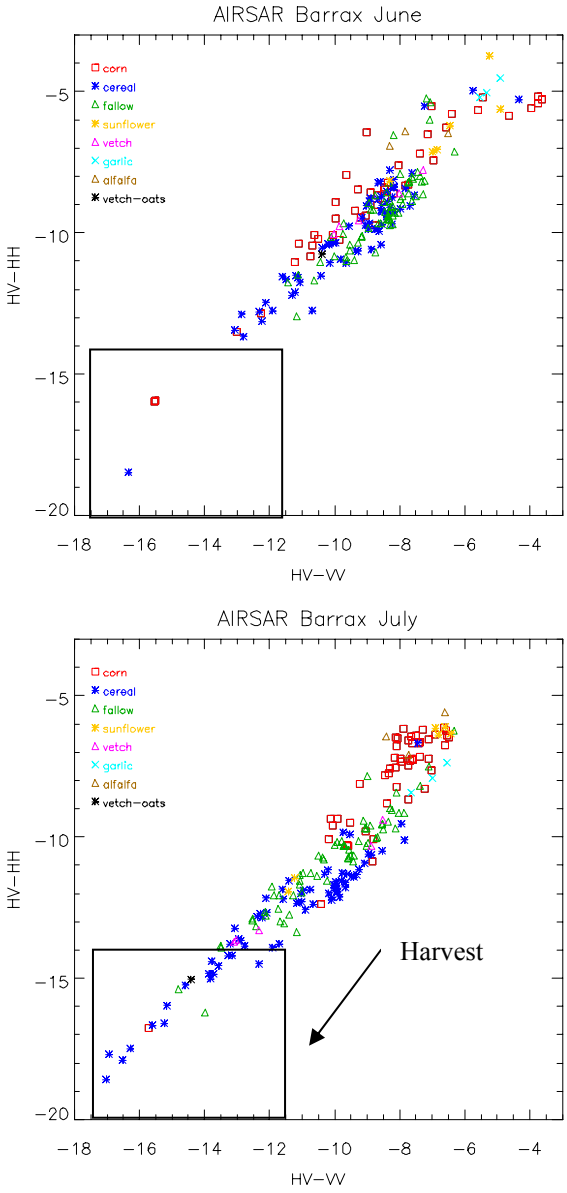

Figure 6.21. HV-HH versus HV-VV scatter plot for crop fields in the area of Barrax during June a) and July b).

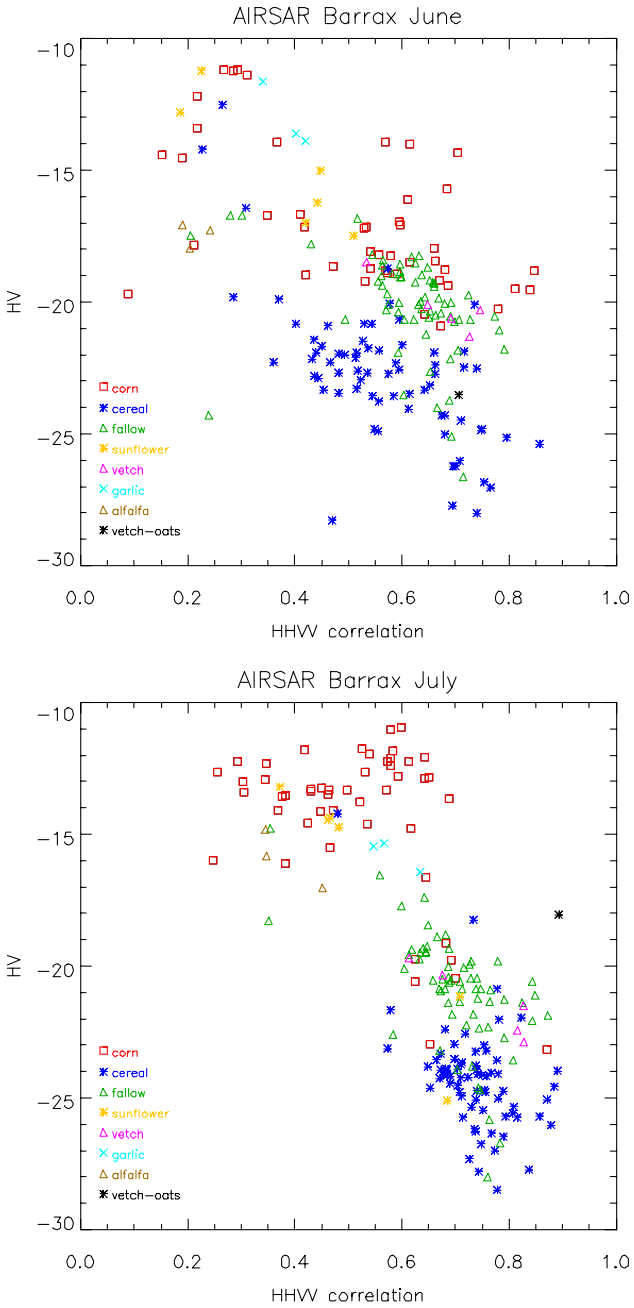

Figure 6.22. HV versus HH-VV correlation scatter plot for crop fields in the area of Barrax during June a) and July b).

Vegetation structure:

Figure 6.23 shows that, as expected, the structural effects are not clear in this case, neither in June or July. This is a consequence of the phenological stage of crops. However, structural changes in corn fields from June to July are well detected.

Biomass level:

Biomass level is given by HV. **Figure 6.24** shows the growing of corn and sunflower fields from June to July.

HV/HH versus HV/VV

The scatter plot resulting from comparing HV/HH versus HV/VV is shown in **Figure 6.25.** For the date in June these polarimetric ratos are not able to discriminate any cluster of type of crops. In July 14 distribution of clusters of this scatter plot is similar to that of HV versus HHVV correlation (**Figure 6.21**). The HH/VV ratio is slightly higher for wheat fields than for fallow fields, but both clusters are very mixed. The small values of HH/VV are a consequence of the phenological stage of wheat (ripening).

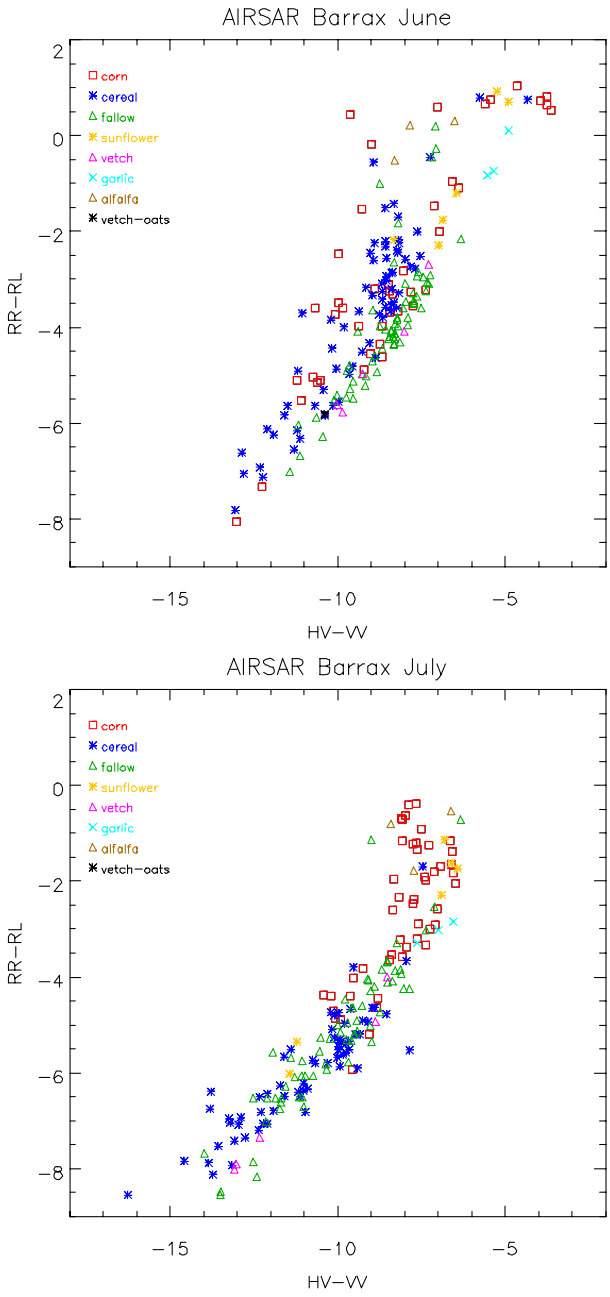

Figure 6.23. RR-RL versus HV/VV scatter plot for crop fields in the area of Barrax during June a) and July b).

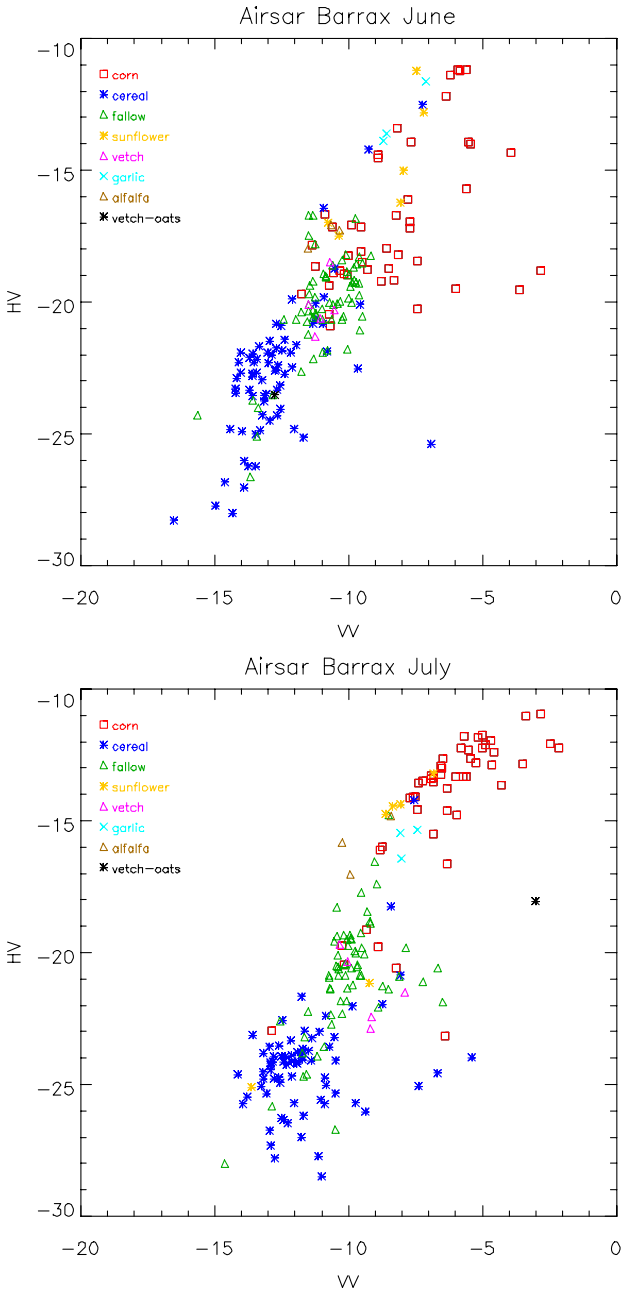

Figure 6.24. HV versus VV scatter plot for crop fields in the area of Barrax during June a) and July b). Cereals in are harvested between June and July.

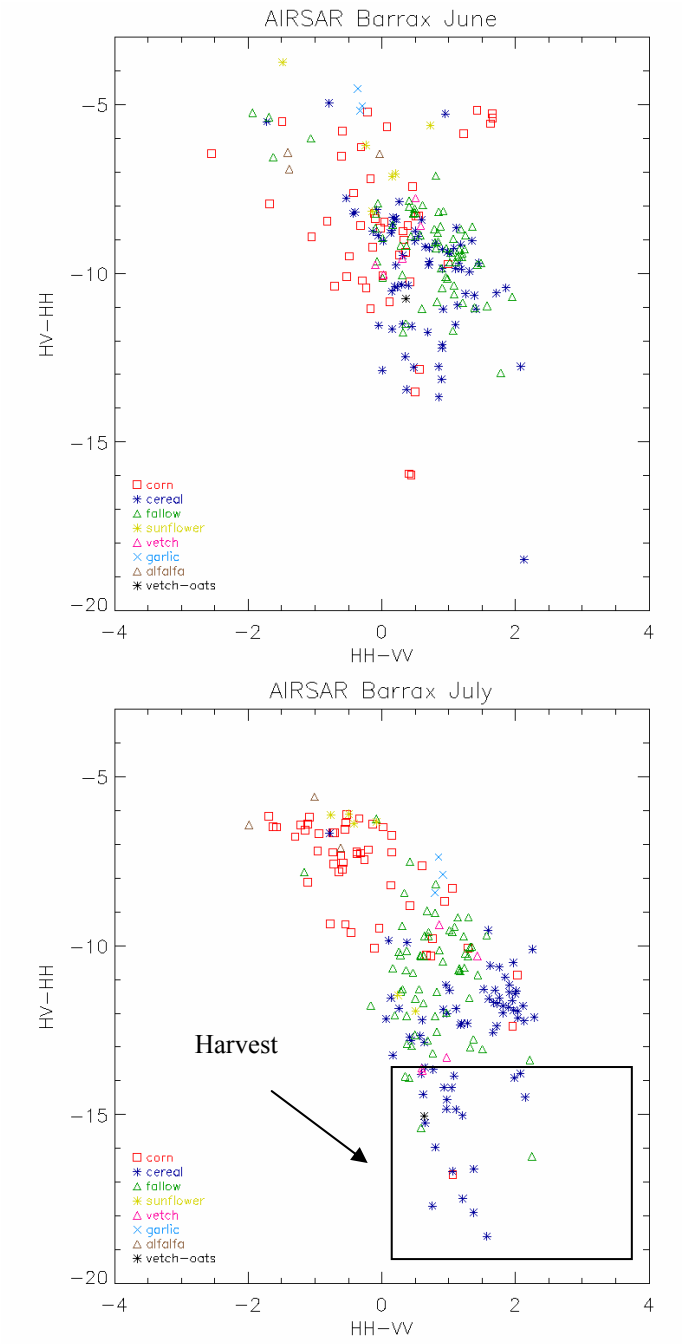

Figure 6.25. HV/HH versus HH/VV scatter plot for crops fields in the area of Barrax during June a) and July b).

Conclusion on the Barrax analysis

The analysis at the Barrax site confirms, as in the case of Flevoland, that the methods of classification based on scattering mechanisms need to take into account the crop calendar for a particular site. In the case of Barrax the acquisition time of the images was not optimal for the type of crops present in the area. Thus, the hierarchical classification method proposed for Flevoland could not be applied with success in this area for the two AIRSAR images available for this study. However, the analysis shows that the algorithm rules are quite robust and better results would be obtained with an image acquired at the end of July/beginning of August and at the beginning of May.

6.9 General conclusion.

The principal conclusions of this study are:

a) The radar data used for the classification of crops need to be adapted to the crop calendar of the area under study. The AIRSAR data available for this study were acquired during the MAC-Europe campaign in July, 1991. This period was well adapted to the characteristics of Flevoland, but it was not the case for Barrax. As a consequence, the same method that gave good results in Flevoland could not be applied in Barrax.

b) A limited set of polarimetric measurements carry the information needed to classify the crops present under northern European agricultural conditions. The most effective set of features appear to be the RR-RL ratio, the HH-VV correlation and the HV backscattering coefficient, together with the HV-VV and HV-HH ratios when bare soil (or harvested

crops) needs to be taken into account. These polarimetric measurements indicate the relevant biophysical characteristics of the crops.

c) The behaviour of these backscattering measurements varies markedly through the growing season, as a consequence of variation in the scattering mechanisms. For Flevoland, mid-July was clearly best suited to classification, with well-separated classes in the measurement space. The situation was not as good in late July, and, in early July.

d) In mid and late July, at Flevoland, the proposed classification algorithm was quite successful, with accuracies of around 73% in mid-July and 65% in late July.

e) This methodology could be adapted to other sites based on the knowledge of crop type and calendar.

CHAPTER 7:
USE OF ENVISAT ASAR-APP DATA FOR CROP STUDIES.

This chapter is dedicated to the analysis of ENVISAT/ASAR data in agricultural regions. The first part describes the experimental measurements done in a wheat field in the area of Toulouse during the year 2003, the available radar data and the processing applied. The second part of this chapter explores the possible application and limitations of the algorithm of crop classification presented in **Chapter 6** using data form the region of Toulouse acquired at several dates in 2003 and data acquired at one date in Barrax. The possibility of retrieving wheat biomass using ASAR data is also investigated.

7.1 Test site and dataset.

The test site of La Masquère (Toulouse) is located in the Midi-Pyrénées region of France (**Figure 7.1**). In Toulouse, the climate is considered as a transition between the Mediterranean and oceanic climates. The mean annual precipitation is higher than in Barrax (>650 mm). Although the dry season is recorded in summer, the seasonal variability is low. The number of rainy days is high but extremes are unusual. However, summer 2003 was atypical in terms of climatology. The growing period (March-September) was a period of pronounced drought with high temperatures.

Figure 7.1. Geographic location of the Toulouse area and La Masquère.

The Bouconne forest, of approximately 2200 ha and constituted of broadleaved and coniferous trees, is an important feature of the Northern part of the area. In the South, East and West, the landscape is hilly.

In the Toulouse region, meadows represent approximately 20% of the total surface. The forests correspond to 10% being mainly deciduous. This area is mainly dedicated to agriculture: crops represent about 65% of the surface. In 2003, the most important crops grown in the area were sunflower, wheat and corn. Other plantations, which were less important in surface, were rapeseed, sorghum, barley, soybean and peas. About 15% of the agricultural surface was let as fallow (**Figure 7.8**). Summer crops in the area need irrigation.

Within the Toulouse region the agricultural site of La Masquère was selected for field work.

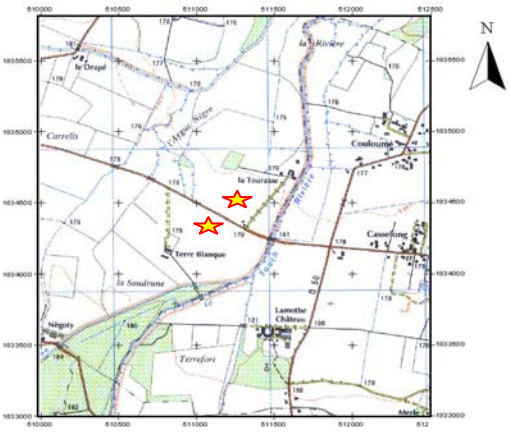

Figure 7.2. Wheat fields emplacement in La Masquère site.

La Masquère:

The test-site is located near the town called La Masquère, (**Figure 7.2**) where the Agricultural Engineering School of Purpan, (l'Ecole Supérieure d'Agriculture de Purpan, ESAP) has its farm (270 ha). The experiment took place in the Tourasse farm, which has its own drainage and its soil is clay.

7.1.1 Description of the field measurements.

As opposite to the experiments that took place in the Barrax site, the field measurements in Toulouse did not take place in an intensive one-week campaign but during the whole growth season and only for a wheat field.

Vegetation measurements consisted on: a) Fresh Biomass b) Dry Biomass, c) Plant Height, d) Stem Density and e) Plant density. Soil moisture was also measured.

Vegetation sampling was done in coincidence with ENVISAT overpasses. Sampling was done along 1 linear meter. Plat height was measured 4 or 5 times at different points along the 1 linear meter. The number of stems and the number of plants was counted before cutting the sample. Once cut, the sample was put in a plastic bag, closed, and kept in coolers for avoiding water losses. Samples were weighted fresh and after drying in an oven. For that purpose the facilities of the University Paul Sabatier were used. The number of samples was ten for dates 13/03 (DOY 72) to 17/04 (DOY 107) and five for the rest of days. This choice was done for practical reasons (space limitation in the oven).

Values of wheat parameters per squared meter were obtained by multiplying the 1 linear m measurements by the number of rows in 1 m, n_r. The number of rows was estimated counting the number of rows in five meters at several emplacements in the field. The average value obtained is $n_r = 6.75$. **Table 7.1** resumes the measurements and the corresponding standard deviations. For biomass, the standard deviation is higher after the period of stem elongation. Plant density values are very variable, as it is more difficult to estimate than stems density. **Figure 7.3** shows the biomass curves and height during the season. Before heading, there was a high correlation

between biomass and height (**see Figure 7.4**). Stems density decreases along the season, probably due to plant competition (**Figure 7.5a**). Finally, from Fresh and Dry Biomass vegetation water content has been estimated and it is displayed in **Figure 7.5b**.

Date	DOY	Phenology	Fresh Biomass (g/m2)	Dry Biomass (g/m2)	Height (cm)	Stem Density (nº/m2)	Plant Density (nº/m2)
13/03	72	Beginning of Tillering	230±80	43±15	18±3	800±100	138±13
22/03	81	Tillering	530±90	120±70	15.8±1.3	820±120	83±17
1/04	91	Tillering	1000±160	170±30	22±3	740±90	90±8
7/04	97	End of Tillering	1100±180	210±30	28.5±1.3	750±60	110±20
17/04	107	Stem Elongation	1500±240	330±60	38±3	660±80	110±30
26/04	116	Booting	2500±900	900±400	55±3	500±200	78±15
12/05	132	Heading	2700±900	700±300	70±4	380±130	78±14
22/05	142	Milky Grain	2100±300	740±120	76.2±0.9	350±150	80±15
10/06	161	Dough Grain	1900±300	1070±180	79±4	380±50	92±16
16/06	167	Hard Grain	1180±180	1040±110	69±3	370±30	100±18

Table 7.1. Vegetation measurements during 2003.

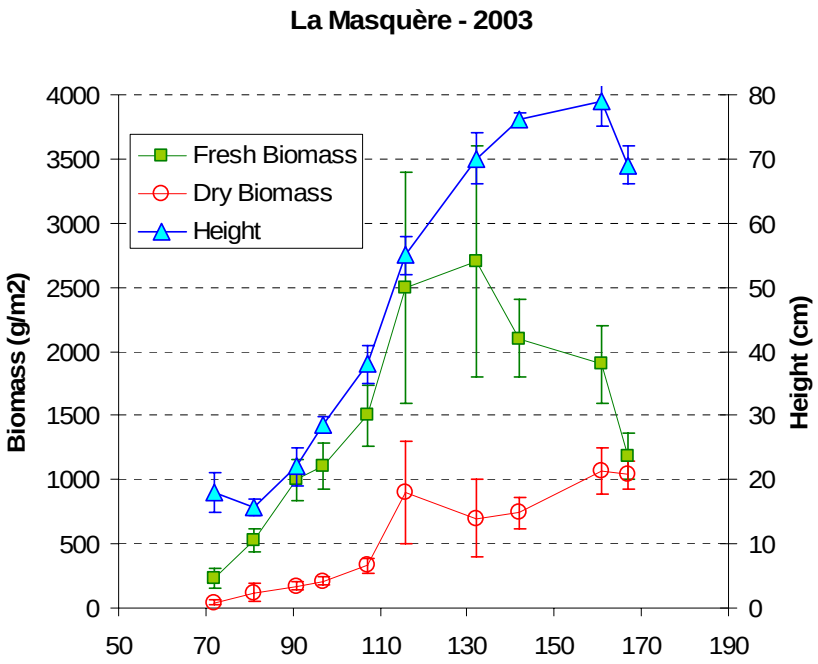

Figure 7.3. Fresh Biomass, Dry Biomass and height for wheat during 2003.

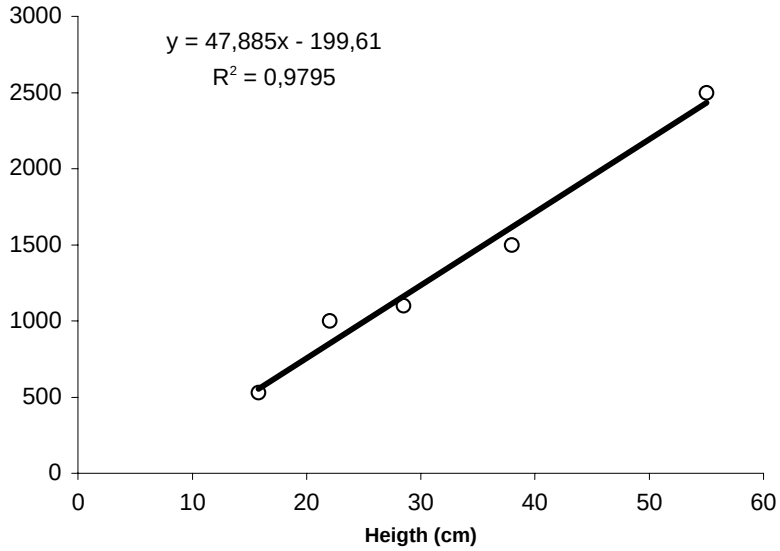

Figure 7.4. Relationship between height and Fresh Biomass for wheat before heading.

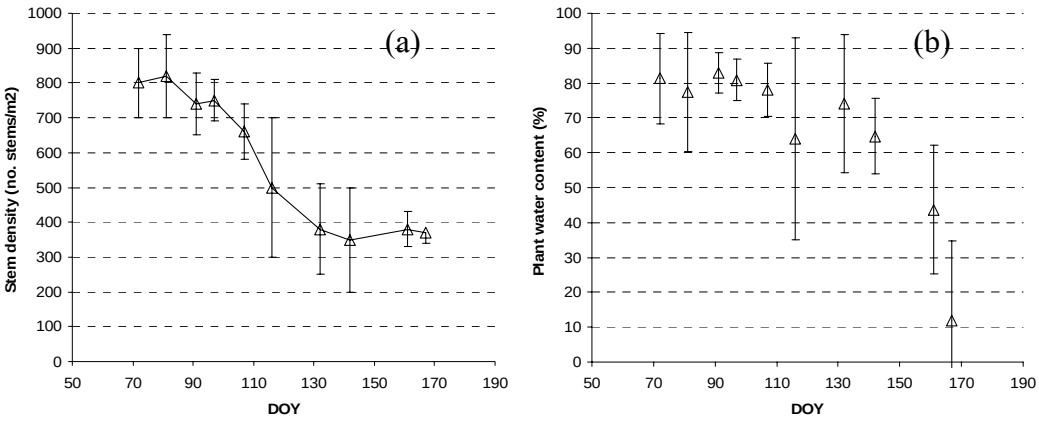

Figure 7.5. Stems density (a) and Plant water content (b) along year 2003.

In addition to these measurements, each date, the average sample was decorticated in leaves, stems and ears (when present) and weighted before and after drying. **Table 7.2** and **Figure 7.6** resume the obtained values.

Date	DOY	Fresh Biomass (g/m2)			Dry Biomass (g/m2)		
		Leaves	Stems	Ears	Leaves	Stems	Ears
13/03	72	90±30	160±50	-	12±4	39±13	-
22/03	81	360±60	170±30	-	70±10	30±4	-
1/04	91	630±50	380±80	-	93±7	69±12	-
7/04	97	560±90	650±110	-	110±18	120±20	-
17/04	107	690±110	870±140	-	160±30	290±50	-
26/04	116	800±300	1600±600	-	180±70	800±300	-
12/05	132	410±140	1400±500	480±160			140±60
22/05	142	290±40	1290±190	699±90	150±20	460±80	210±30
10/06	161		830±140	1060±180		480±80	610±100
16/06	167		560±90	600±100		500±60	570±60

Table 7.2. Distribution of biomass in the plant elements (leaves, stems and ears) for wheat along year 2003.

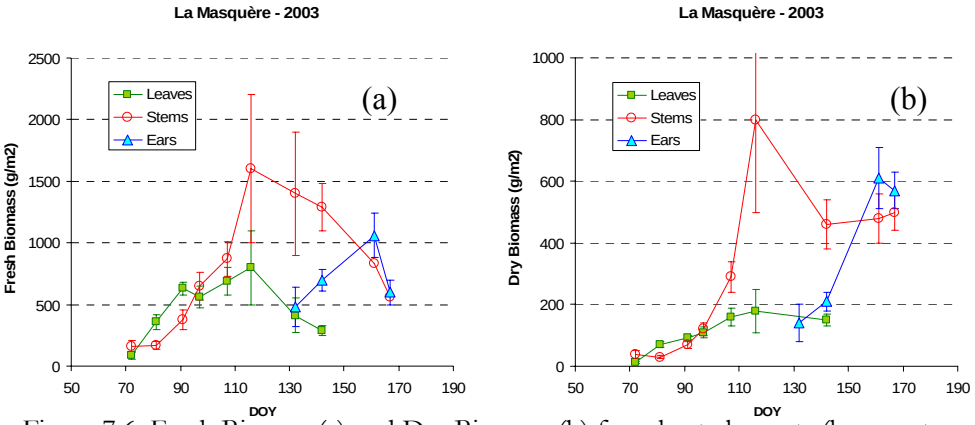

Figure 7.6. Fresh Biomass(a) and Dry Biomass (b) for wheat elements (leaves, stems and ears) during 2003.

Soil moisture w, was measured using the gravimetric method. For that, ten cylindrical pots, distributed along a transect, were filled with 2-3 cm depth soil. Soil was weighted wet, s_w, and after drying, s_d, allowing to soil moisture estimation as follows :

$$w = 100\frac{s_w - s_d}{s_w}\% \qquad \text{[Eq. 7.1]}$$

Date	DOY	Moisture (%)
13/03	72	14.2±1.4
22/03	81	8.6±0.8
1/04	91	11.9±1.2
7/04	97	5.5±0.8
17/04	107	5.3±0.6
26/04	116	17.7±0.9
12/05	132	12.4±1.5
22/05	142	6.0±1.2
10/06	161	4.1±0.6
16/06	167	3.3±0.1

Table 7.3. Soil moisture measurement values.

The values of soil moisture in 2003 are unusually low for the region, due to the drought period. All moisture values **are** below 12%, with the exception of the first measurement date, and a rainfall the 26th of April. Since the beginning of May no precipitations were registered, and soil moisture decreases progressively (**see Figure 7.7**).

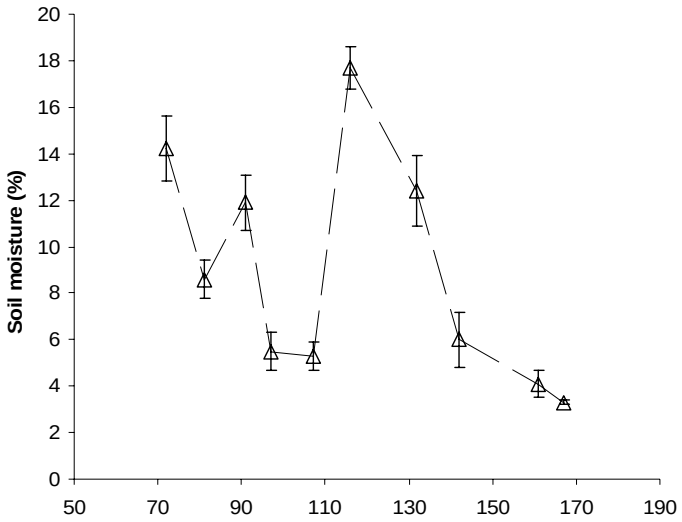

Figure 7.7. Soil moisture measurements values corresponding to the wheat field under study.

7.1.2 Radar Images.

ENVISAT ASAR data characteristics:

ASAR is an advanced SAR (Synthetic Aperture Radar instrument) at C-Band (5.331 GHz) and operating in 5 distinct measurements modes: Image Mode (IM), Alternating Polarisation Mode (AP), Wide Swath Mode (WS), Global Monitoring Mode (GM) and Wave Mode (WV). From all the possible ASAR modes the most adequate to the purpose of this study was the Alternating Polarisation.

The Alternating Polarisation products contain two co-registered images corresponding to one of the three possible polarisation combinations: HH & VV, HH & HV or VV & HV and one of the seven selectable swaths. Each swath corresponds to an incident angle range (see **Table 7.4**). These products are acquired and processed on request and have a spatial resolution of approximately 30m (except swath 1).

Alternating Polarisation products are multi-look, ground range images and can be geo-located (ASAR-APG-1P) or non-geolocated (ASA_APP_1P). In this study, Level 1B Alternating Polarisation Precision Images products were used. In order to preserve as much as possible the radiometric quality of the data, the non-geocoded ASAR-APP products were preferred, because they have minimal geometrical corrections. The pre-processing done by ESA includes, among others, data decompression, and engineering corrections, as antenna elevation pattern compensation and range spreading loss. From now, these data will be referred as ASAR-APP. ASAR-APP products are generated with a technique in which half of the looks of the image are acquired in horizontal polarisation and the other half in vertical polarisation. This leads to a lower radiometric quality compared to the ASAR Image mode, but two polarisations are available.

ASAR-APP images used in this study:

During the growth season of 2003 a number of 7 ASAR-APP images were acquired in the Toulouse area. Among those 7 images, 5 were acquired in HH & VV polarisations and the rest in HV & VV polarisations (see **Table 7.5**). Images out of the wheat season, as well as images from year 2004, were used for speckle filtering. During 2003, more images were requested to ESA

from March to September but unfortunately some of the acquisitions were cancelled.

Swath	Swath with (Km)	Near Range Incidence angle (degrees)	Far Range Incidence angle (degrees)
S1	108.4 - 109.0	14.1 – 14.4	22.2 – 22.3
S2	107.1 – 107.7	18.4 - 18.7	26.1 – 26.2
S3	83.9 – 84.3	25.6 - 25.9	31.1 – 31.3
S4	90.1 – 90.6	30.6 - 30.9	36.1 – 36.2
S5	65.7 – 66.0	35.5 - 35.8	39.2 – 39.4
S6	72.3 – 72.7	38.8 - 39.1	42.6 – 42.8
S7	57.8 – 58.0	42.2 - 42.6	45.1 – 45.3

Table 7.4. ASAR_APP_1P characteristics. Information from ESA web page (http://earth.esa.int).

Date	Polarisation	Swath
13/03/2003	HH & VV	S6
22/03/2003	HH & VV	S1
29/03/2003	VV & HV	S7
17/04/2003	HH & VV	S6
26/04/2003	HH & VV	S1
03/05/2003	VV & HV	S7
16/06/2003	HH & VV	S2
26/06/2003	HH & VV	S6
29/06/2003	VV & HV	S4
05/07/2003	HH & VV	S1
12/07/2003	VV & HV	S7
21/07/2003	HH & VV	S1
31/07/2003	HH & VV	S6

Table 7.5. ASAR-APP images over the study area during year 2003.

7.1.3 Ancillary data.

A classification of crops from the Toulouse region was used (see **Figure 7.8**). This classification is based in a maximum likehood multi-temporal classification method applied to 7 SPOT images (Gouaux et al., pers. comm.).

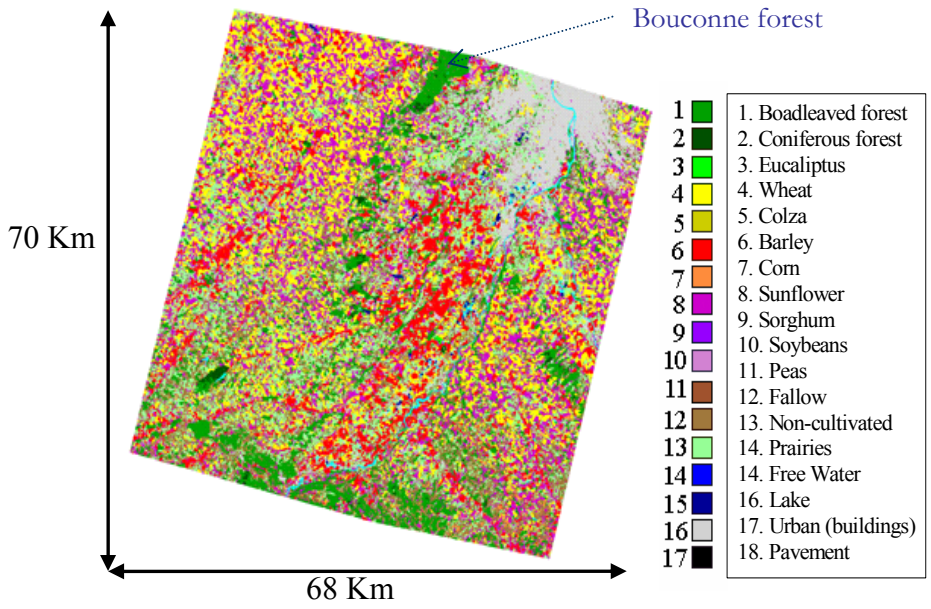

Figure 7.8. Land use classification in the area of Toulouse at 20 m resolution for year 2003 (Gouaux et al., pers. comm.).

7.2 Image processing.

Bouvet et al. (2008) implemented the image processing applied to the ASAR-APP images used in this study. The processing consists on five steps: extraction of the study region, calibration, resizing, co-registration and speckle filtering. The processing was applied following this sequence, as co-registration is a requirement for applying the speckle filtering method. The general scheme

of the processing is illustrated in **Figure 7.9**. Below, some details concerning the processing steps are given.

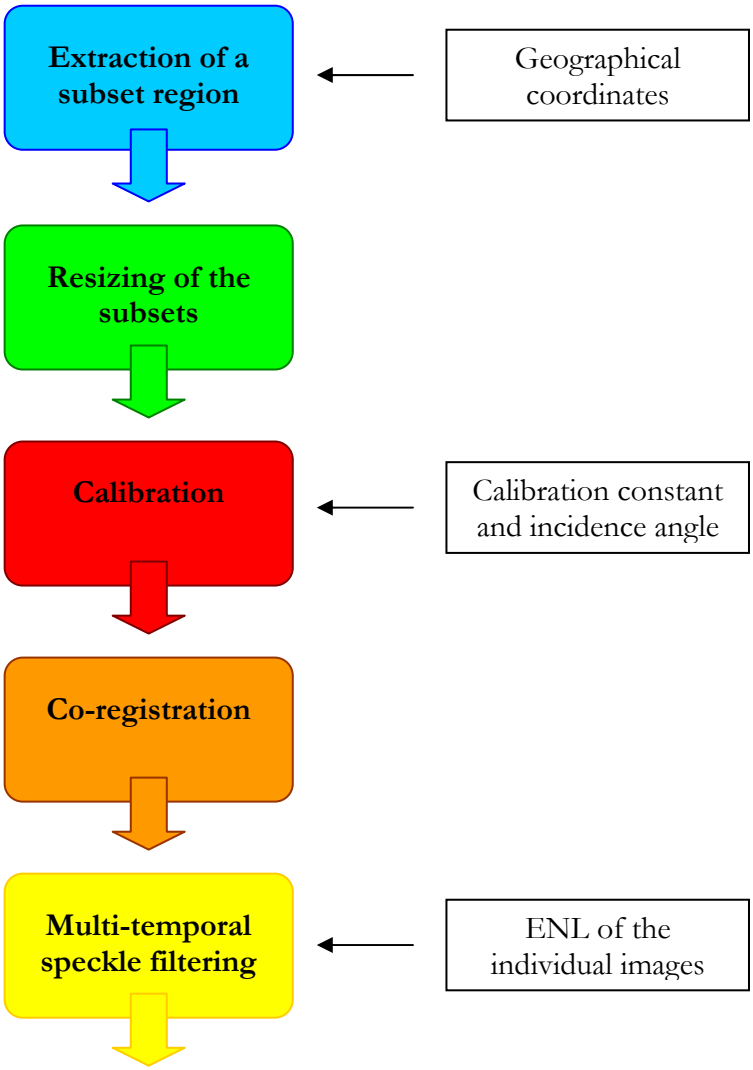

Figure 7.9. Image processing scheme.

Extraction of the region of study:

The extraction of the region of study is done on the SAR images, in a first approximation, using the geographic coordinates of the region. To make the extraction more precise, coordinates of tie-points available in the image header were interpolated.

Calibration:

Calibration is needed to transform the Digital Number (DN) counts of the image into backscattering coefficient, σ. To obtain the backscattering coefficient of a distributed target, following the ESA ASAR Product Handbook (ESA, 2007), it is necessary to know the image calibration constant and the incidence angle for each pixel. The calibration is done using the following equation:

$$\sigma = \frac{\langle A^2 \rangle}{K} \sin\theta \qquad \text{[Eq. 7.2]}$$

where K is the absolute calibration constant, A is the average pixel intensity and θ is the incidence angle. The calibration constant is included in the header of each ASAR image. It is different for every swath and also depends on the image processor used by ESA. **Table 7.5** gives the calibration constants that has been applied to the data in this study.

Date	Polarisation	Swath	Processing version	Acquisition center	Processing center	Calibration constant
13/03	VV / HH	S6	PF-ASAR v3.05	PDAS-F	PDHS-E	944449.9
22/03	VV / HH	S1	PF-ASAR v3.03	PDAS-F	PDHS-E	518800.03
29/03	VV / HV	S7	PF-ASAR v3.05	PDAS-F	PDHS-E	1130383.9
17/04	VV / HH	S6	PF-ASAR v3.03	PDAS-F	PDHS-E	1044720.25
26/04	VV / HH	S1	PF-ASAR v3.05	PDHS-K	UK-PAC	426351.38
03/05	VV / HV	S7	PF-ASAR v3.05	PDHS-K	UK-PAC	1130383.9
16/06	VV / HH	S2	PF-ASAR v3.05	PDAS-F	PDHS-E	543250.3
26/06	VV / HH	S6	PF-ASAR v3.05	PDAS-F	PDHS-E	944449.9
05/07	VV / HH	S1	PF-ASAR v3.05	PDHS-K	UK-PAC	426351.38
12/07	VV / HV	S7	PF-ASAR v3.06	PDAS-F	UK-PAC	1130383.9
21/07	VV / HH	S2	PF-ASAR v3.06	PDAS-F	UK-PAC	543250.3
31/07	VV / HH	S6	PF-ASAR v3.05	PDHS-E	I-PAC	944449.9

Table 7.5. Calibration constants used in the calibration of the ASAR images.

Resizing of the subset images:

The subsets extracted from the SAR images had nearly the same dimensions, differing only in 1 or 2 rows or samples. Before registration, the images were resized to have exactly the same dimensions (a few lines and samples are removed from bigger images).

Co-registration:

Co-registration was done by an automatic method. For images that had the same satellite track and the same incident angle, that is exactly the same acquisition geometry, co-registration could be performed with simple translations. Those translations were done on the basis of an optimum set of GCPs (Ground Control Points). From all the subset images to filter, one was selected as reference image (by default, the first one). Then, ground control points (GCPs) were selected on this reference image. The default GCPs were 9 pixels, equally distributed in the image. The GCPs were chosen to be those that showed the higher correlation between a GCP in the reference image and every pixel in the neighbourhood of the same GCP in each image of the same polarisation.

The advantage of this co-registration method is that the image radiometry is not altered. However, the method fails to co-register images with multiple swaths. For images with a different geometry of acquisition (that results in a different ground pixel size), co-registration cannot be done with simple translations. Some difficulties were also found when the subsets extracted from the original images are big. Co-registration of the Toulouse data was done using only images of the same swath.

Speckle filtering:

ASAR images were speckle filtered using the method developed and described by Lopes et al., (1993), Beaudoin et al., (1994), Le Toan et al., (1997), Bruniquel and Lopes, (1997), Quegan et al., (2000), Quegan and Yu, (2001). This filter, originally developed for ERS images, is a multi-temporal filter. The explicit form of the filter is:

$$J_k(x,y) = \frac{\langle I_k(x,y)\rangle}{M}\sum_{i=1}^{M}\frac{I_i(x,y)}{\langle I_i(x,y)\rangle} \qquad \text{[Eq. 7.3]}$$

where, $I_i(x,y)$ is the radar intensity of the input image, i at pixel (x,y), $\langle I_i(x,y)\rangle$ is the local average intensity of the input image i at pixel (x,y) and $J_k(x,y)$ is the radar intensity of the output image k at pixel (x,y). The filter should be applied over uncorrelated images, but it is only slightly suboptimal for correlated channels. Multi-temporal filtering was applied on all registered images (all dates and all polarisations together).

In principle, the temporal filtering should not degrade the spatial resolution, but the estimates of $\langle I_i(x,y)\rangle$ require to do an spatial averaging within a window in each image. The loss of resolution inherent to the $\langle I_i(x,y)\rangle$ estimation was minimized using an adaptive processing window.

The main objective of removing the speckle is to reduce the uncertainties in the backscattering value estimation by increasing the ENL (Equivalent Number of Looks). Furthermore, it also facilitates visual interpretation of the images.

If there are M uncorrelated multi-temporal images, each consisting of L-look data, then the filtered data will ideally have $M \times L$ looks. However, in practice, errors in the estimates of the $\langle I_i(x,y)\rangle$ results in lower L-look value than would correspond to the ideal case.

In the case of ASAR data, the number of range looks for each image, before filtering, also depends on the swath and the original ESA processing. Some versions of ESA processors applied range multi-looking on high incidence swaths. That leads to different ENL among the images, having high

incidence angles a higher ENL. The images used in this study, corresponding to swaths 6 and 7, are 3 looks, except that of the 17/04/03 that was processed with an older processing version. Details are shown in **Table 7.6**. As a consequence, S6 and S7 look clearer than low incidence angle swaths images.

Figure 7.10 and **Figure 7.11** show the subset image corresponding to La Masquère region, before and after filtering respectively. The 4 available swaths S1, S2, S6 and S7 are displayed clockwise. Each swath was filtered separately. S6 shows an artefact on the right side because one of the images is smaller than the rest and there are no data.

Date	Swath	ENL
13/03	S6	3
22/03	S1	1
29/03	S7	3
17/04	S6	1
26/04	S1	1
03/05	S7	3
16/06	S2	1
26/06	S6	3
05/07	S1	1
12/07	S7	3
21/07	S2	1
31/07	S6	3

Table 7.6. Equivalent number of looks for each one of the ASAR images.

The uncertainty in the backscattering of ASAR images depends on the Equivalent Number of Looks. For images with an original ENL=3, an ENL=240 can be achieved by applying pixel averaging to an area of interest (AOI) of about 240 pixels, depending on the AOI location in range (radiometric resolution is higher at far range than at near range). The related confidence level is of 90% for radiometric resolution bounds of ±0.5 dB.

The backscattering measurements used in this study have been field averaged (with sizes of the order of 200 pixels). In addition the original ENL of the images (**Table 7.6**) were increased thanks to the multitemporal speckle filtering.

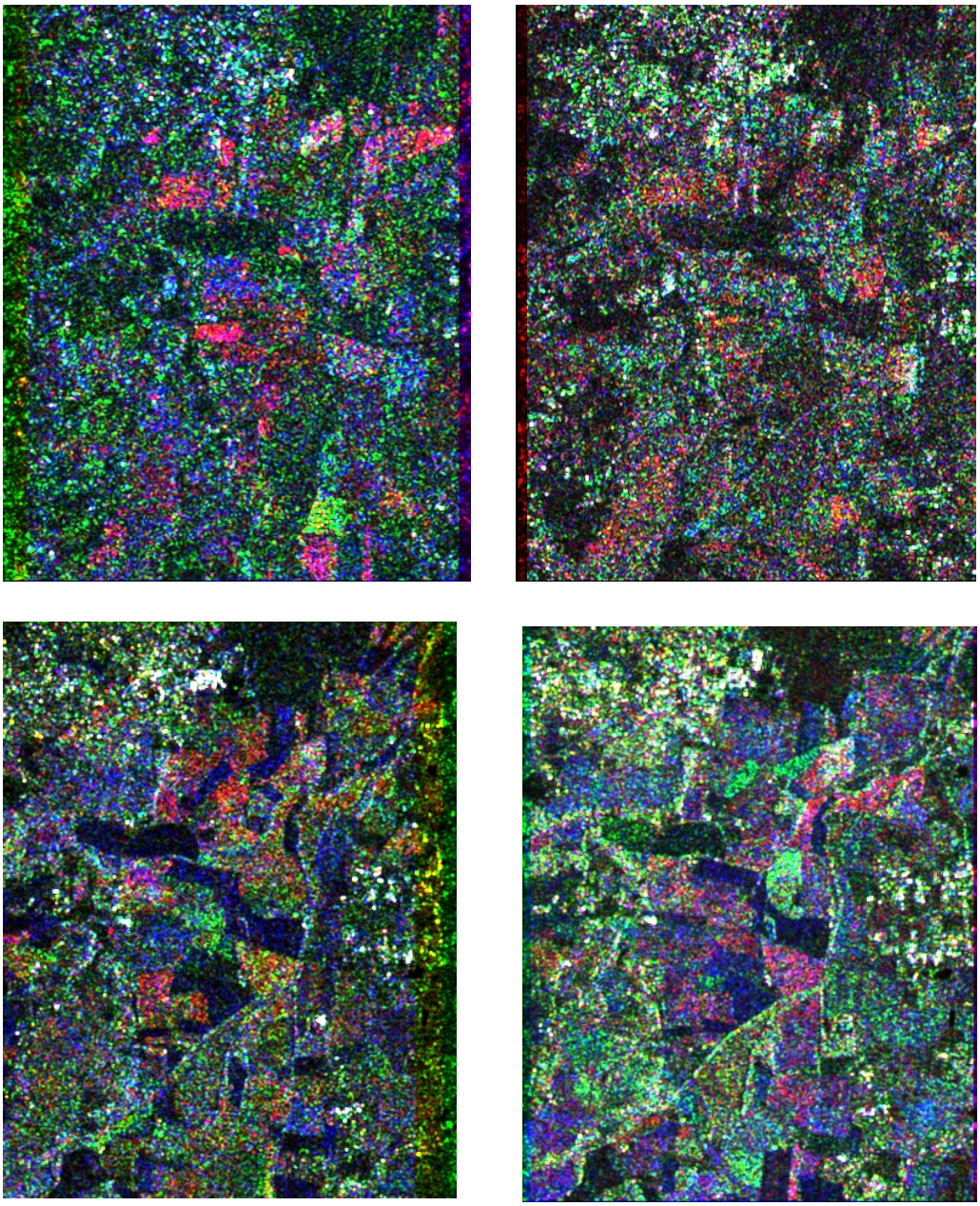

Figure 7.10. Area of La Masquere before filtering. The figures are RGB multi-date composites: a) R(26/04-VV), G(22/03-VV), B(05/07-VV, b) R(16/06-VV), G(21/07-HH), B(21/07-VV) c) R(26/06-VV), G(31/07-VV), B(13/03-VV) and d) R(12/07-VV), G(03/05-VV), B(29/03-VV).

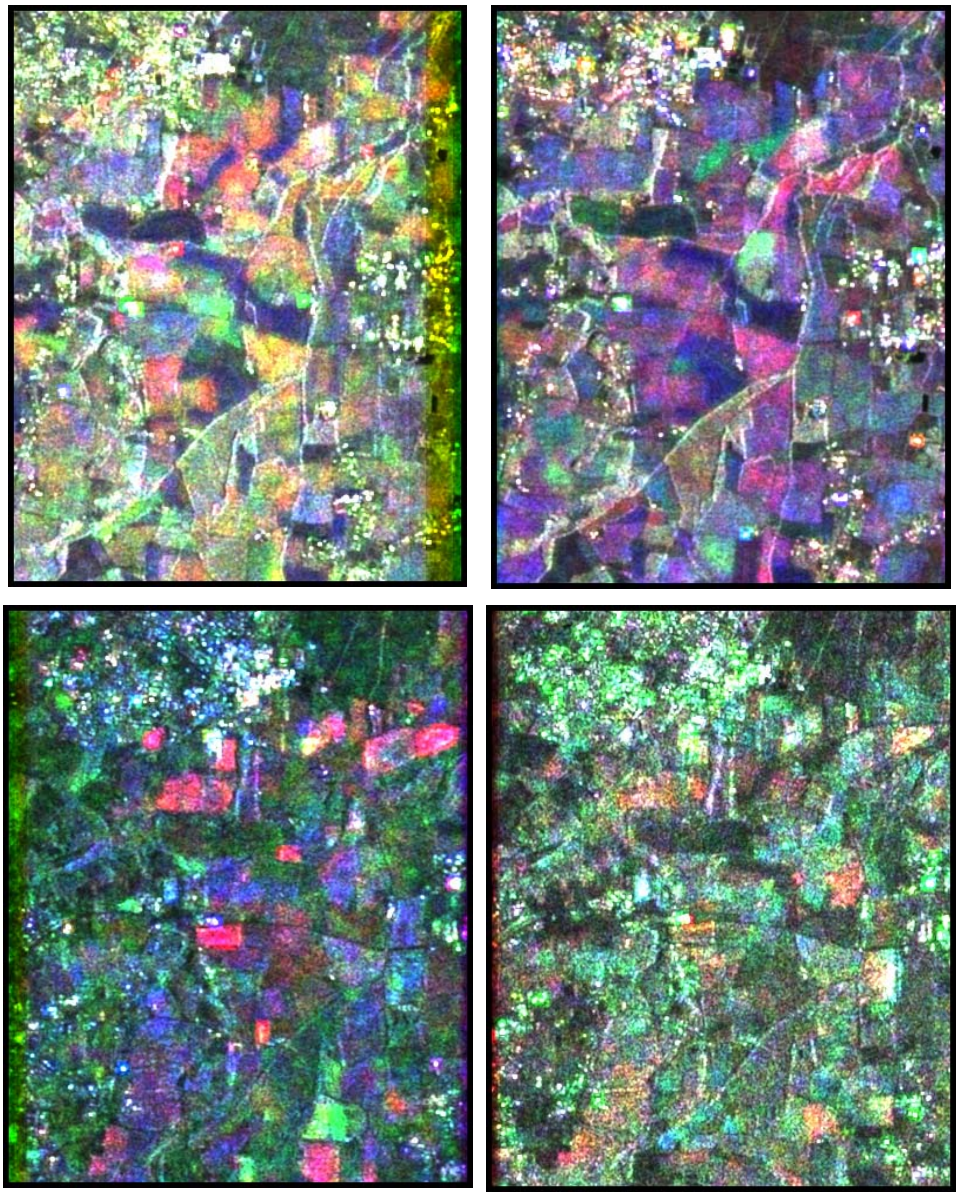

Figure 7.11. Example showing the area of La Masquere after filtering. The number of bands used are x,x,x,x from swath 1 to swath 7. The figures are RGB multi-date composites: a) R(26/04-VV), G(22/03-VV), B(05/07-VV, b) R(05/07-VV), G(22/03-HH), B(26/04-HH) c) R(29/03-VV), G(03/05-VV), B(12/07-VV) and d) R(05/07-VV), G(22/03-VV), B(26/04-VV).

7.3 Evaluation of the consistency of the measured backscattering.

In order to evaluate the consistency of the ASAR-APP data from Toulouse, the backscattering behaviour of a forest is analysed in this section. The temporal, angular and polarisation behaviour of a forest is usually well known. A cover of dense forest is expected to have a stable temporal variation.

The Bouconne forest, that was included in almost all the scenes, was selected. This forest is mainly composed of oaks and there are also other tree species, like beech trees, pine and chestnut trees. Finally, the backscattering values were also compared with ERS measurements in 1998.

Temporal evolution:

The backscattering from a forest depend on its structural and biophysical characteristics, as well as on the soil background, being the soil contribution to the total signal higher in the case of low fraction of vegetation cover. Roughness and soil moisture are parameters that can introduce variations in the temporal signal. Biomass and vegetation moisture are parameters controlling the scattering. The vegetation moisture can introduce variations in the dielectric constant of the vegetation, although, it does not vary significantly, except for the periods of leaves fall. As biomass can be considered constant, and vegetation dielectric constant is relatively stable we expect the Bouconne signal to be also stable, except in the case of a strong contribution of the soil. **Figure 7.12a** shows that the signal is relatively stable but, at the same time, it shows a decreasing trend of the backscattering along the year, in all swaths. The reason for this decrease may be the particular conditions of year 2003, which was characterised by a strong drought. It may

also be due to a reduction of water content in the trees cover, and under-store, also as a consequence of the drought.

Angular behaviour:

The angular behaviour shown in **Figure 7.12a** seems to deviate slightly from a cosines law, decrease of 1dB from 20° to 40° incidence angle. However it is difficult to ensure this statement, as multi-angular acquisitions are not simultaneous.

Polarisation behaviour:

The polarisation response was as expected. The C band waves interact with the tree elements: leaves and small stems. If leaves and small stems are randomly oriented in the space, i.e. there is not a predominant structural orientation. HH and VV response should be similar. The medium will also introduce a de-polarisation of the signal giving a significant cross polarisation (HV) backscattering. An important characteristic of the forest surfaces at C band is that the ratio HH/VV is very stable for all incidence angles (**Figure 7.12b**).

Comparison with ERS data:

In terms of absolute value, ASAR measurements in VV polarisation are in agreement with previous ERS observations. **Figure 7.12a** shows that VV backscattering for low incidence angles (S1) were comparable to those measured by ERS-2 (23° incidence angle) in May 1996 and April/May 1998, being around -7 dB. The ratio HV/VV was higher than -8 dB, which confirms

that the dominant phenomenon was not the surface scattering, but volume scattering (Ferrazzoli et al., 1999).

a)

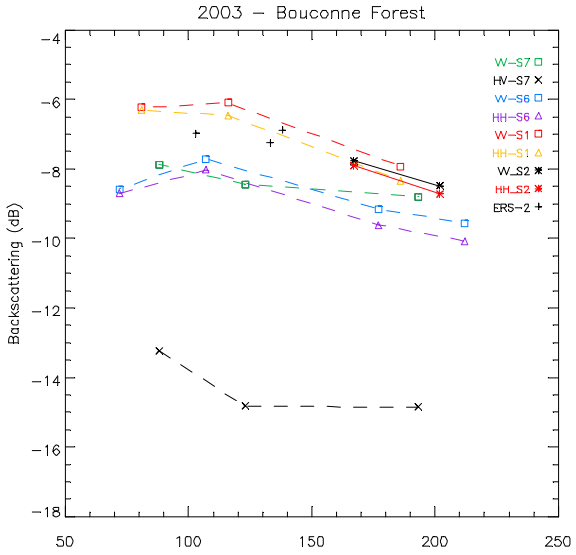

b)

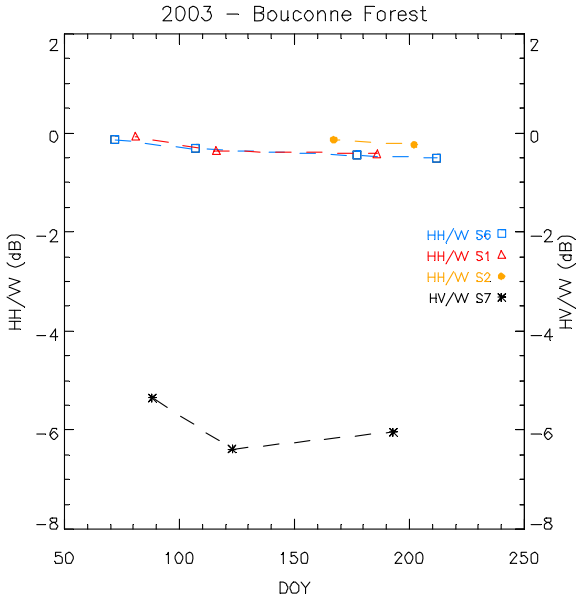

Figure 7.12. a) ASAR Backscattering at HH, VV and HV polarisations in the Bouconne Forest, year 2003. b) HH/VV and HV/VV ratios.

7.4 Analysis of ASAR temporal backscattering measurements of crops.

In **Chapter 6**, a crop classification algorithm for the area of Flevoland, which used fully polarimetric radar data, was presented. This algorithm cannot be directly applied using data acquired with the ASAR instrument, because ASAR can only measure two polarisations at the same time, and therefore it is not a fully polarimetric instrument.

The analysis in **Chapter 6** showed that, from the non-fully polarimetric features, HV and HV/VV ratios were very interesting to discriminate crops. HV was found useful to discriminate crops with different level of biomass and the ratio HV/VV was found to be a good vegetation/non-vegetation discriminator. It was also shown that, the structural effects could also be the basis of a rule for crop separation.

The objective of this section is to confirm the findings of **Chapter 6** using ASAR data. To this aim ASAR data acquired over Toulouse were used (see **Table 7.4**). An image from in the region of Barrax was also used.

Extraction of the crop backscattering:

The average backscattering of agricultural fields identified in the ASAR images was extracted. In the area of Toulouse, three sub-regions were selected in order to cover a variety of spring and summer crops. The identification of the fields in the ASAR images was done with the help of the SPOT based classification of **Figure 7.8**. Analogously, in the Barrax image, the crop backscattering was extracted with the help of the Landat based classification that was shown in **Chapter 3.**

In Toulouse, colza, wheat sunflower and corn fields were analysed, as well as some areas of deciduous forest. The later were selected in order to evaluate the degree of confusion with crops.

In Barrax, alfalfa, small grain spring cereals (non irrigated cereal and spring irrigated cereal), summer irrigated crops (mainly corn and sugar beet), double harvest fields (cropped with cereals in sprint) and some bare soil fields were identified.

Vegetation-non/vegetation:

Figure 7.13 corresponds to the scatter plots HV versus HV/VV in swath 7, for two different dates, 29/03 (**Figure 7.13a**) and 03/05 (**Figure 7.13b**).

In that figure, it can be observed that HV/VV separates two clusters of points: spring crops (colza and wheat) from non-cropped fields (labelled with sunflower and corn) at the end of March. A threshold value around -7 dB could be used for separating the two clusters. At the beginning of May the same was observed, with the exception of a colza field that was confused with the fields that would be cultivated with summer crops. The same threshold could be used.

The situation in mid-July was less favourable for the discrimination of crops (see **Figure 7.14**). The ratio HV/VV could not discriminate between summer crops (sunflower and corn) from harvested wheat and colza. A threshold value around -7dB could separate most of the corn fields. A poor development of sunflower fields, due to the very dry conditions of year 2003, may be the reason for the confusion between sunflower and harvested cereals.

a)

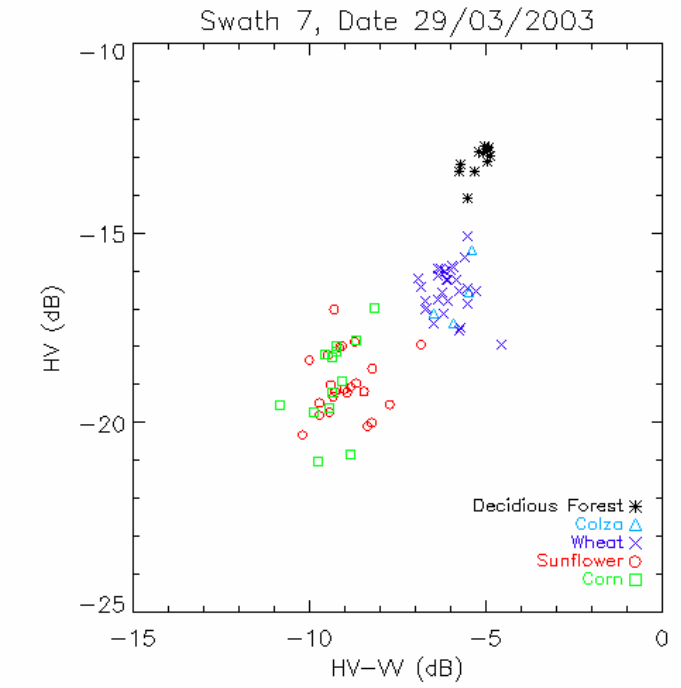

b)

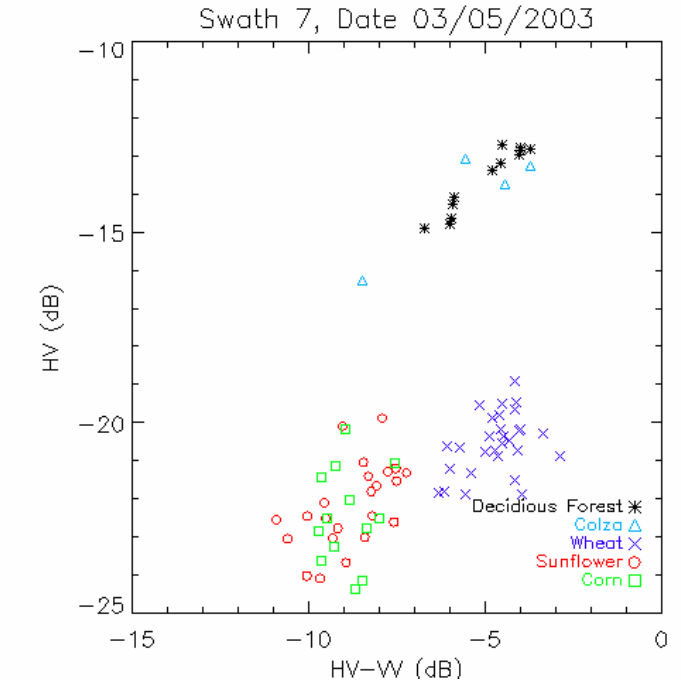

Figure 7.13. HV versus HV/VV ratio in swath 7, corresponding to crops in the area of Toulouse at two different dates a) 29/03/2003 and b) 03/05/2003.

When displaying HV versus HV/VV in Barrax on the 20/04/200 a clear separation between spring crops (labelled as alfalfa, spring irrigated and non irrigated cereals) and bare soils (labelled as bare soils and and summer irrigated) is obtained in the X axis (see **Figure 7.15**). A threshold of around 8dB could be used. The alfalfa field out of the cluster corresponds to an alfalfa field that was harvested.

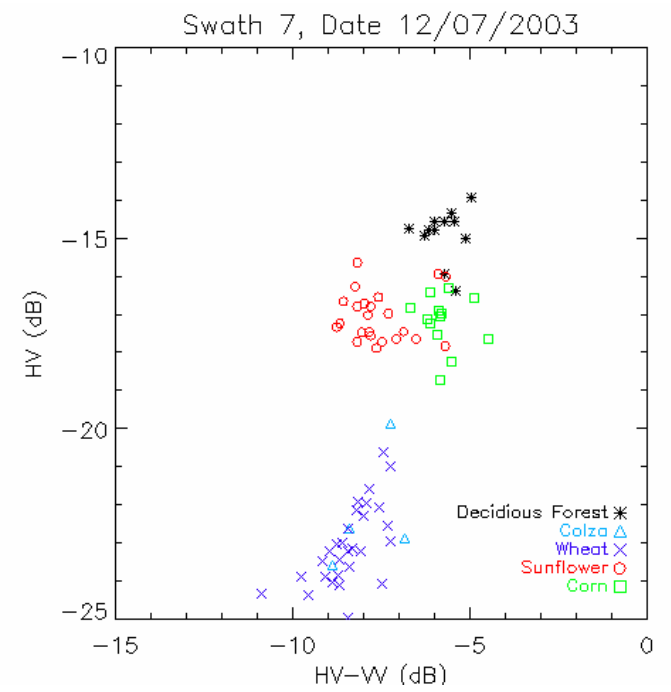

Figure 7.14. HV versus HV/VV ratio in swath 7, corresponding to crops in the area of Toulouse at 12/07/2003.

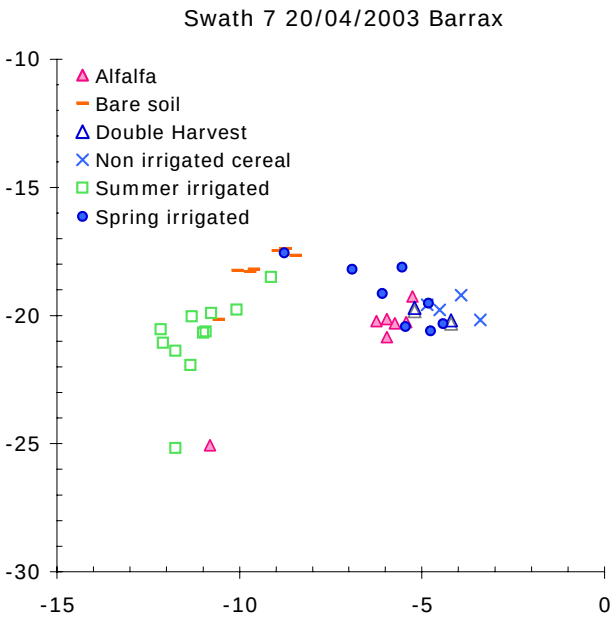

Figure 7.15. HV versus HV/VV ratio in swath 7, corresponding to crops in the area of Barrax at 20/04/2003.

Level of biomass:

In **Chapter 6**, HV was used to separates crops with different levels of biomass. The same capability was found with ASAR data. The situation at the beginning of May was very interesting (**Figure 7.13b**). It corresponds to the moment in which rapeseed pods were present. This was also observed at Flevoland (**Figure 6.9**). At the end of March (**Figure 7.13a**) colza and wheat had similar levels of biomass. In mid-July sunflower and corn fields could not be discriminated with HV because of the same reason.

In Barrax (**Figure 7.15**) on the 20/04/2003 cultivated fields (spring cereals, non irrigated cereals, and alfalfa) had similar levels of biomass. The alfalfa field with a lower level of biomass, due to harvest, was detected.

Deciduous forest:

Deciduous forest showed a relative stability in the HV signature (**Figures 7.3** and **7.14**). This temporal stability could be used to mask forested areas in a classification method.

Structural effects:

At it will be shown in **Section 7.5** of this chapter, the vertical structure of small grain cereals contributes to a higher attenuation of VV compared to HH. This physical phenomenon can also be used for a classification. **Figure 7.16** shows the high increase in the HH/VV ratio at high incident angles for crops with vertical structure (wheat and rapeseed) from mid March (very low biomass level) to mid April (high biomass level). It is important to remark that not, only wheat fields, but also rapeseed fields show the same behaviour. At low incident angles, the same effect occurs. Thus, in **Figure 7.17a** the higher HH/VV ratios correspond to wheat and rapeseed fields.

In July (**Figure 7.17b**) no structural effects are observed.

This analysis shows that the HH/VV ratio could be used as a discriminator for crops with vertical structure, provided they are well developed (April in Toulouse). At early stages (13/03 in Toulouse) some confusion with non vegetated fields was still observed. In our dataset, high incident angles appeared more useful than low incident angles. However this is also a consequence of the acquisition date.

a)

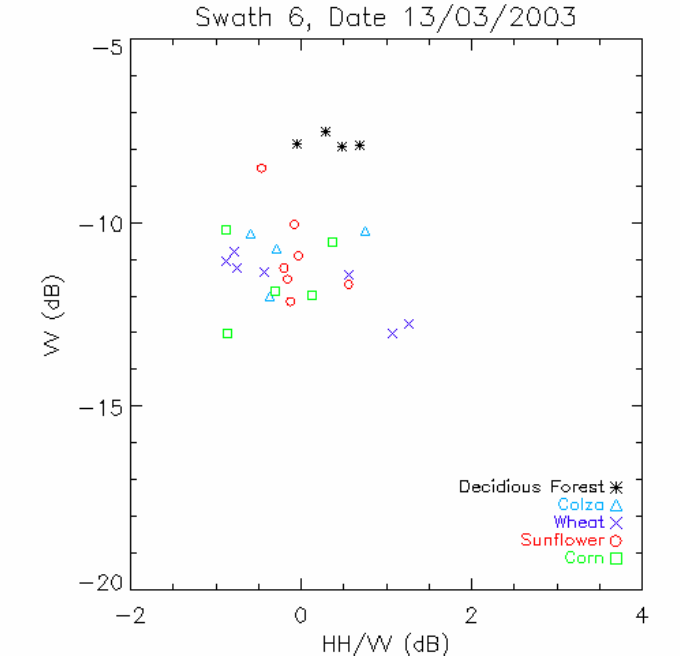

b)

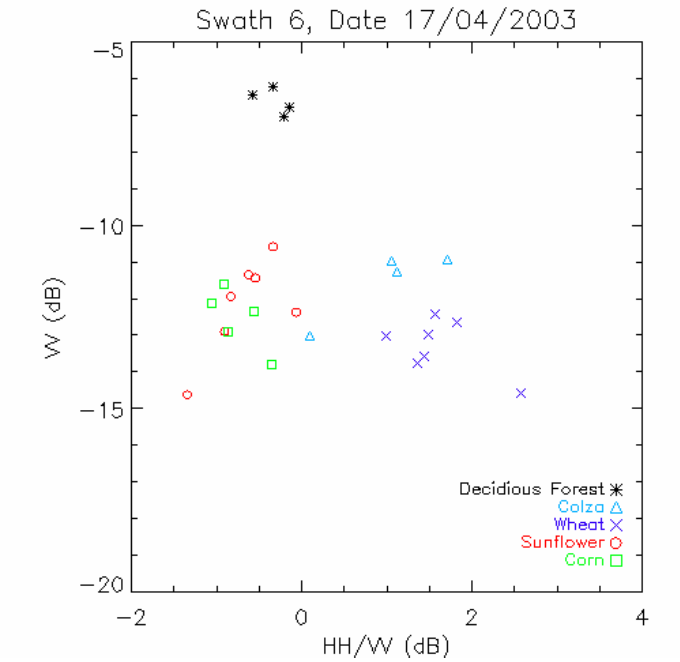

Figure 7.16. VV versus HH/VV ratio in swath 6 for different crops in the area of Toulouse at two dates, a) 13/03/2003 and b) 17/04/2003.

a)

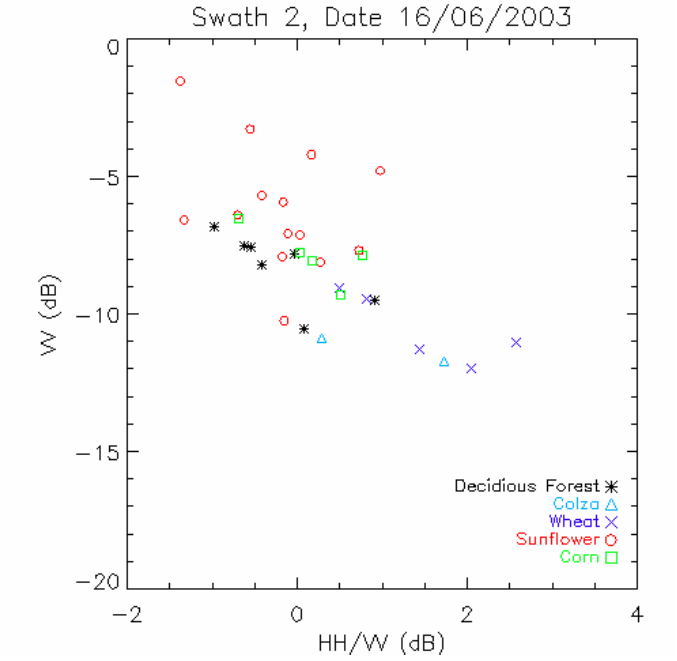

b)

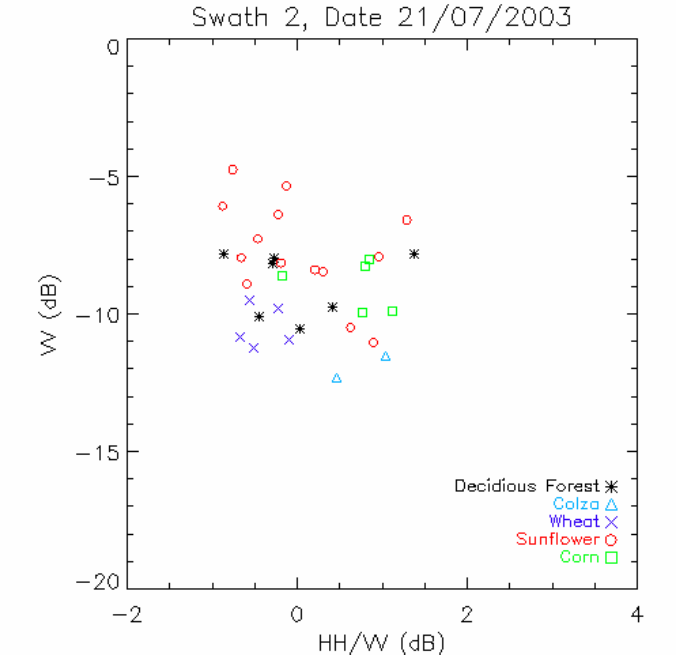

Figure 7.17. VV versus HH/VV ratio in swath 6 for different crops in the area of Toulouse at two dates, a) 16/06/2003 and b) 21/07/2003.

Conclusion on the analysis of the backscattering measurements of crops:

At it was concluded in **Chapter 6,** for a particular area, the crop calendar is critical for the success in crop discrimination. In this sense, the time distribution of the dataset in Toulouse was good. However, the mixture of polarisations and swaths made the analysis of crops signatures difficult.

The analysis using ASAR data in Toulouse confirms that the ratio HV/VV can be used for discriminating between cropped fields and non-cropped fields.

Better results were obtained with high incident angles.

For crop classification studies, there is a need of operational data acquisition with ENVISAT-ASAR, which was not achieved in the area of Toulouse. Future missions like Sentinel-1 will accomplish this requirement.

7.5 Relationship between biomass and the backscattering coefficient for wheat canopies.

The radar signal is sensitive to biomass or other related vegetation parameters such as plant water content or LAI of agricultural fields. Early studies using a ground based radar, showed the correlations between plant water content and the radar basckcattering coefficient, allowing the monitoring of the growth of crops such as corn or wheat (Ulaby and Bush, 1976, Ulaby et al 1984). Higher incidence angles (40° or more) were found more appropriate for an effective monitoring of crop growth.

For the case of wheat, past studies using X-Band scatterometer (**Figure 5.18**) data demonstrated the possibilities of biomass monitoring (Le

Toan et al., 1989). Mattia el al, (2003) concluded that the C-Band HH/VV ratio (with a preference for high incidence angles) can be an indicator of wheat biomass. At some wheat stages VV is strongly attenuated by stems and not HH, as a consequence of the stems vertical structure. This attenuation is stronger at high incidence angles. Biomass can be detected by the attenuation of the soil signal that the canopy produces, rather than by the direct contribution of the canopy to the total measured backscattering. However scattering mechanisms are different at each wheat stage and affect differently VV and HH polarisations. A significant change in the scattering mechanisms occurs when ears appears. In addition the changes on soil moisture and soil roughness affect the temporal backscattering.

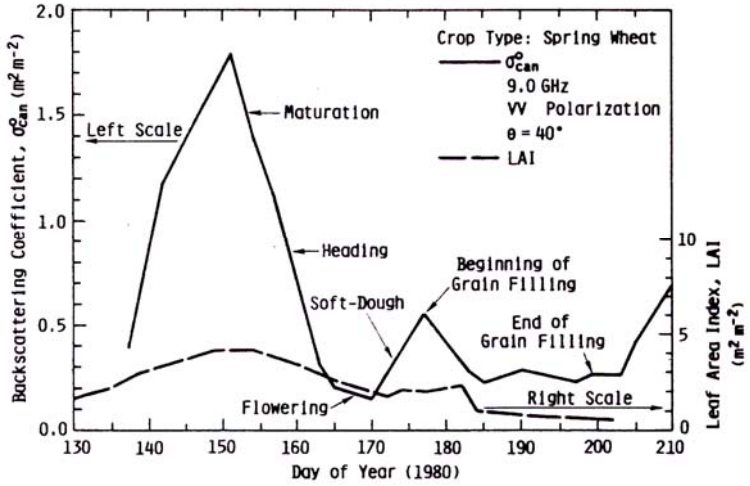

Figure 5.18. Measured temporal patterns of backscattering coefficient and LAI of a spring wheat in France. (From LeToan et al., 1983).

Before heading, HH and VV, at low and at high incidence angles, are related to biomass but, after heading, a unique polarisations does not show a relationship with biomass. The ratio HH/VV was found to enhance sensitivity

to biomass. At low incidence angles, HH/VV was not very correlated with biomass, but at high incidence angles the relationship was clear. Furthermore, it was not sensible to soil moisture. A strong linear correlation between HH/VV and biomass at 40° incidence angle was reported.

Practical applications for the retrieval of wheat biomass using satellite data were not achieved, due to the lack of appropriate multitemporal SAR data over agricultural surfaces. The ESA ASAR sensor onboard the ENVISAT satellite can measure two simultaneous polarisations HH/VV, HH/HV, VV/HV at different incidence angles (not simultaneous) from space. This motivated the study conducted in this work. In this chapter, the capabilities of ENVISAT/ASAR data to monitor wheat biomass, taking advantage of the differences between the HH and VV polarisation measurements that occurs over wheat surfaces, were investigated.

7.6 Backscattering coefficient from a wheat canopy.

The interpretation of the temporal evolution of the backscattering coefficient of a wheat canopy is still a research issue due to the complexity of the phenomena involved. Recently, experimental studies have been conducted to understand the different scattering mechanisms contributing to the backscattering described in **Figure 5.14** of **Chapter 5**. For instance, the work of Brown et al., (2003) using a 3-D radar system of high resolution, permitted to localize the scattering sources within a mature wheat canopy. Their measurements showed that, at HH polarisation, soil dominates the backscattering for all incidence angles. At VV polarisation the soil

backscattering is only dominant for angles less than 35°. For angles >35° contribution of the upper canopy is the dominant term at VV, due to the interaction with ears and flag leaves. The cross-polarized return, HV, is mainly due to the soil and the volume scattering is not the dominant term. An analogous experiment by Gomez-Dans et al, (2006) which used polarimetric interferometry, corroborated the results of Brown et al., (2003).

The previous experiments were done at a particular wheat stage (mature wheat, already with ears). As the structure of wheat changes along the growing season, mutitemporal studies are necessary for the development of retrieval methods. In this sense, the HH and VV backscattering coefficient in C-Band was investigated in an experiment at the Matera site (Italy) for different wheat phenological states and different incident angles, using scatterometer data (Mattia et al., 2003). This work is a very valuable documentation of wheat temporal scattering.

Recent experiments revealed discrepancies with current wheat models, in particular the model of Marliani et al., (2002). This is probably because many of the existing models overestimate the attenuation caused by wheat stems (Cookmartin et al., 2000). The work of Picard et al., (2003) demonstrated the important role of multiple scattering in a wheat canopy and provided a more realistic calculation of the canopy attenuation. However, in this model, the canopy is described only as stems, which has limitations to describe the stages of wheat in which ears and leaves could contribute to the total scattering.

In conclusion, although in the recent years theoretical works for crops have significantly improved (Shriver et al., 1999; Saich and Borgeaud, 2000; Cookmartin et al., 2000; Picard et al., 2003), the quantitative description of the

scattering phenomena in wheat canopies is not yet achieved. Thus, possible inversions methods need to be based on empirical relationships.

7.7 Study of the backscattering coefficient of a wheat canopy.

7.7.1 ASAR measurements in a wheat field in the Toulouse area.

The experimental field of La Masquere was monitored with ASAR during year 2003. ASAR measurements have been done at thirteen different dates (see **Table 7.4**). The field was planted with wheat from the acquisition of date 13/03 to the acquisition of date 26/06 (DOY 170). In that period, 8 images were available, at different polarisations and incidence angles:

- -6 images were acquired at HH&VV polarisations, from which 3 correspond to swath 6, 2 swath 1 and 1 swath 2.
- -2 images were acquired at VV&HV polarisations in swath 7.

The wheat field was harvested after date 26/06. After harvest, 5 more images were acquired and were used for speckle filtering.

The soil roughness of a wheat field does not change significantly along the growing season. Thus it is not taken into account in the analysis.

Temporal variation of HH and VV scattering:

Figure 7.20 reports the HH and VV backscattering measured by the ASAR instrument. Because there were few measurements for each angular range, low incidence angles (swath 1 and swath 2) were grouped, as well as high incidence angles (swath 6 and swath 7), even though this adds some

fluctuations to the temporal profile. When the field was planted with wheat, the backscattering at low incidence angles was higher than at high incidence angles, due to the longer path through vegetation and to the higher attenuation that occurs in the case of high incident angles. These angular differences were affected by the phenology of wheat. After harvest (DOY > 170) the differences of the backscattering among swaths 1-2 and swath 6-7 were more constant.

The soil was relatively dry during the season (see **Figure 7.7**) with the exception of a rainfall event on DOY 116 (26/04). However, soil moisture during that event (18%) was not very high, comparing to other years.

Figure 7.20 confirms the following statements:

a) During the cereal season HH and VV polarisations behaved differently. VV was more attenuated than HH for all incidence angles.
b) The attenuation was different for low and high incidence angles, being also affected by crop phenology.

At high incidence angles, VV decreased due to the growth of wheat: from March 13 (DOY 72) to April 17 (DOY 107) there is a decrease of 5 dBs in the measured backscattering at swath 6, while HH decreases less than 1 dB. On May 3 (DOY 123) VV at swath 7 also showed this strong attenuation.

At low incidence angles, VV also showed a decrease along the season, but it was less important than at high incidence angles: 0.1 dBs from March 22 (DOY 81) to April 26 (DOY 116), and 2.5 dBs from March 22 (swath 1) to June 16 (DOY 167, swath 2). HH increased 3 dBs from March 22 to April 26,

which is explained by the higher soil moisture, and decreases 3 dBs form March 22 to June 16.

After harvest, the behaviour of HH and VV polarisations corresponds to a slightly rough soil surface. The effect of polarisation was weak, being VV slightly higher than HH for all the angles of incidence.

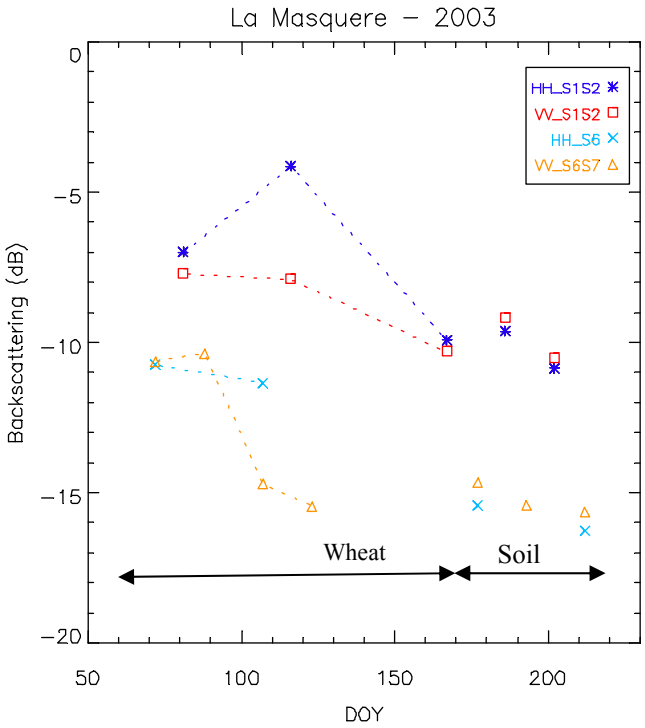

Figure 7.20. HH and VV Backscattering for the experimental site in 2003 at high (swath 6) and low (swath1&2) incidence angles.

Figure 7.21 displays the backscattering ratio HH/VV in dBs, for swaths 1-2 and swaths 6-7, together with the wheat phenological stage. The figure confirms, as shown in Mattia et al., (2003), that the ratio HH/VV follows the development of wheat.

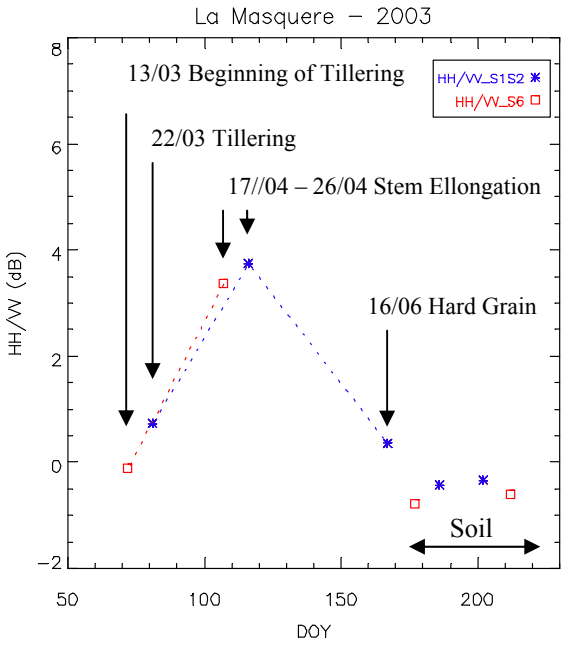

Figure 7.21. Ratio HH-VV for the experimental site in 2003 at high (swath 6) and low (swath1&2) incidence angles.

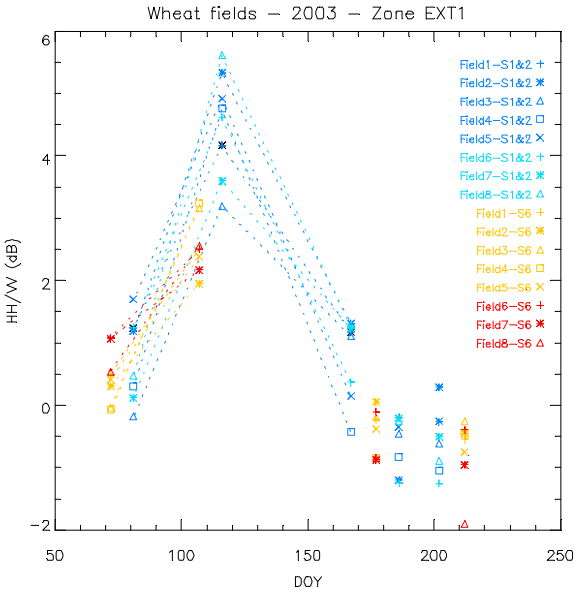

Figure 7.22. Ratio HH/VV for wheat fields in 2003 distributed in two regions of the ASAR images, named as EXT-1 and EXT-2.

The same behaviour has been observed for other wheat fields in the region (**Figure 7.22**).

7.7.2 Biomass relationship.

The biomass relationship obtained for La Masquère site is shown in **Figure 7.23**. It can be observed that the HH/VV ratio follows the biomass curve, both in the case of small incident angles (swath 1 & 2) and high incident angles (swath 6). However, this behaviour may be affected by the rain event of April 26. This, together with the limited number of ASAR acquisitions available for this study does not allow obtaining a meaningful regression between the biomass and the HH/VV ratio.

The swath 6 measurements in Toulouse were compared to other radar measurements that were also acquired at a high incidence angle over wheat. Two kinds of measurements were used. The first set of data are scatterometer measurements from Mattia et al., (2003), acquired in a field in the Matera site (Italy), and from Brown et al., (2003), acquired by the ground-based SAR indoor system of the University of Sheffield in the UK. The second set of measurements used for this comparison are also from the Matera site, but were acquired by ENVISAT-ASAR during 2003 and 2004. The later were extracted from (Mattia et al., 2005). The comparison is shown in **Figure 7.24**.

The comparison of measurements of **Figure 7.24** confirms that there is a relationship between the HH/VV ratio and biomass for high incident angle measurements. It also indicates that the relationship is different for each site, which makes the inversion of biomass difficult.

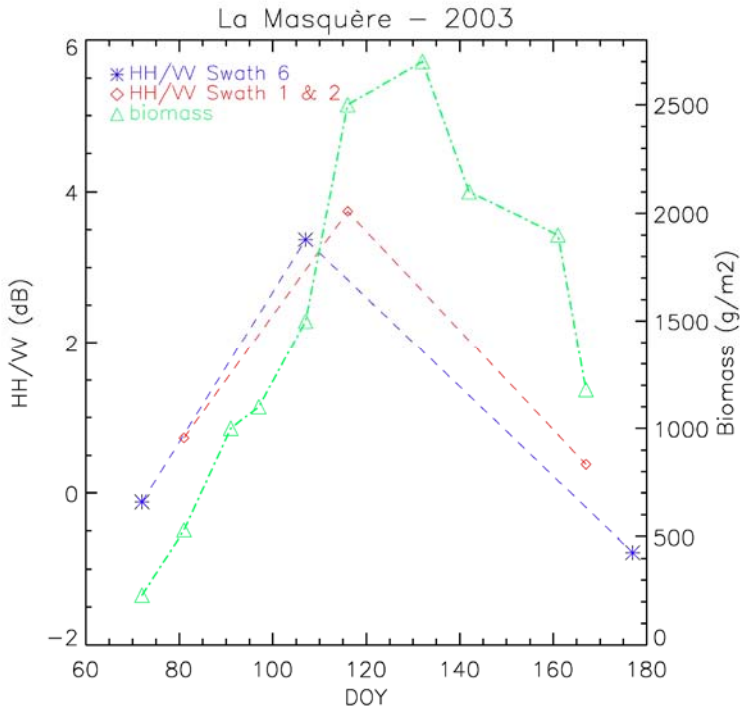

Figure 7.23.. HH/VV and biomass relationship for data in La Masquere 2003.

7.7.3 Discussion and conclusion on the retrieval of wheat biomass.

Unfortunately, this study was limited by the few ASAR images that were possible to acquire in the area of Toulouse. In spite of the few acquisitions, it was shown that the HH/VV ratio can be used to monitor the growth of wheat (**Figures 7.22** and **7.23**). This study also confirmed that the HH/VV ratio increases with biomass (**Figure 7.24**). However, the relationship could be site specific and it is dependent on many factors, including, soil

moisture, wheat density, plant structure and external factors, like wind, that affects the vertical structure of the plant. Theoretical modelling would be very useful to better understand the effect of those factors in the relationship. If more data were available, the biomass could have been established, but, due to the number of external factors that affect the relationship, the robustness of the method seems questionable. Therefore, more research is necessary on this subject.

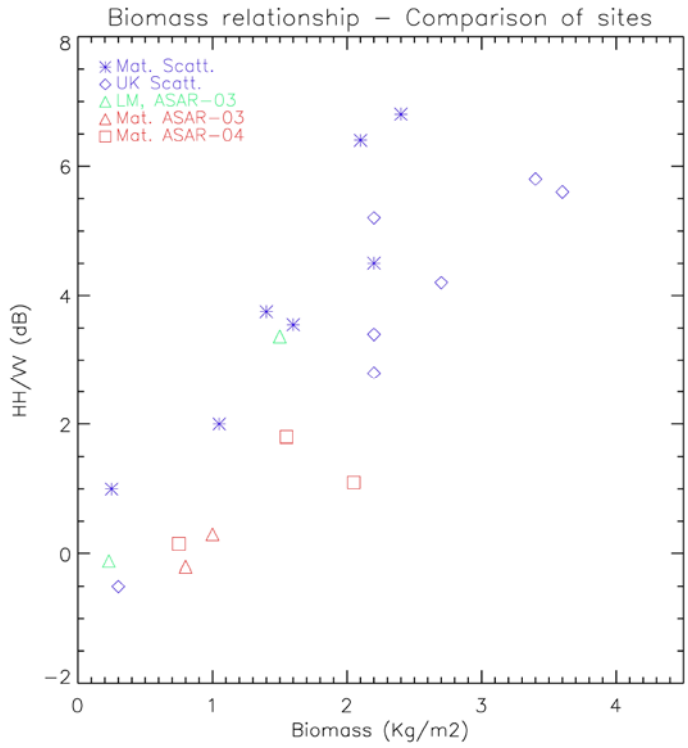

Figure 7.24. HH/VV and biomass relationship for data in La Masquere 2003 (LM), Matera (MAT) and UK.

Another aspect that should be taken into account is the need of developing angular compensation methods. In the case of ENVISAT-ASAR,

these methods are necessary because, to observe the wheat cycle with a temporal resolution higher than 35 days, the ASAR measurements should be acquired with more than 1 swath. In conclusion, due to the dependence of the angular compensation with the phenology of wheat, as was reported by Mattia et al., (2003), more temporal measurements over wheat sites are needed, as they would be very valuable to develop angular compensation methods.

CHAPTER 8:
SUMMARY AND CONCLUSIONS

The objective of this study was the development and assessment of methods for the classification of crops and the estimation of LAI, Chlorophyll and biomass, which are based on the use of optical and radar remote sensing data, with the aim to assist the operational or quasi-operational systems of crop monitoring in agricultural applications.

After an introduction given in **Chapter 1**, the first part of this study starts with an overview of the retrievals of biophysical parameters from optical data given in **Chapter 2**. **Chapter 3** is dedicated to the estimation of LAI in Barrax, an area with diversity of crop types and crop growth cycles. The LAI was retrieved, in a pixel-by-pixel basis, for 12 LANDSAT-TM images covering the agricultural season of year 2003. The PROSPECT+SAIL models were inverted using a technique based on LUTs (Look Up Tables). The results were successfully validated with in situ LAI measurements taken in July. The use of in-situ measurements (leaf chlorophyll content, leaf dry matter, leaf water content) together with other a-priori information (soil background spectra

type, soil background variability, LAI range of variation, plant structure, literature values) was an essential part of the methodology. This information was used as input to the models to construct the LUTs. It was shown that relatively simple methods driven with adequate ground information allow obtaining LAI estimations for many different crops with good accuracy.

For the Barrax region, the assumptions on the soil background variability were valid and did not appear to be a major source of error. Nevertheless, in view of applications to other regions, the effect of the soil background variability (due to soil moisture or soil type) on the LAI retrievals needs to be further investigated.

The comparison of the physically based method with the empirical relationships relating LAI and NDVI allowed us to conclude that these relationships are more dependent on crop type than the physically based approach. Furthermore, the inversion method allowed us to access to higher values of LAI than with the NDVI-LAI relationship, which saturates at smaller values of LAI.

This study was focused on the retrieval of effective LAI, but, in future work, it would be desirable to use clumping corrections to try to obtain the true LAI, in particular, for the case of corn (Duthoit, 2006). Another improvement to the LAI inversion methodology applied in this study would be to add a temporal dependent term in the function that is minimized during the inversions. In **Chapter 4** this aspect was investigated using MERIS data.

Chapter 4 was dedicated to the development of a multi-temporal method to retrieve LAI and chlorophyll using MERIS-FR data, in the area of Barrax. The method also inverts the PROSPECT+SAIL model, with the particularity that temporal dependent terms (temporal constraints) were

introduced in the merit function, which is minimized using an iterative algorithm. The method was applied to small grain cereal fields and the results were compared with date-by-date inversions, which used the same model and iterative inversion method. The comparison showed that the multi-temporal method performed better. Different terms were investigated, and the best results were obtained with a constraint in the temporal evolution of the product LAI x Chlorophyll.

The use of MERIS data for the monitoring of crops in the region of Barrax had serious limitations because of the spatial resolution of MERIS and the field sizes. The accuracy of the results could be improved by correcting the inversions for the percent of soil present in the MERIS pixels. This could be done by means of parameters like the fraction of vegetation cover. However, to be coherent with the SAIL model assumptions (the pixel is homogeneous), the correction should be done previously to the inversion. Un-mixing techniques for MERIS data were proposed by Zurita-Milla et al., (2007) and could be introduced as a previous step in our algorithm. Better results would also be obtained with a higher spectral sampling similar to that of CHRIS-PROBA.

The hypotheses of the models were one of the main limitations of the methodologies used in **Chapter 3** and **4**. These hypotheses are the main source of error, as it was discussed previously, and the quantification of this source of error requires further study. In this sense, the last version of PROSPECT (Feret et al., 2008) is expected to improve the Chlorophyll estimations. However, the retrieval of leaf Chlorophyll Content from satellite data is a difficult task and we believe that much more work is needed at the same time in modelling and inversion techniques.

To observe crops in Northern Europe, radar data were preferred to optical data, due to the high presence of clouds in that region.

The classification of agricultural crops using C-Band polarimetric airborne data was addressed in **Chapter 6,** where a hierarchical algorithm based on five physical rules was proposed. The algorithm rules were developed using the scattering mechanisms and scattering behaviour of the different crop fields. The first rule of the algorithm separates vegetation and non/vegetation using the HV/VV and HV/HH ratios. The second rule separates broad leaf from small stem crops with a condition on the circular polarisation ratio RR/RL. Finally the cross-polarised backscattering, HV, is used to discriminate different levels of biomass in the small stem class and the HH_VV correlation is used to separate subclasses in the broad leaf class. The algorithm was developed for the region of Flevoland, The Netherlands, and validated with a crop map obtaining good results. Accuracies of 73% in mid-July and 65% in late July were obtained.

This classification work permitted to conclude that a limited number of polarimetric measurements had sufficient information content to perform a classification of crops present under northern European agricultural areas. The algorithm could not be applied with success to the area of Barrax (Spain) mainly because the images acquired in that area were not adapted to the actual crop calendar of the region. However, the analysis in Barrax proved that the algorithm rules are robust. HV/HH and HV/VV ratios served to detect the harvest of small grain cereal from June to July. The changes in the structure of crops were detected with the RR/RL ratio, as well as the changes in the biomass level, using HV. Better result could be expected for Barrax with an image acquisition schedule more adapted to the particularities of the region.

Also, in this area of South Europe, were the presence of clouds is not a limitation, classification algorithms using optical data would give much better results.

The main conclusion is that the methodology proposed seems robust and can be adapted to other sites provided there is a knowledge of the crop calendar and the crop types present in the area.

The final part of this work, presented in **Chapter 7**, consisted of the analysis or ENVISAT-ASAR images acquired in Toulouse. The mixture of polarisations and swaths limited the analysis of the ENVISAT-ASAR images for crop discrimination. Nevertheless this analysis confirmed that the HV backscattering coefficient was a good discriminator of biomass level. Also the HV/VV ratio was found robust for discriminating between cropped and non cropped fields. In Toulouse, better results were obtained in terms of discrimination of crop fields when using high incident angles.

Another advantage of radar data compared to optical is that they contain information useful for the retrieval of biomass. The second objective of **Chapter 7** was to investigate the estimation of wheat biomass by means of the HH/VV polarisation ratio. To this aim a dedicated campaign for the acquisition of ground measurements in a wheat field was conducted in year 2003. This study permitted to confirm previous investigations (Le Toan et al., 1998; Mattia et al., 2003), which showed that HH/VV ratio increases with biomass. The results with ENVISAT-ASAR show that the HH/VV ratio can be used for the monitoring of wheat growing. However, the inversion of wheat biomass encountered a limitation, which was the lack of a sufficient number of acquisitions with the same incident angle. The comparison of our results with other studies shows that the HH/VV and biomass relationship could be site

specific and much more work is needed for the development of a biomass inversion method. The relationship depends on many factors: soil moisture, density of wheat, plant structure. Also, a precise knowledge or the wheat phenological is very important for the interpretation of the backscattering measurements. A recommendation for future work is to guarantee the best possible characterisation of all the relevant parameters related with the wheat structure and phenology. More work is also needed for developing angular compensation methods.

In this work, the relationship between backscattering and biomass was investigated for one type of crop. But certainly other types of relationships may hold (as suggest **Chapter 6**) for different crops and backscattering measurements. Particularly interesting appears the cross polarisation, HV.

General conclusions:

This study showed the importance of using multi-temporal datasets for crop studies. Remote sensing of biophysical parameters is by essence an inverse problem. The monitoring of biophysical parameters requires the acquisition of images with high temporal resolution and an adequate spatial resolution. This is often a limitation in the application of remote sensing methods, due to the lack of this kind of data for a given site. This work benefited from an un-usual dataset (12 LANDSAT images along the same year) and demonstrated the practical applicability of LAI inversion in a large area. It was also shown, by using a temporal constraint in the LAI & Chlorophyll inversion from MERIS data, how the temporal dimension itself could be used to improve the biophysical parameter retrieval. Recent missions like FORMOSAT and future VENUS, that will be able to provide a high

temporal frequency and spatial resolution, will offer new perspectives for the methods explored in this work.

With respect to crop classification using radar data the same conclusion applies. Classification methods benefit from multi-temporal acquisitions. If the temporal resolution is not sufficient, it is not possible to observe some important changes in the structure of crops. Indeed, the experience in Flevoland demonstrated that, to optimize the results, it is required to use weekly observations due to the dynamics of crops. Furthermore, it was shown that the use of C-band polarimetry is a good mean to improve the classification of crops. The algorithm proposed in this study is particularly suitable for application to the new RADARSAT-2 data.

Finally, this is one of the few studies that show in practice the possibilities offered by the combination of different types of data (radar and optical), in order to obtain the maximum information useful for crop monitoring. The combination of optical and radar data provides estimations of LAI and biomass, which are two key variables for the understanding and modelling of crop growth. Nevertheless, the acquisition of simultaneous optical and radar satellite data with an adequate spatial resolution is not yet a reality. However, current satellite data offer many perspectives for the synergy of both types of data.

REFERENCES

Allen, R. G. (2000). Using the FAO-56 dual crop coefficient method over an irrigated region as part of an evapotranspiration intercomparison study. *Journal of Hydrology*, *229*(1), 27-41.

Andrieu, B., Baret, F., Jacquemoud, S., Malthus, T., and Steven, M. (1997). Evaluation of an improved version of SAIL model for simulating bidirectional reflectance of sugar beet canopies. *Remote Sensing of Environment*, *60*(3), 247-257.

Arbiol, R., Zhang, Y. and Palà, V. (2006). Advanced classification techniques: a review. *Proceedings of the ISPRS Mid-term Commission VII Symposium, 292-296*.

Atzberger, C. (2004). Object-based retrieval of biophysical canopy variables using artificial neural nets and radiative transfer models. *Remote Sensing of Environment*, *93*(1-2), 53-67.

Bach, H., Verhoef, W., and Schneider, K. (2001). Coupling remote sensing observation models and a growth model for improved retrieval of (geo)

biophysical information from optical remote sensing data. *In Remote Sensing for Agricultura, Ecosystems, and Hydrology II, Manfred Owe, Guido d'Urso and Eugenio Zilioli (Ed.). Proceedings of SPIE,* Vol. 4171, pp. 1-11.

Bacour, C., Baret, F., Bal, D., Weiss, M., and Pavageau, K. (2006). Neural network estimation of LAI, fAPAR, fCover and LAICab, from top of canopy MERIS reflectance data: Principles and validation. *Remote Sensing of Environment*, *105*(4), 313-325.

Bacour, C., Jacquemoud, S., Leroy, M., Hautecoeur, O., Weiss, M., Prévot, L., et al. (2002). Reliability of the estimation of vegetation characteristics by inversion of three canopy reflectance models on airborne POLDER data. *Agronomie*, *22*(6), 555-565.

Bally, P., and Fellah, K. (1995). Evaluation of the Accuracy of the Backscatter Coefficient Measurement In SAR Data Products. *ESA/ESTEC/Earth Sciences Devision Technical Note*, July, 1995.

Bannari, A., Khurshid, K., Staenz, K., and Schwarz, J. (2007). A Comparison of Hyperspectral Chlorophyll Indices for Wheat Crop Chlorophyll Content Estimation Using Laboratory Reflectance Measurements. *IEEE Transactions on Geoscience and Remote Sensing*, *45*(10), 3063-3074.

Baret, F., and Guyot, G. (1991). Potentials and limits of vegetation indices for LAI and APAR assessment. *Remote Sensing of Environment*, *35*(2-3), 161-173.

Baret, F., Weiss, M., Allard, D., Garrigues, S., Leroy, M., Jeanjean H., Fernades, R., Myneni, R., Privette, J., Morisette, J., Bohbot, H., Bosseno, R., Dedieu, G., Di Bella, C., Duchemin, B., Espana, M., Gond, V., Fa Gu, X., Guyon, D., Lelong, C., Maisongrande, P., Mougin, E., Nilson, T., Veroustraete, F., Vintilla, R. VALERIE: a network of sites and a methodology for the validation of land satellite products. *Remote Sensing of Environment*, submitted.

Barnes, J. D., Ollerenshaw, J. H., and Whitfield, C. P. (1995). Effects of Elevated Co2 And/or O3 on Growth, Development and Physiology of Wheat (triticum Aestivum L.). *Global Change Biology*, *1*(2), 129-142.

Bartholomé, E., and Belward, A. S. (2005). GLC2000: a new approach to global land cover mapping from Earth observation data. *International Journal of Remote Sensing*, *26*, 1959-1977.

Beaudoin, A., Toan, T. L., Goze, S., Nezry, E., Lopes, A., Mougin, E., et al. (1994). Retrieval of forest biomass from SAR - data. *International Journal of Remote Sensing*, *15*(14), 2777-2796.

Begiebing, S., and Bach, H. (2004). Analyses of hyperspectral and directional CHRIS data for agricultural monitoring using a canopy recflectance model. *In Proceedings of the 2nd ESA CHRIS/Proba Workshop, Frascati, Italy 28-30 April*, ESA/ESRIN SP-578, July 2004.

Berger, M., Rast, M., Wursteisen, P., Attema, E., Moreno, J., Müller, A., et al.

(2001). The DAISEX campaigns in support of a future land-surface-processes mission. *ESA Bulletin*, *105*, 101-111.

Berk, A., Anderson, G. P., Bernstein, L. S., Acharya, P. K., Dothe, H., Matthew, M. W., et al. (1999). MODTRAN4 radiative transfer modeling for atmospheric correction. *Optical Spectroscopic Techniques and Instrumentation for Atmospheric and Space Research III, Denver, USA, Proceedings of the SPIE*, Vol. 3756, 348-353.

Bicheron, P., and Leroy, M. (1999). A Method of Biophysical Parameter Retrieval at Global Scale by Inversion of a Vegetation Reflectance Model. *Remote Sensing of Environment*, *67*(3), 251-266.

Boegh, E., Soegaard, H., Broge, N., Hasager, C. B., Jensen, N. O., Schelde, K., et al. (2002). Airborne multispectral data for quantifying leaf area index, nitrogen concentration, and photosynthetic efficiency in agriculture. *Remote Sensing of Environment*, *81*(2-3), 179-193.

Bondeau, A., Kicklighter, D. W., Kaduk, J., and the participants of the Postdam NPP Intercomparison Project. (1999). Comparing Global Models of Terrestrial Net Primary Productivity (NPP): Importance of Vegetation Structure on Seasonal Npp Estimates. *Global Change Biology*, *5*(s1), 35-45.

Booker, F. L., Prior, S. A., Torbert, H. A., Fiscus, E. L., Pursley, W. A., and Hu, S. (2005). Decomposition of Soybean Grown Under Elevated

Concentrations of Co2 and O3. *Global Change Biology*, *11*(4), 685-698.

Bouvet, A., Le Toan, T., and Lam Dao, N. (2008). Monitoring of the rice cropping system in the Mekong delta using ENVISAT/ASAR dual polarisation data. *IEEE Transactions on Geoscience and Remote Sensing*, (submitted).

Brèda, N. J. J. (2003). Ground-based measurements of leaf area index: a review of methods, instruments and current controversies. *Journal of Experimental Botany*, *54*(392), 2403-2417.

Brisson, N., Mary, B., Ripoche, D., Jeuffroy, M. H., Ruget, F., Nicoullaud, B., et al. (1998). STICS: a generic model for the simulation of crops and their water and nitrogen balances. I. Theory and parameterization applied to wheat and corn. *Agronomie*, *18*(5-6), 311-346.

Broge, N. H., & Leblanc, E. (2001). Comparing prediction power and stability of broadband and hyperspectral vegetation indices for estimation of green leaf area index and canopy chlorophyll density. *Remote Sensing of Environment*, *76*(2), 156-172.

Brown, S. C. M., Quegan, S., Morrison, K., Bennett, J. C., and Cookmartin, G. (2003). High resolution measurements of scattering in wheat canopies – implications for crop parameter retrieval, *IEEE Transactions on Geoscience and Remote Sensing,* 41(7), 1602-1610.

Bruinsma, J. (2003). *World Agriculture: Towards 2015/2030: an FAO Perspective*. Ed. Earthscan.

Bruniquel , J., and Lopes, A. (1997). Multi-variate optimal speckle reduction in SAR imagery. *International Journal of Remote Sensing*, *18*, 603-627.

Chen, J. M., and Black, T. A. (1992). Defining Leaf Area Index for Non-Flat Leaves. *Plant, Cell and Environment*, *15*(4), 421-429.

Chen, J. M. (1996). Optically-based methods for measuring seasonal variation of leaf area index in boreal conifer stands. *Agricultural and Forest Meteorology*, *80*(2-4), 135-163.

Chen, K. S., Huang, W. P., Tsay, D. H. and Amar, F. (1996). Classification of Multifrequency Polarimetric SAR imagery using a Dynamic Learning Neural Network. *IEEE Transactions on Geoscience and Remote Sensing*, *34(3),* 814-820.

Chen, J. M., Pavlic, G., Brown, L., Cihlar, J., Leblanc, S. G., White, H. P., et al. (2002). Derivation and validation of Canada-wide coarse-resolution leaf area index maps using high-resolution satellite imagery and ground measurements. *Remote Sensing of Environment*, *80*(1), 165-184.

Cho, M. A., & Skidmore, A. K. (2006). A new technique for extracting the red edge position from hyperspectral data: The linear extrapolation method. *Remote Sensing of Environment, 101*(2), 181-193.

Clevers, J., and van Leeuwen, H. J. C. (1996). Combined Use of Optical and Microwave Remote Sensing Data for Crop Growth Monitoring. *Remote Sensing of Environment*, *56*, 42-51.

Clevers, J., Vonder, O. W., Jongschaap, R. E. E., Desprats, J. F., King, C., Prévot, L., et al. (2002a). Using SPOT data for calibrating a wheat growth model under mediterranean conditions. *Agronomie*, *22*, 687-694.

Clevers, J. G. P. W., De Jong, S. M., Epema, G. F., Van Der Meer, F. D., Bakker, W. H., Skidmore, A. K., et al. (2002b). Derivation of the red edge index using the MERIS - standard band setting. *International Journal of Remote Sensing, 23*(16), 3169.

Cloude, S., and Pottier, E. (1997). An entropy based classification scheme for land applications of polarimetric SAR. *IEEE Transactions on Geoscience and Remote Sensing*, *35*(1), 68-78.

Combal, B., Baret, F., and Weiss, M. Improving canopy variables estimation from remote sensing data by exploiting ancillary information. Case study on sugar beet canopies. (2002a). *Agronomie*, *22*, 205-215.

Combal, B., Baret, F., Weiss, M., Trubuil, A., Macé, D., Pragnère, A., Myneni, R., Knyazikhih, Y., and Wang, L. (2002b). Retrieval of canopy biophysical variables from bidirectional reflectance: Using prior information to solve the ill-posed inverse problem. *Remote Sensing of Environment*, *84*(1), 1-15.

Confalonieri, R., and Bechini, L. (2004). A preliminary evaluation of the simulation model CropSyst for alfalfa. *European Journal of Agronomy*, *21*(2), 223-237.

Cookmartin, G., Saich, P., Quegan, S., Cordey, R., Burgess-Allen, P., and Sowter, A. (2000). Modeling microwave interactions with crops and comparison with ERS-2 SAR observations. *IEEE Transactions on Geoscience and Remote Sensing*, *38*(2), 658-670.

Curran, P. J. (1989). Remote sensing of foliar chemistry. *Remote Sensing of Environment*, *30*(3), 271-278.

Curran, P., Dungan, J., and Gholz, H. (1990). Exploring the relationship between reflectance red edge and chlorophyll content in slash pine. *Tree physiology*, *7*(1_2_3_4), 33-48. doi: 14972904.

Curran P. J., and Dash J. (2005). ESA MERIS Algorithm Theoretical Basis Document ATBD 2.22 Chlorophyll Index.

D'Alba, L., and Colagrande, P. (2005). *MERIS Smile effect characterization and correction*. Technical Note, ESA-PCF MERIS Team.

Daughtry, C. S. T., Walthall, C. L., Kim, M. S., Colstoun, E. B. D., & McMurtreyIII, J. E. (2000). Estimating Corn Leaf Chlorophyll Concentration from Leaf and Canopy Reflectance. *Remote Sensing of Environment*, *74*(2), 229-239.

Dawson, T. P., Curran, P. J., and Plummer, S. E. (1998). LIBERTY--Modeling the Effects of Leaf Biochemical Concentration on Reflectance Spectra. *Remote Sensing of Environment*, *65*(1), 50-60.

Demarez, V., Gastellu-Etchegorry, J. P., Mougin , E., Marty , G., Proisy, C., Dufrene, E., et al. (1999). Seasonal variation of leaf chlorophyll content of a temperate forest. Inversion of the PROSPECT model. *International Journal of Remote Sensing*, *20*(16), 879-894.

Dong, Y., Milne, A. K., and Forster B. C. (2001). Segmentation and classification of vegetated areas using polarimetric SAR image data. *IEEE Transactions on Geoscience and Remote Sensing*, *39(2)*, 321-329.

Doraiswamy, P., McCarty, G., Hunt, J., Yost, R., Doumbia, M., and Franzluebbers, A. (2007). Modeling soil carbon sequestration in agricultural lands of Mali. *Agricultural Systems*, *94*(1), 63-74.

Duchemin, B., Hadria, R., Erraki, S., Boulet, G., Maisongrande, P., Chehbouni, A., et al. (2006). Monitoring wheat phenology and irrigation in Central Morocco: On the use of relationships between evapotranspiration, crops coefficients, leaf area index and remotely-sensed vegetation indices. *Agricultural Water Management*, *79*(1), 1-27.

Duke, C., and Guérif, M. (1998). Crop Reflectance Estimate Errors from the SAIL Model Due to Spatial and Temporal Variability of Canopy and Soil Characteristics. *Remote Sensing of Environment*, *66*(3), 286-297.

Duthoit S. (2006) Prise en compte de l'agrégation des cultures dans la simulation du transfert radiatif : importance pour l'estimation de l'indice foliaire (LAI), de la parcelle au paysage. Thesis, *Université Paul Sabatier*, Toulouse.

ESA. (2007). ASAR Product Handbook, Issue 2.2. ESA. Available from: http://envisat.esa.int/handbooks/asar/.

España, M. L., Baret, F., Aries, F., Chelle, M., Andrieu, B., and Prévot, L. (1999). Modeling maize canopy 3D architecture: Application to reflectance simulation. *Ecological Modelling*, *122*(1-2), 25-43.

Estellés, V., Utrillas, M. P., Martínez-Lozano, J. A., Alcántara, A., Alados-Arboledas, L., Olmo, F. J., et al. (2006). Intercomparison of spectroradiometers and Sun photometers for the determination of the aerosol optical depth during the VELETA-2002 field campaign. *Journal of Geophysical Research*, *111*, D17207. doi: 10.1029/2005JD006047.

Fang, H., and Liang, S. (2003). Retrieving leaf area index with a neural network method: simulation and validation. *IEEE Transactions on Geoscience and Remote Sensing, 41*(9), 2052-2062.

Fang, H., Liang, S., and Kuusk, A. (2003). Retrieving leaf area index using a genetic algorithm with a canopy radiative transfer model. *Remote Sensing of Environment*, *85*(3), 257-270.

Feret, J., François, C., Asner, G. P., Gitelson, A. A., Martin, R. E., Bidel, L. P., et al. (2008). PROSPECT-4 and 5: Advances in the leaf optical properties model separating photosynthetic pigments. *Remote Sensing of Environment*, *112*(6), 3030-3043.

Ferrazzoli, P., Guerriero, L., and Schiavon, G. (1999). Experimental and model investigation on radar classification capability. *IEEE Transactions on Geoscience and Remote Sensing*, *37*(2), 960-968.

Fomferra, N., and Brockmann, C. (2005). Beam–the ENVISAT MERIS and AATSR Toolbox. *Proceedings of the MERIS (A) ATSR Workshop 2005 (ESA SP-597). 26-30 September 2005 ESRIN, Frascati, Italy. Editor: H. Lacoste. Published on CDROM., p. 13.1.*

Fourty, T. (1996). Estimation du contenu biochimique d'un couvert végétal à partir de données haute résolution spectrale acquises au niveau satellitaire. *Université Paul Sabatier*, Toulouse, France.

Freeman, A. and Durden, S., L. (1998). A three-component scattering model for polarimetric SAR data. *IEEE Transactions on Geoscience and Remote Sensing*, *32,* 963-973.

Frost, V. S., Stiles, J. A., Shanmugan, K. S., and Holtzman, J. C. (1982). A model for radar images and its application to adaptive digital filtering of multiplicative noise. *IEEE Transactions on Pattern Analysis and Machine Intelligence*, *4*, 157-166.

Fung, A. K. (1994). *Microwave Scattering and Emission Models and Their Applications* (pág. 592). Artech House Publishers.

Ganapol, B. D., Johnson, L. F., Hlavka, C. A., Peterson, D. L., and Bond, B. (1999). LCM2: A coupled leaf/canopy radiative transfer model. *Remote Sensing of Environment*, *70*(2), 153-166.

Gandía, S., Fernández, G., García, J. C., and Moreno, J. (2004). Retrieval of vegetation biophysical variables from CHRIS/PROBA data in the SPARC campaign. *In Proceedings of the 2nd ESA CHRIS/Proba Workshop, Frascati, Italy 28-30 April*, ESA/ESRIN SP-578, July 2004.

Gao, W., and Lesht, B. M. (1997). Model inversion of satellite-measured reflectances for obtaining surface biophysical and bidirectional reflectance characteristics of grassland. *Remote Sensing of Environment*, *59*(3), 461-471.

Garrigues, S., Allard, D., Baret, F., and Weiss, M. (2006). Influence of landscape spatial heterogeneity on the non-linear estimation of leaf area index from moderate spatial resolution remote sensing data. *Remote Sensing of Environment*, *105*(4), 286-298.

Gastellu-Etchegorry, J. P., Martin, E., and Gascon, F. (2004). DART: a 3D model for simulating satellite images and studying surface radiation budget. *International Journal of Remote Sensing*, *25*(1), 73.

Gielson, A., Merzlyak, M., and Lichtenthaler, H. (1996). Detection of red edge position and chlorophyll content by reflectance measurements near 700 nm. *Journal of Plant Physiology*, *148*, 501-508.

Giorgi, F., and Lionello, P. Climate change projections for the Mediterranean region (2008). *Global and Planetary Change*, (In Press, Corrected Proof.).

Gitelson A. A., and Merzlyak M. N. (1997). Remote estimation of chlorophyll content in higher plant leaves. *International Journal of Remote Sensing*, *18*, 2691-2697.

Gitelson, A. A., Viña, A., Ciganda, V., Rundquist, D. C., and Arkebauer, T. J. (2005). Remote estimation of canopy chlorophyll content in crops. *Geophysical Research Letters*, *32*, L08403. doi: 10.1029/2005GL022688.

Gitelson, A. A., Viña, A., Verma, S. B., Rundquist, D. C., Arkebauer, T. J., Keydan, G., et al. (2006). Relationship between gross primary production and chlorophyll content in crops: Implications for the synoptic monitoring of vegetation productivity. *Journal of Geophysical Research*, *111*, D08S11. doi: 10.1029/2005JD006017.

Gobron, N., Pinty, B., Verstraete, M. M., and Govaerts, Y. (1997). A semidiscrete model for the scattering of light by vegetation. *Journal of Geophysical Research*, *102*(D8), 9431–9446.

Goel, N.S. (1988). Models of vegetation canopy reflectance and their use in

estimation of biophysical parameters from reflectance data. *Remote Sensing Reviews*, 4, 1-222.

Gomez-Dans, J. L., Quegan, S., and Bennett, J. C. (2006). Indoor C-Band Polarimetric Interferometry Observations of a Mature Wheat Canopy. *IEEE Transactions on Geoscience and Remote Sensing, 44*(4), 768-777.

González-Sanpedro, M., Le Toan, T., Moreno, J., Kergoat, L., and Rubio, E. (2008). Seasonal variations of leaf area index of agricultural fields retrieved from Landsat data. *Remote Sensing of Environment*, *112*(3), 810-824.

Govaerts, Y. M., and Verstraete, M. M. (1998). Raytran: a Monte Carlo ray-tracing model to compute light scattering in three-dimensional heterogeneous media. *IEEE Transactions on Geoscience and Remote Sensing*, *36*, 493-505.

Govaerts, Y. M., Jacquemoud, S., Verstraete, M. M., and Ustin, S. L. (1996). Three-dimensional radiation transfer modeling in a dicotyledon leaf. *Applied Optics*, *35*(33), 6585-6598.

Goze, S., and Lopes, A. (1993). A MMSE Speckle Filter for Full Resolution SAR Polarimetric Data. *Journal of Electromagnetic Waves and Applications*, *7*, 717-737.

Guanter, L., Alonso, L., and Moreno, J. (2005). First results from the

PROBA/CHRIS hyperspectral/multiangular satellite system over land and water targets. *IEEE*, *Geoscience and Remote Sensing Letters, 2*(3), 250-254.

Guanter, L., González-Sanpedro, M. D. C., and Moreno, J. (2007). A method for the atmospheric correction of ENVISAT/MERIS - data over land targets. *International Journal of Remote Sensing*, *28*(3), 709.

Haboudane, D., Miller, J. R., Tremblay, N., Zarco-Tejada, P. J., & Dextraze, L. (2002). Integrated narrow-band vegetation indices for prediction of crop chlorophyll content for application to precision agriculture. *Remote Sensing of Environment*, *81*(2-3), 416-426.

Haboudane, D., Miller, J. R., Pattey, E., Zarco-Tejada, P. J., and Strachan, I. B. (2004). Hyperspectral vegetation indices and novel algorithms for predicting green LAI of crop canopies: Modeling and validation in the context of precision agriculture. *Remote Sensing of Environment*, *90*(3), 337-352.

Hadria, R., Duchemin, B., Lahrouni, A., Khabba, S., Erraki, S., Dedieu, G., et al. (2006). Monitoring of irrigated wheat in a semiarid climate using crop modelling and remote sensing data: Impact of satellite revisit time frequency. *International Journal of Remote Sensing*, *27*(5-6), 1093-1117.

Henderson, F. M., and Lewis, A. J. (1998). *Principles and Applications of Imaging Radar: Manual of Remote Sensing, vol. 2*. Wiley, New York.

Hoekman, D. H. And Quiñónez, M., J. (2000). Land cover type and biomasa classification using AirSAR data for evaluation of monitoring scenarios in the Colombian Amazon. *IEEE Transactions on Geoscience and Remote Sensing*, *38,* 685-696.

Hoogenboom, G., Jones, J. W., and Boote, K. J. (1992). Modeling growth, development, and yield of grain legumes using soygro, pnuogro, and beangro: a review. *Transactions of the ASAE*, *35*(6), 2043-2056.

Hosgood, B., Jacquemoud, S., Andreoli, G., Verdebout, J., Pedrini, G., and Schmuck, G. (1995). *Leaf optical properties experiment (LOPEX 93), European Commission, Joint Research Center, Institute For Remote Sensing Applications, Ispra (Italy)*. Report EUR-16095-EN.

Jacquemoud, S., and Baret, F. (1990). PROSPECT: A model of leaf optical properties spectra. *Remote Sensing of Environment*, *34*(2), 75-91.

Jacquemoud, S. (1993). Inversion of the PROSPECT + SAIL canopy reflectance model from AVIRIS equivalent spectra: Theoretical study. *Remote Sensing of Environment*, *44*(2-3), 281-292.

Jacquemoud, S., Baret, F., Andrieu, B., Danson, F. M., and Jaggard, K. (1995). Extraction of vegetation biophysical parameters by inversion of the PROSPECT + SAIL models on sugar beet canopy reflectance data. Application to TM and AVIRIS sensors. *Remote Sensing of Environment*,

52(3), 163-172.

Jacquemoud, S., Ustin, S. L., Verdebout, J., Schmuck, G., Andreoli, G., and Hosgood, B. (1996). Estimating leaf biochemistry using the PROSPECT leaf optical properties model. *Remote Sensing of Environment*, *56*(3), 194-202.

Jochum, A. and Calera, A. (2006). Operational Space-Assisted Irrigation Advisory Services: Overview Of And Lessons Learned From The Project DEMETER. *In Proceedings of the International Conference on Earth Observation for vegetation monitoring and water management*, *Naples, Italy, 10-11 November 2005. AIP Conference Proceedings, August 23, 2006, Vol. 852 (pp 3-13).*

Jones, C. A., and Kiniry, J. R. (1986). *CERES-Maize: A Simulation Model of Maize Growth and Development*. Texas AandM University Press College Station (USA).

Jones, G. V., and Davis, R. E. (2000). Using a synoptic climatological approach to understand climate-viticulture relationships. *International Journal of Climatology*, *20*(8), 813-837.

Jones, J. W., Hoogenboom, G., Porter, C. H., Boote, K. J., Batchelor, W. D., Hunt, L. A., et al. (2003). The DSSAT cropping system model. *European Journal of Agronomy*, *18*(3-4), 235-265.

Jones, P. D., and Moberg, A. (2003). Hemispheric and Large-Scale Surface Air Temperature Variations: An Extensive Revision and an Update to 2001. *Journal of Climate*, *16*(2), 206-223 .

Jong-Sen Lee, Grunes, M., and de Grandi, G. (1999). Polarimetric SAR speckle filtering and its implication for classification. *IEEE Transactions on Geoscience and Remote Sensing, 37*(5), 2363-2373.

Kalubarme, M. H., Potdar, M. B., Manjunath, K. R., Mahey, R. K., and Siddhu, S. S. (2003). Growth profile based crop yield models: a case study of large area wheat yield modelling and its extendibility using atmospheric corrected NOAA - AVHRR - data. *International Journal of Remote Sensing*, *24*(10), 2037.

Karl, T. R., and Easterling, D. R. (1999). Climate Extremes: Selected Review and Future Research Directions. *Climatic Change*, *42*(1), 309-325.

Kaufman, Y. J. (1989). The atmospheric effect on remote sensing and its correction. *Theory and Applications of Optical Remote Sensing*, 336-428.

Kimes, D. S., Privette, J. L., Abuelgasim, A. A., Knyazikhin, Y., and Gao, F. (2000). Inversion methods for physically-based models (for extracting vegetation variables using bidirectional and spectral data from modern-borne sensors). *Remote Sensing Reviews. Vol. 18*, *18*(2-4), 381-439.

Kneubühler, M. (2002). Spectral Assessment of Crop Phenology Based on

Spring Wheat and Winter Barley. PhD Dissertation, *Remote Sensing Series*, Vol. *38,* University of Zurich, pp: 149.

Koetz, B., Baret, F., Poilv, H., and Hill, J. (2005). Use of coupled canopy structure dynamic and radiative transfer models to estimate biophysical canopy characteristics. *Remote Sensing of Environment*, *95*(1), 115-124.

Kuan, D. T., Sawchuk, A. A., Strand, T. C., and Chavel, P. (1987). Adaptive restoration of images with speckle. *IEEE Transactions on Acoustics Speech and Signal Processing*, *35*, 373-383.

Kuusk, A. (1995). A fast, invertible canopy reflectance model. *Remote Sensing of Environment*, *51*(3), 342-350.

Lacaze, R., Chen, J. M., Roujean, J., and Leblanc, S. G. (2002). Retrieval of vegetation clumping index using hot spot signatures measured by POLDER instrument. *Remote Sensing of Environment*, *79*(1), 84-95.

Lanjeri, S., Melia, J., and Segarra, D. (2001). A multi-temporal masking classification method for vineyard monitoring in central Spain. *International Journal of Remote Sensing*, *22*(16), 3167-3186.

Launay, M., and Guerif, M. (2005). Assimilating remote sensing data into a crop model to improve predictive performance for spatial applications. *Agriculture, Ecosystems and Environment*, *111*(1-4), 321-339.

Lauvernet, C., Baret, F., Hascoºt, L., and LeDimet, F. X. (2005). Improved estimates of vegetation biophysical variables from meris toa images by using spatial and temporal constraints. In *Proceedings of the 9th ISPMSRS, Beijing, China*.

Le Maire, G., François, C., and Dufrêne, E. (2004). Towards universal broad leaf chlorophyll indices using PROSPECT simulated database and hyperspectral reflectance measurements. *Remote Sensing of Environment*, *89*, 1-28.

Le Toan, T., Laur, H., Mougin, E., and Lopes, A. (1989). Multitemporal and dual-polarization observations of agricultural vegetation covers by X-band SAR images. *Geoscience and Remote Sensing, IEEE Transactions on*, *27*(6), 709-718.

Le Toan, T., Lopes, A., and Malavaud, A. (1983). Relationships between radar backscattering and the characteristics of a crop canopy: considerations on the effect of structure. *Proceeding of the ESA IGARSS 84. Remote Sensing: From Res. Towards Operational Use*, Vol. 1 p 155-160.

Le Toan, T., Ribbes, F., Li-Fang Wang, Floury, N., Kung-Hau Ding, Jin Au Kong, et al. (1997). Rice crop mapping and monitoring using ERS-1 data based on experiment and modeling results. *IEEE Transactions on Geoscience and Remote Sensing, 35*(1), 41-56.

Le Toan, T., Lopes, A., and Huet, M. (1984). On the relationships between

radar backscattering Coefficient and Vegetation Canopy Characteristics. *Proceedings of the International Geoscience and Remote Sensing Symposium*, 155-160.

Lee, J. (1986). Speckle suppression and analysis for synthetic aperture radar images. *Optical Engineering*, *25*, 636-643.

Lee, J. S., Grunes, M., and Kwok R. (1994). Classification of multi-look polarimetric SAR images based on complex Wishart distribution. *International Journal of Remote Sensing, 15*(11), 2299-2311.

Lee, J., Grunes, M., and de Grandi, G. (1999). Polarimetric SAR speckle filtering and its implication for classification. *IEEE Transactions on Geoscience and Remote Sensing*, *37*(5), 2363-2373.

Lombardo, P., Olivier, C. J., Macri Pellizzeri, T., and Meloni, M. (2003). A new maximu-likehood joint segmentation technique for multitemporal SAR and multiband optical images. *IEEE Transactions on Geoscience and Remote Sensing*, *41*, 2478-2487.

Long, S. P., Ainsworth, E. A., Leakey, A. D., and Morgan, P. B. (2005). Global food insecurity. Treatment of major food crops with elevated carbon dioxide or ozone under large-scale fully open-air conditions suggests recent models may have overestimated future yields. *Philosophical Transactions of the Royal Society B: Biological Sciences*, *360*(1463).

Lopes, A., Nezry, E., Touzi, R., and Laur, H. (1993). Structure detection and statistical adaptive speckle filtering in SAR - images. *International Journal of Remote Sensing*, *14*(9), 1735-1758.

Lopes, A., and Sery, F. (1997). Optimal speckle reduction for the product model in multilook polarimetric SAR imagery and the Wishart distribution. *IEEE Transactions on Geoscience and Remote Sensing*, *35*, 632-647.

Loveland, T. R., Reed, B. C., Brown, J. F., Ohlen, D. O., Zhu, Z., Yang, L., et al. (2000). Development of a global land cover characteristics database and IGBP - DISCover from 1 km AVHRR - data. *International Journal of Remote Sensing*, *21*(6), 1303.

Maier, S. W., Lüdeker, W., and Günther, K. P. (1999). SLOP : A Revised Version of the Stochastic Model for Leaf Optical Properties. *Remote Sensing of Environment*, *68*(3), 273-280.

Major, D. J., Schaalje, G. B., Wieg, C., and Blad, B. L. (1992). Accuracy and sensitivity analyses of SAIL model-predicted reflectance of maize. *Remote Sensing of Environment*, *41*(1), 61-70.

Marliani, F., Paloscia, S., Pampaloni, P., and Kong, J. (2002). Simulating coherent backscattering from crops during the growing cycle. *Geoscience and Remote Sensing, IEEE Transactions on*, *40*(1), 162-177. doi: 10.1109/36.981358.

Martínez, B., Camacho-de Coca, F., García-Haro, F. J., Meliá, J. (2005). Methdology for direct validation of LAI/FVC/FAPAR coarse satellite derived products. In: ESA-SPARC Proceedings, ISSN:1022-6656.

Mattia, F., Le Toan, T., Picard, G., Posa, F., D'Alessio, A., Notarnicola, C., et al. (2003). Multitemporal C-band radar measurements on wheat fields. *IEEE Transactions on Geoscience and Remote Sensing*, *41*(7), 1551-1560.

Mattia, F., Dente, L., Satalino, G., and Le Toan, T. (2005). Sensitivity of ASAR AP data to wheat crop parameters. *In Proceedings of the 2004 Envisat & ERS Symposium, Salzburg, Austria, 6-10 September 2004,* ESA SP-572, CDROM. Ed. H. Lacoste and L. Ouwehand.

McCown, R. L., Hammer, G. L., Hargreaves, J. N. G., Holzworth, D. P., and Freebairn, D. M. APSIM: a novel software system for model development, model testing and simulation in agricultural systems research. *Agricultural Systems*, *50*(3), 255-271.

Miller, J. R., Berger, M., Jacquemoud, S., Moreno, J., Mohammed, G., Moya, I., et al. (2004). Overview of FluorMOD: A project to develop an integrated leaf-canopy fluorescence simulation model. *2nd International Workshop on Remote Sensing of Vegetation Fluorescence, 17-19 November, 2004, Montreal (Canada).*

Mkhabela, M. S., Mkhabela, M. S., and Mashinini, N. N. (2005). Early maize yield forecasting in the four agro-ecological regions of Swaziland using NDVI data derived from NOAA's-AVHRR. *Agricultural and Forest*

Meteorology, *129*(1-2), 1-9.

Montaldo, N., and Albertson, J. D. (2003). Multi-scale assimilation of surface soil moisture data for robust root zone moisture predictions. *Advances in Water Resources*, *26*(1), 33-44.

Moreno, J., and participants of the SPARC campaigns. (2004). The SPECTRA Barrax Campaign (SPARC): overview and first results from CHRIS data. *In Proceedings of the 2nd ESA CHRIS/Proba Workshop, Frascati, Italy 28-30 April*, ESA/ESRIN SP-578, July 2004.

Moulin, S., Bondeau, A., and Delecolle, R. (1998). Combining agricultural crop models and satellite observations: from field to regional scales. *International Journal of Remote Sensing*, *19*(6), 1021.

Nicodemus, F. E., Richmond, J. C., Hsia, J. J., Ginsberg, I. W., and Limperis, T. (1977). Geometrical considerations and nomenclature for reflectance. *NBS Monograph*, *160*, 52.

Nilson, T., and Kuusk, A. (1989). A reflectance model for the homogeneous plant canopy and its inversion. *Remote Sensing of Environment*, *27*(2), 157-167.

Norman, J. M., Kustas, W. P., and Humes, K. S. (1995). Source approach for estimating soil and vegetation energy fluxes in observations of directional radiometric surface temperature. *Agricultural and Forest*

Meteorology, *77*(3-4), 263-293.

Oliver, C., and Quegan, S. (1998). Understanding Synthetic Aperture Radar Images Boston. *MA: Artech House*.

Picard, G. (2002). *Modélisation radar des couverts végétaux, application à la télédétection de couverts forestiers et agricoles*. Thèse. Université Paul Sabatier, Toulouse, France.

Picard, G., Le Toan, T., and Mattia, F. (2003). Understanding C-band radar backscatter from wheat canopy using a multiple-scattering coherent model. *IEEE Transactions on Geoscience and Remote Sensing*, *41*(7), 1583-1591.

Pierce, L. E., Ulaby, F. T., Sarabandi, K., and Dobson, M. C. (1994). Knowledge-based classification of polarimteric SAR images. *IEEE Transactions on Geoscience and Remote Sensing*, *32*, 1081-1086.

Pinty, B., Verstraete, M. M., and Dickinson, R. E. (1990). A physical model of the bidirectional reflectance of vegetation canopies. 2. Inversion and validation. *Journal of Geophysical Research*, *95*, 11767-11775.

Press, W. H., Flannery, B. P., Teukolsky, S. A., and Vetterling, W. T. (1992). *Numerical Recipes in FORTRAN 77: The Art of Scientific Computing* (2º ed., pág. 992). Cambridge University Press.

Privette, J. L., Emery, W. J., and Schimel, D. S. (1996). Inversion of a vegetation reflectance model with NOAA AVHRR data. *Remote Sensing of Environment*, *58*(2), 187-200.

Qaim, M., and Zilberman, D. (2003). Yield Effects of Genetically Modified Crops in Developing Countries. *Science*, *299*(5608), 900-902.

Qi, J., Kerr, Y. H., Moran, M. S., Weltz, M., Huete, A. R., Sorooshian, S., et al. (2000). Leaf Area Index Estimates Using Remotely Sensed Data and BRDF Models in a Semiarid Region. *Remote Sensing of Environment*, *73*(1), 18-30.

Qin, W., Gerstl, S. A. W., Deering, D. W., and Goel, N. S. (2002). Characterizing leaf geometry for grass and crop canopies from hotspot observations: A simulation study. *Remote Sensing of Environment*, *80*(1), 100-113.

Quegan, S., and Jiong Jiong Yu. (2001). Filtering of multichannel SAR images. *IEEE Transactions on Geoscience and Remote Sensing, 39*(11), 2373-2379.

Quegan, S., Le Toan, T., Yu, J., Ribbes, F., and Floury, N. (2000). Multitemporal ERS SAR analysis applied to forest mapping. *Geoscience and Remote Sensing, IEEE Transactions on*, *38*(2), 741-753.

Ranson, K. J. and Sun, G. (2000). Effects of environmental conditions on boreal forest classification and biomass estimates with SAR. *IEEE*

Transactions on Geoscience and Remote Sensing, *38,* 1242-1252.

Räisänen, J. (2007). How Reliable Are Climate Models? *Tellus A*, *59*(1), 2-29.

Richter, R. (1997). Correction of atmospheric and topographic effects for high spatial resolution satellite imagery. *International Journal of Remote Sensing*, *18*, 1099-1111.

Ritchie, J. T., and Otter-Nacke, S. (1985). *CERES-Wheat. A simulation model of wheat growth and development*, ARS(1985). (págs. 159-175). US Department of Agriculture.

Royo, C., Aparicio, N., Villegas, D., Casadesus, J., Monneveux, P., and Araus, J. (2003). Usefulness of spectral reflectance indices as durum wheat yield predictors under contrasting Mediterranean conditions. *International Journal of Remote Sensing*, *17*, 4403-4419.

Ruget, F., Brisson, N., Delécolle, R., and Faivre, R. (2002). Sensitivity analysis of a crop simulation model (STICS) in order to determine the accuracy needed for the parameters. *Agronomie*, *22*, 133-158.

Saich, P., and Borgeaud, M. (2000). Interpreting ERS SAR signatures of agricultural crops in Flevoland, 1993-1996. *IEEE Transactions on Geoscience and Remote Sensing, 38*(2), 651-657.

Schotten, C. G. J., Van Rooy, W. W. L., and Janssen, L. L. F. (1995).

Assessment of the capabilities of multi-temporal ERS-1 SAR data to discriminate between agricultural crops. *International Journal of Remote Sensing*, *16*(14), 2619-2637.

Schou, J., and Skriver, H. (2001). Restoration of polarimetric SAR images using simulated annealing. *IEEE Transactions on Geoscience and Remote Sensing, 39*(9), 2005-2016.

Schröter, D., Cramer, W., Leemans, R., Prentice, I. C., Araujo, M. B., Arnell, N. W., et al. (2005). Ecosystem Service Supply and Vulnerability to Global Change in Europe. *Science*, *310*(5752), 1333-1337.

Simonneaux, V., Duchemin, B., Helson, D., Er-Raki, S., Olioso, A., and Chehbouni, A. G. (2008). The use of high-resolution image time series for crop classification and evapotranspiration estimate over an irrigated area in central Morocco. *International Journal of Remote Sensing*, *29*(1), 95.

Skriver, H., Svendsen, M., and Thomsen, A., G. (1999). Multitemporal C- and L-band polarimetric signatures of crops. *IEEE Transactions on Geoscience and Remote Sensing, 37(5)*, 2413-2429.

Skriver, H., Dall, J., Le Toan, T., Quegan, S., Ferro-Famil, L., Portier, E., Lumsdon, P., and Moshammer, R. (2005). Agriculture classification using PolSAR data. *Proceedings or the POLinSAR Workshop.*

Skriver, H. (2007). Signatures of Polarimetric Parameters and their

Implications on Land Cover Classification. *Proceedings or the Geoscience and Remote Sensing Symposium, IGARSS 2007,* 4195-4198.

Solomon, S., Qin, D., Manning, M., and Marquis, M. (2007). *Climate change 2007: the physical science basis contribution of Working Group I to the fourth assessment report of the Intergovermental Panel on Climate Change*. Cambridge University Press, Cambridge.

Spitters, C. J. T., van Keulen, H., and van Kraalingen, D. W. G. (1989). A simple and universal crop growth simulator: SUCROS87. *Simulation and Systems Management in Crop Protection*, 147-181.

Strahler, A., Muchoney, D., Borak, J., Friedl, M., Gopal, S., Lambin, E., et al. (1999). MODIS land cover product, algorithm theoretical basis document (ATBD), version 5.0.

Suits, G. H. (1972). The calculation of the directional reflectance of a vegetative canopy. *Remote Sensing of Environment*, *2*, 117-125.

Tanré, D., Herman, M., and Deschamps, P. Y. (1981). Influence of the background contribution upon space measurements of ground reflectance. *Applied Optics*, *20*(20), 3676-3684.

Tanré, D., Deroo, C., Duhaut, P., Herman, M., Morcrette, J. J., Perbos, J., et al. (1990). Technical note Description of a computer code to simulate the satellite signal in the solar spectrum: the 5S code. *International Journal of*

Remote Sensing, *11*(4), 659.

Tarantola, A. (2005). Inverse Problem Theory and Methods for Model Parameter Estimation. SISM (Society for Industrial and Applied Mathematics). ISBN:0-89871-572-5, 342 pp.

Tian, Y., Wang, Y., Zhang, Y., Knyazikhin, Y., Bogaert, J., and Myneni, R. B. (2003). Radiative transfer based scaling of LAI retrievals from reflectance data of different resolutions. *Remote Sensing of Environment*, *84*(1), 143-159.

Tso, B., and Mather, P. M. (1999). Crop discrimination using multi-temporal SAR - imagery. *International Journal of Remote Sensing*, *20*(12), 2443.

Turner, D. P., Cohen, W. B., Kennedy, R. E., Fassnacht, K. S., and Briggs, J. M. (1999). Relationships between Leaf Area Index and Landsat TM Spectral Vegetation Indices across Three Temperate Zone Sites. *Remote Sensing of Environment*, *70*(1), 52-68.

Ulaby, F., and Bush, T. (1976). Corn growth as monitored by radar. *IEEE Transactions on Antennas and Propagation, 24*(6), 819-828.

Ulaby, F., Allen, C., III, G. E., and Kanemasu, E. (1984). Relating the microwave backscattering coefficient to leaf area index. *Remote Sensing of Environment*, *14*(1-3), 113-133.

Ulaby, F. T., Moore, R. K., and Fung, A. K. (1986). *Microwave Remote Sensing: Active and Passive, from Theory to Applications* (pp. 1120). Artech House Publishers.

Van Zyl, J. (1989). Unsupervised classification of scattering behaviour using radar polarimetry data. *IEEE Transactions on Geoscience and Remote Sensing*, *27*(1), 36-45.

Verhoef, W. (1984). Light scattering by leaf layers with application to canopy reflectance modeling: The SAIL model. *Remote Sensing of Environment*, *16*(2), 125-141.

Verhoef, W. (1998). *Theory of radiative transfer models applied in optical remote sensing of vegetation canopies*. PhD Dissertation. *Wageningen Agricultural University*, The Netherlands.

Verhoef, W. (2002). Improved modelling of multiple scattering in leaf canopies: The model SAIL++. *In Proceedings of the 1st International Symposium on Recent Advances in Quantitative Remote Sensing, 16-20 September, Torrent, Spain*, pp. 11-20.

Verhoef, W., and Bach, H. (2003). Simulation of hyperspectral and directional radiance images using coupled biophysical and atmospheric radiative transfer models. *Remote Sensing of Environment*, *87*(1), 23-41.

Verhoef, W., Jia, L., Xiao, Q., and Su, Z. Unified Optical-Thermal Four-

Stream Radiative Transfer Theory for Homogeneous Vegetation Canopies. *IEEE Transactions on Geoscience and Remote Sensing, 45*, 1808-1822.

Vermote, E. F., Tanré, D., Deuzé, J. L., Herman, M., and Morcrette, J. L. (1997). Second Simulation of the Satellite Signal in the Solar Spectrum, 6S: An overview. *IEEE Transactions on Geoscience and Remote Sensing, 35*, 675-686.

Vicente-Serrano, S. (2007). Evaluating the Impact of Drought Using Remote Sensing in a Mediterranean, Semi-arid Region. *Natural Hazards*, *40*(1), 173-208.

Vicente-Serrano, S., Cuadrat-Prats, J., and Romo, A. (2006). Early prediction of crop production using drought indices at different timescales and remote sensing data: application in the Ebro Valley (northeast Spain). *International Journal of Remote Sensing*, *27*, 511-518.

Viña, A., Rundquist, D. C., Keydan, G., Leavitt, B., and Schepers, J. (2004). Monitoring maize (Zea mays L.) phenology with remote sensing. *Agronomy Jounal*, *96*, 1139-1147.

Wang, Z. J., Wang, J. H., Liu, L. Y., Huang, W. J., Zhao, C. J., and Wang, C. Z. (2004). Prediction of grain protein content in winter wheat (Triticum aestivum L.) using plant pigment ratio (PPR). *Field Crops Research*, *90*(2-3), 311-321. doi: 10.1016/j.fcr.2004.04.004.

Weiss, M., and Baret, F. (1999). Evaluation of Canopy Biophysical Variable Retrieval Performances from the Accumulation of Large Swath Satellite Data. *Remote Sensing of Environment*, *70*(3), 293-306.

Weiss, M., Myneni, R. B., Pragnère, A., and Knyazikhin, Y. (2000). Investigation of a model inversion technique to estimate canopy biophysical variables from spectral and directional reflectance data. *Agronomie*, *20*, 3-22.

Weiss, M., Troufleau, D., Baret, F., Chauki, H., Prévot, L., Olioso, A., et al. (2001). Coupling canopy functioning and radiative transfer models for remote sensing data assimilation. *Agricultural and Forest Meteorology*, *108*(2), 113-128.

Yoder, B. J., and Pettigrew-Crosby, R. E. (1995). Predicting nitrogen and chlorophyll content and concentrations from reflectance spectra (400–2500 nm) at leaf and canopy scales. *Remote Sensing of Environment*, *53*(3), 199-211.

Zarco-Tejada, P. J., Miller, J. R., Harron, J., Hu, B., Nol, T. L., Goel, N., et al. (2004). Needle chlorophyll content estimation through model inversion using hyperspectral data from boreal conifer forest canopies. *Remote Sensing of Environment*, *89*(2), 189-199.

Zhang, Q., Xiao, X., Braswell, B., Linder, E., Baret, F., and Moore III, B. (2005). Estimating light absorption by chlorophyll, leaf and canopy in a

deciduous broadleaf forest using MODIS data and a radiative transfer model. *Remote Sensing of Environment*, *99*(3), 357-371.

Zurita-Milla, R., Kaiser, G., Clevers, J., Schneider, W., and Schaepman, M. E. (2007). Spatial unmixing of MERIS data for monitoring vegetation dynamics. *In Proceedings of the Envisat Symposium, 23-27 April 2007, Montreux (Switzerland)*. ESA SP-636, July 2007.

APPENDIX I

RESUMEN EXTENSO EN CASTELLANO

Esta memoria se ha redactado originalmente en inglés. El presente anexo, en castellano, es un resumen extenso de la misma y se ha introducido para cumplir con la normativa de la Universidad de Valencia. La versión original en inglés es mucho más completa y contiene todos los detalles del trabajo científico que se defiende en esta tesis doctoral.

INTRODUCCIÓN

A.1. Contexto científico.

A.1.1. Necesidad de una monitorización agrícola.

El aumento de la población mundial, la incertidumbre en los cambios de producción causados por el cambio climático, así como la importancia social y económica que el sector agrícola tiene en muchas regiones del mundo, hace que sea muy importante desarrollar métodos que permitan hacer un seguimiento del estado de los cultivos, mejorar la gestión de los mismos, así como poder realizar una estimación temprana de la producción. Esta necesidad se ve reforzada por cuestiones referentes al cambio climático y a la evolución de las prácticas agrícolas.

En cuanto a las actividades humanas, la Organización de las Naciones Unidas para la Agricultura y la Alimentación (FAO) señala que la población mundial aumentará a un ritmo de 43 millones por año en el período 2045 - 2050 (Bruinsma, 2003). Este aumento de población será consecuencia del crecimiento en los países en vías de desarrollo (45 millones), y el pronóstico es que la mitad de este aumento se llevará a cabo en el África sub-sahariana (23 millones). En los países en vías de desarrollo, especialmente en África, el aumento de población agravará aún más el estado actual de desnutrición en el mundo. Se espera que los países industrializados reaccionen para aumentar la producción de alimentos de acuerdo al crecimiento de la población. Es un hecho que existe una preocupación general por la necesidad de aumentar la producción agrícola.

Además, en el marco de lo que se conoce como estrategias de seguridad alimenticia, hay un interés en la predicción de problemas como las plagas y las infecciones en los períodos de sequía, que pueden dañar la producción de cultivos. En las regiones áridas y semiáridas del mundo los frecuentes períodos de sequía generan grandes pérdidas en la producción agrícola, las cuales se traducen en hambrunas así como en importantes pérdidas económicas en los países en vías de desarrollo. Se espera que estos problemas aumenten con el cambio climático, principalmente en la región del Mediterráneo, que podría ser una de las regiones más vulnerables al cambio global. Los estudios para la región mediterránea muestran una reducción de las zonas agrícolas y pérdidas de potencial agrícola durante el siglo XX (Schröter et al., 2005) debido a la disminución pronunciada de las precipitaciones tal como predicen Giorgi y Lionello (2008).

El cambio de hábitos alimentarios que se está produciendo en la actualidad en países emergentes importantes, tales como India y China, está aumentando la demanda de productos agrícolas. En estos países, un sector de la población cada vez mayor tiene suficientes recursos económicos para cambiar una dieta vegetariana, principalmente a base de arroz y otros cereales, por una dieta que incluye más proteínas de origen animal. El ganado debe ser alimentado con cereales, lo que aumenta la demanda y, en consecuencia, los precios de mercado. Por otra parte, algunos países desarrollados están aumentando su producción de bio-combustibles, lo cual disminuye la cantidad de los cultivos destinados al consumo humano. Esto también contribuye a incrementar los precios de los cereales. Por último, pero no por ello menos importante, la tendencia al alza de los precios está atrayendo especuladores a los mercados. El aumento general de los precios está causando tensiones políticas, como ocurrió durante la primavera de 2008 en países como Haití, donde el primer ministro tuvo que dimitir, Camerún, Senegal, pero así mismo, Egipto o Tailandia. Un modo de limitar el aumento de los precios sería aumentar la producción, lo que también requeriría aumentar la productividad agrícola. De hecho, durante la cumbre de la FAO de junio de 2008, se afirmó que se necesitan más inversiones para aumentar la productividad agrícola.

La necesidad de un aumento de la producción ha inducido cambios importantes en las prácticas agrícolas durante las últimas décadas. Por ejemplo, el uso de fertilizantes se ha extendido en todo el mundo y los cultivos modificados genéticamente se utilizan como una solución para un aumento "sostenible" de la producción (Qaim y Wilberman, 2003). También existe una preocupación por los impactos asociados a estas nuevos prácticas agrícolas. La

expansión de la agricultura debe hacerse de forma sostenible ya que el uso generalizado de fertilizantes o la sobre-explotación de los recursos hídricos representa riesgos para el medio ambiente y puede incluso tener consecuencias para la salud humana. El aumento de los procesos intensivos tales como la irrigación y / o el uso indebido de fertilizantes también puede producir consecuencias negativas sobre la calidad del agua y la degradación de tierras de regadío, por ejemplo, como consecuencia de la salinización.

Por último, otro cambio notable en la agricultura moderna es que, cada vez con más frecuencia, las rotaciones de los cultivos son decididas por las fluctuaciones del mercado y por reglamentos en materia de política (sobre todo en la UE). Esto introduce una nueva dinámica en la distribución de cultivos que hace necesaria una actualización frecuente de los mapas de cultivos.

La otra cuestión importante por la cual se requiere un sistema de seguimiento de los cultivos es el impacto del cambio climático en la agricultura. Los estudios realizados durante las últimas décadas han aportado pruebas acerca de las modificaciones de varios parámetros climáticos (Salomón et al., 2007). Por ejemplo, durante el siglo XX se han observado tendencias claras en las temperaturas de la superficie a escala mundial (Jones y Moberg, 2003). Las observaciones de satélite realizadas con datos AVHRR y ATSR han confirmado un aumento de la temperatura global del mar (+0,13 º C en una década). También se ha registrado un aumento de fenómenos extremos como olas de calor, sequías y eventos de precipitación extrema en diferentes regiones (Karl y Easterling, 1999). Los modelos climáticos actuales están de acuerdo

sobre el aumento de las temperaturas de la superficie del planeta durante el segundo semestre del siglo XXI. Por ejemplo, con una duplicación de la concentración de CO2, el aumento de la temperatura estará probablemente en un rango que va desde 2 a 4,5 ° C, con la mejor estimación en 3 ° C. Sin embargo, aunque esta es la pauta general prevista a escala global, los modelos indican una diversidad espacial importante en la manifestación de los efectos del clima (Räisänen, 2007).

El efecto retroactivo del cambio climático sobre la agricultura es complejo. El aumento de la temperatura y el aumento en la concentración de CO2 atmosférico podrían afectar a los procesos biológicos de la planta (fotosíntesis, respiración, crecimiento, etc) (Barnes et al., 1995; Booker et al., 2005). El efecto fertilizante del carbono en la atmósfera podría producir un aumento general de la actividad de la vegetación y de la producción (Long et al., 2005). Sin embargo, la respuesta positiva de la actividad de vegetación y de la producción con el cambio climático sólo se espera en zonas con una adecuada disponibilidad de agua, por el contrario, las zonas afectadas por un aumento de la temperatura y la evapotranspiración, junto con una disminución de las precipitaciones, van a sufrir de un mayor estrés hídrico en la vegetación, que, a su vez, causaría una disminución de la producción (Vicente-Serrano et al., 2006). Por último, los fenómenos extremos (olas de calor, sequías, precipitaciones extremas) tiene un efecto negativo en la producción de cultivos (Vicente-Serrano, 2007). Los efectos indeseables que el cambio climático puede tener en la producción de cultivos muestran que actualmente hay una importante necesidad de realizar un seguimiento de los cultivos, que debe mantenerse en el futuro.

A.1.2. Seguimiento de cultivos.

En la sección anterior se puso de relieve que la relación entre la agricultura y el clima, y los cambios importantes en las prácticas agrícolas que se han producido durante la última parte del siglo XX, muestran que los sistemas de seguimiento de cultivos son necesarios. Para ser eficaces, esos sistemas deben satisfacer al menos los tres requisitos enumerados a continuación: deberían ser capaces de proporcionar un mapa de cultivos regularmente, realizar un seguimiento del crecimiento de los cultivos y, si es posible, predecir el rendimiento. A continuación, cada uno de estos requisitos se examina con más detalle.

Cartografía de cultivos.

El aumento sustancial de la agricultura intensiva, junto con la influencia de los reglamentos en materia de política, y las demandas del mercado, se traduce en cambios muy frecuentes en la superficie que se destina a la agricultura y en la distribución de los cultivos dentro de la tierra dedicada a la agricultura. Por lo tanto, para poder realizar estimaciones del rendimiento es necesaria una identificación regular de los cultivos, un inventario y una cartografía. Además de ser útil para la evaluación de la producción, la cartografía de cultivos también es útil para la gestión de los recursos hídricos o para realizar estimaciones del carbono fijado por el suelo, entre otros.

Seguimiento del crecimiento de los cultivos.

El seguimiento del crecimiento de los cultivos consiste en monitorizar, durante el período de crecimiento, varios parámetros de la planta y del suelo, que son indicadores del status de la planta, junto con su estado fenológico. Estos parámetros son, por ejemplo, la altura de planta, el LAI (Índice de Área Foliar), la biomasa o el contenido en nitrógeno. Normalmente, la monitorización del crecimiento de los cultivos se centra en las siguientes cuestiones, que están a su vez interconectadas:

- Desarrollo fenológico: que es la sucesión de eventos biológicos durante la vida de la planta. El estudio de la fenología implica, por ejemplo, la observación del momento exacto en el que determinados órganos del cultivo aparecen (por ejemplo, las espigas del trigo). La fenología se suele simular en términos de la suma de grados-día y características específicas de los cultivos, como son por ejemplo los factores de vernalización.

- Desarrollo de la cubierta vegetal: puede ser cuantificada mediante la medición del LAI, la biomasa o a la altura de la planta. En términos de procesos biológicos, el desarrollo de la cubierta vegetal es el resultado de la fotosíntesis, la respiración y la repartición de biomasa. La cantidad de energía recibida y la capacidad de la planta para utilizar esta energía van a determinar la producción de biomasa. La cantidad de radiación interceptada es una función del LAI. Sólo una parte de la radiación interceptada, denominado fPAR, es utilizada de forma eficiente por los cultivos para la acumulación de biomasa. La forma en que se realiza la repartición es

específica a cada tipo de cultivo. En la modelización del desarrollo de la cubierta vegetal, la diversidad estructural está controlada por variables genéticas que intervienen en esta repartición.

- Crecimiento de las raíces y capacidad de absorción: la función de las raíces de las plantas es la absorción de agua y nutrientes del suelo. Esto está estrechamente relacionado con las propiedades químicas y físicas del suelo, así como sus condiciones de humedad. Cualquier carencia de nutrientes, especialmente nitrógeno, o cualquier deficiencia en agua tiene un impacto negativo en el desarrollo de la planta. La escasez de minerales o nutrientes básicos en el suelo puede detectarse con análisis periódicos de muestras de suelo y compensarse mediante fertilización. El seguimiento de las condiciones de humedad también es necesario. En cuanto a aspectos biológicos, hay una gran diferencia entre el sistema racinal de los cultivos anuales (por ejemplo, trigo, maíz, patatas...) y el de los cultivos perennes (por ejemplo, los viñedos).

- Balance de agua entre la planta, el suelo y la atmósfera. Las necesidades de agua de un cultivo en un determinado momento dependen de variables ambientales (por ejemplo, la temperatura del aire), las condiciones del suelo y la fenología de los cultivos. Los procesos que intervienen en el balance hídrico incluyen la evaporación y transpiración, tanto en el suelo como en la planta. La lista de variables que intervienen en el balance de agua, principalmente describiendo la situación del suelo y el comportamiento del agua en el suelo, puede ser muy extensa (albedo del suelo, coeficientes de drenaje, etc....) pero lo más importante es la humedad del suelo.

- Balance de nitrógeno en el suelo y en la planta. El contenido de nitrógeno en el suelo puede cambiar como resultado de descomposiciones orgánicas, fertilización, etc. Los cultivos absorben nitrógeno a través del sistema racinal y lo fijan en sus diferentes elementos. El contenido de nitrógeno en las hojas se relaciona con el contenido en clorofila, el cual es más fácil de medir que el contenido de nitrógeno.

La información obtenida mediante el seguimiento de los puntos anteriores a través de la cuantificación de varios parámetros es de gran valor para la gestión de los campos, y es la base de las intervenciones humanas, como el uso de fertilizantes o la aplicación de un calendario de regadío concreto. Sin embargo, el seguimiento de los parámetros de los cultivos a lo largo de una temporada de cultivo es caro y consume mucho tiempo. Por lo tanto, hay una necesidad de desarrollar técnicas de teledetección que sean de utilidad en este contexto.

Predicción del rendimiento de los cultivos.

Varias técnicas han sido utilizadas para obtener una predicción temprana de la producción de cultivos, la mayoría de ellas basadas en observaciones de las condiciones climáticas que se sintetizan por medio de índices de sequía, índices de vegetación obtenidos a partir de datos de teledetección (por ejemplo, Mkhabela et al., 2005; Kalularme et al., 2003; Royo et al., 2003) y una combinación de ambos índices (Vicente-Serrano et al., 2006). Dichos métodos se basan en modelos de regresión entre el rendimiento final de las cosechas, datos climáticos e índices de vegetación. Aunque estos

métodos son ampliamente utilizados, tienen el problema de que las predicciones son dependientes de las medidas locales en la zona de estudio y a veces la extrapolación espacial es difícil, como consecuencia de la diversidad geográfica y las diferencias entre los cultivos. Para resolver estos problemas, también se pueden utilizar modelos más complejos, basados en procesos biofísicos. Estos modelos tienden a ser más generales que los métodos estadísticos basado en regresiones locales. Un modelo de crecimiento de los cultivos describe cómo una planta crece, es decir, la forma en que el carbono se ha fijado en la planta. Estos modelos requieren datos meteorológicos diarios: radiación solar, temperatura y precipitaciones. Muchos modelos se han desarrollado o adaptado a un único cultivo, a un número reducido de ellos o condiciones particulares de los cultivos tales como estrés hídrico, estrés de nitrógeno, condiciones de salinidad, etc. y hacen uso de muchos parámetros. De este modo, los beneficios de la utilización de sistema de seguimiento de cultivos que proporcione parámetros capaces de describir el desarrollo de la cubierta vegetal, por ejemplo el LAI serían muy importantes para la calibración del modelo, forzado, etc.

En la literatura científica existe una gran diversidad de modelos de crecimiento de cultivos. Algunos de éstos modelos bien conocidos y sus correspondientes «familias» son SUCROS (Simple y Universal Simulador de crecimiento de los cultivos) (Spitters et al., 1989), CERES (Crop Medio Ambiente Recursos de síntesis) (Kiriny y Jones, 1986; Ritchie et al., 1985) que fue desarrollado para los cereales, CROPGRO (Hoogenboom, 1992) es una familia de modelos para leguminosas y STICS (Simulateur mulTIdisciplinaire pour les Cultures estándar) (Brisson et al. 1998) desarrollado en el INRA,

Francia. También hay "paquetes" de software como DDSAT (Decisión Sistema de Apoyo para Agrotechnology Transfer) (Jones et al., 2003) y APSIM (la Producción Agrícola Simulador de Sistemas) (McCown, 1986) que integran varios de los modelos anteriormente citados.

Sin embargo, a pesar de la gran utilidad de estos modelos, hay notables limitaciones en relación a su calibración. Los parámetros de cultivo que describen el desarrollo de la cubierta vegetal y su dinámica son en general necesarios para la calibración de los modelos. Esto implica tiempo y toma de muestras sobre el terreno, con el consecuente coste económico. Desgraciadamente, muy a menudo hay una falta de representación espacial, principalmente en áreas en las cuales la diversidad espacial de los cultivos, así como la diversidad en las características del suelo y el clima, son importantes. Por lo tanto, debido a estas limitaciones, hay una necesidad de desarrollar métodos basados en datos de teledetección, que permitan el seguimiento de parámetros de cultivo en áreas extensas, para mejorar la predicción del rendimiento.

A.2. El papel de la teledetección en el seguimiento de los cultivos.

El seguimiento de los cultivos se puede hacer por medio observaciones sobre el terreno a escala local. Sin embargo, a escala regional, la teledetección es más adecuada, tanto en términos de cobertura espacial como cobertura temporal.

Cartografía de cultivos.

Como se dijo antes, la cartografía de cultivos es necesaria para los estudios de cambio de usos de suelo, el cambio climático, estudios hidrológicos y otras aplicaciones, como la predicción del rendimiento y la gestión eficiente de los recursos hídricos, ésta última se basa en estimaciones de la evapotranspiración (Simonneaux et al., 2008). Los mapas de cultivos se suelen utilizar en combinación con modelos de crecimiento de cultivos para la predicción de la cosecha o para la predicción del carbono fijado en el suelo (Doraiswamy et al., 2007).

Debido a la cantidad de aplicaciones, la clasificación de los cultivos mediante imágenes de teledetección es un tema de investigación importante dentro del campo de la teledetección. Las ventajas de utilizar técnicas de teledetección, en lugar de las observaciones sobre el terreno, son un coste económico más bajo y la posibilidad de cubrir áreas extensas. Otra razón importante es que las clasificaciones son más fáciles de actualizar, debido a la posibilidad de repetir las adquisiciones de datos a lo largo del tiempo.

Las metodologías para la cartografía de cultivos basadas en el uso de datos de teledetección procedentes de sensores ópticos están bien establecidas y han demostrado ser casi operacionales. La clasificación de cultivos utilizando datos ópticos es a menudo realizada con datos de una resolución espacial compatible con el tamaño del campo: en general a escala regional se utilizan Landsat-TM o SPOT-HRV. Los datos de resolución media (200 Km - 1 kilómetro) y los datos de baja resolución espacial (> 1 kilómetro) se consideran a menudo como insuficiente en relación con el tamaño de los campos. Esos

datos (AVHRR, MODIS, MERIS, SPOT-VGT) se utilizan sobre todo para seguimientos temporales multi-anuales, y para obtener mapas de usos de suelo o de cobertura del suelo a escala continental o mundial (Loveland et al., 2000; Strahler et al. 1999; Bartholomé y Belward, 2005). Una limitación conocida de los datos ópticos es la presencia de nubes, que impide la adquisición de imágenes en el momento deseado. Los datos de radar, por el contrario, tienen la ventaja de ser independientes de la cobertura nubosa y, por tanto, presentan un alto potencial para la clasificación de cultivos. También puede suceder que la vegetación necesite ser observada en un momento fenológico concreto. Este es el caso, por ejemplo, cuando dos cultivos tienen un comportamiento similar durante su ciclo de vida, excepto en una fase concreta de desarrollo. Sin embargo, los datos de satélite radar no han sido utilizados a menudo para este propósito, (Saich y Borgeaud, 2000; Schotten et al., 1995; GRT y Mather, 1999) principalmente porque, hasta hace muy poco tiempo, los satélites sólo eran capaces de medir una única polarización lineal y en una sola frecuencia: ERS-1 y ERS-2 operan en banda C con polarización VV, RADARSAT en banda C y polarización HH y JERS en la banda L, polarización HH. Las misiones futuras medirán la matriz completa de dispersión en una única frecuencia y es necesario desarrollar métodos de clasificación adecuados.

Varios algoritmos utilizan los datos radar para la clasificación de cultivos. De manera general, pueden clasificarse en métodos basados en una base de conocimientos (knowledge-based approaches), clasificación por mecanismos de dispersión, y métodos estadísticos (Oliver y Quegan, 1998). Los métodos basados en una base de conocimientos se fundamentan en en el análisis de la física que determina la retrodispersión medida para cada tipo de

cultivo. Estos clasificadores tienen la ventaja de ser más robustos y fáciles de adaptar a las condiciones específicas de la zona que se clasifica.

Seguimiento de la condición y del crecimiento de los cultivos por medio de datos de teledetección.

Los datos de teledetección pueden ser utilizados para estimar parámetros biofísicos, los cuales son indicadores de la condición en que se encuentran los cultivos a lo largo de su ciclo de crecimiento. Las estimaciones multi-temporales de estos parámetros contribuyen al seguimiento del crecimiento. Las variables biofísicas como el LAI, fracción de radiación fotosintéticamente activa (fPAR), la biomasa o el contenido de nitrógeno son importantes porque contribuyen a la comprensión de la dinámica de los cultivos y de la dinámica medioambiental a cualquier escala espacial. A pesar de la disponibilidad de los datos de radar independientemente de las condiciones meteorológicas, la inversión de parámetros biofísicos se realiza con mayor frecuencia utilizando datos ópticos, principalmente debido a que la interacción entre la señal radar y la vegetación es más compleja que en el caso de la señal en el óptico, y por lo tanto es más difícil establecer relaciones biofísicas. En general, éstas sólo pueden ser establecidos para un tipo de cultivo, porque tiene una estructura particular. Además, el manejo de datos radar es más complejo que el de datos ópticos. Se ha publicado una gran cantidad de artículos sobre la obtención de parámetros biofísicos de la cubierta vegetal mediante datos ópticos. Así, pueden encontrarse muchos ejemplos para el LAI (Turner et al., 1999; Weiss et al. 2000; Combal et al, 2002a; Duchemin et al., 2006), fPAR, contenido en agua de la cubierta vegetal y contenido en clorofila de la hoja. En

el caso de los cultivos agrícolas, en los cuales los cambios temporales son más rápidos que, por ejemplo, en las superficies forestales, las observaciones multi-temporales son muy importantes. Sin embargo, pocos trabajos se han referido a la inversión efectiva de imágenes de satélite multi-temporales y de alta resolución espacial para diversos tipos de cultivos. Por lo tanto, es necesario realizar más estudios para la inversión de parámetros biofísicos utilizando datos multi-temporales.

En la región radar, los datos multi-angulares, polarimétricos e interferométricas han demostrado ser de interés para la inversión de parámetros bio-geofísicos de cultivos, tales como la altura de la planta, el contenido en agua, el LAI y la biomasa (Le Toan et al., 1984). Estos estudios se realizaron principalmente con las bandas X y C. Se ha demostrado que si la cubierta vegetal tiene componentes con orientaciones específicas, la profundidad de penetración, el volumen de dispersión, y la atenuación puede ser diferente para los diferentes estados de polarización (Ferrazzoli et al., 1999; Picard et al., 2003, y Mattia et al. 2003). Este fenómeno fue la base utilizada para desarrollar un algoritmo de clasificación de campos de arroz (Le Toan et al., 1989).

Al igual que ocurre con la cartografía de cultivos la inversión de parámetros biofísicos utilizando datos de satélite radar se han visto limitados por el tipo de datos disponibles. El sensor ASAR a bordo de ENVISAT permitió, por primera vez, la medida simultánea de dos polarizaciones: HH / VV, HH / HV y VV / HV , para varios ángulos de incidencia no simultáneos, todo ello en banda C. Esta fue la motivación de estudios sobre el uso de la

polarimetría para la inversión de la biomasa del trigo (Mattia et al., 2003). El presente trabajo estudia el potencial de los datos radar polarizados para la inversión de la biomasa de cereales de grano pequeño utilizando datos ENVISAT-ASAR.

El papel de la Teledetección en combinación con los modelos de crecimiento de cultivos para la predicción de la cosecha.

En los modelos de crecimiento de cultivos es difícil tener en cuenta la heterogeneidad espacial de la vegetación y de las condiciones de suelo, así como las dificultades inherentes a la fenología. El crecimiento de los cultivos depende de muchos factores (clima, especies, el estado del suelo, las características del suelo y las estrategias de gestión) y, en consecuencia, los modelos necesitan muchos parámetros. Por ejemplo STICS v3.0 depende de 132 parámetros (Ruget et al. 2002). Es frecuente que algunos de estos parámetros, tales como la fecha de siembra, no se conozcan, o tengan que ser ajustados para cada tipo de cultivo o ubicación geográfica. Una solución consiste en calibrar los modelos utilizando las mediciones de parámetros biofísicos (por ejemplo, Brisson et al., 1998; Spitters et al., 1989; Bondeau et al., 1999; Launay y Guerif, 2005). El LAI, que representa la superficie de hoja que intercepta la radiación incidente, y la biomasa, son variables clave para calibrar los modelos de crecimiento de cultivos.

La calibración se puede hacer con la medida in-situ de parámetros biofísicos. Sin embargo, las mediciones in-situ son caras, requieren mucho tiempo y, en general, sólo puede hacerse en un número limitado de campos. Así, la calibración corre el riesgo de convertirse en dependiente de la zona de

estudio y del cultivo. En este contexto la teledetección por satélite es útil cuando se integra con los modelos de crecimiento de los cultivos, ya que proporciona información espacial sobre la vegetación. La teledetección se puede utilizar para estimar variables claves de los modelos: LAI, la biomasa aérea de cultivos y otras características, como la clorofila o contenido en nitrógeno. Esta información se puede integrar en el proceso de calibración utilizando, por ejemplo, métodos de forzado (Clevers y van Leeuwen, 1996; Moulin et al., 1998).

A.3. Objetivos del estudio.

El objetivo general de esta tesis doctoral es la evaluación y el desarrollo de métodos basados en datos de teledetección, que sean útiles para el seguimiento de los cultivos, y puedan contribuir, cuando se combinen con otros métodos, a la mejora de la predicción del rendimiento. La tesis se centrará en dos temas principales: la clasificación de los tipos de cultivos y la inversión de parámetros de vegetación. Por otra parte, uno de los aspectos relevantes que se aborda en esta tesis es el beneficio que puede derivarse de utilizar datos multi-temporales. Para lograr los objetivos de este estudio ha sido necesario tratar con la complejidad añadida de la utilización de diferentes instrumentos, tipos de datos, zonas de estudio y medidas de campo.

Este estudio se basa en dos tipos de datos de teledetección: óptico y radar. Los instrumentos de satélites ópticos que se utilizan son LANDSAT-TM y ENVISAT-MERIS. Los datos radar provienen del instrumento a bordo del satélite ENVISAT-ASAR, así como de un sensor aerotransportado, JPL-

AirSAR. En los capítulos siguientes se darán más detalles acerca de estos sensores y satélites.

En el caso de las aplicaciones agrícolas, el uso de ambos datos ópticos y de radar es necesario para superar las limitaciones que cada uno de los tipos de datos tienen por separado. Por ejemplo, aunque existen métodos operativos para la clasificación de los cultivos utilizando datos ópticos, estos métodos no pueden ser aplicadas en regiones cubiertas frecuentemente por nubes. En este sentido, este estudio es una demostración de la la complementariedad de ambos tipos de datos en los estudios de cultivos. Los datos ópticos se utilizan para llevar a cabo un seguimiento multitemporal del LAI, y para invertir LAI y clorofila. Datos de satélites recientes, y datos similares a los que se obtendrán mediante satélites futuros, se utilizan para la cartografía de cultivos. Por último, la inversión de la biomasa utilizando datos de radar también se investiga.

En cuanto a la inversión de parámetros biofísicos, los objetivos de este estudio son tres:

- La estimación de las variaciones de LAI a lo largo de un ciclo, a partir de imágenes LANDSAT, para los diferentes cultivos de una misma zona agrícola.
- El desarrollo de un método multi-temporal para la inversión de LAI y clorofila utilizando datos MERIS-FR.
- La investigación del seguimiento de cereales de grano pequeño con datos ASAR-APP, así como las posibilidades de invertir la biomasa de este tipo de cereales.

En cuanto a la cartografía de los cultivos, el objetivo de esta tesis es el desarrollo de un método de clasificación jerárquico y su validación. En vista de las aplicaciones a datos de satélites actuales y disponibles en un futuro reciente, se utilizan datos polarimétricos en banda C del instrumento AirSAR. En la última parte de este trabajo, también se investiga el potencial de los datos ENVISAT-ASAR.

Este estudio se ha desarrollado en tres zonas agrícolas de Europa:

- Barrax en Castilla-La Mancha, España. El capítulo 3 describe más detalladamente la región , así como las medidas de campo adquiridas durante la campaña ESA/SPARC-2003.
- Flevoland, al norte de los Países Bajos. En el capítulo 6 se dan más detalles sobre esta zona.
- Toulouse, al sur de Francia. La descripción del experimento llevado a cabo en un campo de trigo, con el objetivo de medir la biomasa del trigo, así como otras medidas se realiza en el capítulo 7.

A.4 Organización de la memoria.

La presente tesis doctoral se ha organizado en dos partes: óptico y radar. La tesis proporcionará los conceptos básicos necesarios para la comprensión de la señal de teledetección con respecto a los cultivos agrícolas. El capítulo 1 es una introducción general.

En la Parte I se presentan los resultados obtenidos a partir de los datos ópticos en la zona de Barrax.

- El capítulo 2 da las bases físicas de la teledetección en el óptico. Se presenta una descripción de los modelos utilizados para la inversión de datos ópticos, así como una revisión de los algoritmos utilizados para la inversión de LAI, clorofila y biomasa. El método de corrección atmosférica que se se aplica a los datos ópticos también se describe en este capítulo.

- El capítulo 3 se centra en la inversión de LAI usando datos LANDSAT-TM. El estudio se lleva a cabo en la región de Barrax. El LAI se ha invertido a partir de imágenes en doce fechas repartidas a lo largo del año 2003 y se ha validado con las medidas de campo pertenecientes a la campaña ESA/SPARC-2003.

- El capítulo 4 presenta los resultados de la inversión de LAI y clorofila a partir de datos MERIS-FR utilizando un método multi-temporal. El estudio también se ha realizado en la región de Barrax.

La parte II expone el trabajo realizado utilizando datos radar. Las mismas tres áreas de estudio están involucradas. Los capítulos 5 al 7 se organizan de la siguiente manera:

- El capítulo 5 da el contexto teórico de la teledetección radar necesario para los capítulos 6 y 7.

- El capítulo 6 expone un método jerárquico de clasificación de cultivos, basado en datos polarimétricos de radar de apertura sintética en banda C. Se han utilizado datos AirSAR acquiridos sobre la región de Flevoland, en el marco de la campaña de la Agencia Espacial Europea, MAC-Europe, así como datos de la biblioteca del proyecto ERA-ORA (European RAdar-Optical Research Assemblage, http://eraora.disp.uniroma2.it/) financiado por la Unión Europea. Los resultados obtenidos en la clasificación de 5 tipos de cultivos y una clase de suelo se han validado con un mapa de cultivos de la zona realizado mediante observaciones sobre el terreno. Algunas de las reglas del algoritmo también han sido examinadas en la región de Barrax.

- El capítulo 7 trata sobre la aplicación de datos ASAR-APP para la clasificación de cultivos, y sobre la inversión de la biomasa de cereales de grano pequeño utilizando datos ENVISAT-ASAR, en la región de Toulouse. En este capítulo se describe la campaña de campo que se llevó a cabo en Toulouse, para medir los parámetros biofísicos de un campo de trigo. También se exponen los resultados sobre el uso de datos ASAR-APP para la clasificación de cultivos en Barrax. Por último se describe el tratamiento aplicado a los datos ENVISAT-ASAR.

- El capítulo 8 contiene las conclusiones generales y las perspectivas de este trabajo.

CAPÍTULO 1: Introducción

El capítulo 1 de esta tesis doctoral es una introducción al tema de estudio y se ha trascrito íntegramente en castellano en la sección precedente.

CAPÍTULO 2: Parámetros biofísicos y datos ópticos.

En este capítulo se da una breve introducción a la base conceptual de la teledetección óptica, antes de proceder a la evaluación de los métodos de teledetección. Estos conceptos se presentan como los antecedentes pertinentes a la tesis, con el fin de entender las relaciones entre la señal medida por los sensores ópticos y las propiedades de la vegetación. En primer lugar, se describe un esquema del problema general de teledetección. Se explica el efecto de la atmósfera sobre la radiación solar y se presenta el método de corrección atmosférica que se ha aplicado a los datos. Los modelos que han sido utilizados en este trabajo para describir la interacción de la radiación solar con la cubierta de vegetación son también presentados. El capítulo termina con una revisión de bibliografía relativa a la obtención de parámetros biofísicos, LAI y contenido en clorofila de la hoja utilizando datos ópticos.

CAPÍTULO 3: Variaciones del Indice de Area Foliar a lo largo de un ciclo en cultivos agrícolas mediante datos LANDSAT.

El cálculo del índice de área foliar (LAI) mediante datos de satélites ópticos ha sido objeto de una gran cantidad de estudios. Por el contrario, son pocos los trabajos que han realizado una inversión multi-temporal efectiva utilizando imágenes de satélite de resolución espacial alta para los distintos cultivos de una determinada región. El presente estudio se centra en la evaluación de un método de inversión de LAI basado en un modelo físico y aplicado a datos multi-temporales ópticos, adquiridos sobre una región agrícola con una diversidad de cultivos y de calendarios agrícolas. Tanto el método de inversión como el tipo de datos se han seleccionado por su amplia utilización. Los cultivos en la región de estudio (Barrax, Castilla-La Mancha, España) son los siguientes: cereales, maíz, alfalfa, remolacha, cebolla, ajo, adormidera. Algunos de los tipos de cultivos (cebolla, ajo, adormidera) no se han abordado en trabajos previos.

En este estudio se usan medidas in-situ y valores obtenidos de la literatura científica para establecer los a priori que se utilizan en el modelo PROSPECT+SAIL con el que se generan Look Up Tables (LUTs). Estas LUTs se utilizan posteriormente para invertir las imágenes Landsat-TM y Landsat ETM+ (12 fechas de marzo a septiembre de 2003). Las LUTs se han adaptado a los cultivos presentes en la zona, los cuales se han identificado en las imágenes gracias a una clasificación LANDSAT de la región. El LAI obtenido se ha comparado con las medidas in-situ, que se realizaron durante la

campaña de campo que se llevó a cabo a mediados de julio del 2003. Se ha obtenido un buen acuerdo (una alta correlación lineal) para valores de LAI comprendidos entre 0.1 y 6.0. Por lo tanto se han producido mapas de LAI para cada una de las 12 fechas. La variación temporal del LAI manifiesta una gran coherencia con el estado fenológicos de los cultivos. El método de inversión se ha comparado de forma favorable con un método de inversión de LAI basado en la relación empírica existente entre el LAI y el NDVI a partir de datos LANDSAT. Esto ofrece perspectivas para los futuros datos de satélite ópticos, que garantizarán una resolución espacial y una frecuencia temporal altas.

CAPÍTULO 4: Inversión de LAI y Clorofila utilizando datos multi-temporales.

En el capítulo 3, el LAI se obtuvo mediante la aplicación de un método simple para la inversión del modelo PROSPECT+SAIL y datos LANDSAT-TM, con buenos resultados. Como se discutió, la utilización de la dimensión temporal podría ser una nueva mejora en la inversión. El objetivo de este capítulo es investigar las posibilidades de inversión, de LAI y contenido en clorofila de la hoja, conjuntamente, en campos agrícolas, aprovechando, en la medida de lo posible, la información contenida en los datos multi-temporales. Esto se hace mediante la adición de una ligadura temporal en el procedimiento de inversión. Entre los posibles métodos de inversión, se ha seleccionado un método numérico de búsqueda directa, puesto que la ligadura

temporal era fácil de implementar en este tipo de método. Así mismo, se ha preferido el uso de datos ENVISAT-MERIS frente a los datos LANDSAT-TM, debido a su mayor frecuencia temporal, a pesar de tener una resolución espacial menor. El método se aplica a la zona de Barrax (España) con especial interés en los campos de cereales de grano pequeño.

CAPÍTULO 5: Bases físicas de la teledetección radar activa.

En este capítulo se da una breve introducción a los fundamentos de la teledetección por radar y los conceptos utilizados en el capítulo 6 y el capítulo 7.

CAPÍTULO 6: Datos de Polarización en banda C para la clasificación de cultivos.

Como ya se ha discutido en el capítulo 1, los métodos para la clasificación de cultivos utilizando datos ópticos están bien establecidos. Sin embargo, en las zonas agrícolas con cobertura nubosa frecuente, como ocurre en el Norte de Europa, hay una necesidad de desarrollar métodos basados en datos de radar.

En este capítulo se ha desarrollado un método de clasificación de cultivos utilizando datos radar polarimétricos en banda C. En el capítulo 5 se

afirmó que los datos en banda C son los más adaptados a la agricultura frente a otras longitudes de onda de radar. La elección de longitud de onda se ha realizado en vistas a las aplicaciones a datos de satélite radar existentes (ENVISAT / ASAR, RADARSAT-2) y a las aplicaciones en las misiones futuras de satélites (Sentinel-1).

Una dificultad para el desarrollo de este tipo de estudio es la falta de datos polarimétricos multi-temporales en banda C, ya sea adquiridos desde satélite como desde avión, junto con un mapa de cultivos detallado, el cual es necesario para el análisis y la validación de los resultados. En consecuencia, el estudio se ha llevado a cabo con los datos aerotransportados del sensor AirSAR, imágenes adquiridas en 1991 de julio en Flevoland (Países Bajos), que constituye un conjunto completo de datos con sus correspondientes observaciones de campo. La primera parte del capítulo está dedicado al análisis de datos AirSAR de la base de datos ERA-ORA. Los resultados de este análisis se utilizarán para desarrollar el método de clasificación. El método proporciona buenos resultados, como se indica en la sección 6.5 de esta memoria. Por último, los datos AirSAR correspondientes a la zona de Barrax (España) también han sido estudiados con el fin de evaluar las reglas del algoritmo en una región diferente.

CAPÍTULO 7: Uso de datos ENVISAT-ASAR APP para el estudio de cultivos.

Este capítulo está dedicado al análisis de datos ENVISAT / ASAR en regiones agrícolas. En la primera parte se describen las medidas experimentales realizadas en un campo de trigo, en la zona de Toulouse, durante el año 2003, los datos de radar disponibles y el tratamiento aplicado a dichos datos. La segunda parte de este capítulo analiza las posibles aplicaciones y las limitaciones del algoritmo de clasificación de cultivos presentado en el capítulo 6, utilizando datos de la región de Toulouse, que fueron adquiridos en varias fechas a lo largo de año 2003, así como datos obtenidos para una fecha en Barrax. También se ha investigado la posibilidad de invertir la biomasa de trigo utilizando datos ASAR.

CAPÍTULO 8: RESUMEN Y CONCLUSIONES

El objetivo de este estudio fue la elaboración y la evaluación de métodos para la clasificación de cultivos y para la estimación de LAI, clorofila y biomasa, basados en el uso de datos de teledetección ópticos y radar, cuyo interés es ayudar a sistemas operativos, o quasi-operativos, de seguimiento de cultivos en aplicaciones agrícolas.

Después de la introducción que figura en el capítulo 1, la primera parte de este estudio se inicia con un panorama sobre la inversión de

parámetros biofísicos con datos ópticos, expuesta en el capítulo 2. El capítulo 3 se dedica a la estimación del LAI en Barrax, un área con una diversidad de tipos de cultivos y de ciclos de crecimiento. El LAI se invirtió, para 12 imágenes LANDSAT-TM, que cubren la temporada agrícola del año 2003. El modelo PROSPECT+SAIL se invirtió utilizando una técnica basada en LUTs (Look Up Tables). Los resultados fueron validados con éxito utilizando medidas in-situ de LAI en julio. El uso de medidas in situ (contenido de clorofila en la hoja, materia seca en la hoja, contenido de agua en la hoja), junto con otra información a-priori (espectro del tipo de suelos, variabilidad del suelo, rango de variación del LAI, estructura de planta, valores obtenidos de la literatura científica) es un parte esencial de la metodología. Esta información fue utilizada como input de los modelos para la construcción de las LUTs. Se demostró que los métodos relativamente simples ayudados de suficiente información terreno, permiten obtener estimaciones de LAI para diferentes cultivos con buena precisión.

En la región de Barrax, las hipótesis sobre la variabilidad del suelo eran válidas y no parecen ser una fuente de error importante. No obstante, en vista de las aplicaciones a otras regiones, el efecto de la variabilidad del suelo (debido a la humedad del suelo o al tipo de suelo) en la inversión de LAI necesita más investigaciones.

La comparación del método físico con el método basado en relaciones empíricas entre el LAI y el NDVI permitió concluir que estas relaciones son más dependientes de tipo de cultivo que el método físico. Por otra parte, el método de inversión permite el acceso a mayores valores de LAI

que la relación el NDVI-LAI, la cual se satura para valores más pequeños de la LAI que el método físico.

Este estudio se centró en la inversión del LAI efectivo, pero, en trabajos futuros, sería deseable utilizar correcciones de clumping para tratar de obtener el LAI verdadero, en particular, para el caso de maíz (Duthoit, 2006). Otra mejora para la metodología de inversión de LAI aplicada en este estudio sería añadir una ligadura temporal en la función que se minimiza durante el inversiones. En el capítulo 4 se investigó este aspecto mediante el uso de datos MERIS.

El capítulo 4 se dedica al desarrollo de un método multi-temporal para inversión de LAI y clorofila, utilizando datos MERIS-FR en la zona de Barrax. El método también invierte el modelo PROSPECT+SAIL, con la particularidad de que los términos temporales dependientes (limitaciones temporales) se introdujeron en la función de mérito, que se minimiza usando un algoritmo iterativo. El método se aplicó a campos de cereales de grano pequeño y los resultados se compararon con los resultados de las inversiones fecha a fecha, que utilizan el mismo modelo y el mismo método iterativo para la inversión. La comparación reveló que el método multi-temporal funcionó mejor. Se investigaron diferentes términos de ligadura, y los mejores resultados se obtuvieron para una ligadura temporal sobre la evolución del producto LAI x clorofila.

El uso de los datos MERIS para el seguimiento de cultivos en la región de Barrax tiene serias limitaciones debido a la resolución espacial de

MERIS y los tamaños de los campos. La precisión de los resultados de las inversiones podría mejorarse mediante la corrección del porcentaje de suelo presente en los píxeles de MERIS. Esto podría hacerse por medio de parámetros como la fracción de la cubierta vegetal. Sin embargo, para ser coherente con las hipótesis del modelo SAIL (el píxel es homogéneo), la corrección debe hacerse previamente a la inversión. Zurita-Milla et al., (2007) han propuesto técnicas de unmixing para datos MERIS y podrían ser introducidas como un paso previo a nuestro algoritmo. También podrían mejorarse las inversiones con un mayor muestreo del espectro similar al de CHRIS-PROBA.

La hipótesis realizadas por los modelos son una de las principales limitaciones de las metodologías utilizadas en el capítulo 3 y 4. Estas hipótesis son la principal fuente de error, como se discutió anteriormente, y la cuantificación de esta fuente de error requiere un estudio más a fondo. En este sentido, se espera que la última versión de PROSPECT (Feret et al., 2008) mejore las estimaciones de clorofila. Sin embargo, la inversión del contenido de clorofila de la hoja mediante datos de satélite es una tarea difícil y requiere más investigaciones, dedicando esfuerzos, al mismo tiempo a la elaboración de modelos y a las técnicas de inversión.

Para observar los cultivos en el norte de Europa, los datos radar son preferibles a los datos ópticos, debido a la alta presencia de nubes en esa región. La clasificación de cultivos agrícolas utilizando datos aerotransportados polarimétricos en banda C fue abordada en el capítulo 6, donde se propuso un algoritmo jerárquico basado en cinco reglas físicas. Las reglas del algoritmo

fueron desarrolladas en base a los mecanismos de dispersión y el comportamiento de la dispersión de los diferentes cultivos. La primera regla del algoritmo separa entre vegetación y no / vegetación utilizando los cocientes HV / HV y VV / HH . La segunda regla separa los cultivos de hoja ancha de los cultivos de tallo pequeño, mediante una condición sobre el coeficiente de polarización circular RR / RL. Por último, el coeficiente de retrodispersión de polarización cruzada, HV, se utiliza para discriminar diferentes niveles de biomasa en la clase de cultivos de tallo pequeño, y la correlación HH_VV se utiliza para separar las subclases en la clase de hoja ancha. El algoritmo ha sido desarrollado para la región de Flevoland, Países Bajos, y se ha validado con un mapa de cultivos obteniéndose buenos resultados. Se ha obtenido una precisión del 73% a mediados de julio y del 65% a finales de julio.

Este trabajo de clasificación permite concluir que un número limitado de las medidas polarimétricas contiene información suficiente para realizar una clasificación de los cultivos presentes en las zonas agrícolas del norte de Europa. El algoritmo no pudo aplicarse con éxito a la zona de Barrax (España), principalmente porque las imágenes adquiridas en esa zona no estaban adaptadas al calendario de cultivos real de la región. Sin embargo, el análisis en Barrax ha demostrado que las reglas de algoritmo son robustas. Los cocientes HV / HH y HV / VV han servido para detectar la cosecha de cereales de grano pequeño, de junio a julio. Los cambios en la estructura de los cultivos se detectaron con el cociente RR / RL, así como los cambios en el nivel de biomasa, utilizando HV. Un mejor resultado se podría esperar en Barrax con un calendario de adquisición de imagen más adaptado a las

particularidades de la región. Así mismo, en esta zona del sur de Europa, donde la presencia de nubes no es una limitación, los algoritmos de clasificación utilizando datos ópticos darían resultados mucho mejores.

La principal conclusión es que la metodología propuesta es sólida y se puede adaptar a otros sitios siempre que exista un conocimiento del calendario agronómico y del tipo de cultivos presentes en la zona.

La última parte de este trabajo, presentada en el capítulo 7, consistió en el análisis de imágenes ENVISAT-ASAR adquiridas en Toulouse. La mezcla de polarizaciones y swaths ha sido una limitación en el análisis de las imágenes ENVISAT-ASAR para la discriminación de cultivos. No obstante, este análisis confirma que el coeficiente de retrodispersión HV era un buen discriminador de la biomasa. Así mismo, el cociente HH / VV se ha encontrado robusto en la discriminación entre campos cultivados y no cultivados. En Toulouse, se obtuvieron mejores resultados en la discriminación de cultivos cuando se utilizan ángulos de incidencia elevados. Otra ventaja de los datos de radar en comparación con los datos ópticos es que contienen información útil para la inversión de la biomasa. El segundo objetivo del capítulo 7 es investigar la estimación de biomasa de trigo por medio del cociente de polarizaciones HH / VV. Con este objetivo, en el año 2003 se realizó una campaña dedicada a la adquisición de mediciones de terreno en un campo de trigo. Este estudio ha permitido confirmar las investigaciones anteriores (Le Toan et al., 1998; Mattia et al., 2003), que mostraron que el cociente HH / VV aumenta con la biomasa. Los resultados con ENVISAT-ASAR muestran que el cociente HH / VV puede utilizarse para la monitorización del crecimiento de trigo. Sin embargo,

la inversión de la biomasa del trigo se vio limitada por la falta de un número suficiente de las adquisiciones con el mismo ángulo de incidencia. La comparación de nuestros resultados con otros estudios muestran que la relación entre el cociente HH / VV y la biomasa podría ser dependiente de la zona de estudio y el desarrollo de un método de inversión de la biomasa requiere más trabajo. La relación depende de muchos factores: la humedad del suelo, la densidad de trigo, la estructura de la planta, etc. Por otra parte, para la interpretación de las mediciones de retrodispersión es muy importante un conocimiento exacto de la fenología del trigo. Una recomendación para futuros trabajos es garantizar la mejor caracterización posible de todos los parámetros relacionados con la estructura de trigo y su fenología. También, más estudio es necesario para el desarrollo de métodos de compensación angular.

En este estudio, la relación entre la biomasa y de retrodispersión fue investigado por un único tipo de cultivo. Pero, ciertamente, otros tipos de relaciones pueden existir (como sugiere el capítulo 6) entre los diferentes cultivos y las medidas de retrodispersión. Especialmente interesante parece la polarización cruzada, HV.

Conclusiones generales:

Este estudio ha demostrado la importancia de utilizar datos multi-temporales en el estudio de cultivos. La teledetección de parámetros biofísicos es en esencia un problema inverso. El seguimiento de parámetros biofísicos requiere la adquisición de imágenes con alta resolución temporal y una adecuada resolución espacial. Esto es a menudo una limitación en la aplicación

de métodos de teledetección, debido a la falta de este tipo de datos en un determinado sitio. Este trabajo se benefició de una serie de datos inusual (12 imágenes LANDSAT a lo largo del mismo año) y demostró la aplicación práctica de la inversión de LAI en una zona amplia. También se mostró, mediante una ligadura temporal en la inversión de LAI y clorofila con datos MERIS, cómo la dimensión temporal en sí misma puede ser utilizada para mejorar la inversión de parámetros biofísicos. Las misiones recientes como FORMOSAT y la futura misión Venus, que será capaz de ofrecer una frecuencia temporal y resolución espacial muy altas, ofrecen nuevas perspectivas para los métodos explorados en este trabajo.

En lo que respeta a la clasificación de cultivos utilizando datos radar, la misma conclusión se aplica. Los métodos de clasificación de cultivos se benefician de las adquisiciones multi-temporales. Si la resolución temporal no es suficiente, no es posible observar algunos cambios importantes en la estructura de los cultivos. De hecho, la experiencia en Flevoland ha demostrado que, para optimizar los resultados, es necesario hacer observaciones semanales, debido a la dinámica de los cultivos. Por otra parte, se ha demostrado que el uso de la polarimetría en banda C es un buen medio para mejorar la clasificación de cultivos. El algoritmo propuesto en este estudio es particularmente adecuado para su aplicación a los datos del nuevo satélite RADARSAT-2.

Por último, este es uno de los pocos estudios que demuestran en la práctica las posibilidades que ofrece la combinación de diferentes tipos de datos (radar y óptico), con el fin de obtener la máxima información útil para el

seguimiento de cultivos. La combinación de datos ópticos y de radar proporciona estimaciones de LAI y de la biomasa, que son dos variables clave para la comprensión y la modelización del crecimiento de los cultivos. Sin embargo, la adquisición simultánea de datos ópticos y de radar, con una resolución espacial adecuada, mediante satélite, no es todavía una realidad. Sin embargo, los datos de satélite actuales ofrecen muchas perspectivas para la sinergia de ambos tipos de datos.